SSC PC-001
296 PAGES

A Research and Development Program

To Continue the Development of Precision Instrumentation for The study of Muons in the TeV Region

submitted to

The Superconducting
Super Collider Laboratory

A Research and Development Proposal Submitted by

G. Gratta, R. Mount, H. Newman
California Institute of Technology

I. Brock, A. Engler, T. Fergusen, H. Vogel
Carnegie Mellon University

L. Wilk
Charles Stark Draper Laboratory

P. McBride, I. Scott, K. Strauch
Harvard University

H. Akbari, J.Z. Bao, C. Spartlotis
John's Hopkins University

D. Duchane, W. Kinnison, W. Miller, G. Sanders, H. Ziock
Los Alamos National Laboratory

U. Becker, P. Berges, J.D. Burger, Y.H. Chang, R. Clare
T.S. Dai, M. Fukushima, C. Grinnell, G. Herten, Q. Li,
D. Luckey, S.C.C. Ting, T. Wenaus, M. White, B. Wyslouch
Massachusetts Institute of Technology

R. Beckers, H. Cohen, A. Gabriel, J. Johnson, D. Kuban
F. Plasil, M. Rennich, G. Young
Oak Ridge National Laboratory

P. Denes, P. Piroue, D. Stickland
Princeton University

A. Bujak, L. Gutay, T. McMahon, B. Stringfellow
Purdue University

CONTENTS

Chapter I Introduction

Muon Physics at the Superconducting Super Collider

1.1 Physics considerations

1.2 Physics objectives

1.3 Experience

1.4 Worldwide interest in precision muon physics at the Superconducting Super Collider

1.5 Organization of this proposal

Chapter II **Precision Measurement of Muons at the Superconducting Super Collider**

2.1 Introduction

2.2 Plans for research and development for a complete detector

Chapter III **Research and Development for the Construction and Design of Muon Chambers at the Superconducting Super Collider**

3.1 Need for research and development

3.2 Chamber structure

3.3 Wire alignment

3.4 Drift cell optimization

3.5 Test modules

3.6 Scope, schedule, milestones and funding estimates

3.7 Funding requests

Chapter IV **Research and Development Program to Determine a Suitable Gas for a Large SSC Precision Muon Detector**

4.1 Need for research and development

4.2 L3 experience and comparison with the SSC

4.3 Research and development goals

4.4 Research and development program

4.5 Prototype chamber for final tests

4.6 Scope, schedules and milestones

4.7 Funding requests

Chapter V **Research and Development for the Support and Alignment of Muon Chambers at the Superconducting Super Collider**

5.1 Structural design

(a) The need for research and development in the structural design

(b) Structural design considerations

(c) L3 structural design review

(d) A proposed SSC muon chamber support structure design

(e) Scope, schedule and milestones of research and development for the structural design

(f) Request for support of the structural design research and development

5.2 Structural analysis

(a) The Need for structural analysis research and development

(b) L3 structural analysis review

(c) Scope, schedule and milestones of research and development for the structural analysis

(d) Request for support of the structural analysis research and development

5.3 Alignment systems

(a) The need for research and development in alignment systems

(b) L3 alignment system review

(c) A proposed SSC muon chamber alignment scheme

(d) Scope and schedule of research and development for the alignment systems

(e) Support for the research and development on alignment systems

Chapter VI **Coordination of Engineering**

6.1 The need for coordination of engineering support

6.2 Scope of engineering coordination

6.3 Request for support of the engineering coordination

Chapter VII **Summary**

7.1 Summary of activities for the SSC muon detector research and development program

7.2 Summary of milestones for the SSC muon detector research and development program

7.3 Summary of contributions by participating institutes in the SSC muon detector research and development program

7.4 Summary of requests for support of the SSC muon detector research and development program to the Swiss Government

7.5 Summary of requests for support of the SSC muon detector research and development program to D.O.E.

Appendix I **Description of the L3 Muon Chamber System**

Appendix II **Development of Large Area Precision Muon Detectors**

Appenidx III **Synergy between Industry and High Energy Physics for Market Relevant New Methods in High Precision Laser Survey Techniques, High Resolution Time Measurement and Parallel Optical Data Transmission.**

Appendix IV **"Drift Velocity and Drift Angle Measurements"** C.M.Ma et al, Massachusetts Institute of Technology, Laboratory for Nuclear Science Report. Technical Report Number 129, October 22, 1982.

* * * * * * *

CHAPTER I

INTRODUCTION : MUON PHYSICS AT THE SUPERCONDUCTING SUPER COLLIDER

1.1 Physics considerations :

Advancements in physics are based on the close interplay between experiment and theory. Advancements in theory are based on the ability of theorists to explain existing experimental results and to predict new phenomena to be confirmed by experiments. Revolutions in physics occur when an experimental result contradicts the theoretical prediction which leads to the creation of new theory. There is no theory that can disprove an experimental result, whereas a theory, however logical and elegant, cannot be valid if it does not conform to experimental observations. Over the last quarter of the century, careful experimentation in physics, such as the discovery of the J particle, the observation of CP violation in K decay, and the discovery of high temperature superconductors have opened up new fields of research in physics. These observations were carried out by experiments even though there was no apriori theoretical interest.

Over a period of a quarter of a century, there have been many fundamentally important discoveries in elementary particle physics. These discoveries have enabled us to have more confidence in the Standard Model. These discoveries were all made by precision experimentations on leptonic final states. Indeed, one can recall the following examples :

1) The discovery of two neutrinos [1.1] was done by measuring μ and e final states.
2) The discovery of the J particle [1.2] (shown in Fig.1.1) was done by an experiment on e^+e^- final states with a mass resolution of 0.1% and a hadron background rejection of $1/10^{10}$.
3) The discovery of the Tau lepton [1.3] (shown in Fig.1.2) was done by an experiment with a 4π detector measuring coincidence of μe final state.
4) The discovery of the Upsilon particle [1.4] (shown in Fig.1.3) was done by an experiment with a μ pair mass resolution of 2%.

5) The discovery of the Z° particle [1.5] (shown in Fig.1.4) was done with a large 4π detector measuring e^+e^- final states. Fig.1.5 shows the measured muon pair spectrum by UA1 (CERN) clearly indicating the discovery potential of measuring muon pairs.

6) The discovery of $W\pm$ [1.6] was done by measuring their large momentum single muon decays.

These facts enable us to make the following observations :

i) These discoveries were not predicted when the original accelerators were constructed (with exception of Z and W).

ii) None of these discoveries were made by detecting hadronic final states.

iii) In general, the decay rate of heavy particles into single lepton and lepton pairs is much smaller than the decay rate into hadrons. However, since the background of single lepton and lepton pair is generally very small, if an experiment can be done cleanly and precisely and with good resolution and good hadron rejection, one can easily distinguish the signals from the background, as shown in Figs.1.1 to 1.5.

iv) The need for resolution can be easily established by recalling not only the history of the J particle but also by the recent precision muon pair experiment done at Fermi National Laboratory where the original resonance seen in Fig.1.3 was shown to be a composite of many states [1.7] (Fig.1.6).

1.2 Physics objectives

The purpose of this proposal is to request support to enable us to continue twenty-five years of experience in the physics of leptons and to develop precision instrumentation for the study of muons in the TeV region.

We intend to propose a 4π detector to be used at the SSC Laboratory to measure precisely inclusive leptons with a hadron rejection $\frac{\ell\pm}{h} \approx 10^{-6}$ for $P_t > 0.1$ TeV and measure lepton pairs with a mass resolution $\frac{\Delta m}{m} \approx 1\%$. The purpose of this experiment is to search not only for particles predicted by existing theories, such as Higgs, but more importantly to look for new and

unpredicted phenomena, which is the main purpose for the construction of the Superconducting Super Collider.

1.3 Experience

It has taken us nearly twenty-five years to develop the techniques of performing an experiment measuring leptons and lepton pairs with high precision and large solid angle. The graph below is a summary of this learning process.

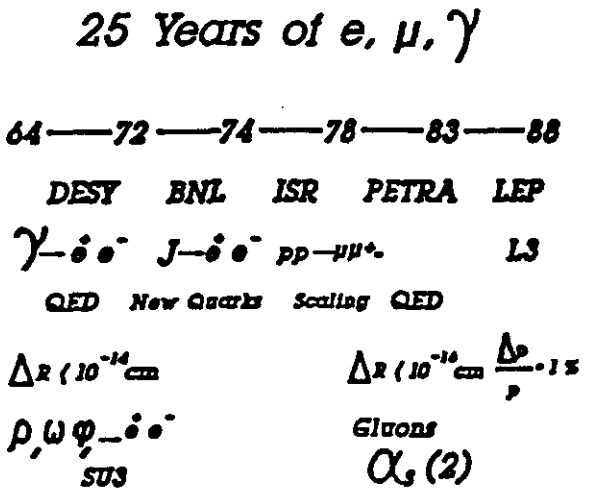

Twenty-five years ago, at DESY, in the process of checking the validity of quantum electrodynamics and studying leptonic decay of vector mesons, we developed techniques to measure leptons in a high intensity photon beam of 10^{11} per second. We obtained a $\frac{ee}{hh} = \frac{1}{10^6}$ rejection and a mass resolution of $\frac{\Delta m}{m} \approx 1\%$.

In the early seventies, at Brookhaven, based on the experience learned at DESY, we designed a spectrometer able to measure lepton pairs in a high intensity proton beam of 10^{12} per second (equivalent to the luminosity of 10^{36} cm^2/sec) with a $\frac{ee}{hh} = \frac{1}{10^{10}}$ rejection and a mass resolution of $\frac{\Delta m}{m} \approx 0.1\%$. This led to the discovery of the J particle.

Subsequently, we designed an experiment at the ISR, CERN, with a 2π solid angle measuring μ pair production with a luminosity between 10^{31} and 10^{32}. This experiment was carried out with the classical method of surrounding intersection regions with a vertex chamber followed by magnetized iron sandwiched with large drift chambers [1.8]. As such, its ability to study inclusive muons was limited because of the limited hadron rejection

ratio, and its ability to search for narrow resonances was limited since the mass resolution was limited to $\frac{\Delta m}{m} \approx 10\%$ due to multiple scattering. This experiment enabled us to measure $pp \rightarrow \mu\mu$ scaling very precisely.

In the late seventies, at PETRA, we built a 4π calorimeter detector [1.9] (MARK J) measuring electrons, muons and hadron jets. This experiment enabled us to measure precisely muon pair assymetry with a systematic error of 1%. The result confirmed the prediction of the Standard Model. The measurement of hadron jets lead to the discovery of gluons.

At LEP, we have built a 4π detector L3 (see Appendix I) which measures a 100 GeV particle decaying into a pair of muons with a mass resolution of 1.4%. L3 also measures electrons and photons with a coordinate resolution of ± 1mm, an energy resolution of 5% at 100 MeV and an energy resolution of 1% at 2 GeV. The hadron calorimeter in L3 measures hadron energy with a resolution of $(55/\sqrt{E}+5)\%$ and $\Delta\Theta = 2.5°$, $\Delta\Phi = 3.5°$ for jets. The L3 vertex chamber was built with a time expansion principle which enables us to measure single particle tracks of 40μm resolution.

The L3 detector described above enables us to obtain good hadron rejection. The momentum of muons is measured twice, first in the vertex chamber with a value of P_v, and second, by the precision muon chambers with a value P_μ. The muon energy loss ΔE is measured by the sampling calorimeter which also monitors large angle photon radiation. The energy balance,

$$P_v = \Delta E + P_\mu$$

enables us to eliminate hadron decays and hadron punch-throughs from muon signals.These properties of L3 make it the only LEP detector adaptable for use at the LEP Hadron Collider (LHC).

Since 1976, Professor U. Becker and his colleagues have conducted a continuous systematic R & D effort to investigate precision instrumentation for muon physics. Appendix II summarizes some of this effort spanning over 10 years, which originated from the first R & D project to build a precision muon detector at ISABELLE. This research effort has covered the following areas :

i) Gas study : selection of the best gas for large area drift chambers in a magnetic field.

ii) Chamber construction : development of methods to build simple high resolution muon chambers which cover areas of a $1000m^2$.

iii) Supporting structure : development of supporting structures for precise alignment of the chambers.

iv) Alignment systems : development of high precision alignment systems with UV laser verification.

This program involved the coordinated efforts of many universities in the United States and of research centers in Spain, The Netherlands, Switzerland and Italy. The success of this program enabled us to build the ISR and PETRA experiments on time and within specifications. The success of this program is one of the main reasons why we have been able to build the ultra precise L3 detector at LEP.

The present R & D proposal therefore represents a natural continuation of the work of this group and will enable new levels of precision to be developed based on the knowledge and experience already obtained.

1.4 Worldwide interest in precision muon physics

The physics potential of precision study of muon at the SSC has attracted not only the L3 collaboration but also many other universities and national laboratories, worldwide. Together, we are forming a collaboration which now has the following members :

a) United States universities : University of Alabama , Boston University, California Institute of Technology, University of California, San Diego, Carnegie-Mellon, Harvard University, Iowa University, John's Hopkins University, Massachusetts Institute of Technology, University of Mississipi, Northeastern University, Princeton University, Purdue University.

b) United States national laboratories : Charles Stark Draper Laboratory, Los Alamos National Laboratory, Oak Ridge National Laboratory, .

c) The Soviet Union national institutes : Dubna, Institute of Theoretical and Experimental Physics (ITEP), Kruchatov Institute, Leningrad, Novossibirsk, Serpukhov, and others.

d) Switzerland : E.T.H. Zurich, University of Geneva, University of Lausanne.

e) Federal Republic of Germany : First Physics Institute, RWTH, Aachen and others.

f) Democratic Republic of Germany : High Energy Physics Institute, Zeuthen, Berlin.

g) Spain : Barcelona University, CIEMAT-Madrid, Santander University, Santiago de Compostela, University of Sevilla, Valencia University.

h) Italy : University of Florence, University of Naples, University of Rome.

i) The Netherlands : National Institute of High Energy Physics, NIKHEF, Amsterdam and Nijmegen.

j) People's Republic of China : Institute of High Energy Physics, Beijing, Chinese University of Science and Technology, Hefei, Shanghai Institute of Ceramics, Shanghai.

k) India : Tata Institute of Fundamental Research, Bombay.

l) Bulgaria : Bulgarian Academy of Sciences, Sofia.

m) Hungary : Central Physics Research Institute, Budapest.

In addition, there are many large national laboratories, industries and research centers which are currently discussing with us the possibility of a joint effort.

1.5 Organization of this proposal

This proposal presents a plan for R & D to include three major areas of effort : chamber construction, gas studies and support structure design to be implemented and carried out concurrently and in close coordination over a period of three to four years. Details are set forth in Chapters 3, 4 and 5, respectively, and include the description and scope of work, time schedules and milestones, as well as estimates of manpower, equipment and budgetary needs. Chapter 6 presents the plan for ensuring these three activities are carefully coordinated. Chapter 7 presents the summary of all activities, milestones, contributions by participating institutes and requests for financial support.

The following Chapter, entitled "Precision measurement of muons at the Superconducting Super Collider", is a perspective view of this R & D proposed program vis-a-vis the unique physics potential of the SSC. It also relates this R & D program to our experience at L3 and to other complementary R & D programs already in progress, such as the Swiss national effort in muon physics (partly included in this document as Appendix III) and the efforts of our other collaborators in the United States, Europe and U.S.S.R. These programs will culminate in a full detector design to be proposed to the SSC. Management at the appropriate time.

References

[1.1] Phys. Rev. Let. 9, (1962) 36.

[1.2] Phys. Rev. Let. 33, (1974) 1404.

[1.3] Phys. Rev. Let. 35, (1975) 1489.

[1.4] Phys. Rev. Let. 39, (1977) 252.

[1.5] Phys. Lett. 126B, (1983) 398.

[1.6] Phys. Lett. 122B, (1983) 103.

[1.7] Mark R. Adams, University of Illinois Preprint.

[1.8] U. Becker et al., NIM 128 (1975), 593.

[1.9] D.P. Barber et al, Phys. Report 63 (7) 333.

Figure Captions

Fig.1.1 **The discovery of the J particle :**
Electron positron spectrum from $p + B_e \rightarrow e^+e^- + X$ at Brookhaven National Laboratory. The spectrum was observed with a detector with a mass resolution of 0.1%. The peak at 3.1 GeV is the first evidence of the J particle.

Fig.1.2 **The discovery of Tau lepton :**
Fig. a) : The correlation of electron and muon momentum from MARK 1 detector at SLAC.
Fig. b) : The production cross-section of τ shows the threshold behavior.

Fig.1.3 **The discovery of Upsilon particle :**
Muon pair spectrum observed at Fermi National Laboratory with a detector having a mass resolution of 2%

Fig.1.4 **The discovery of Z^o particle :**
the spectrum shows a e^+e^- energy correlation from Z^o decay at UA1, CERN.

Fig.1.5 **The discovery of W particle :**
The discovery of W^{+-} particle was done by the UA1 group at CERN by measuring the large transfer momentum $\mu^+\mu^-$ from W decays.

Fig.1.6 The Upsilon spectrum as observed at Fermi National Laboratory with a precision muon pair spectrometer. The graph comes from a preprint by Mark R. Adams, University of Illinois, Chicago.

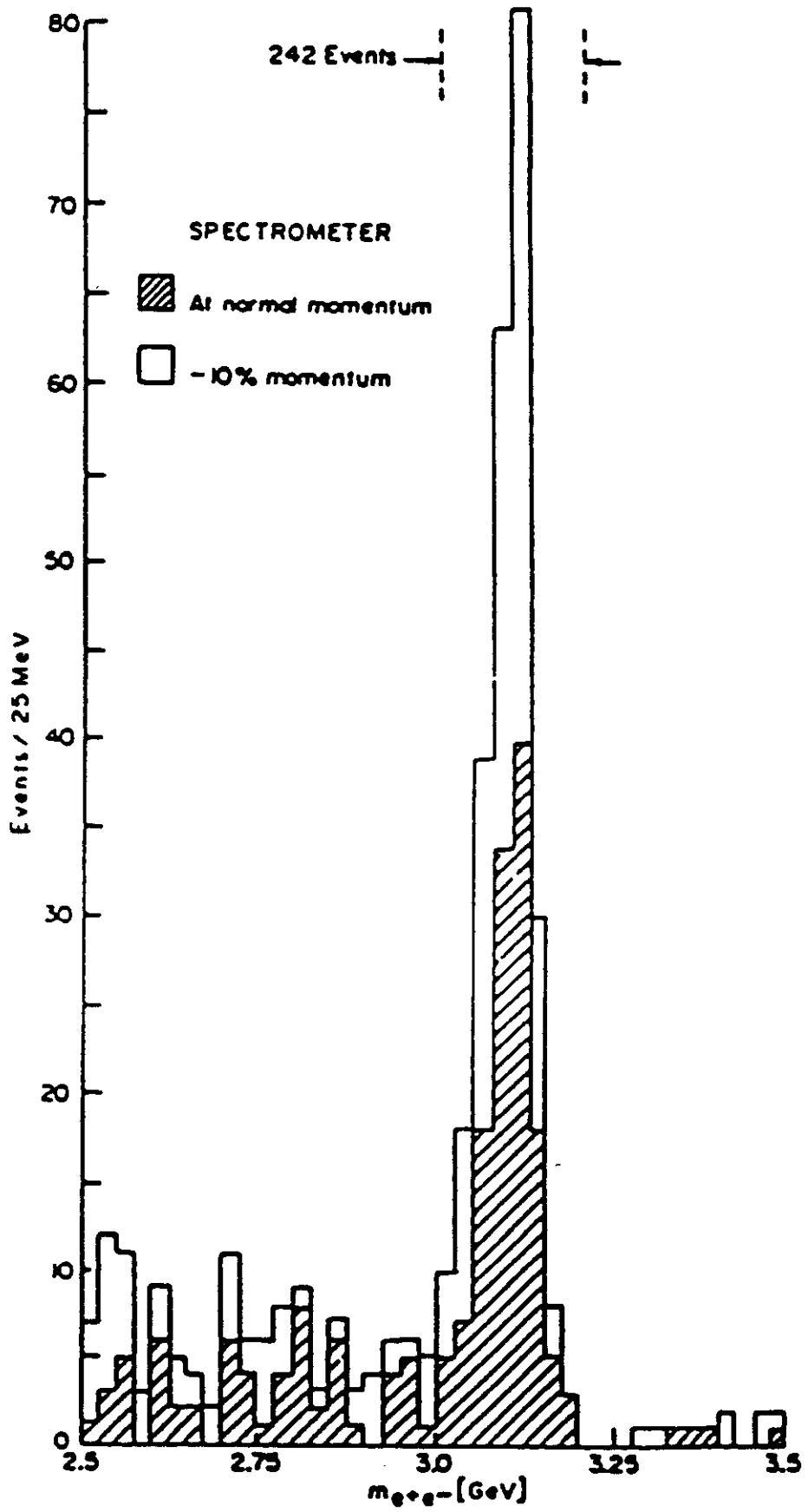
242 Events
SPECTROMETER
At normal momentum
-10% momentum
Events / 25 MeV
0
10
20
30
40
50
60
70
80
2.5
2.75
3.0
3.25
3.5
$m_{e^+e^-}$ [GeV]

Fig. 1.1

a)

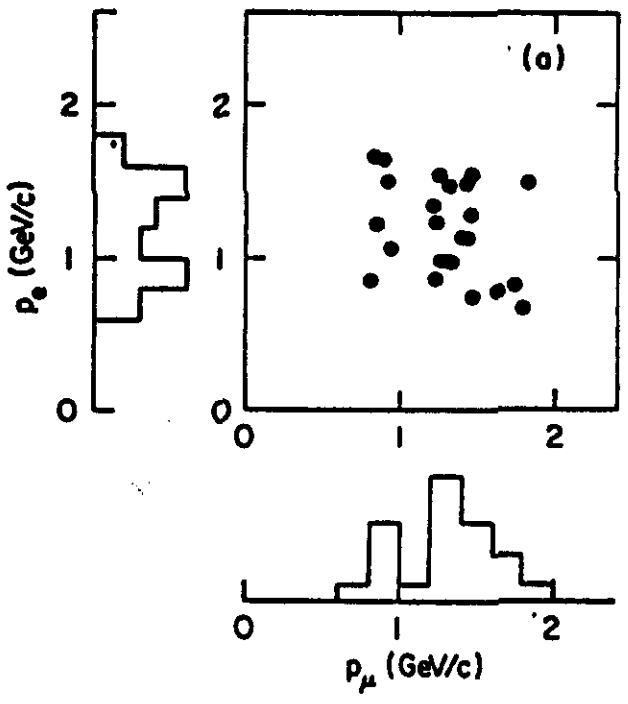
(a)
p_e (GeV/c)
p_μ (GeV/c)
0
1
2

b)

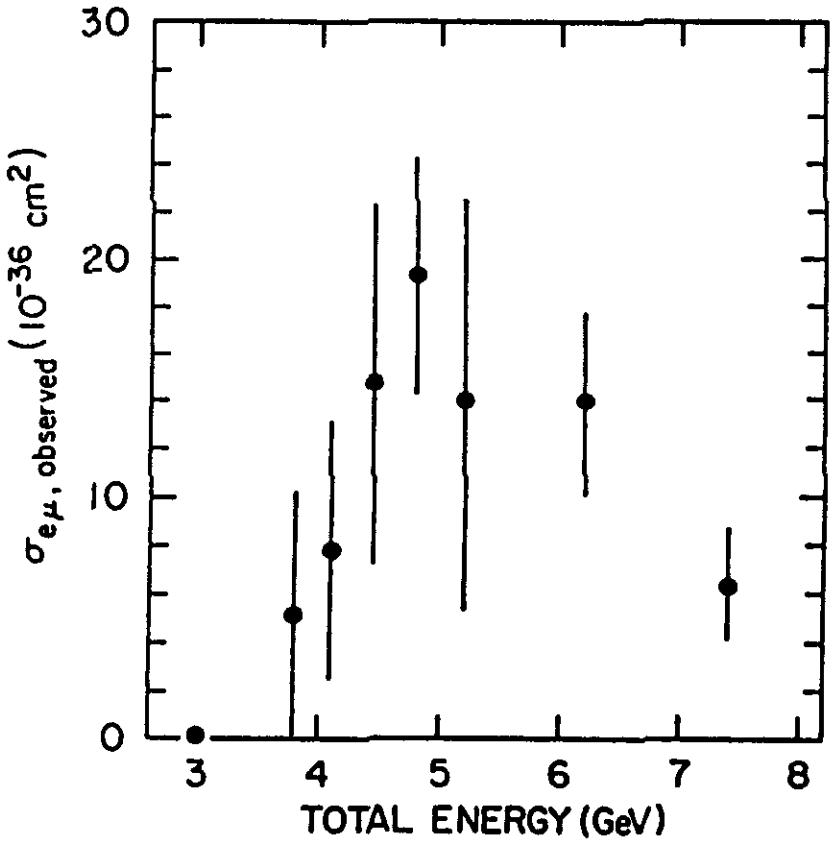
$\sigma_{e\mu,\ observed}$ (10^{-36} cm^2)
TOTAL ENERGY (GeV)
0
10
20
30
3
4
5
6
7
8

Fig. 1.2

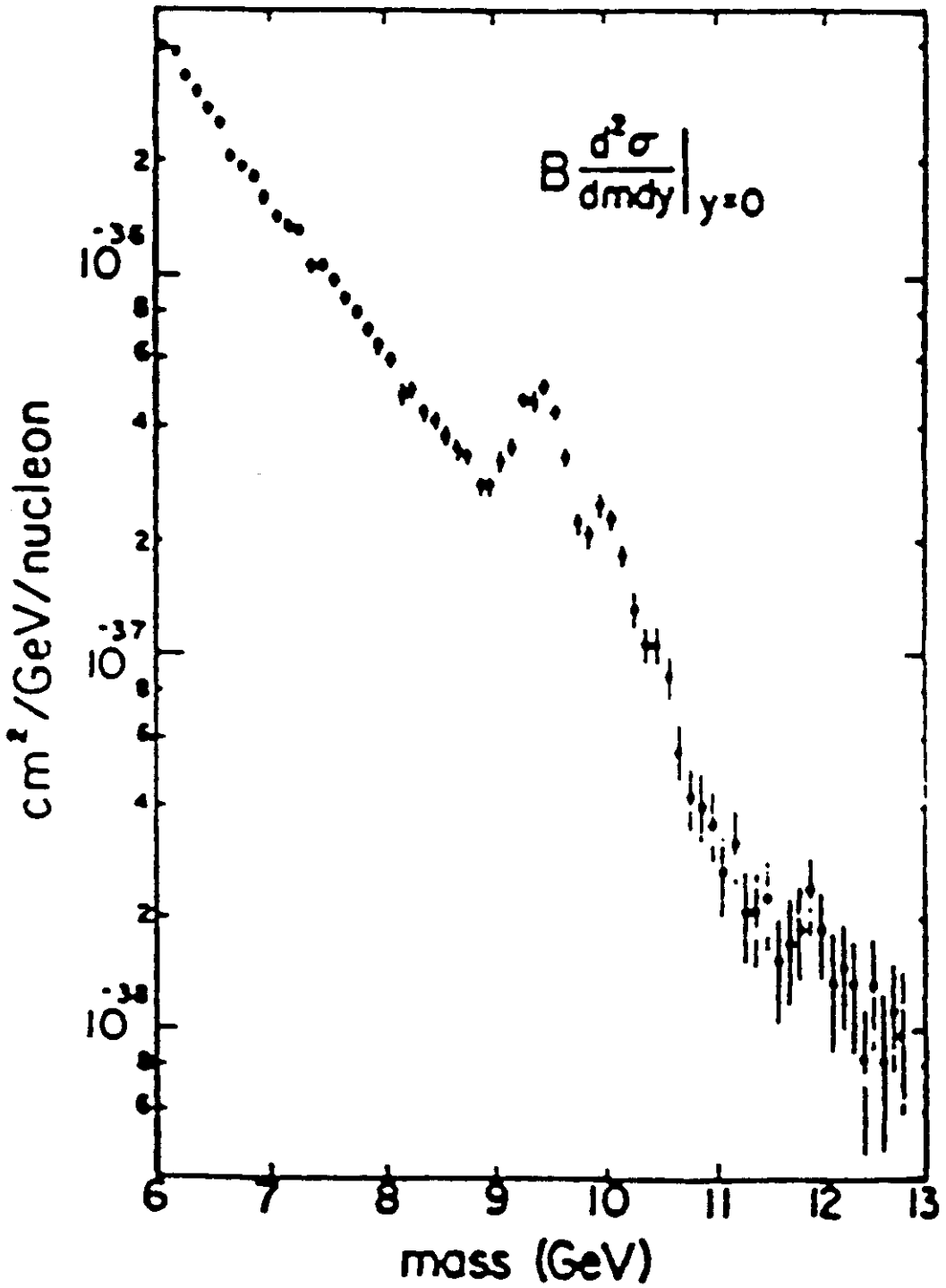
$B \frac{d^2\sigma}{dm\,dy}\Big|_{y=0}$
cm²/GeV/nucleon
mass (GeV)
6
7
8
9
10
11
12
13

Fig. 1.3

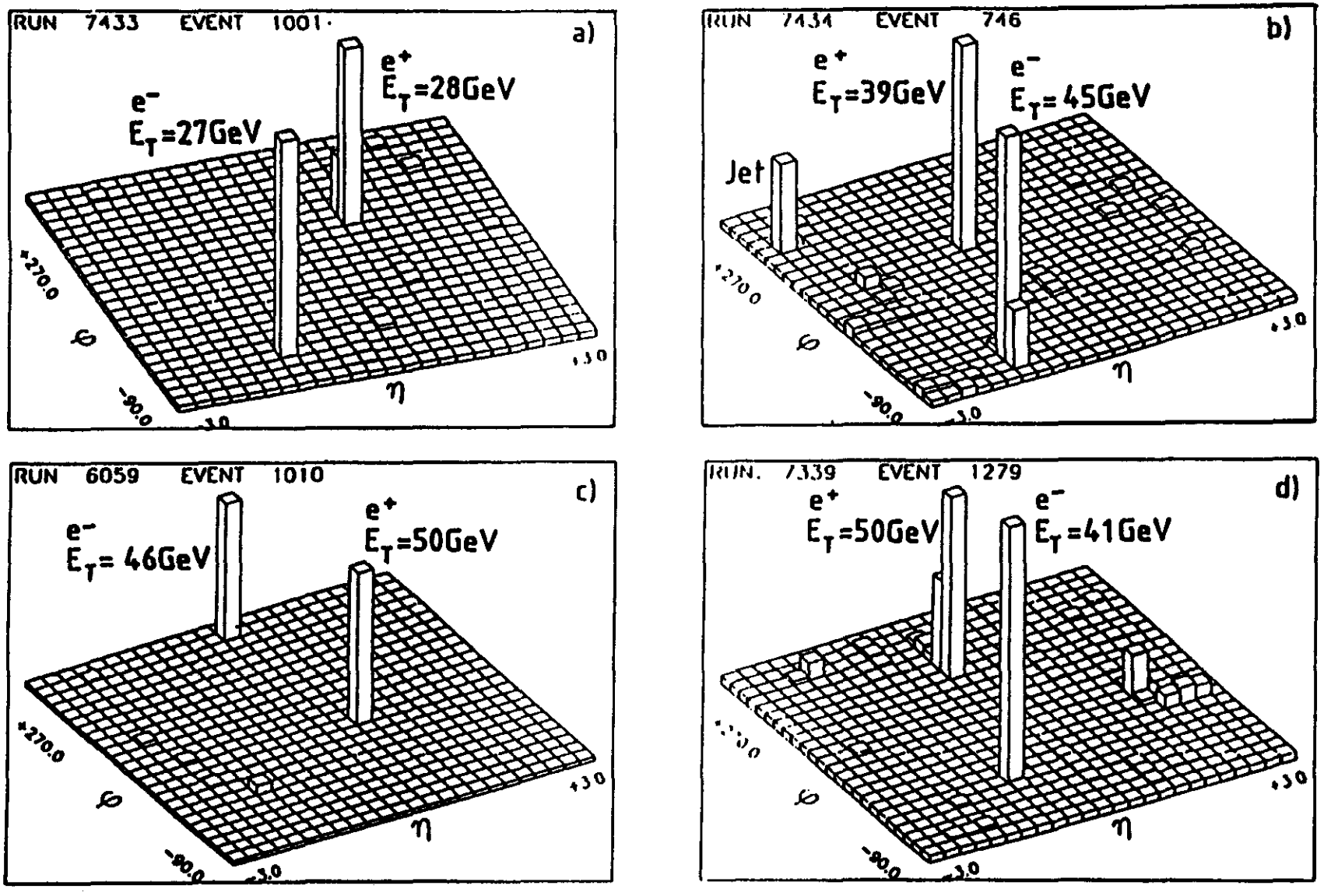
RUN 7433 EVENT 1001
a)
e⁻
E_T=27GeV
e⁺
E_T=28GeV
+270.0
φ
-90.0
η
RUN 7434 EVENT 746
b)
e⁺
E_T=39GeV
e⁻
E_T=45GeV
Jet
+270.0
φ
-90.0
η
RUN 6059 EVENT 1010
c)
e⁻
E_T= 46GeV
e⁺
E_T=50GeV
+270.0
φ
-90.0
η
RUN. 7339 EVENT 1279
d)
e⁺
E_T=50GeV
e⁻
E_T=41GeV
φ
η

Fig. 1.4

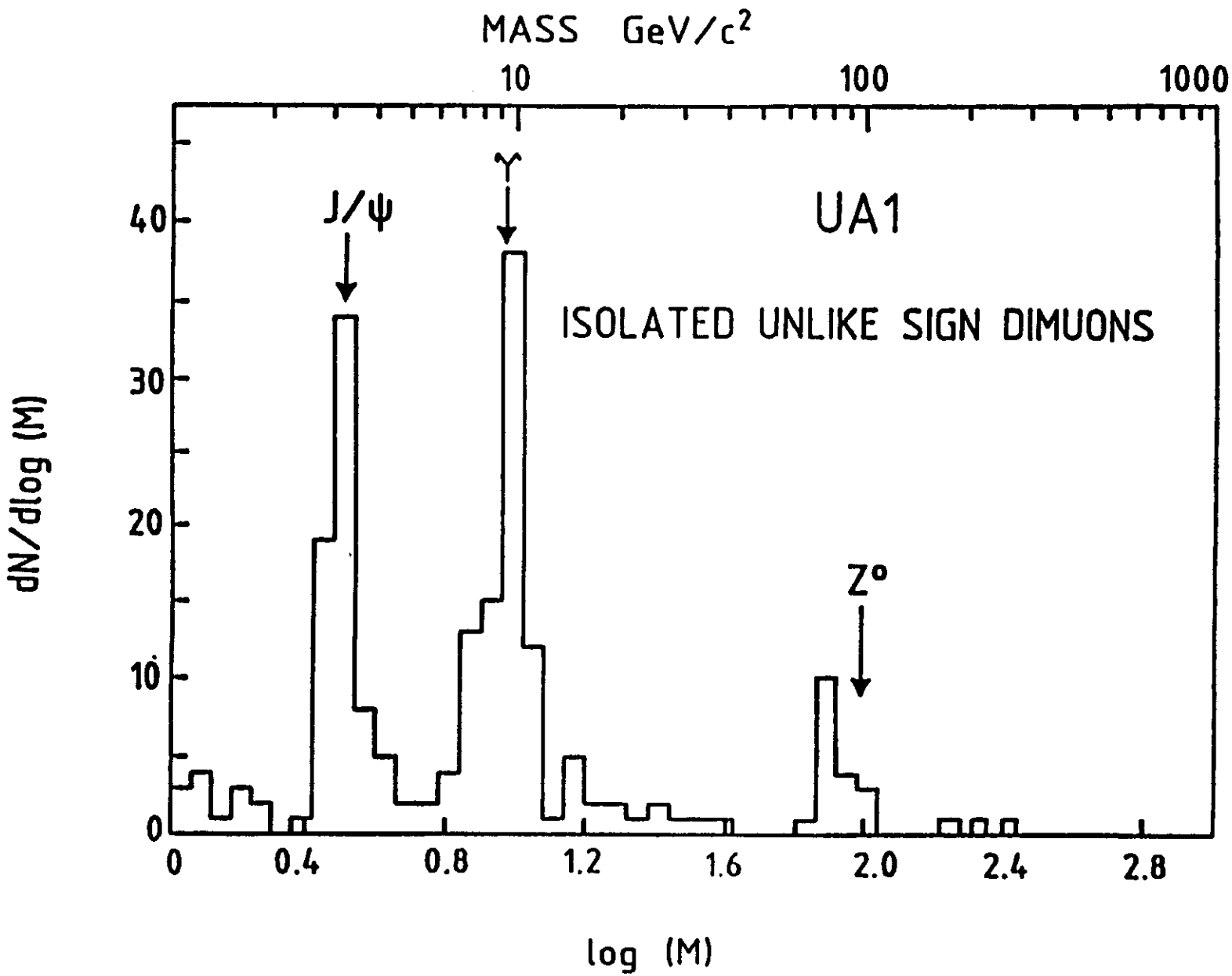
MASS GeV/c²
10
100
1000
J/ψ
ϒ
UA1
ISOLATED UNLIKE SIGN DIMUONS
Z°
dN/dlog (M)
40
30
20
10
0
0
0.4
0.8
1.2
1.6
2.0
2.4
2.8
log (M)

Fig. 1.5

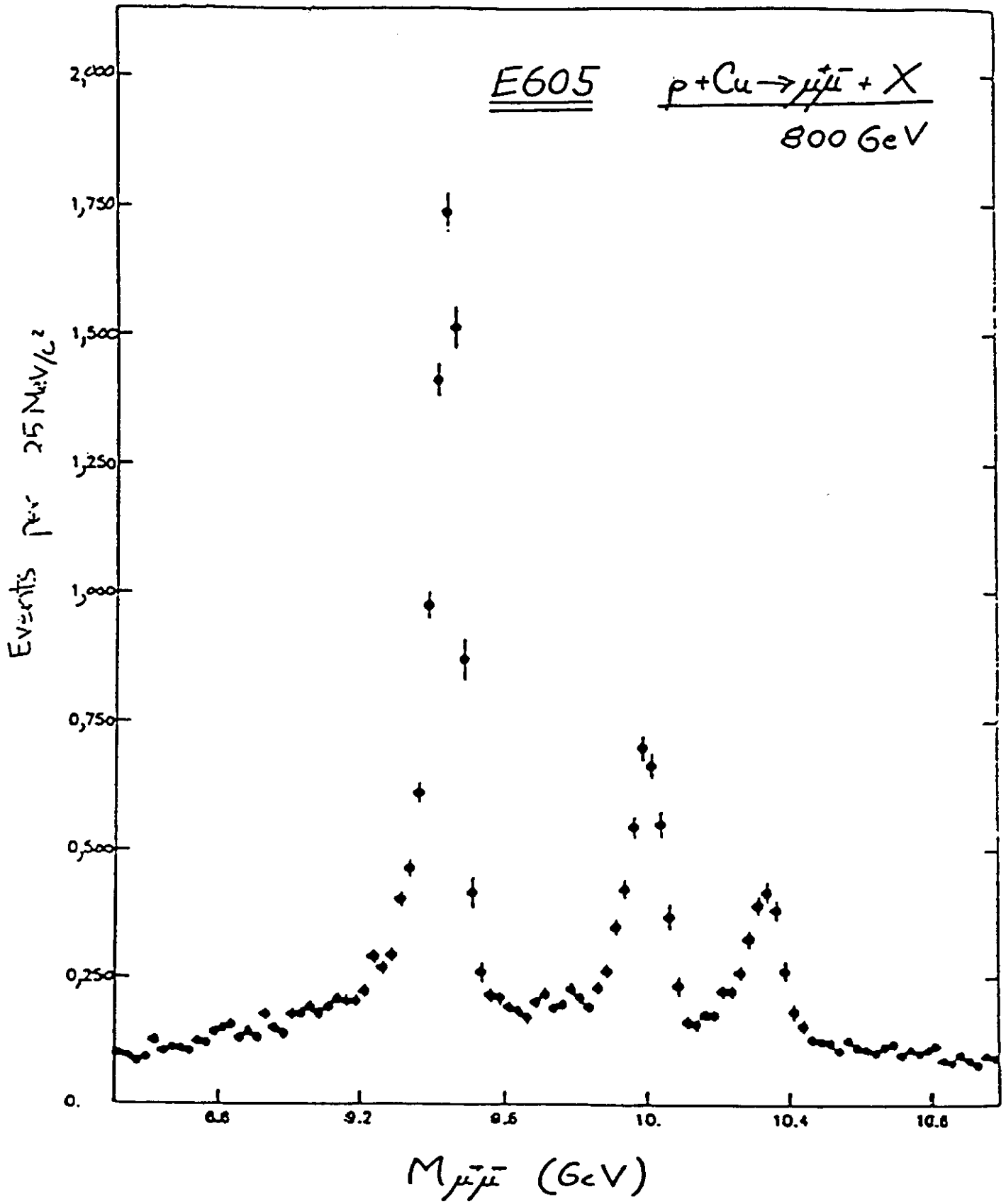
E605
p+Cu→μ+μ⁻+X
800 GeV
2,000
1,750
1,500
1,250
1,000
0,750
0,500
0,250
0.
Events per 25 MeV/c²
8.8
9.2
9.6
10.
10.4
10.8
Mμ⁺μ⁻ (GeV)

Fig. 1.6

CHAPTER II

PRECISION MEASUREMENT OF MUONS AT THE SUPERCONDUCTING SUPER COLLIDER

2.1 Introduction

The most important property of the SSC is that it provides both high energy (40 TeV) and high intensity (luminosity $10^{33}/cm^2$ sec). This feature provides a unique opportunity to search for rare and unexpected phenomena. However, in order to be able to use the SSC, it is important to realize that at 40 TeV, the pp total cross-section will be 100 mb and there are

$$10^{33}/cm^2 \text{ sec} \times 100 \times 10^{-27} cm^2 = 10^8 \text{ interactions per second.}$$

Each interaction produces about 100 hadrons. Therefore we must cope with 10^{10} hadrons per second. This rate makes it exceedingly difficult to study the details of hadron production at the SSC. Consequently, the detection of muons is the most reliable way to search for new phenomena at the SSC.

There are two ways of measuring muons :

a) **First method** : <u>the conventional way</u> is the iron ball where the intersection region is surrounded with a vertex chamber followed by magnetized iron absorber sandwiched with drift chambers as drawn below.

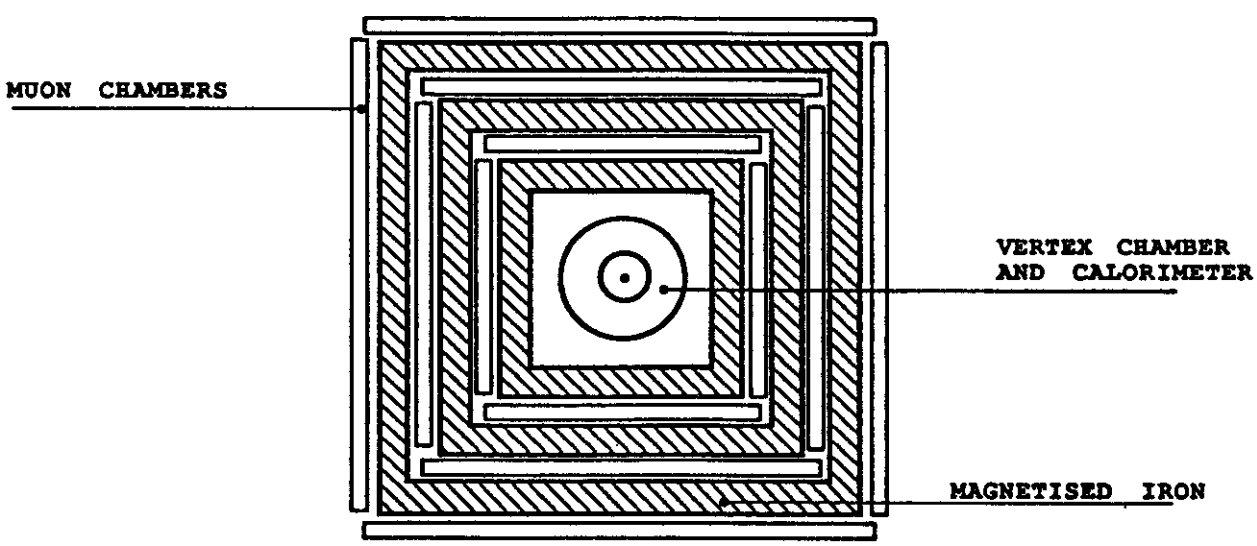

Indeed, this is exactly what we did at I.S.R., CERN and PETRA for many years. These types of experiments have the following characteristics :

i) Since multiple scattering in the iron ($\Delta\Theta$) behaves like $\frac{1}{p}$ in the same way as the bending Θ of muons :

$$\Delta\Theta = \frac{0.015}{p}\sqrt{\frac{\ell}{\ell_o}}$$

$$\Theta = 0.3\,\frac{B\ell}{p}$$

$$\frac{\Delta p}{p} = \frac{\Delta\Theta}{\Theta} = 0.22\,\frac{1}{\sqrt{\ell}} \text{ for iron}$$

therefore, the resolution improves very slowly with the length $\sqrt{\ell}$ and it is independent of muon momentum. Ultimately the resolution of the chambers sandwiched in the iron and the ability to align the chamber system in the iron limit the resolution. In practice, the $\frac{\Delta p}{p}$ has a limit of 10% to 15%.

ii) This method measures the muon momentum only in magnetized iron; therefore the hadron decay background, hadron punch-through and particularly large angle photon emission are difficult to eliminate. In practice our experience at the ISR shows that it is very difficult to study inclusive muons at a luminosity above $10^{32}/cm^2$ sec.

b) **Second method : <u>the precise way</u>**

The best way to study muon physics is to track muons continuously from their production at the intersection point, by roughly measuring the momentum within the vertex chamber, by tracking muon behavior with a fine grain sampling calorimeter absorber and by measuring precisely the muon momentum in a large free space. This principle was adopted by the L3 experiment where one has been able to obtain a mass resolution at Z° of $\frac{\Delta m}{m} = 1.4\%$. It is important to note the following :

i) The muon momentum $P\mu$ is measured very precisely in a large free space of 2.9m with three layers of ultra-precise drift chambers. Each chamber measures the coordinate to 50μm and angle to 1-2 mrads. There are a total of 80 chambers. These chambers are supported by a supporting structure which is aligned and monitored to an accuracy of 30μm.

ii) The fine grain of the sampling in the hadron calorimeter enables us to follow the energy loss for muons as well as the emission of large angle photons, as shown in Figs.2.1 and 2.2.

Figs.2.3 and 2.4 illustrate a conceptual design of an SSC detector layout to measure muon pairs with mass resolution of 1.5% for a 1 TeV particle decaying into a muon pair, in the angle region $\Theta > 15°$. These designs are an extension of the L3 experience and have the following properties :

i) Since the resolution on $P\mu$ improves as $\frac{1}{B\ell^2}$, the most effective way to obtain good resolution is to have a large magnet providing long free space ℓ. In Fig.2.3 and Fig.2.4, we have shown a design with B = 7.5 KGauss and ℓ (max.) = 9.5m and ℓ (for muon measurement) = 5.25m.

ii) Muon momentum ($P\mu$) is measured precisely in a free space ℓ by 3 layers of large area drift chambers with precision supporting structures, precision alignment and monitor systems. There are 16 chambers in each layer. In the first and last layers, each chamber has 32 signal wires. In the middle layer, each chamber has 64 wires.

iii) The fine sampling calorimeter absorber measures the energy loss of muons (ΔE) and the emission of large angle photons.

iv) A vertex chamber surrounding the intersection region, the muon momentum (p_v) is first measured to a $\frac{\Delta p}{p} \approx 50\%$. The energy balance

$$P_v = \Delta E + P\mu$$

enables us to eliminate hadron decays and hadron punch-throughs from muon signals.

The table hereafter is a comparison between the L3 and SSC muon detectors.

Comparison between the L3 and the SSC Muon Detectors

	L3	SSC
Magnet		
- BL^2 for entire magnet	180 KGauss-m^2	677 KGauss-m^2
- BL^2 for muon detecting volume	42 KGauss-m^2	207 KGauss-m^2
Muon Chambers		
- Volume (LxWxH)	5.5x2.25x0.4=5m^3	6.7x3.3x0.5=11m^3
- Maximum area (LxW)	5.6x2.25=12.6m^2	6.7x3.3=22m^2
- Total wires in central region	250,000	1,500,000
- Wire plane height/signal wires	0.5m/24	0.9m/64
- Number of chambers	80	160
Gas		
- Volume	250m^3	2250m^3
- Resolution from gas	250μm	150-200μm
- Flammability classification	flammable	nonflammable
Mechanical Support		
- Maximum unsupported length	5.8m	13.5m
- Complete mechanical stability	2.5m	5.0m
- Module weight	6 tons	10 tons
Alignment		
- Wires within a module	30μm over 3m	20μm over 9m
- Wires to the intersection region	± 2mm at 4m	± 1mm at 6.5m
Years of R & D		
- Z chambers	1975-1982	1990-1992
- P chambers	1978-1983	1990-1992

The purpose of this proposal is to investigate and to solve some of the practical problems associated with precision measurement of muons in a large free space provided by the magnet.

2.2 Plans for research and development for a complete detector

We have started a worldwide comprehensive research and development program to design a precision muon detector to measure the reaction

$$p + p \rightarrow T + X$$

$$T \rightarrow \mu^+\mu^-$$

$$\frac{\Delta M}{M} \approx 1\%$$

Our efforts can be summarized as follows :

i) The magnet R & D effort will be provided by a national effort from Soviet Union.

ii) The high rate vertex chamber R & D program will be carried out by a joint U.S.S.R and United States effort.

iii) The calorimeter R & D effort will be carried out by U.S.S.R, Germany and the United States.

iv) The muon system R & D effort to measure muon momentum will be a collaboration between participants of this proposal and a Swiss national effort, supported by K.W.F., Switzerland (Swiss Commission for the Promotion of Applied Scientific Research). The muon system R & D effort to measure muon production angle will be carried out by a Spanish national team currently being organized.

The principle of accuracy of measuring Pμ is shown in the drawing below where ℓ is the maximum free space inside of which three layers of drift chambers with wires N1, N2 = 2N1, N1, each providing an individual resolution σ, and enables us to measure precisely sagitta s.

Principle of Accuracy

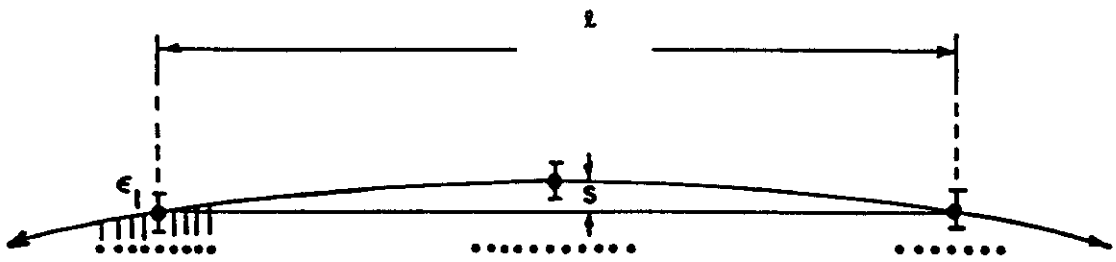

N1 wires	N2	N1
$\varepsilon_1 = \frac{\sigma}{\sqrt{N1}}$	ε_2	$\varepsilon_3 = \varepsilon_1$

$$\Delta s = (\varepsilon_{1/2}^2 + \varepsilon_2^2)^{1/2}$$

$$s = \frac{\theta \ell}{8} = \frac{0.03}{8} \frac{B\ell^2}{Pt}$$

$$\frac{\Delta Pt}{Pt} = \frac{\Delta s}{s} = 267\sigma \left(\frac{1}{2N1} + \frac{1}{N2}\right)^{1/2} \cdot \frac{Pt(GeV)}{B\ell^2(m)}$$

The following examples illustrate the close relation between the various parameters N1, N2, N3, ℓ and σ in determining the resolution and the need to understand the practical limit of these parameters, in order to have a $\frac{\Delta m}{m}$ = 1.5% for a 1 TeV particle with muon-hadron decaying into a pair of muons :

σ	N1	N2	N3	ℓ
150	32	64	32	5.25
200	60	120	60	5.25
200	32	64	32	6.0

Since the resolution $P\mu$ improves as $\frac{1}{\ell^2}$, the best way to improve it is to build a large magnet. Since in reality the size of the magnet is limited by mechanical and economical reasons, a moderately increased field from 5 to 7.5 KGauss is also necessary to improve the resolution. These facts imply the necessity of carrying out research and developments activities as follows :

(1) The technology to construct larger chambers, each with a larger number of wires (N1 and N2), with high resolution σ. This is the main R & D effort outlined in Chapter 3.

(2) Selecting a suitable gas with a volume of 2 000 cubic meters which would operate at higher magnetic field and be nonflammable. This the main R & D effort outlined in Chapter 4.

(3) Designing a support structure for the muon chambers to cover a volume of 10000 m^3 ($0.35 \times 10^6 ft^3$). This is the main R & D effort outlined in Chapter 5.

(4) Designing the alignment system for the muon detector. This effort will be carried out by the Swiss universities and industry.

(5) Designing and constructing new electronics with better time resolution to match the space resolution σ. This effort will be provided by the Swiss universities and industry (see Appendix III).

(6) As seen in the table below which gives a first order comparison between the L3 and the SSC muon detector on cables, wires and connectors, it is necessary to select an effective optical fiber system to transmit the signals from the chambers to the control room. This effort will be provided by the Swiss universities and industry (see Appendix III).

Muon Spectrometer Data Transfer

	L3		SSC	
Wires	250000		1500000	
Cables	8000		50000	
Connectors	25000		150000	
Wire length	6000	km	80000	km
Cable length	160	km	4000	km

(7) At the SSC, it is important to measure muons down to a very forward region $15° > \theta > 5°$. There are many designs of a magnet system, with field perpendicular to the muon trajectory in this region. A final design will be chosen after prototype studies are completed by our Soviet collaborators in Moscow. The chambers and supporting structures for this region may be different and will be the subject of R & D effort at a later time.

Figure Captions

Fig.2.1 A $Z^\circ \rightarrow \mu^+\mu^-$ decay in L3, recorded in August 1989 at LEP, shown in the side, or non bending view. A 3 GeV photon, emitted into the lower BGO barrel is clearly visible.

Fig.2.2 The same $Z^\circ \rightarrow \mu^+\mu^-$ event, front view. The muon momenta are 40 and 44 GeV. Data from the hadron calorimeter proved the particles to be minimum ionizing.

Fig.2.3 A conceptual design of an SSC detector layout to measure muon pairs with mass resolution of 1.5% for a 1 TeV particle decaying into a muon pair, in the angle region $\theta > 15°$. The region $15° > \theta > 5°$ may request different magnet and chamber configuration.

Fig.2.4 Sectional view of of Fig.2.3.

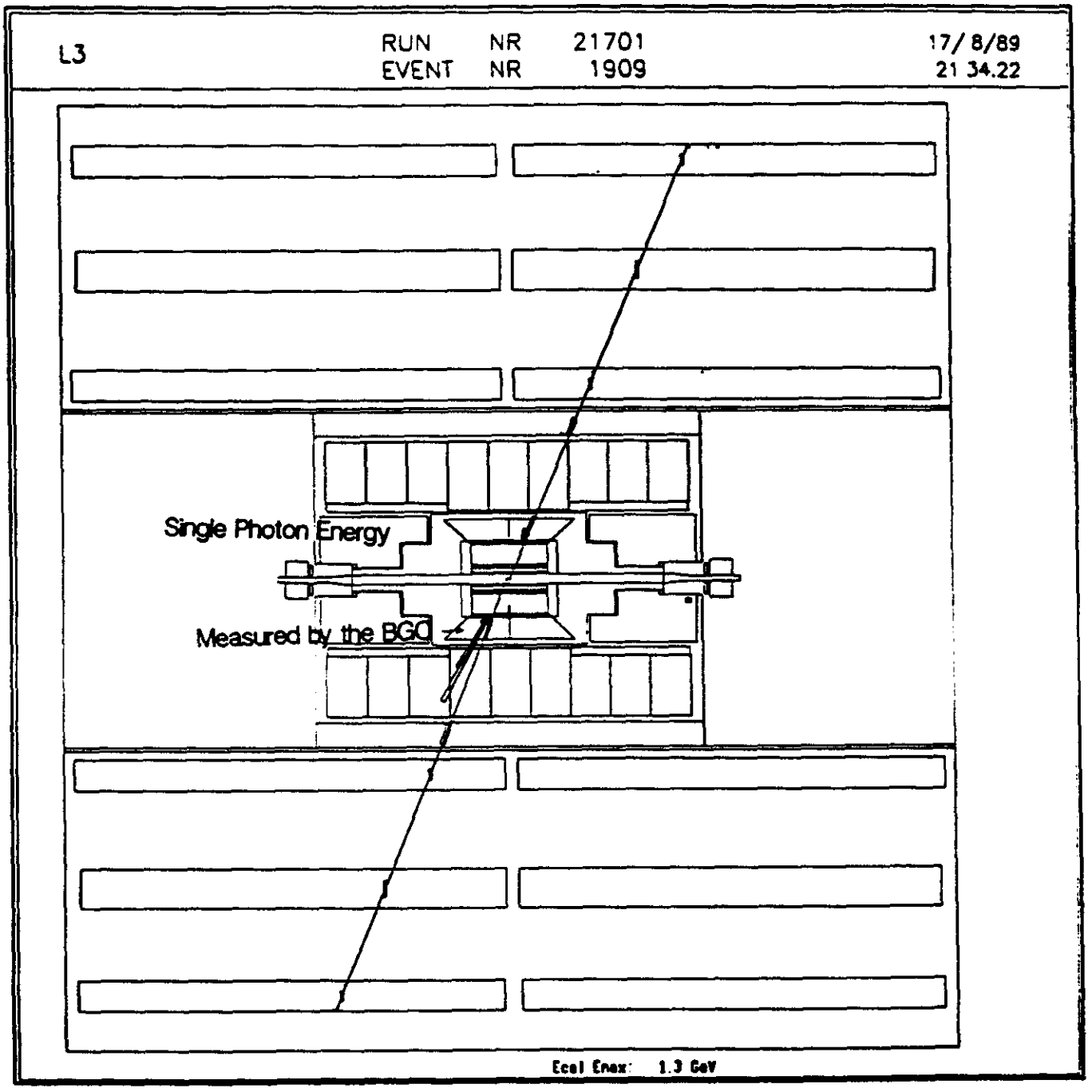
L3
RUN NR 21701
EVENT NR 1909
17/ 8/89
21 34.22
Single Photon Energy
Measured by the BGO
Ecal Emax: 1.3 GeV

FIG.2.1

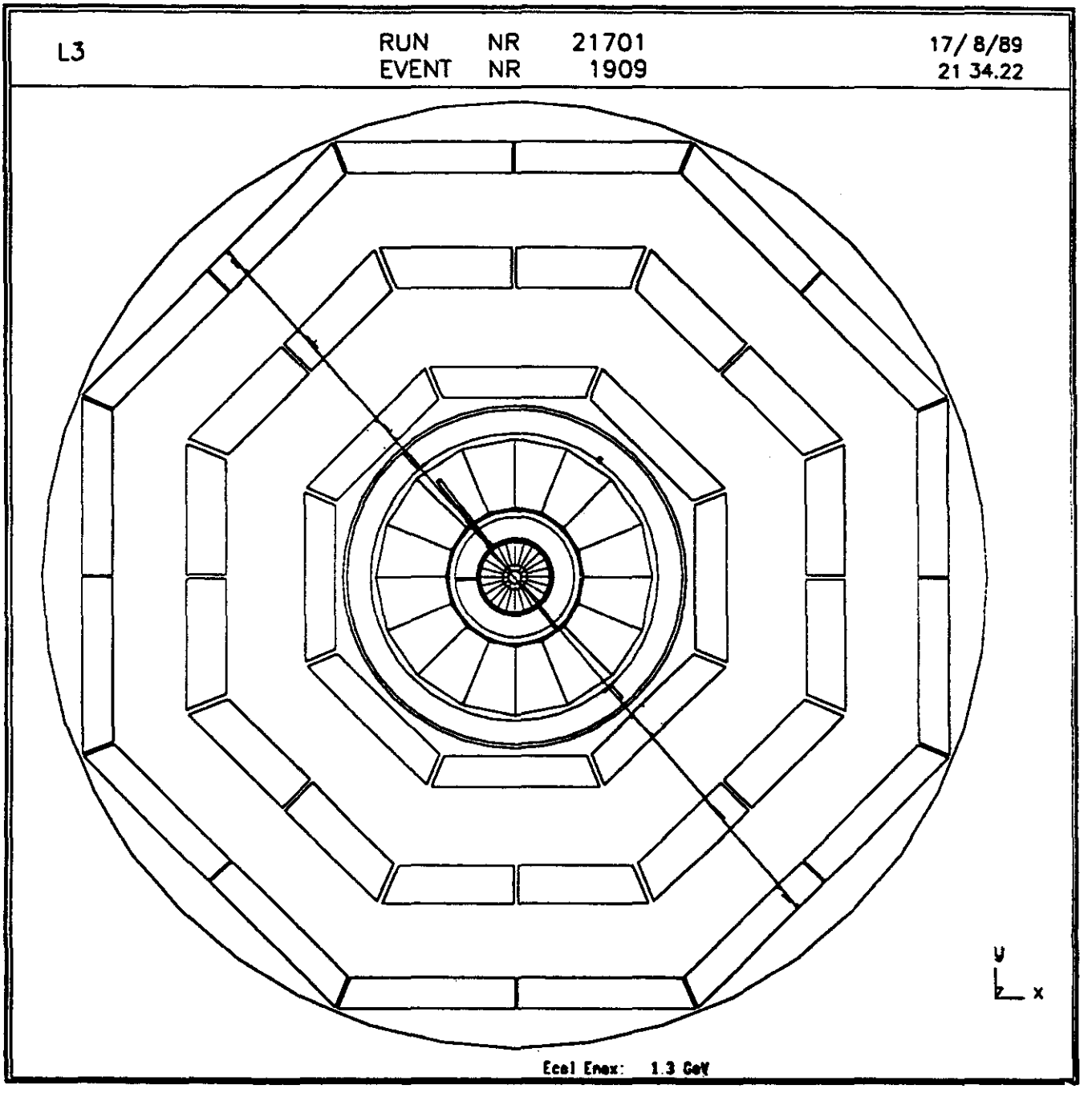

FIG.2.2

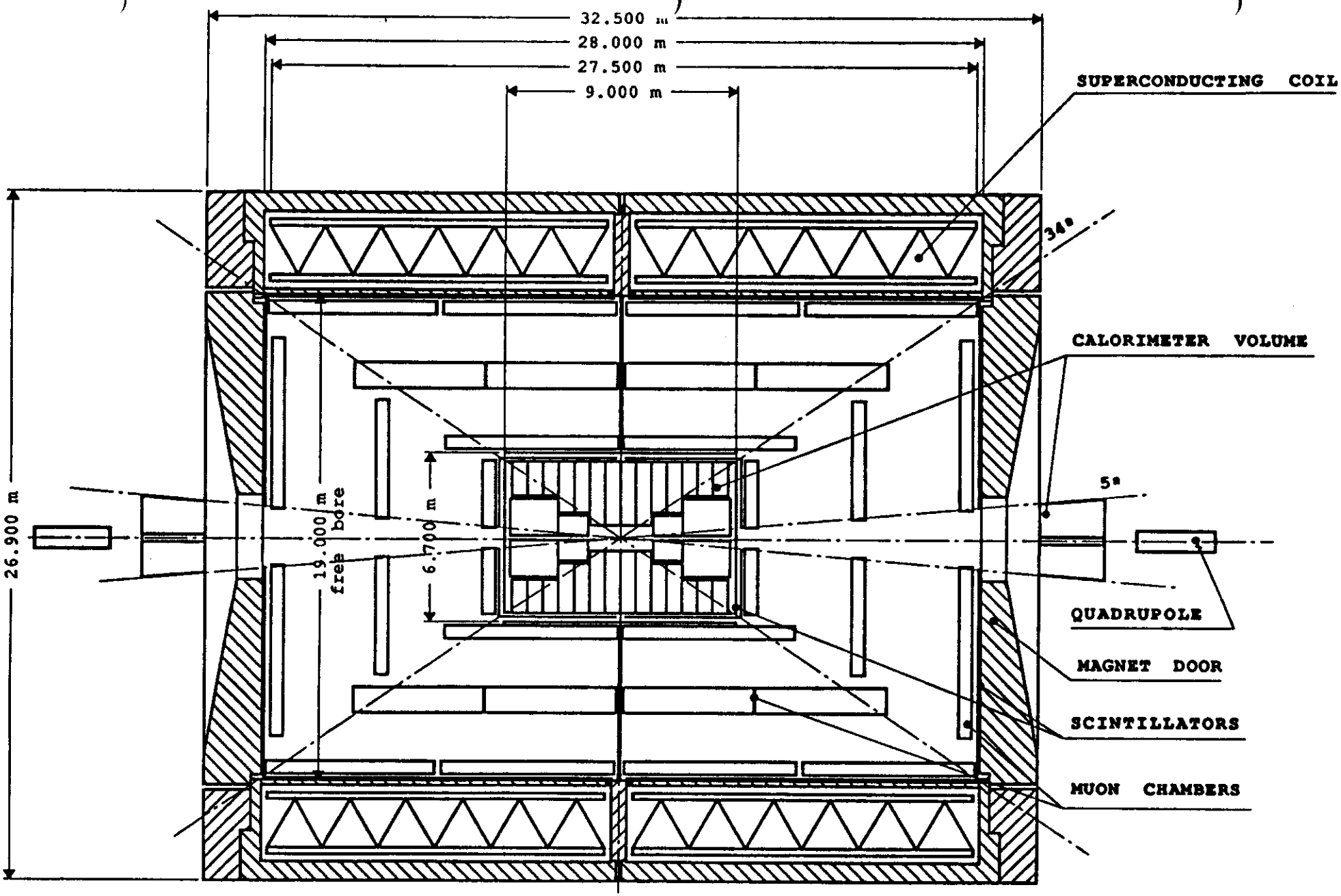

DETECTOR LAYOUT

Scale 1:200
18 September 1989

FIG. 2.3

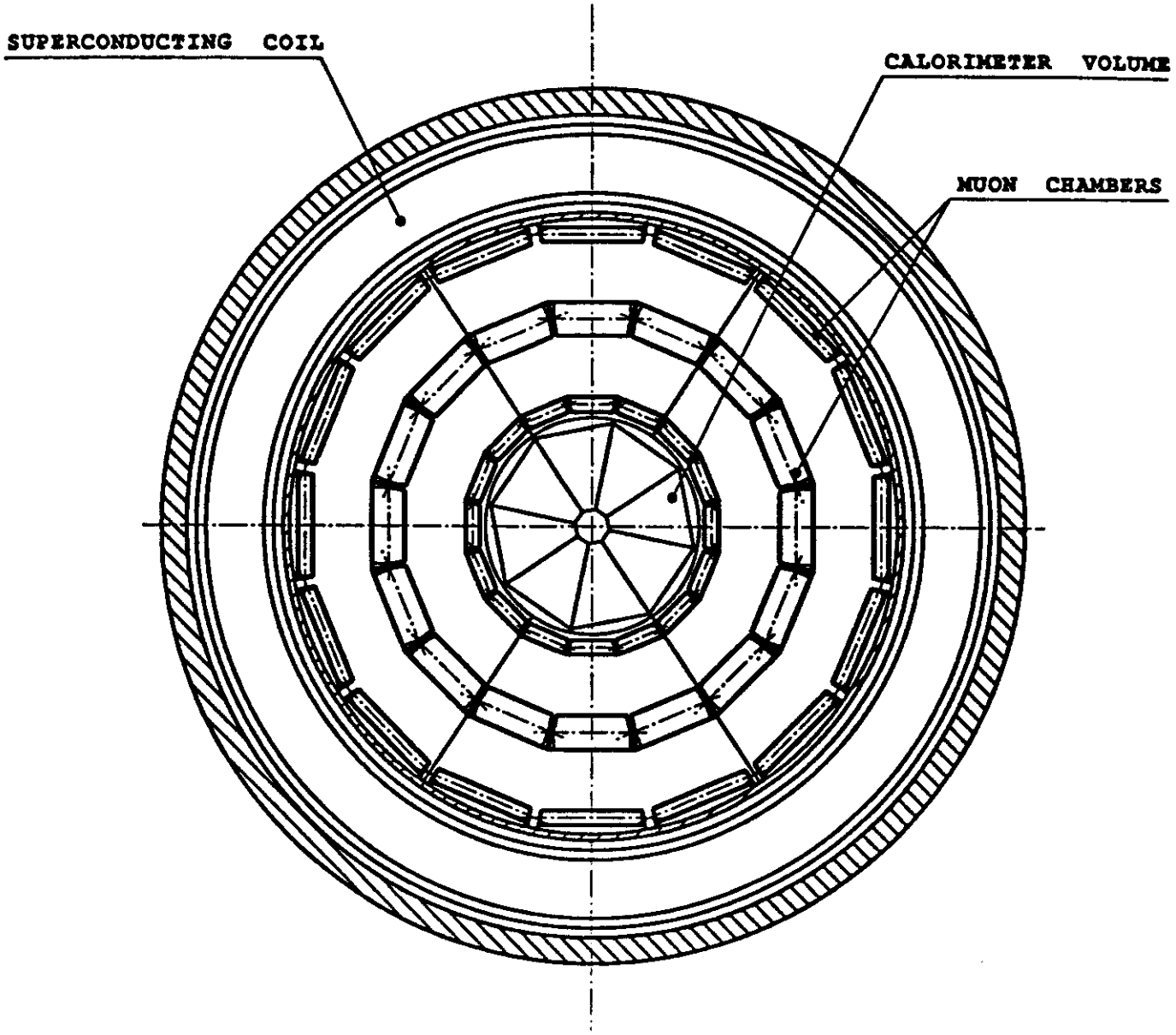

CROSS SECTION

DETECTOR LAYOUT

SUPERCONDUCTING VERSION

0.75 Tesla

Scale 1:200
19 SEPTEMBER 1989

FIG. 2.4

CHAPTER III

RESEARCH AND DEVELOPMENT FOR MUON CHAMBERS AT THE SUPERCONDUCTING SUPER COLLIDER

I. Brock, A. Engler, T. Fergusen, H. Vogel,
Carnegie Mellon University, Pittsburgh, PA
H. Akbari, J.Z. Bao, C. Spartlotis
John's Hopkins University, Baltimore, MD
P. Berges, R. Clare, T.S. Dai, M. Fukushima, Q. Li, M. White
Massachusetts Institute of Technology, Cambridge, MA
D. Kuban, F. Plasil, M. Rennich, G. Young
Oak Ridge National Laboratory, Oak Ridge, TN
P. Denes, P. Piroué, D. Stickland
Princeton University, Princeton, NJ
A. Bujak, T. McMahon, B. Stringfellow
Purdue University, Lafayette, IN

Contact Person: M. White

The goal of this R & D project is to design large precision muon chambers for the SSC, and to establish a model for SSC muon chamber production. The chamber should provide good resolution, be able to be aligned to ± 20μm tolerances, be optimized for high reliability, and be suitable for mass production.

3.1 Need for research and development

In our experience at L3, we have been successful in designing and constructing a muon detector which is unique in its ability to detect dimuons with 1.4% mass resolution at the Z° mass. The critical feature, that of detecting straight (infinite momentum) tracks with < 30μm error, has been achieved in all production modules. However, drift chamber detectors which can accurately measure muons in the few hundred GeV region will still require substantial research and development. Although the main features of an SSC precision muon detector, such as the one shown in Figs.2.3 and 2.4, will be similar to L3, the increased size and degree of complexity cannot be reached by simple extrapolation from our present system. Nevertheless, much of the

experience gained at L3 can be applied to our approach in developing a more precise muon detector suitable for the SSC.

The higher energies at SSC will produce higher momentum muons than LEP. The design resolution of $\Delta m/m = 1.5\%$ at 1 TeV leads to increased demands on the intrinsic alignment and measuring accuracy of the system.

The sagitta of a 0.5 TeV muon traversing the 0.75 Tesla field of a possible detector with L=5.25m (see Figs.2.3 and 2.4) is:

$$s[mm] = BL^2/8x0.033P\ [GeV/KGaussm^2] = 1.57\ mm$$

To optimize the use of the magnet's analyzing power, one possible wire plane configuration would be to group the wires into three layers, similar to what was done at L3. This concept is illustrated in Fig.3.1 which also shows the number of wires sampling a track in each chamber. If the single wire resolution in a chamber is 150μm, we would measure the center of gravity to within

$$\varepsilon_1 = \varepsilon_3 = 150\mu m/\sqrt{0.94*32} = 27\mu m \text{ and}$$
$$\varepsilon_2 = 150\mu m/\sqrt{0.94*64} = 19\mu m$$

using 94% of the wires in each chamber. The mass resolution is then given by:

$$\Delta m/m = 1/\sqrt{2}\Delta s/s = \sqrt{(27^2/2+19^2+\Delta S^2_{sys})}/\sqrt{2}x1570 = 1.5\%$$

where ΔS^2_{sys} represents all other systematic errors. These errors must be kept below 20μm in order to achieve the design resolution, as is shown above.

To continue our work in precision muon physics instrumentation as it applies to SSC physics, we consider in depth studies on the following inter-related components to be essential :

a) Chamber construction R & D with particular attention to achieving a single wire resolution of between 150μm and 200μm in these larger volume SSC chambers. Structural analyses and stability studies must be carried out and understood for all major chamber parts due to the larger size. This chapter will address the issues concerning chamber construction with particular

emphasis on structure, wire alignment, drift cell optimization, and production of test modules.

b) Gas studies in order to identify a cool, nonexplosive gas. Determining the correct gas is critically important for reasons of safety, better chamber resolution, higher magnetic field, and chamber aging. This subject will be addressed in Chapter 4.

c) System R & D will be necessary to design structures and new alignment methods, since systematic errors for the entire muon detector must now be kept below 20μm rather than 30μm in L3. Likewise, a scheme to calibrate such a system must be devised. This area will be the subject of Chapter 5.

3.2 Chamber structure

1) Principles of chamber design

The SSC muon detector volume is about ten times the L3 volume. The number of chambers to be produced and their dimensions have increased and the system is generally more complicated. The SSC multisampling chambers will require a greater quantity of wires than in L3 to obtain the desired centroid accuracy in each track segment and thus to have a good resolution at high energies. This implies that relative wire positions must be known to very high precisions (systematic errors $\leq$ 20μm). SSC chambers must also perform well in high rate environments.

The following items must be integrated into the total chamber design:

alignment systems
survey references
electronics
a calibration scheme for the chamber
gas seals
connectors for gas, signals, HV, and calibration
feedthrus for gas, signals, HV, and cables
cable supports
chamber supports
actuators
wire plane and foil attachments
transport and handling provisions

Active Θ measuring covers are the research efforts of our European and Soviet collaborators.

The size and complexity of a final SSC muon detector configuration practically precludes the dismantling of major portions for maintenance. It is therefore crucial that individual components be carefully chosen for reliability and all major subsystems be accessible. Access to the interior of the chambers is foreseen to be provided in the endframe designs.

Structural, gas, and electrical safety considerations are important factors to be accounted for in the design. Methods of production, handling, transport, operation, maintenance, and repair will be determined from the beginning of the project onwards to ensure the safety of the personnel and of the equipment.

2) Principles of chamber production

a) General considerations : As indicated in Figs.2.3 and 2.4, the fact that there are many more chambers in the SSC muon detector than in the L3 muon detector means that techniques of economical production must be considered in the design, to avoid wasting time, manpower, and expensive materials. Chamber parts should be standardized whenever possible to take advantage of cost effective mass production. Some of the complex and labor intensive processes used in assembly of L3 chambers must be simplified. Automation of some procedures, and overall quality control contribute to improved accuracy of the detector.

b) Chamber frames : SSC muon chamber frames will have at least a factor of three higher wire tension load than their counterparts in L3, and therefore must be made stronger.

We will work with industry to study possibilities of improving the quality of castings, and also to search for alternative ways to manufacture endframes. Combinations of extruded and welded structures, such as the one shown in Fig.3.2, will be studied to determine suitability, adaptation to mass production, and cost effectiveness. At L3 endframe castings were used but this technique might not be suitable for SSC type chambers. Cast aluminum is of nonuniform quality and labor intensive machining is required to meet production tolerances.

c) **Chamber side panels** : Studies will be made to decide whether prefabricated side panels can be manufactured. The height of L3 middle chamber side panels was already at the maximum possible for European industry but we will actively pursue the possibility that a method can be developed in which larger panels can be fabricated industrially. L3 panels required extensive machining after extrusion to meet tight tolerances for gas seals and joints to the other structural parts. The gas seals between side panels and covers must be reliable, and we are studying improved designs, such as that shown in Fig.3.3. Methods allowing us to relax fabrication tolerances on individual elements and minimize machining will be pursued.

3.3 Wire alignment

Greater accuracy requirements and increased chamber sizes have implications for the wire support system. The structure maintaining wire tension will be independent of the structure which actually sets the wire position. Due to increased chamber width, we will develop an integrated bridge and wire plane support system with negligible thermal expansion but of larger size than L3. One possibility is shown in Fig.3.4.

Applying the L3 wire alignment method to SSC chambers :

The L3 success of precisely positioning 250,000 wires using glass and carbon fiber bridges has never been matched by any machining method. For this reason, bridge-like structures will be used to position the wires in an SSC detector. Bridges will precisely position wires relative to other wires in the same chamber. However, SSC muon detector chambers, such as those shown in Figs.2.3 and 2.4, are wider and higher than their counterparts in L3. Detailed structural analyses will be performed to optimize the bridge designs and ensure stability (see Chapter 5).

The wires in our present L3 system are already stretched to near maximum in order to minimize gravitational sag (now 95μm). If the chamber length is increased to 6.7m while maintaining the present 3 bridge support system, the resulting maximum wire sag is 140μm. For this reason, the accuracy to which wire tensions were adjusted in the L3 method must be improved if a three bridge system is used in SSC chambers.

A large part of this R & D effort will be directed toward improving the wire tension uniformity and the position accuracy both during wire winding, and after installation in the chamber. Tension adjustment and wire alignment inside the chamber, as well as attachment of the aligned wire planes to the bridges were labor intensive and time consuming processes in L3. There is a definite need for automation. Automation and simplification of several of the processes will save time, will contribute to the ultimate accuracy of the chamber, and will also lead to greater consistency from chamber to chamber. Consequently, we will study methods to automate and improve the accuracy of wire tension measurement and adjustment.

An optional technique, that of reducing the unsupported wire length by using two additional bridges (Fig.3.5.) is under study. This scheme will require the development of a complex alignment system (see Chapter 5).

Actuators will move bridges to within range of the alignment systems and allow compensation for thermal and gravitational deflections. New actuators will be needed to move the larger bridges with the required precision. This R & D effort includes the design, construction, and testing of actuators.

Alignment systems, actuators, and bridge supports must be developed and then integrated into the bridge design. Precise and accessible references for survey and alignment must be foreseen in the chamber design.

3.4 Drift cell optimization

Wire size, configuration, materials, and attachment methods will be studied to optimize chamber resolution, and to improve chamber reliability.

The feasibility of replacing field-shaping wire planes with foils or mesh planes will be studied (see Fig.3.6). This is important to reduce the number of wires. As seen in Chapter 2, there are nearly 1.5 million chamber wires to be strung in an SSC detector such as that shown in Figs.2.3 and 2.4. If it is possible to accurately position foil or mesh planes, chamber reliability would be greatly increased. The risk of wire breakage would be reduced, and less of the expensive tungsten wire would be required. Another advantage is that if a wire does break, losses are confined to a very small area of the chamber. These methods will increase the force on the endframes,

and that must be taken into account in the endframe and bridge designs. Tensioning methods for foils and meshes must be developed, with a view toward suitability for chamber mass production.

Electrostatic studies of the chamber ends will be used to help ensure good electrical behavior, and test modules will be constructed for final verification.

3.5 Test modules

After design studies, models of some of the critical structural elements will be constructed and tested. Some of the models to be constructed within the framework of this chamber R & D proposal are:

endframes
side panels
actuators

(see Figs.3.2, 3.3, and 3.4)

Further, test wire planes will have to be wound, since wire winding and tension adjustment play a very important role in achieving the ultimate accuracy of SSC muon chambers. We will use existing facilities to wind wire planes for the initial investigations. However, a larger winding drum will eventually be needed to produce longer planes.

An improved alignment method will be developed to align wires more accurately and consistently during the winding process.

Prototype modules (see Fig.3.6) for foil cathodes and mesh cathodes as well as several other ways to increase wire plane reliability will be studied in order to adapt these methods to mass production.

Test chambers have to be constructed to verify the cell design (see Figs.3.2, 3.3, 3.4 and 3.6).

3.6 Scope, schedule, milestones and funding estimates.

1) Scope

Dr. Marion White will coordinate this research and development effort for SSC muon chambers.

a) Manpower Needs : The physicists listed below will be supported by their home institutes, and will join in this effort on a part time basis. This will ensure not only the success of the research and development effort, but will also ensure that the technical experience is widespread enough to enable chamber production to be carried out in several different institutes.

I. Brock, A. Engler, T. Fergusen, H. Vogel,
Carnegie Mellon University, Pittsburgh, PA
H. Akbari, J.Z. Bao, C. Spartlotis
John's Hopkins University, Baltimore, MD
P. Berges, R. Clare, T.S. Dai, M. Fukushima, Q. Li, M. White
Massachusetts Institute of Technology, Cambridge, MA
D. Kuban, F. Plasil, M. Rennich, G. Young
Oak Ridge National Laboratory, Oak Ridge, TN
P. Denes, P. Piroué, D. Stickland
Princeton University, Princeton, NJ
A. Bujak, T. McMahon, B. Stringfellow
Purdue University, Lafayette, IN

In order to ensure the successful and timely completion of this project, existing expertise gained in the design and construction of L3 must be taken advantage of. Techniques developed after years of effort in L3 should be improved and modified, not reinvented. For this reason, two technicians (H. Meier and C. Haller) who have already gained invaluable experience in the construction of L3 precision chambers, as well as G. Faber, who has done a very large part of the L3 chamber design, will be supported by this request.

Table 1

Tasks	
Designer	- Develop prototypes of endframes, side panels and evaluate mechanical measurements to test suitability of the design. - Design such fixtures as are necessary for wire winding, alignment, and tension measuring.
2 Technicians	- Construct prototypes of endframes and side panels and make mechanical measurements to test suitability of designs. - Construct actuator prototypes and measure accuracy, reproducibility and stability of the design. - Develop and construct such fixtures as are necessary for the wire winding, alignment and tension measuring.

b) Equipment needs : Much of the equipment required is already in existence from L3 and will be used for this R & D project. Nonetheless, some new equipment will have to be purchased,

frequency meter
oscilloscope
sine wave generator
amplifiers
high voltage supplies
microscope
laser
personal computer

Other necessary equipment will include:

- Drift chamber wire, in several different diameters and materials.
- A larger winding drum will be designed and fabricated, and new systems for alignment of wires on the drum will be developed and tested.
- Additional precision measuring instruments must be acquired for stability and deflection tests of endframes, side panels, and actuators. These will include precision straight edges and rulers, dial gauges, depth gauges, and digital micrometers. Test equipment such as voltmeters and temperature measuring devices will also be procured.

Major structural design and analysis will be performed at the Charles Stark Draper Laboratory in Cambridge, MA (see Chapter 5).

c) Travel expenses

The travel budget is for travel foreseen between collaborative institutes.

2) **Schedule**

This R+D program for SSC chambers is anticipated to extend over a three year period. Since the goal of this R & D project is to design and to construct a prototype of a muon chamber for the SSC, we anticipate the following tasks will be systematically and successfully completed:

First Year Goals :

Wire attachment and alignment, chamber structure, and cell design studies will proceed in parallel during the first year.

Methods will be developed to improve position and tensioning accuracy in wire planes. The feasibility of replacing cathode wire planes by mesh or foil planes will be determined. Methods to align and tension them will be studied.

The chamber envelope and main structural elements (endframes, side panels, covers, as shown in Fig.2.14 will be determined. Production methods for major structural parts will be studied.

Tasks For Cell Design and Wire Alignment:

1) Studies of manufacturing and alignment techniques for foil and mesh planes will be completed, including tests.
2) Studies will be made to select materials for wires, foils or meshes, and wire plane or foil attachments. Samples will be evaluated.
3) Test wire planes will be produced to develop methods to increase tension uniformity, to obtain higher position accuracy and improved attachment.
4) Development of new tension measuring devices for wire planes, foils, and meshes will begin.
5) Designs of wire aligning structures [bridges] and actuators will be studied to optimize positioning accuracy and stability.

6) Studies of electric field distortions at the ends of the chamber will be initiated, both by calculation and with the help of test modules (this requires interaction with the gas R & D program, see Chapter 4). This includes calculation of critical areas that could cause unwanted gas amplification [sparks]. Software simulation of chamber resolution will also be undertaken.

Tasks for Chamber structure:

1) Conceptual studies of mechanical structures with at least three times higher wire load than L3 will be carried out.
2) Investigation of materials, production methods, and standardization for several mechanical chamber frame designs will be made. Samples will be evaluated. Production methods suited to eventual chamber mass production will be studied for endframe and side panel structures in collaboration with industry.
3) Concepts of the design with regard to repair, transport, handling, fabrication will be developed.
4) Manpower and time for mass production for several different structural designs and production methods will be estimated and evaluated.

First Year Milestones :

1) Determine whether foil or mesh planes can be manufactured and aligned to the required tolerances.
2) Freeze chamber structural design with regard to major conceptual changes.

Second Year Goals

Chamber structure details should be finalized. Optimization of wire alignment, and cell design will continue during the second year. Prototypes and models will be constructed.

Wire, foil, and mesh alignment, tensioning, and attachment trials will continue. Automated methods to improve position and tensioning accuracy in wire planes will be developed. Wire plane attachment will be optimized.

Tasks for Chamber structure:

1) Stability of the chamber body especially at attachment points, as well as temperature induced deformations of the structure will be studied by computer modeling.
2) A model of the endframe will be produced.
3) Structural verifications with models will be carried out.
4) Methods allowing us to relax fabrication tolerances and minimize machining will be studied in collaboration with industry. Investigations to find ways of automating fabrication processes will be started. Tests will be made.

Tasks for Cell Design and Wire Alignment:

1) Electrostatic modeling and studies of electric field distortions at the ends of the chamber will be continued, to optimize the design for reliability. Simulations to study chamber resolution will continue.
2) Prototypes of improved, automatic tension measuring devices will be constructed and tested.
3) Wire planes will be produced to test improved tensioning and higher position accuracy.
4) Trials will be made of improved wire attachment to the bridges inside chambers.

Second Year Milestones :

1) Produce and evaluate a model of the endframe, and test its stability
2) Produce and evaluate a model for cell verification
3) Produce prototype of wire alignment device
4) Produce prototype tensioning device

Third Year Goals :

Production method for chamber structure should be finalized. Cell design should be finalized in the beginning of that year. Optimization of wire alignment and cell design can continue to mid-year. Prototypes and models will be constructed. Automated methods to improve position and tensioning accuracy in wire planes and foils will be finalized. All designs and methods for construction of a full scale prototype chamber will be finalized.

Major Tasks:

1) Integration of the following into the final chamber body design will be carried out:

   alignment systems
   survey references
   electronics
   a calibration scheme for the chamber
   gas seals
   connectors for gas, signals, HV, and calibration
   feedthroughs for gas, signals, HV, and cables
   cable supports
   chamber supports
   actuators
   wire plane and foil attachments
   transport, handling, and safety precautions

2) A global review of the design with regard to repair, transport, handling, fabrication will be carried out.
3) We will continue to test possible methods and devices for better and automatic tension measurement and wire positioning.
4) A full length model will be constructed to test the alignment system and to study signal calibration methods.
5) Electrostatic modeling and resolution studies will continue.

Third Year Milestones :

1) Chamber design and production methods finalized.
2) Materials plus production, attachment, and alignment methods for wire and foil or mesh planes defined.
3) Full length model constructed and evaluated.

3) Funding requests

CATEGORY/ITEM *		FY90 K$	FY91 K$	FY92 K$
a)	**Personnel costs** Designer 2 Technicians Total	205	220	230
b)	**Materials & Services** Chamber components, tools machine shop, wire, foil, mesh, industrial samples, component metals Total	100	140	150
c)	**Travel**	15	20	20
d)	**Equipment** Test and precision measuring equipment, meters and tools, power supplies, personal computer, laser, microscope, amplifier, oscilloscope Total	60	30	35
Total		**380**	**410**	**435**

* Includes where applicable an estimate of university overheads based on MIT practice.

The funding requests for FY91 and FY92 are summarized in Chapter 7.

Figure captions

Fig.3.1 The wire plane configuration in a possible SSC detector is shown, with a 5.25m center to center distance between the inner and outer chambers. A muon trajectory is indicated.

Fig.3.2 A possible hybrid endframe made of extruded profiles and welded plates is shown.

Fig.3.3 An improved gas seal design in the region between the chamber frame and cover is shown.

Fig.3.4 A possible chamber endframe with its wire plane support frame and precision wire positioning plates is shown.

Fig.3.5 An exploded view of a possible SSC muon chamber with wires supported by 5 bridges.

Fig.3.6 A standard L3 drift cell is shown, along with 3 ideas for field shaping wire plane replacements.

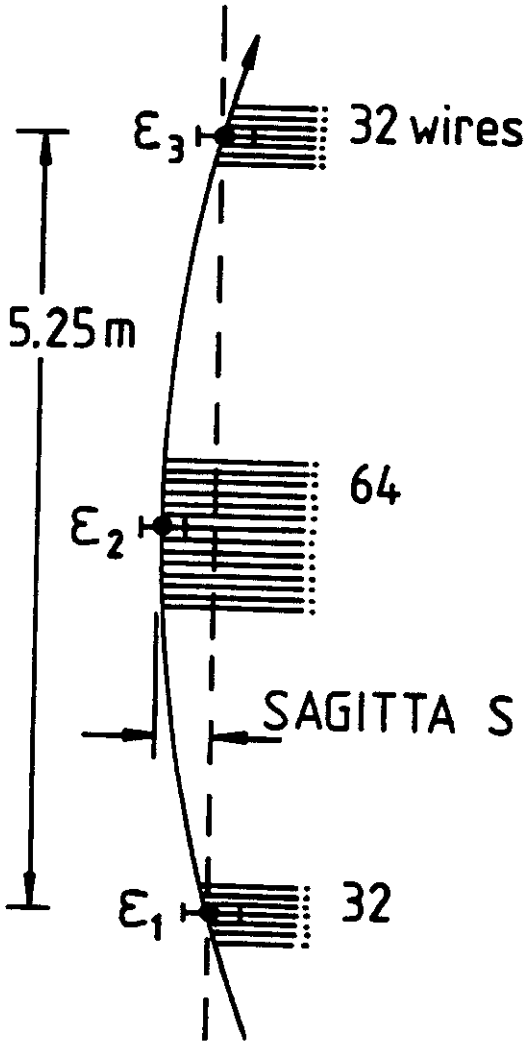
32 wires
ε_3
5.25 m
64
ε_2
SAGITTA S
ε_1
32

FIG. 3.1

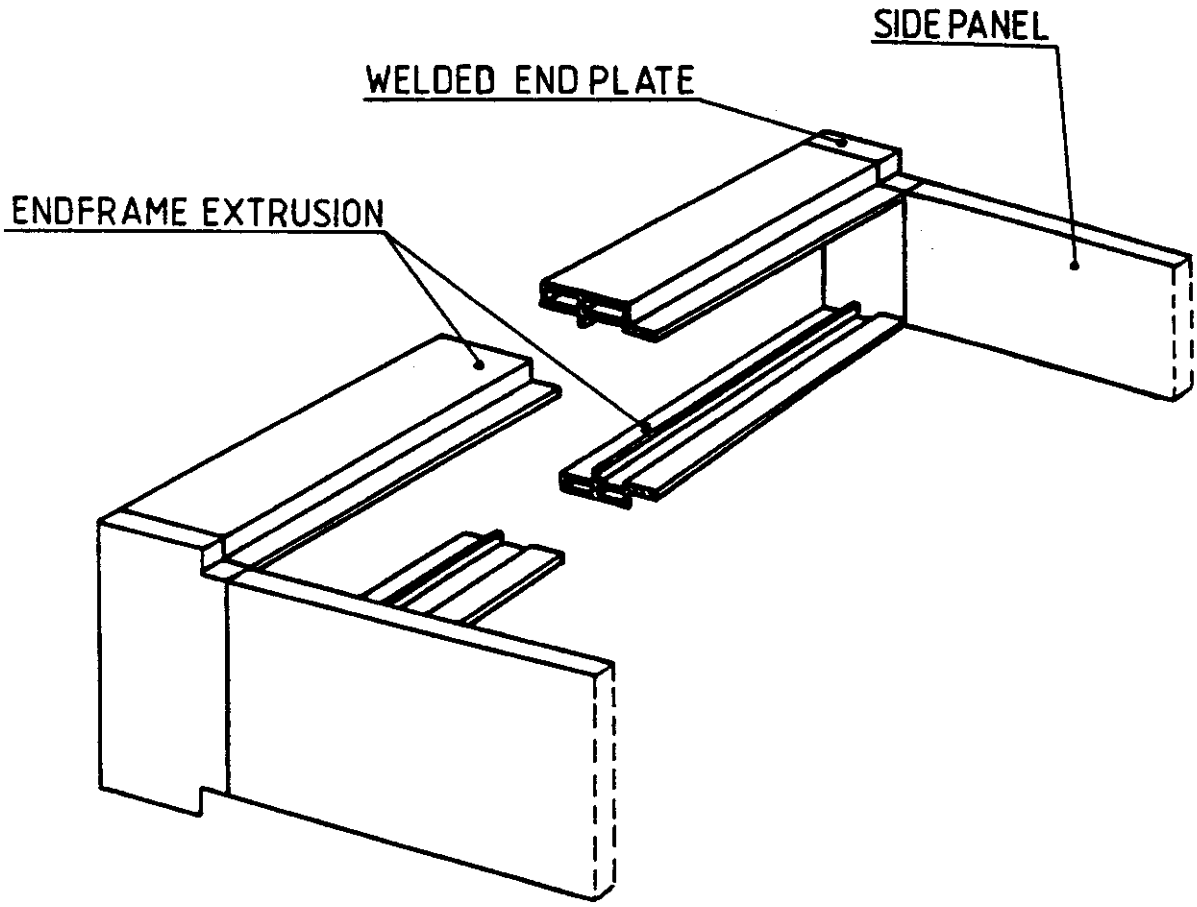

ENDFRAME AL. EXTRUSION

FIG. 3.2

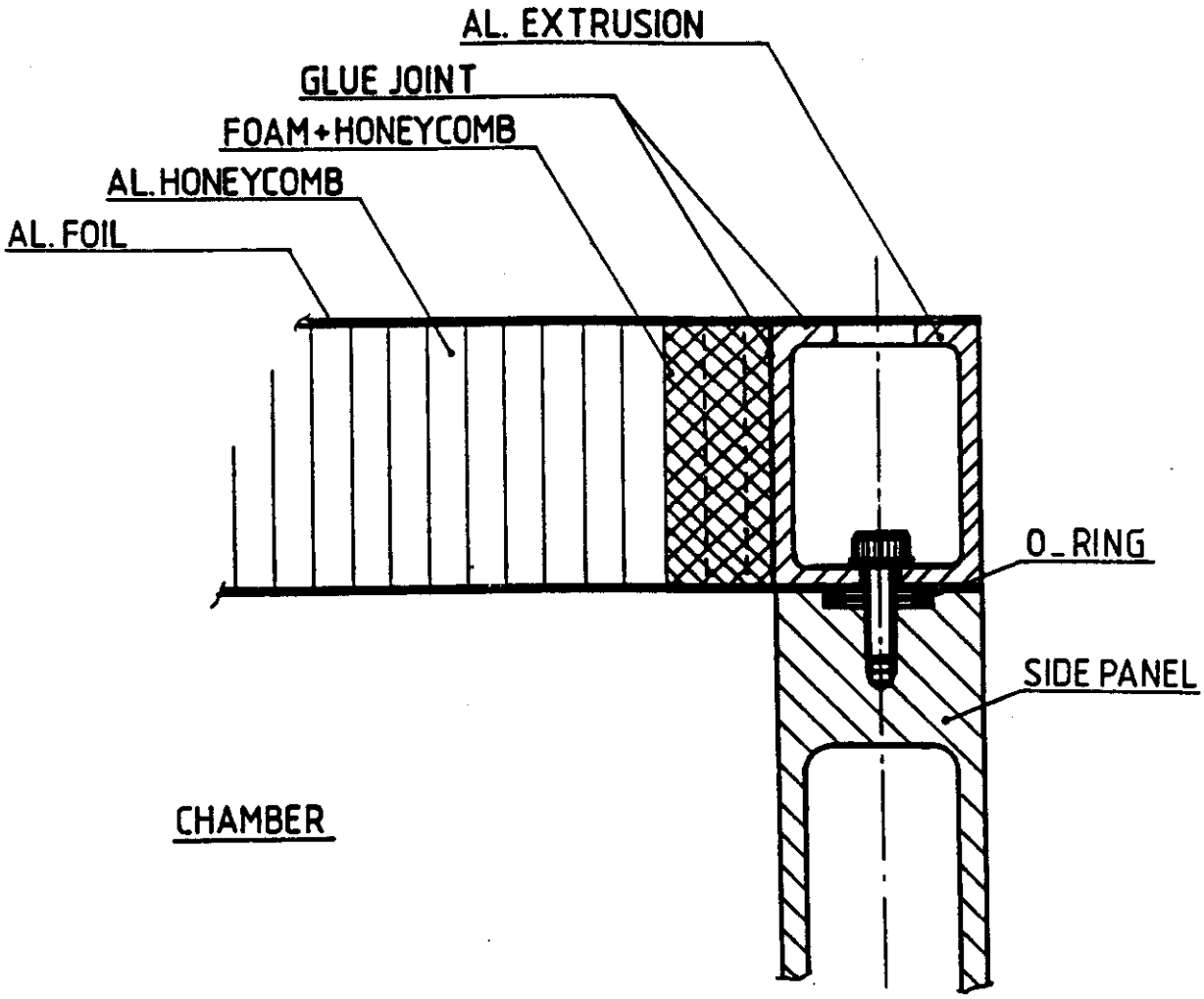

SIDE PANEL_HONEYCOMB COVER JOINT WITH GASSEAL

FIG. 3.3

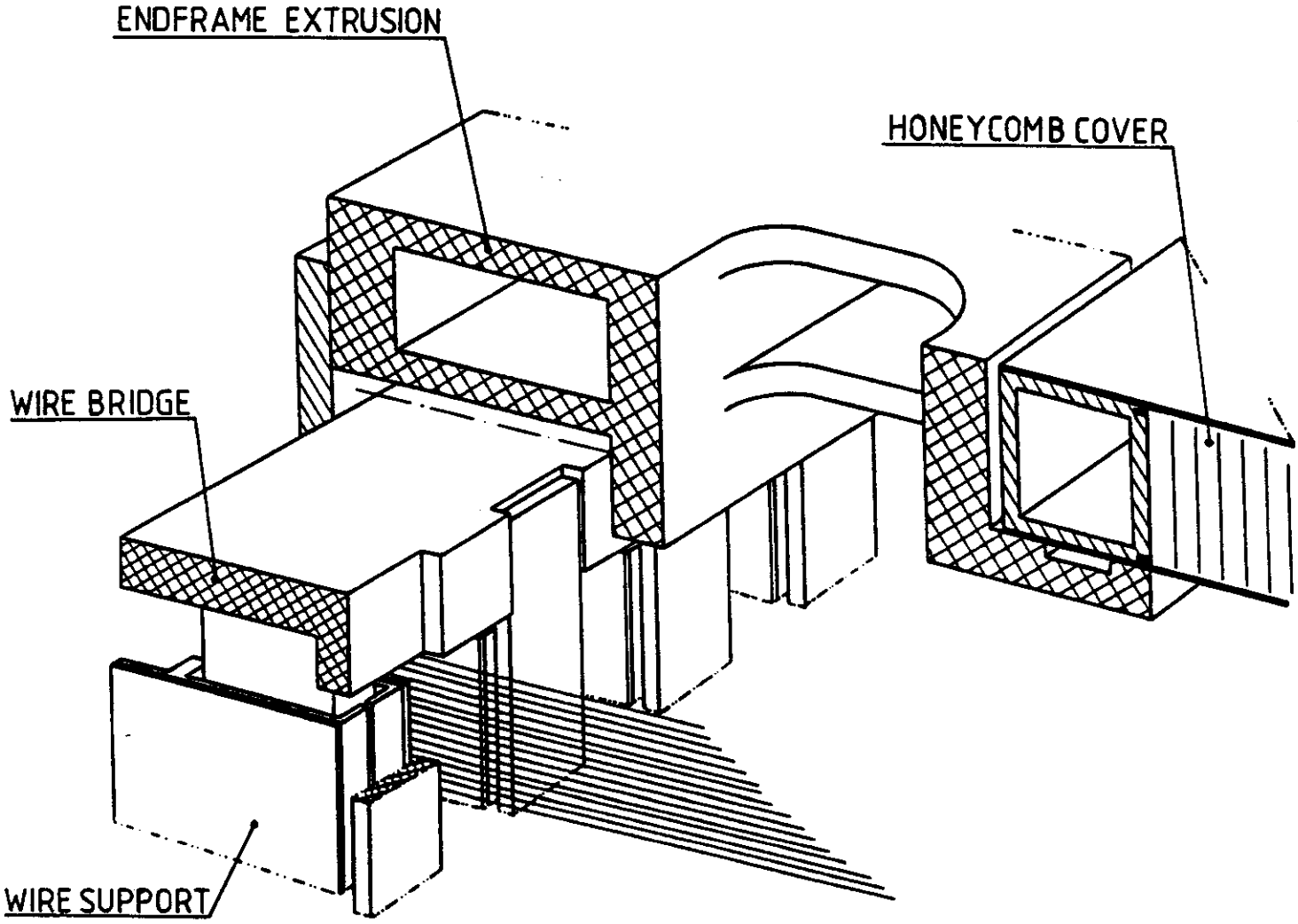

ENDFRAME WITH BRIDGE AND WIRE SUPPORT

FIG. 3.4

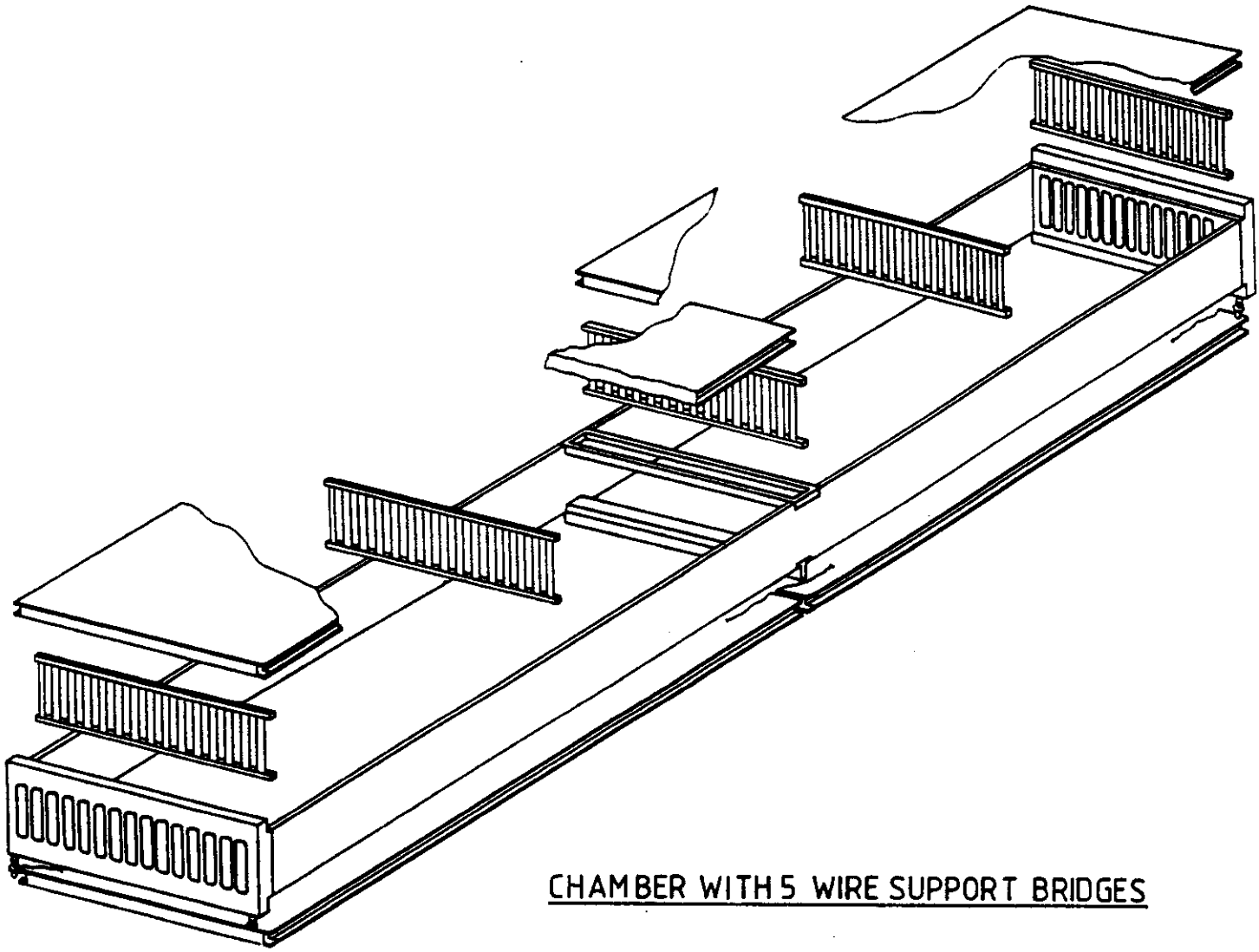

FIG. 3.5

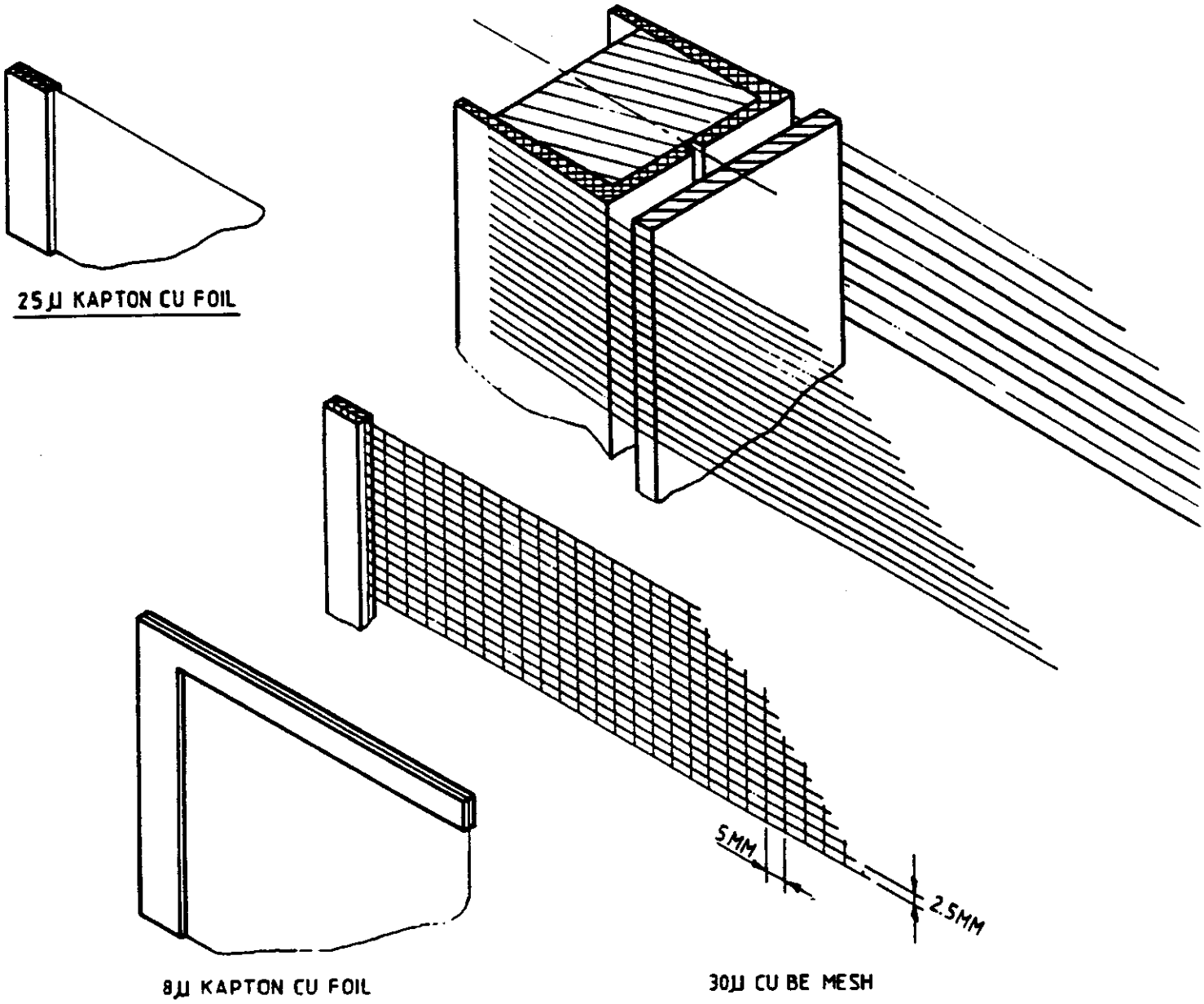

FIELD SHAPING WIRE PLANE REPLACEMENTS

FIG. 3.6

CHAPTER IV

RESEARCH & DEVELOPMENT PROGRAM TO DETERMINE A SUITABLE GAS FOR A LARGE SSC PRECISION MUON DETECTOR

U. Becker, Y.H. Chang, G. Herten, T. Wenaus, B. Wyslouch
Massachusetts Institute of Technology, Cambridge, MA
P. Mc Bride, K. Strauch, I. Scott
Harvard University, Cambridge, MA

Contact Person : U. Becker

The size and precision of muon detectors at the SSC will require drift chambers of unprecedented size and accuracy. One of the central issues will be selection of a suitable gas, since it dictates the detector design in a irreversible way. The gas should have low diffusion to allow high tracking accuracy. Owing to the large volumes involved, it must be nonexplosive. High rate capability and reliability are requirements for the choice of the gas in conjunction with the specific constructions of the chambers. These are the precision multi-sampling chambers with performance demonstrated in L3. The determination of suitable gases together with the operational conditions for these chambers is the objective of this proposal.

4.1) Need for research and development

The most fundamental question in High Energy Physics is the one for the origin of mass and its quantization rules. Presently the quantum H of the Higgs field is expected to emerge at SSC energies. A multitude of reactions and background will overshadow its decays, except the clear decay mode of $H \rightarrow ZZ \rightarrow 4\mu$. The precision detection of the $Z \rightarrow \mu\mu$ decay has been verified by the L3 detector [4.1]. The detection principle can be applied at TeV energies [4.2]. The corresponding SSC detector is depicted in Figs.2.3., 2.4 and Fig.4.1. At the SSC, high resolution will be absolutely imperative to extract the Z from background of heavy quark decays [4.3]. Fig.4.2a shows how a Z can be identified thanks to high (1-2%) resolution, as opposed to a background dominated measurement when the resolution is degraded to 15% (Fig.4.2b).

To obtain the necessary accuracies, the choice and operating conditions of the gas mixture are of primary importance.

In 1982, we carried out a thorough study of drift chamber gases [4.4], (Appendix IV). More than 300 mixture and pressure combinations were measured and are cited in publications [4.5], and standard reference books [4.6]. As a result of these studies, and taking advantage of the low rates expected at LEP, an argon ethane mixture was chosen for the L3 drift chambers.

However, the ten times bigger volume of an SSC detector forbids the use of this explosive gas. Also the aging behavior is not adequate for $10^{33}cm^{-2}\ s^{-1}$ luminosities at 40 TeV. The higher magnetic fields require a search for new gases as well.

The principles guiding the design of L3 were aimed to be applicable to TeV energies [4.2]. We describe therefore the relevant considerations for the original choice of the gas here and compare later to the SSC situation. Fig 4.3 shows how the muon momentum is determined in L3 with high accuracy, by measuring the bend in the magnetic field with 3 layers of drift chambers. The key point in measuring the sagitta of the curved track is illustrated in Fig.4.4. Each chamber samples the track with N wires, so that the average coordinate is given by

$$\langle x \rangle = X \pm \frac{\sigma_o}{\sqrt{N}} \qquad (1)$$

Whereas the accuracy of the track measurement increases by adding more wires according to $\sqrt{N}$, the single wire accuracy, σ_o enters linearly. **σ_o is directly related to the gas used.**

Fig.4.5 gives the details and parameters of the L3 multi-sampling chambers with the computed drift paths and the drift times for a muon passing at 44mm from the signal wire plane. Clearly σ_o will depend on the diffusion of the electrons drifting to the wire.

By the Lorentz force the magnetic field imposes an angle, α, on the drift path. Again, α depends on the gas. The angle should be small, since the distortions grow proportional to cos α, i.e rapidly for $\alpha > 20°$.

In the following we describe the past R & D effort which lead to the selection of the L3 gas, because similar procedures must be repeated in the search for a new nonflammable gas.

In a four years program we tested 300 different gas mixtures [4.4] and selected Argon:Ethane for L3. A mixture of 50:50% showed insensitivity to variations of the composition (Fig.4.6). In addition, the working drift field, E_o, could be chosen such, that

$$\left.\frac{dv}{dE}\right|_{E_o} = 0 \qquad (2)$$

as seen from Fig.4.6.

This means the drift velocity, v, is insensitive to small deviations of the drift field - for example - by space charge, which is hard to control. This gas is very reliable, non-sparking and shows high and stable gas gain. It is not optimal for aging. However, the muon rates at LEP are two orders of magnitude below the level at which this would become of concern.

Unfortunately the 250m³ of Argon:Ethane = 50:50 gas lead to explosion risk classification of class 3 by European standards, which is unacceptable. The L3 mixture was thus changed to 38% Ethane for this reason. A detailed computer program [4.7] was tuned to describe the existing measurements. It then was used to calculate the absolute drift velocity as a function of drift field for this mixture (Fig.4.7a). Also, the projected drift velocity $v_{//}$ was calculated (Fig.4.7b), which is used to determine the coordinate orthogonal from the wire plane by the relation:

$$x = v_{//}\ t \qquad (3)$$

The knowledge of $v_{//}$ as function of E enabled us to determine the operational field for B = 5 KGauss, E_B, from

$$\left.\frac{\partial v_{//}}{\partial E}\right|_{E_B} = 0 \qquad (4)$$

as indicated by the marker in Fig.4.7b.

Since all curves scale with the variable (electrical field/pressure), they depend critically on the gas pressure and temperature, a dependence which was measured separately. Careful calculations were made to determine the maximum variation of 26 parameters in the muon detector which could in the worst case cause a 11μm systematic error in the measured sagitta of a charged particle track.

As seen in Table 1 eight critical parameters are related to the gas, not counting the intrinsic features like gas gain, stability, contamination sensitivity and diffusion. Table 1 has been verified by thorough measurements with a test chamber [4.8].

It should be noted that these computations can be used as a guide for interpolations only and some parameters cannot be calculated reliably. In particular, direct measurements are needed to determine:

1) **Diffusion.** Early classical calculations of the diffusion constant $D_\perp$ are not applicable to the situation of drifting electrons. The diffusion $D_{\parallel}$ along the direction of the drift motion is substantially lower than $D_\perp$ as seen from measurements of Fig.4.8a. Therefore systematic measurements [4.9] of the relevant diffusion must be carried out experimentally like the ones in Fig.4.8b.

2) **Gas gain.** The multiplication process in the vicinity of the wire cannot be reliably calculated. Careful determinations [4.10] of pulse height and dark current by experiment are necessary. As an example Fig.4.9 shows the measurement of pulse height due to Fe^{55} sources (5.9 keV). In Fig.4.9a the pulse height of wire 1 is markedly higher than the others, because the edge wires had normal potentials. In Fig.9b the edge wires compensate for the influence of the outer chamber body at ground potential.In the Argon:Ethane mixture used, we now see equal amplification for all wires in accordance with the configuration of Fig.4.5.

3) **Reliability.** <u>It must be measured in the exact and final chamber.</u> In Fig.4.10 reliability is demonstrated for Argon:Ethane in an L3 chamber. Because as a function of increasing high voltage, the increase of dark current is exactly proportional to the signal. This constitutes ideal behavior and must be checked for each candidate gas. When raising the

TABLE 1

SOURCE OF ERROR	VARIATION GIVING 11 MICRON ERROR	SUGGESTED TOLERANCE
High voltage plane position in x	205 microns	50 microns
High voltage plane position in y	1 mm	500 microns
Position of ground plane	5 mm	5 mm
HV voltages on wires (Gas dep.)	6 volts	3 volts
B field (Gas dep.)	0.37% at 5 kg	0.037%
Gas mixture	0.1%	0.08% Ethane
Barometrique pressure	2.6 mm Hg	1 mm Hg
Gas temperature	1.0 deg. C	0.5 deg. C
Gas contamination	< 50 ppm O	50 ppm O
Gas gain variation	3.1%	3.1%
Amplification/threshold	3.1%	3.1%
Wire diameter	0.4 microns	0.4 microns
Calibration system timing chanel to chanel	0.2 nsec	0.2 nsec
Cal. stop vs. beam crossing stop, relative timing	0.2 nsec	0.2 nsec
Systematic TDC error	0.2 nsec	0.2 nsec
Position of wire in x relative to pyrex	11 microns	11 microns
Wire tension	10%	5%
Position of wire in y relative to disk	46 microns	30 microns
x position of pirex plate center in bridge	8 microns	8 microns
y position of disk in bridge	33 microns	33 microns
x position of bridges relative to chamber feet	11 microns	11 microns
y position of bridges relative to chamber feet	33 microns	33 microns
x position of middle bridge relative to end bridges	11 microns	11 microns
y position of middle bridge relative to end bridges	46 microns	46 microns
x positioning of chambers by Draper stand	11 microns	11 microns
y positioning of chambers	46 microns	46 microns

high voltage even more, eventually the plateau ends when the current increases more rapidly than the signal. However, we observed experimentally that a small addition of DEA extended the plateaus by more than 200V.

4) **Aging.** It is clearly beyond the scope of calculations. Drastic examples [4.11] of deposits on signal and cathode wires respectively were observed. The prevention and cures are debated extensively. Whereas the use of super pure gases and extreme care in the selection of connections and materials promise longer life [4.11], these measures are unrealistic for the operation and construction of a large volume SSC detector. As predicted by Walenta [4.12], addition 0,5% of water extend the chamber life substantially,(Fig.4.11). It can revitalize aged chambers. Present understanding attributes this to the suppression of the Malter effect by water making the covering layers on the wires conductive. Other additions like alcohols have been used successfully too.

The four points discussed above will be the objective of the R & D and will be specified in Chapter 4.3.

4.2 L3 experience and comparison with the SSC

In L3 an Argon:Ethane = 62: 38% vol, mixture at atmospheric pressure is supplied by a well stabilized gas system, which recirculates 97% of the gas.

The parameters are given in Table 2, and the flow diagram in Fig.4.12. Careful design avoids safety risks and ensures reliable operation. The monitored mixture stability is displayed in Fig.4.13. The stability achieved is better than demanded in Table 1. After 4.5 days, new chambers containing Argon only were added, changing the volume by 30%. The system recovery is dominated by the 8 hour recycling time and adapts exactly to the final value.

Using a high intensity Fe^{55} source aging studies were carried out [4.14]. For the 16 wires of a test chamber, Fig.4.14 shows how the gain deteriorates over the course of 35 days. Fig.4.15a shows the surface of the aged signal wire. The deposit analysis [4.16] in Fig.4.15b reveals silicon, oxygen and carbon as ingredients.

TABLE 2

MUON CHAMBER GAS SYSTEMS

- Mixture :

	p chamber
Total volume	250 m^3
Recycling rate	50 m^3 / h
Fresh gas rate	1.5 m^3 / h
Chamber pressure	0.75 - 1.25 mbar
Mixture stabil.	38% +/ - 0.2%

- Impurities :

Oxygen < 50 ppm

Nitrogen < 500 ppm

- Addition :

Water = 5000 ppm

Adding 0.5% of water restores the gain instantly as shown in Fig.4.16. All measurements have been corrected for the daily atmospheric pressure changes, which are substantial [4.15] (Fig.4.17). As a safety measure, the L3 system adds 0.5% water to the gas mixture.

The intrinsic wire resolution depends on the structure of the primary ionization and the chamber configuration. For L3 we measure the resolution as a function of the discriminator level. The result in Fig.4.18 shows that discrimination at < 10% of the pulse height gives the best resolution. The specifics of the ionization structure of the track are that knock-on electrons can distort the track recording. Therefore, considering only 94% of the measurements will improve the resolution, Fig.4.19 gives a track where the two worst of 16 measurements were dropped in the fit. The resulting resolution of 136μm is given in Fig.4.20.

80 chambers were built. They all have identical resolutions given in Fig.4.21 as function of x, the track distance from the wire plane. Due to diffusion, a contribution proportional to $\sqrt{x}$ is visible. The fact that all chambers arrive at this resolution verifies the reliability of the gas choice and chamber construction.

Fig.4.22 shows a cosmic ray recorded in the L3 muon detector in details. The muon momentum in the upper octant module is measured to be 14.5 GeV. The muon then traverses the 300 ton uranium calorimeter where it is expected to lose 4.5 GeV by dE/dx losses and 0.4-0.9 GeV by Bremstrahlung. Indeed, the measured lower muon momentum is to be 9.1 GeV.

The first $Zo \rightarrow \mu^+ \mu^+$ decay at LEP are documented in Figs.2.1 and 2.2, showing the end view and the side view, respectively. With LEP at 91 GeV, the measured muon momenta are 40 and 44 GeV with a dE/dx loss of about 4 GeV and a photon of 3 GeV emitted in the BGO adding up to 91.1 ± 1.3 GeV. The muons emerge from the expected interaction region within < 3mm.

This measurement is of unprecedented accuracy and shows the full potential of our approach to exploit SSC muon physics.

In comparison, the SSC detector of Fig.2.3 has a nearly ten times higher gas volume than L3. Already there, the $250m^3$ volume of the detector compelled us to use a slightly lower than ideal concentration of ethane (38%) in order to avoid the explosive gas classification 3 (European Standard, CERN Manual 1981, Section 2).

Even then, the imposed safety conditions i.e metal tubing, nonflammable cables, complicated feed throughs, double seals, and gas monitors throughout the detector volume imposed serious constraints. These will become unmanageable at the SSC detector dimensions. Table 3 shows how the parameters change from L3 to an SSC muon detector based on the concept of Fig.2.3.

Since the magnetic field changes from 5 to 7.5 KGauss the drift angle would increase from 18.8°to 28° if the same gas mixture were used. A gas with $\alpha < 28°$ must be searched for.

More chambers and wires require higher reliability. The design calls for a resolution of σ_o = 150-200μm, which was reached experimentally with Ethane mixture in 5 KGauss, and must now be achieved with a different gas at 7.5 KGauss.

4.3 Research and development goals

From the above discussion, considering the larger volumes of an SSC detector, and the much higher rates to be expected, the gas to be used in chambers should meet the following specifications :

(a) **Safety** : The gas should contain a minimum of flammable components; a nonflammable gas will be aimed at.

(b) **High reliability** : Good gas amplification ($> 2.10^4$) and low tendency to spark are essential. These features can only be determined by experimentally.

(c) **High accuracy** : "Cool gases", with low diffusion, will allow us to obtain good position resolution (150-200μm).

TABLE 3

L 3 → SSC MUON Detector

==========

VOLUME : 250 m^3 → ≈ 2250 m^3

	avoid class III		1250 m^3 central
	explosive by		1000 m^3 forward
a)	ethane 50 -> 38%		new gas
b)	5 kgauss		7,5 kgauss
c)	40 000 signal w.	→	200 000 signal w.
d)	$\sigma_{wire} < 250\ \mu m$	→	$\sigma_{wire} < 200\ \mu m$
e)	rates low	→	rates high

(d) **Low aging** : Slow aging properties will be vital for the muon detector when the SSC reaches full design luminosity.

With regard to point (a) we note that besides the improved safety, a nonflammable mixture reduces cost because many complications of construction can be avoided. This will eliminate alarm equipment, safety halon gas injection, guarding personnel on shift, and monitoring sensors and computers.

4.4 Research and development program

Using drift chambers in magnetic fields up to 7.5 KGauss, measurements of drift velocity as a function of drift field will be carried out. A set up similar to the one described [4.4] in Appendix IV can be used for the selection of gases.

Fig.4.23 gives a magnet set up providing a homogeneous field up to 8 KGauss. Schematically indicated is test chamber I, inside, where ionization electrons will drift under the influence of the electrical field E towards a grid of positively charged wires. Migrating through the grid, the electrons come into the amplification gap with the more positive signal wires. The arrival of the wire signals, Δt is recorded by a TDC of 0.2ns resolution with respect to the trigger signal of the UV laser or X ray tube creating the ionization.

Having entrance holes of defined distance Δx as indicated in the close up of the particular test chamber in Fig.4.24, the drift velocity is determined by

$$v = \frac{\Delta x}{\Delta t} \qquad (6)$$

The rigid chamber body allows to change the pressure and determine the velocity dependence on this parameter. Also, this chamber can be evacuated, which enables us to quickly study many clean gas mixtures.

Fig.4.25 gives the top view of the chamber displaying the Lorentz angle of the drift motion in the magnetic field. Behind the signal wire is a delay line. The induced signals travel to both ends and are recorded at times t_1 and t_2. The difference t_2-t_1 is proportional to Δy, the coordinate along the

wire. Therefore, the Lorentz angle is measured by the simple relation

$$\tan \alpha = \frac{\Delta y}{\Delta x} \qquad (7)$$

Fig.4.26 gives the drift velocity for Argon:CO_2 mixtures from reference [4.4], Appendix IV. This mixture is nonflammable and has good diffusion behavior. However, the reliability is not sufficient. Also, it is very sensitive to mixture changes. More advanced is the mixture of Fig.4.27, having some propane as quenching agent which enhances the reliability of the chamber operation. But still the mixture sensitivity is worrisome, because the systematic error of the sagitta measured with the SSC muon detector is :

$$20\mu m \ .$$

This allows only drift velocity variations of $< 2.10^{-4}$, and necessitates R & D to look for other mixtures or a very accurate system guaranteeing a highly stable mixture ratio.

Whereas test chamber I is suited to measure v and α, a different chamber type II of Fig.4.28 will be used to determine the longitudinal diffusion. Let wire 1 and wire 2 belong to two different cells of multiple sampling chambers. There, we expect for tracks parallel to signal planes:

$$t_1 + t_2 = \text{const.} \pm \Delta$$

where Δ is a measure of the longitudinal diffusion.

An independent method is to measure the rise time of X ray induced pulses as a function of distance x. We have shown that this method gives reasonable results. It is based on the fact that X rays of 5-10 keV generate pointlike clusters of 180-360 electrons which undergo diffusion while drifting to the wire. From these measurements candidate gases will be selected according to the features a),b),c),d) listed above.

4.5 Prototype chamber for final tests

Most important, the specifications (a-d) must be verified with chambers of the final design, i.e. SSC multiple sampling muon chambers.

The prototype chamber to be constructed will be exactly like an SSC chamber namely full size, except in length. This is necessary, because magnets with 5-6m gap are not available. On the other hand we expect no problems, because we know from studies of 5.4m wires [4.17] compared to 0.5m wires, already the relative difference. It is 25% attenuation in pulse height and a slightly slower rise time.

As a measure of reliability the resolution is monitored over several weeks. This and the other measurements in the magnet require a fastbus data acquisition system for several hundred wires. The same system will be used in test beam measurements.

In addition the pulse height and shape will be studied carefully. Fig.4.29 shows the electrical signals of four consecutive wires in an L3 chamber with 5.4m length of wires from a cosmic muon. The simultaneous recording with 2.5ns/point gives a precise measurement of the rise time [4.18]. It is very similar to pulses observed from a chamber of 0.5m wire length. The reason is that the rise time is dominated by diffusion spread and roughness in the incoming ionization.

The later point is illustrated in Fig.4.30, where we looked at cosmic tracks going parallel to the electric field through a chamber in the "wrong" direction. The incoming ionization is clearly recorded by the digital scope. In fact, we plan to use this method to determine the absolute ionization and the cluster structure for each gas studied.

The prototype chamber has 3 cells to ensure unperturbed electrostatic configuration in the middle cell which will be used for all precision tests. The side cells serve as calibrated references, which is particularly important for pulse height and aging tests.

The final verification with this SSC chamber will be in a test beam at Harvard or Bates. This will provide us with a field map of drift velocity measurements as a function of electrical, magnetic fields, pressures and mixture variations over the fiducial volume.

Using the pulsed X ray tube [4.19], aging tests will be performed on a few of the most promising mixtures, to measure the lifetime and determine what materials are permitted in the chambers and the gas system.

4.6 Scope, schedules and milestones

a) Scope and schedules

The program is to be carried out at MIT with the following staff and institute supported personnel :

Responsible	:	U. Becker, MIT
Harvard University	:	P. Mc Bride, K. Strauch, I. Scott
M.I.T.	:	Y.H. Chang, G. Herten, T. Wenaus, B. Wyslouch

G. Herten and B. Wyslouch will continue the effort during the time U. Becker works at L3 (50%).

New personnel requested :

1	PhD physicist	to carry out measurements
2	Students	to process data
1	technician	to construct 2 test chambers and 1 prototype chamber.
0.5	electro-mechanical technician	to wire the chambers and adapt electronics.

The first year will be dedicated to the setup of the chamber in the magnet and all data taking equipment. We will select first candidate gases for a proposal.

In the second year, this research will continue with emphasis on diffusion and reliability measurements.

Aging tests and test beam measurements form the program of the third year. Availability of test beam time and detailed check measurements may extend into a fourth year.

b) Milestones

- By the end of 1990, completion of setup for measurements.
- By the end of 1991, measurement of diffusion and reliability for ten gas mixures.
- By the end of 1992, construction of a prototype chamber and test beam measurements at Bates Linear Accelerator or Harvard Cyclotron.

4.7 Funding requests

Travel between collaborative institutions for coordination of efforts and test beam measurements is requested.

Materials include test chambers and the set up in the magnet. Very specialized laboratory equipment such as gas mixtures systems, lasers, precision motion devices, electronics, computer read out, gases, control and safety systems have to be acquired for the initial set up.

Table 4 summarizes the cost estimates for this program, consisting of yearly running costs and an initial set up (see also Chapter 7).

Table 4

CATEGORY/ITEM *		FY90 K$	FY91 K$	FY92 K$
a)	**Personnel costs**			
	one postdoctoral			
	two graduate research assistant			
	0.5 electromechanical technician			
	Total	188	197	205
b)	**Materials & services**			
	gases, system components			
	tapes, read out			
	components for chambers			
	LNS shops (drafting, electronics			
	machine shops ..)			
	Total	124	130	136
c)	**Travel**			
	Travel pertinent to SSC meetings, collaboration meetings, test beam..	13	14	16
	TOTAL a)+b)+c)	325	341	357
d)	**Equipment**			
	UV laser, optics	14		
	Gas mixture system	18	15	15
	Magnet set up	23		
	FASTBUS electronics	15	7	10
	Computer read out	36		
	Precision motion devices	12		
	TOTAL FY a)+b)+c)+d)	443	363	382

* Includes where applicable an estimate of university overheads based on MIT practice.

We expect the program to extend over 3-4 years in order to finish careful R & D and to ensure the successful construction of a muon detector which will be in the 100M$ region.

References

[4.1] L3 Technical Proposal 5/83 (LEPC-L3),
B.Adeva et al NIM. to be published

[4.2] U. Becker et al NIM A 253 (1986), 15,
U. Becker et al NIM A 263 (1988), 14

[4.3] G. Herten et al MIT LNS report 163 (1988)

[4.4] C.M. Ma, U. Becker, D.A. Ma, A.H. Walenta MIT-LNS
Technical report 129, Oct 1982, see Appendix II.

[4.5] U. Becker et al. NIM 196, 381 (1982), 381
D. Antreasyan, et al. NIM A252 (1986) 304 SLAC summer school 1985, 207

[4.6] A. Peisert, F. Sauli CERN 84-08, J. Fehlmann, ETH IHP August 1983

[4.7] Program "WIRCHA"

[4.8] J. Branson et al. to be published
H. Onvlee, thesis, NIKHEF 89

[4.9] a) J.A. Jaros, SLAC-PUB-2647 (1980), A. Mellissinios et al.
b) J.Fehlmann et al. ETH Zurich report (1982)

[4.10] "Gain in the L3 chambers" D. Antreasyan, U. Becker, Y.H. Cheng et al.
L3 internal report 88/17 to be published
"Fe^{55} measurement in Muon chambers " Mao Yufang CERN CMS 4.20.88

[4.11] Workshop "Radiation Effects at the SSC, 7-9 March 89, Berkeley
also F. Sauli Summer lectures CERN 88, 89

[4.12] H.A. Walenta " A little H_2O in good for chambers" quotation to U.
Becker 6/1979

[4.13] De Wulf et al., CERN EP 86-26 (1986)

[4.14] D. Antreasyan et al. to be published

[4.15] Some confusion in the contemporary scientific literature originates
from neglecting this correction.

[4.16] J.D. Adams, CERN ST/TE 88/11/006

[4.17] U. Becker, C.M. Ma, A.H.Walenta, BNL 81-4
P.Duinker et al NIM A273 (1988),814

[4.18] Gould digital 4 channel scope 2.5 ns/point

[4.19] Kevex, pulsed X ray tube with self made grid pulsing amplifier.

Figure Captions

Fig.4.1 a. Perspective view of a large SSC detector with precision muon measurement.

Fig.4.2 Signal from the process chain pp → Hx, H → ZZ, Z → μμ, with background from pp → TT → Wb μμx, (Monte Carlo).
a. for the detector of Fig 4.1
b. for an iron toroid detector.

Fig.4.3 End view of one octant in L3 with curved muon track, showing multi-sampling drift chambers, sampling the track 16-24-16 times.

Fig.4.4 Principle of accuracy in L3. The middle chamber has honeycomb enclosures to minimize multiple scattering and will measure the track to better than $\sigma_o/\sqrt{N} = 250/\sqrt{24}$ μm accuracy.

Fig.4.5 Operational parameters and computer modeling in 5.0 KGauss field. Drift time for all wires from a muon track at 44 mm in a chamber cell.

Fig.4.6 Drift velocity in Argon:Ethane mixtures from ref.[4.4]

Fig.4.7 Drift velocity calculation, ref.[4.7] for Argon:Ethane = 62:38 %
a. absolute velocity
b. velocity parallel to the x-axis for 5 KGauss magnetic field.

Fig.4.8 a. Coefficients of longitudinal and transverse diffusion as function of the reduced field. Data from Ref.4.9.
b. Drift velocity and longitudinal diffusion for Ar. (50%)+ C_2H_6 (25%) + $(CH_3)_2O$(25%) at 1 atm. Data from ref.[4.9].

Fig.4.9 a. Measured pulse height of Fe^{55} signals on 4 wires with guard wires uncompensated.
b. Same with compensated guard wires. Note all signals are of equal height now.

Fig.4.10 Measured pulse height and dark current in L3 multi-sampling chambers as a function of high voltage.

Fig.4.11 Influence of water addition on chamber life time. From ref.[4.13].

Fig.4.12 Schematic of L3 gas system.

Fig.4.13 Gas mixture stability of the L3 gas system in one week. Also shown : recovery from major perturbation.

Fig.4.14 Gain measurement by Fe^{55} for 16 wires of a test chamber. The radiation/cm of signal wire is largest at wire 10 and corresponds to several m Coulombs of charge.

Fig.4.15 a. Surface of a 30μm signal wire after aging.
b. Deposit analysis of coated compared to a clean wire.

Fig.4.16 Same as Fig.4.14. However, adding 0.5 % H_2O to the gas restores the gain.

Fig.4.17 Gain variation under small atmospheric pressure changes.

Fig.4.18 Resolution vs, discrimination level in L3 chamber with Argon:Ethane.

Fig.4.19 Individual track with residuals in mm. Two measurements were omitted in the track fit.

Fig.4.20 Resolution achieved with cosmic muons fitting 14 of 16 measurements.

Fig.4.21 Resolution of L3 production chambers, showing the $\sqrt{x}$ increase due to diffusion in the gas.

Fig.4.22 Cosmic muon event in the L3 detector with enlarged details of the chamber tracks.

Fig.4.23 Set up in a magnet with homogeneous field. Ionization is generated by UV laser or pulsed X ray tube and compared to Fe^{55} signals.

Fig.4.24 Close up of test chamber I. Different inlet holes define Δx.

Fig.4.25 Top view of chamber I. C are field shaping walls, D potential wire grid, E signal wires, F delay line with 7 ns/cm.

Fig.4.26 Pressure and mixture dependence of argon-CO_2 gas. Although this is a cool gas, high voltage breakdown occurs. C.M. Ma et al. MIT Technical Report 129 (1982).

Fig.4.27 Gas mixture with low diffusion, similar to that shown in Fig.4.29 but with considerably better high voltage breakdown behavior. Note the insensitivity to E, since $dV/dE \approx 0$ at high E fields. From C.M.Ma, ibid.

Fig.4.28 Schematic principle of test chamber II.

Fig.4.29 Four simultaneous wire signals recorded on a digital scope of 2.5ns/point from a cosmic ray passing a L3 chamber. Note the jitter due to primary ionization.

Fig.4.30 Measurement of the primary ionization structure in 2 cells of drift chamber from a cosmic traversing 90° from normal situation.

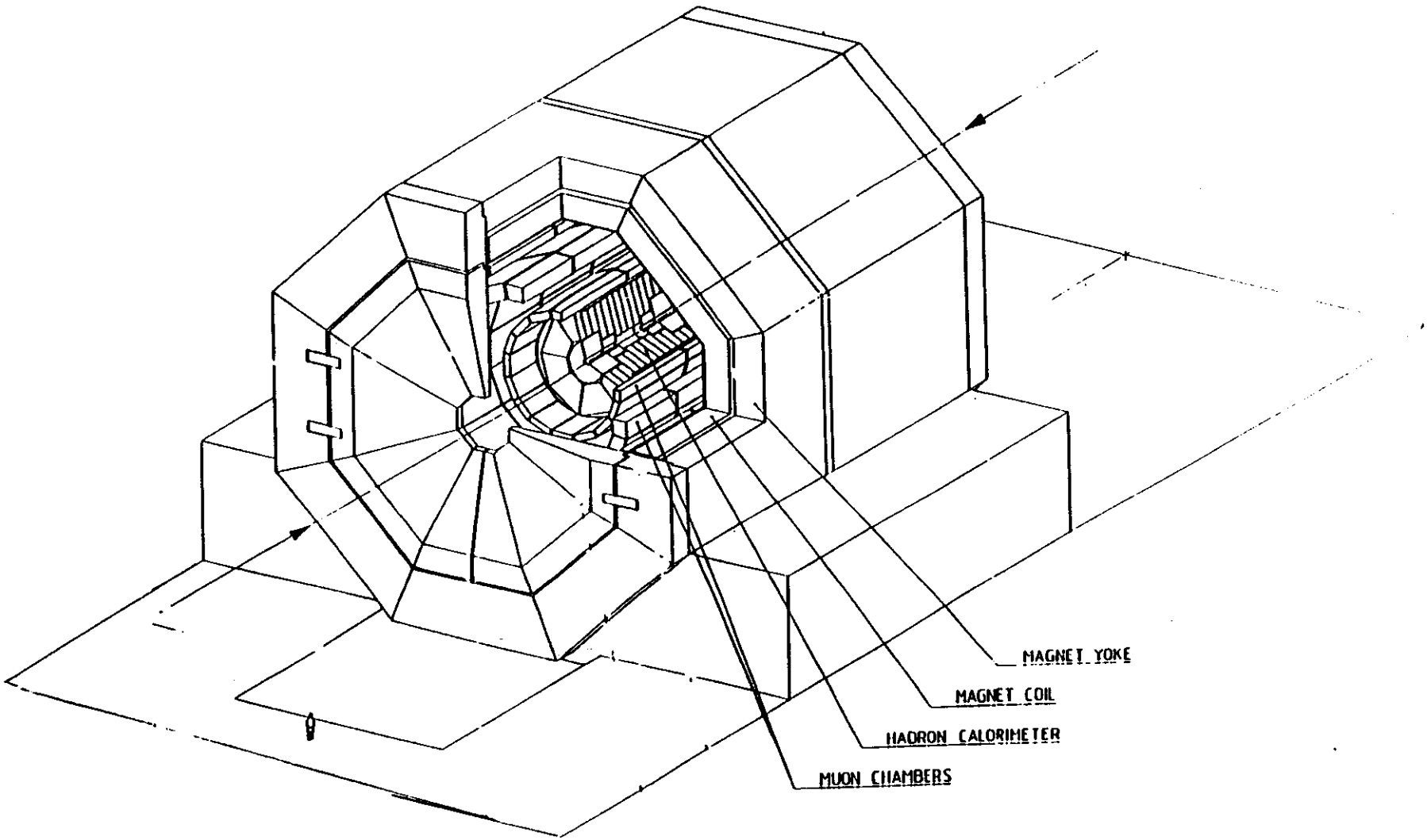

FIG. 4.1

Resolution is imperative!

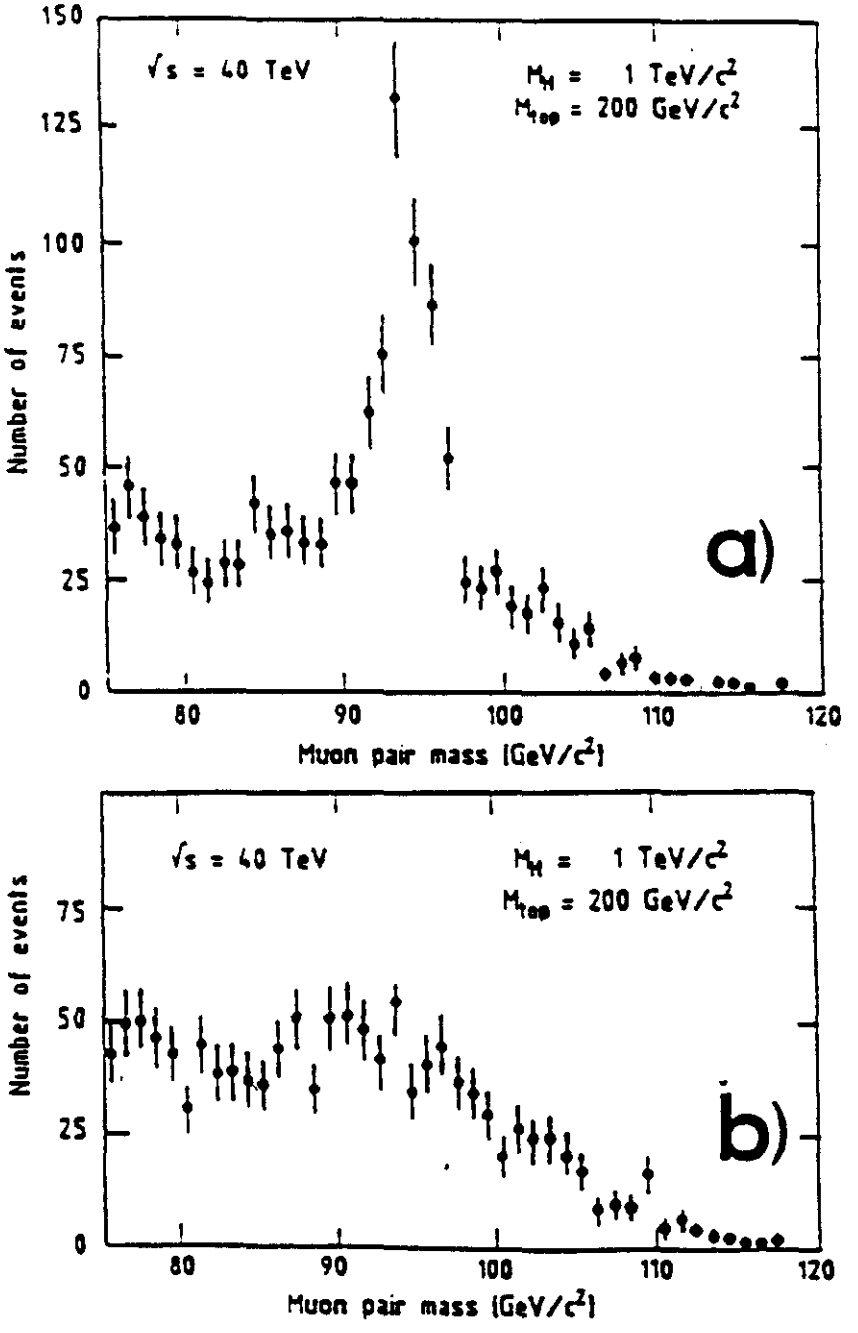

FIG. 4.2

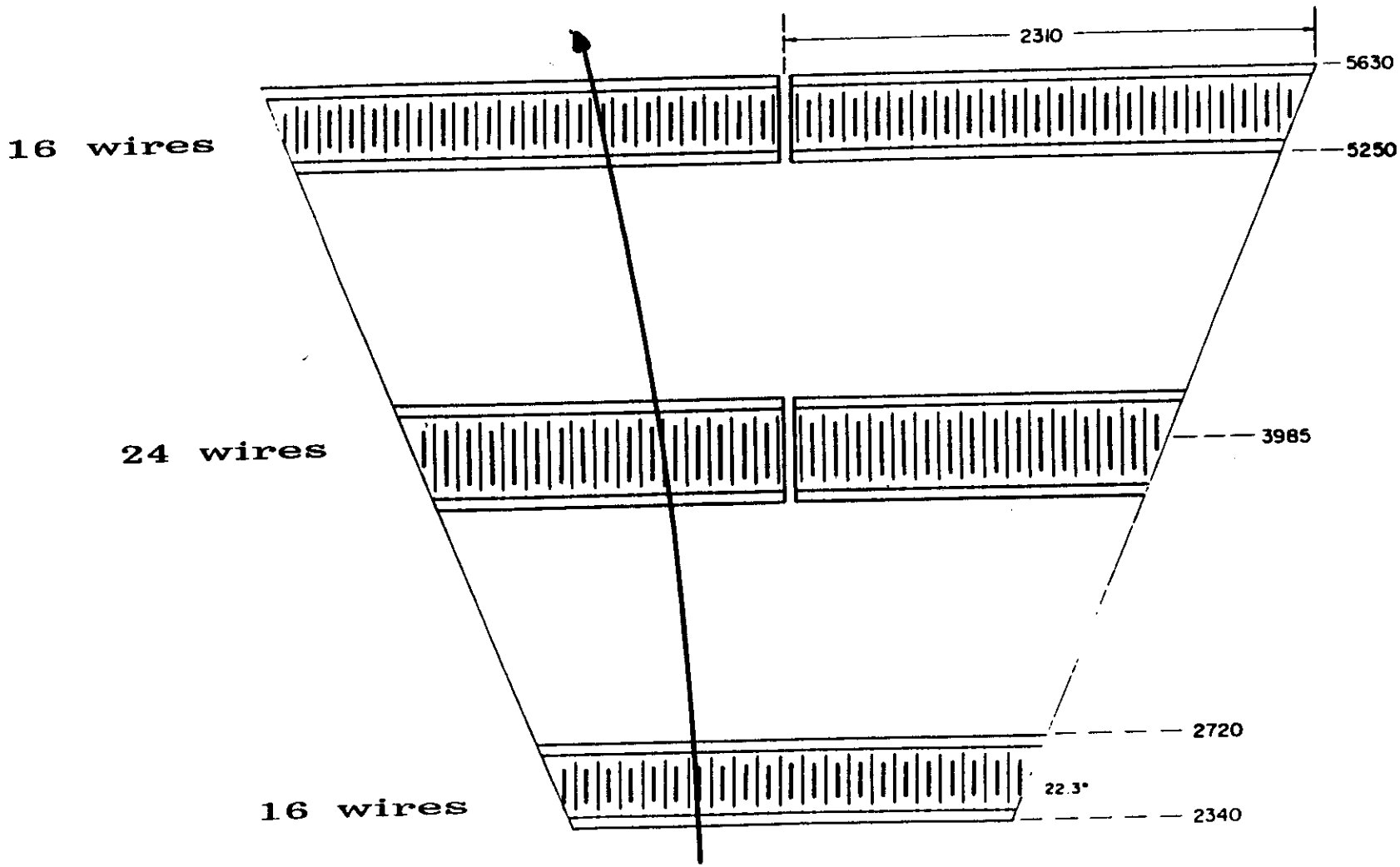

FIG. 4.3

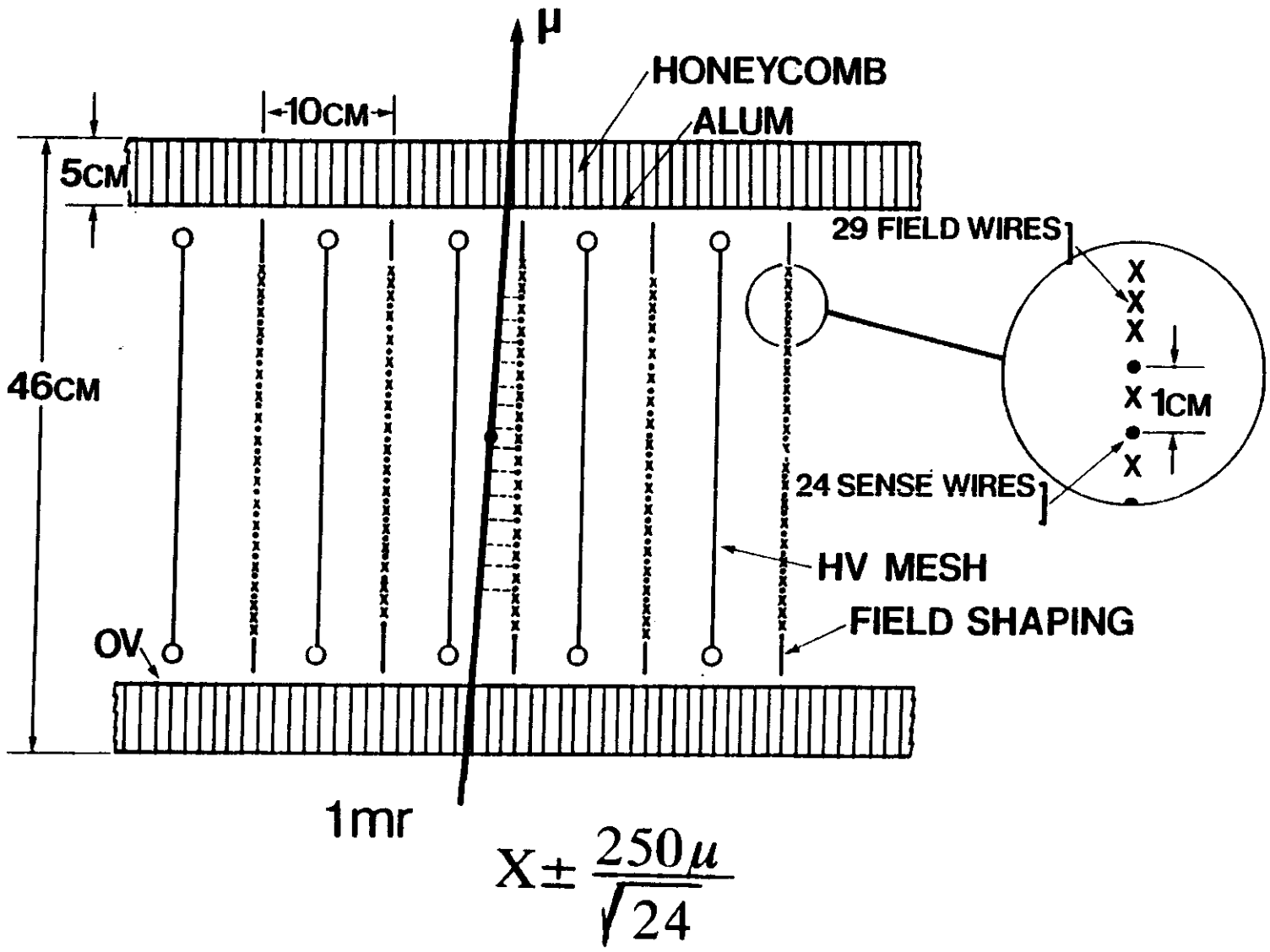
μ
HONEYCOMB
ALUM
10CM
5CM
46CM
29 FIELD WIRES
1CM
24 SENSE WIRES
HV MESH
FIELD SHAPING
OV
1mr
$X \pm \frac{250\mu}{\sqrt{24}}$

FIG. 4.4

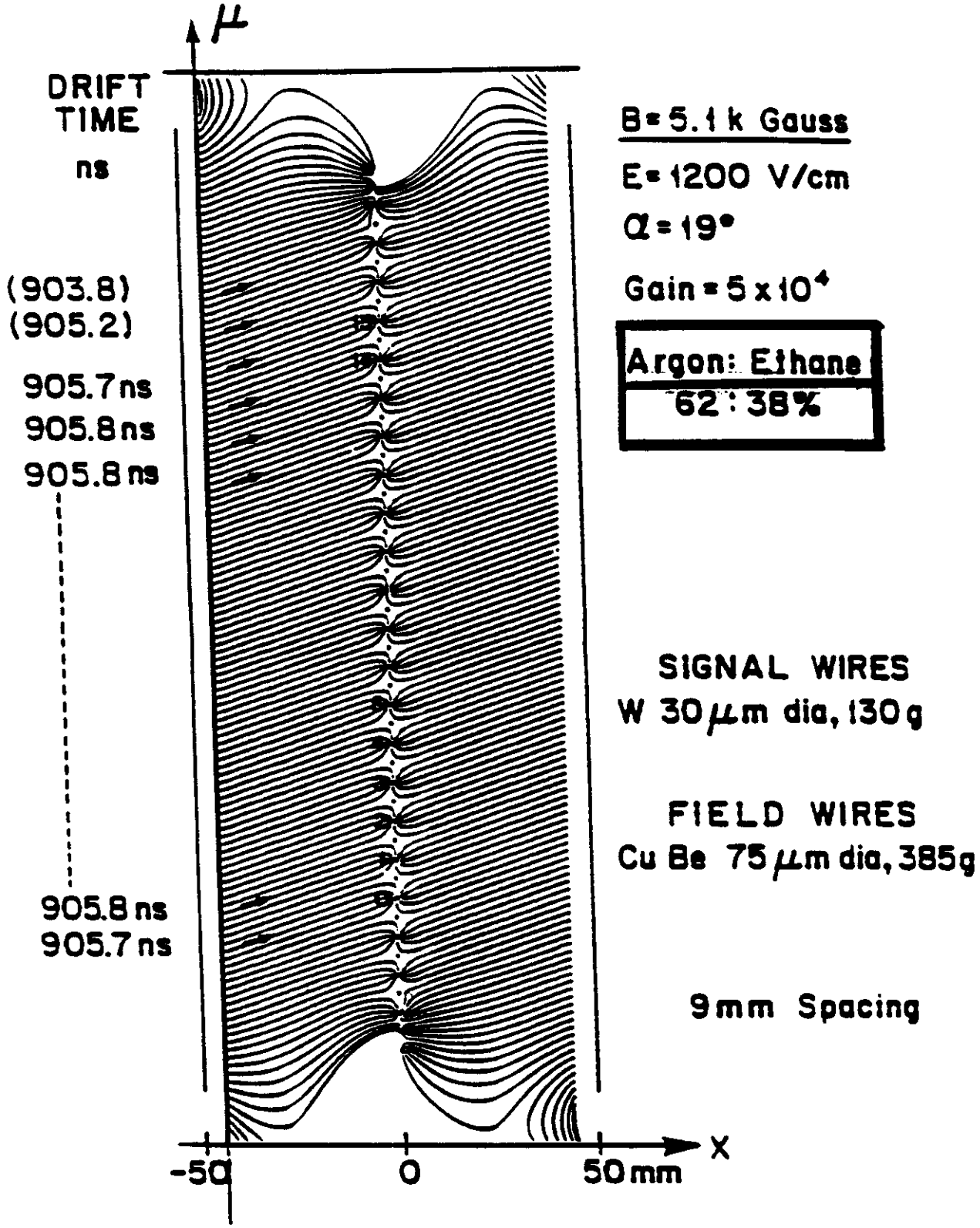
μ
DRIFT TIME ns
(903.8)
(905.2)
905.7 ns
905.8 ns
905.8 ns
905.8 ns
905.7 ns
B = 5.1 k Gauss
E = 1200 V/cm
α = 19°
Gain = 5 x 10⁴
Argon: Ethane
62 : 38%
SIGNAL WIRES
W 30 μm dia, 130 g
FIELD WIRES
Cu Be 75 μm dia, 385 g
9 mm Spacing
-50
0
50 mm
X

FIG. 4.5

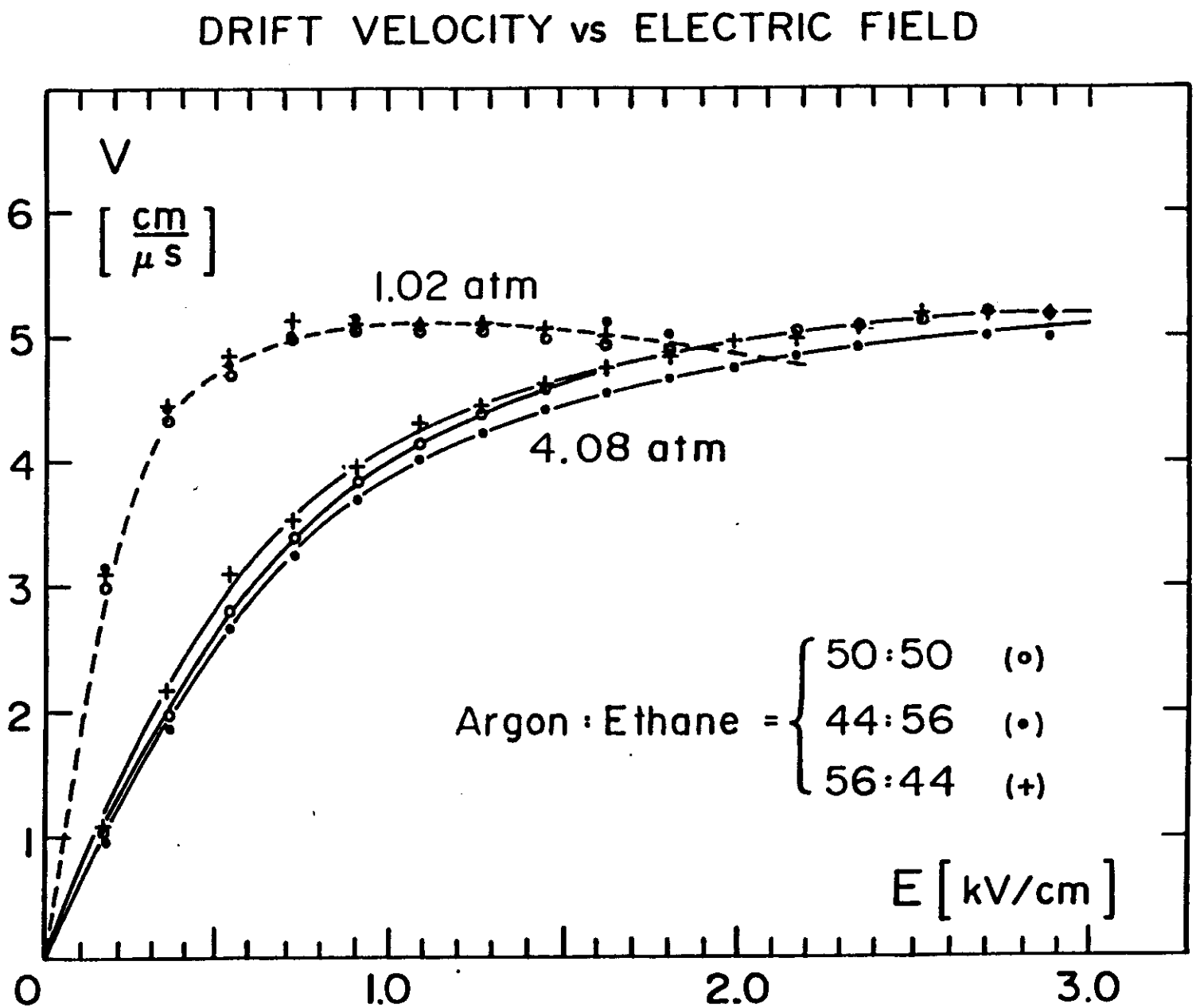
DRIFT VELOCITY vs ELECTRIC FIELD
V
[cm / μs]
1.02 atm
4.08 atm
Argon : Ethane = 50:50 (o)
44:56 (•)
56:44 (+)
E [kV/cm]
0
1.0
2.0
3.0
1
2
3
4
5
6

FIG. 4.6

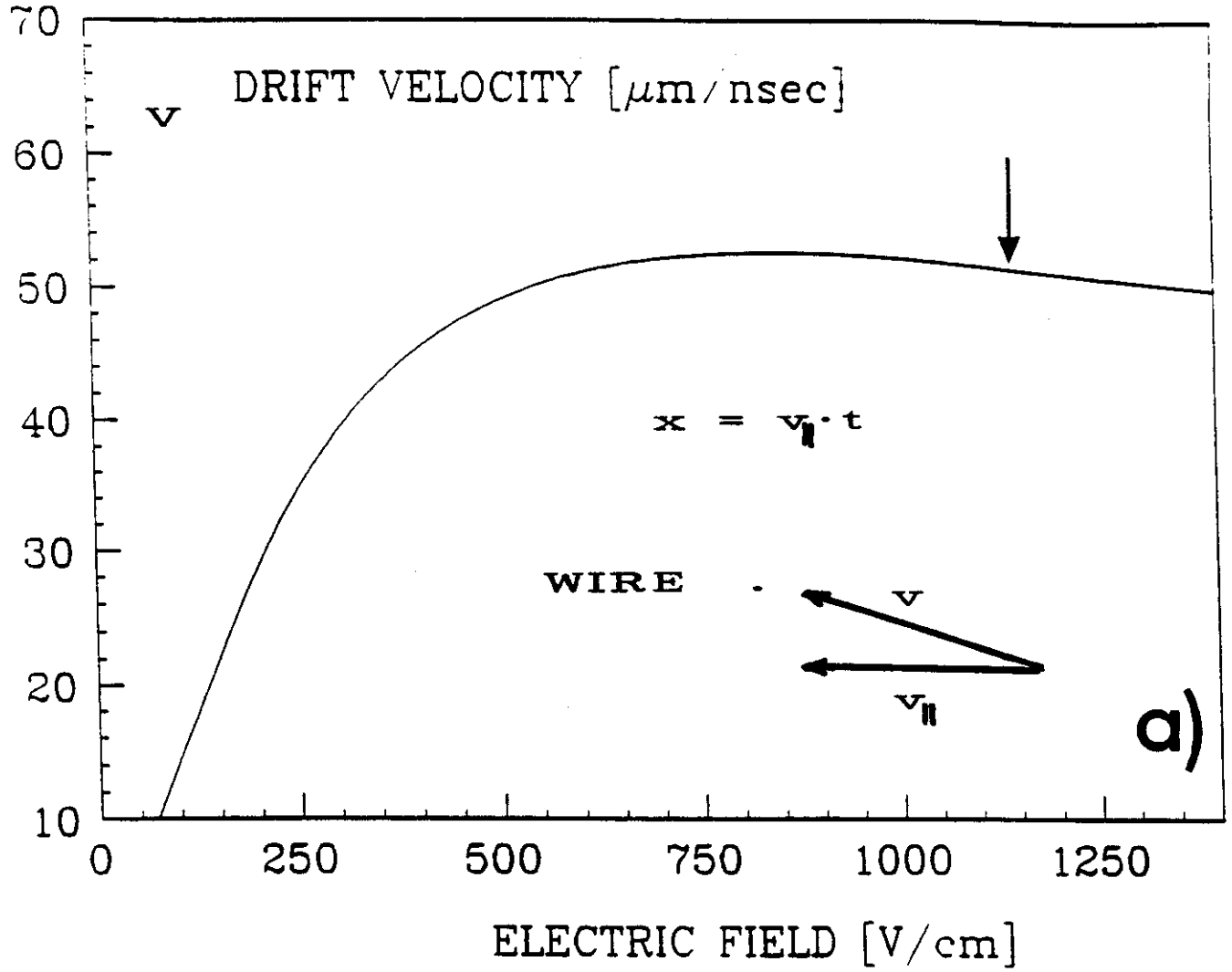
DRIFT VELOCITY [μm/nsec]
v
x = v∥ · t
WIRE
v
v∥
a)
70
60
50
40
30
20
10
0
250
500
750
1000
1250
ELECTRIC FIELD [V/cm]

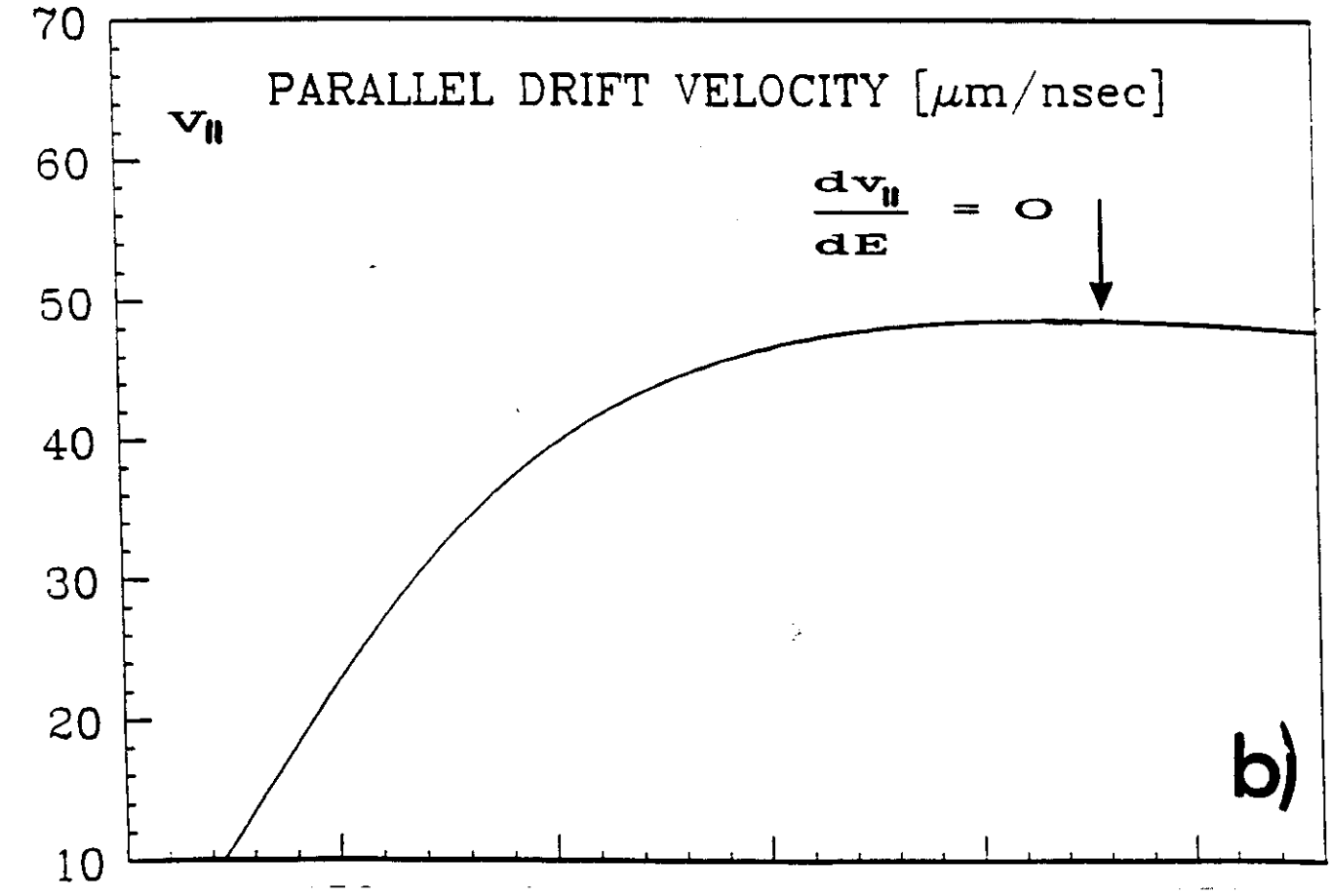
PARALLEL DRIFT VELOCITY [μm/nsec]
v∥
dv∥/dE = 0
b)
70
60
50
40
30
20
10

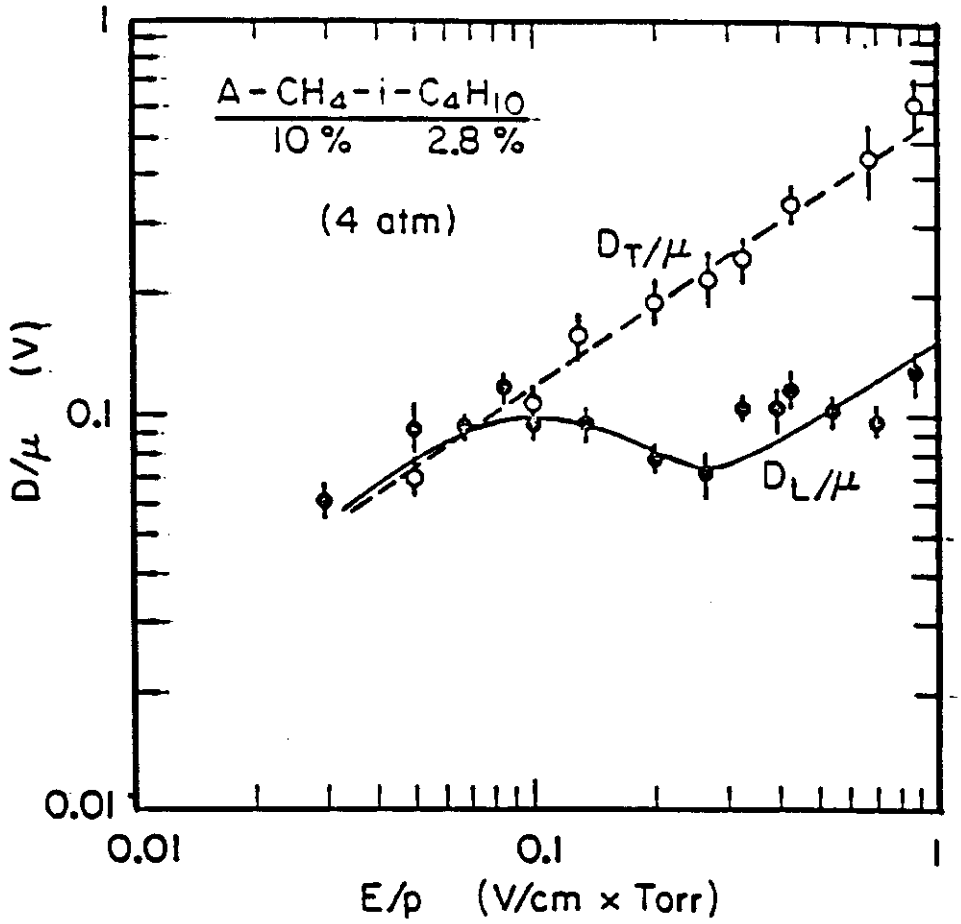
A - CH4 - i - C4H10
10 % 2.8 %
(4 atm)
DT/μ
DL/μ
D/μ (V)
E/p (V/cm × Torr)
1
0.1
0.01
0.01
0.1
1

a)

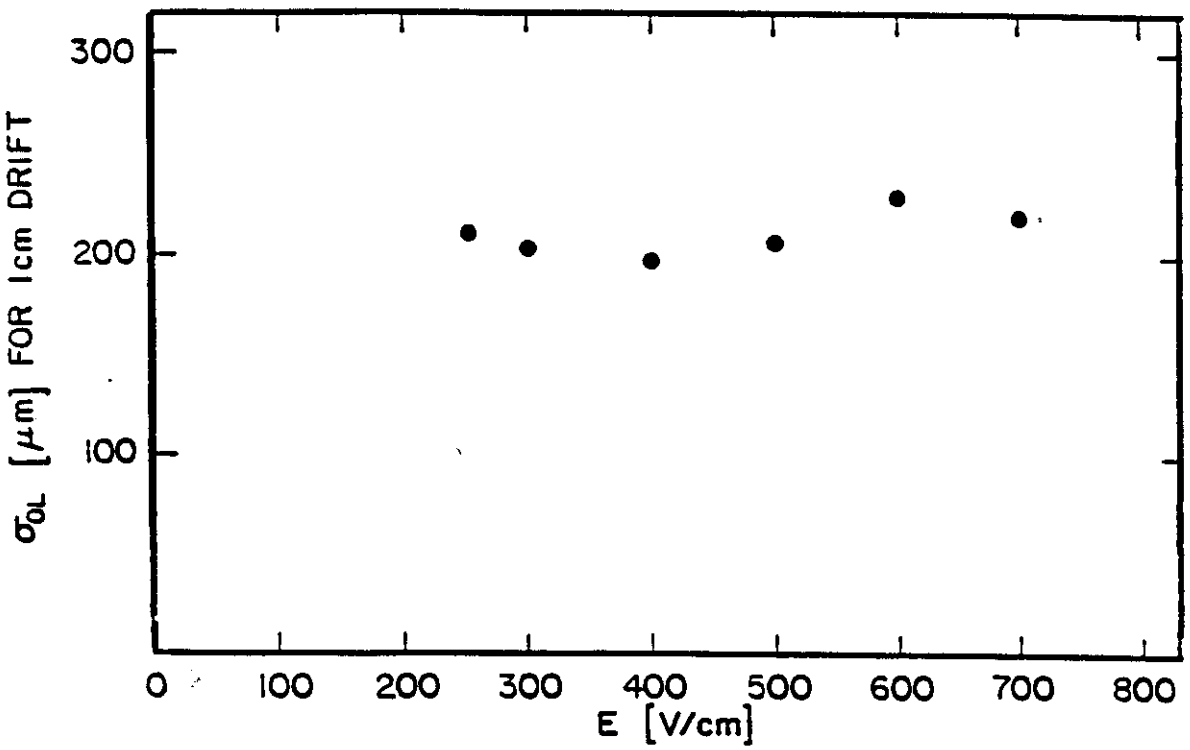
σ0L [μm] FOR 1cm DRIFT
E [V/cm]
300
200
100
0
100
200
300
400
500
600
700
800

b)

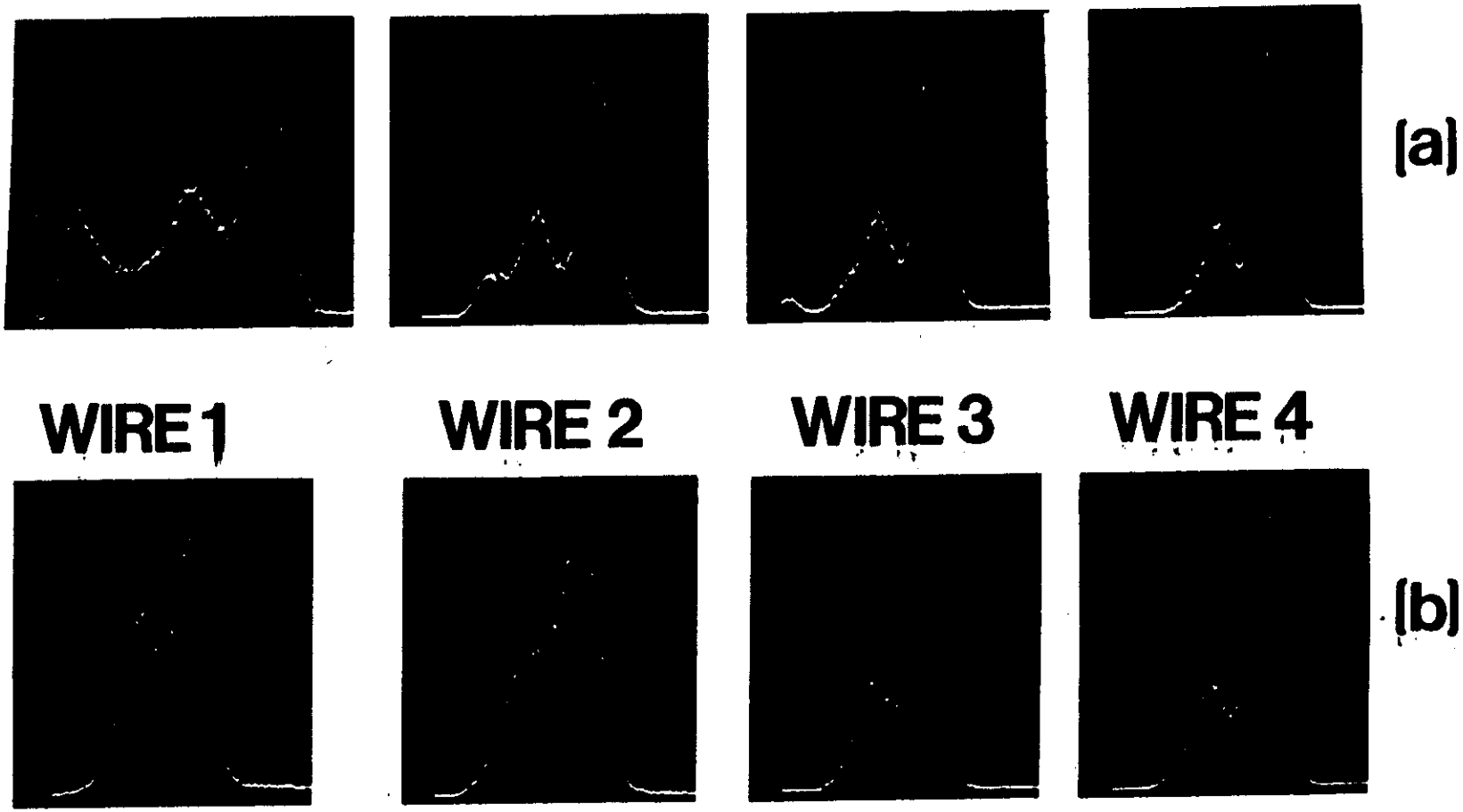

FIG. 4.9

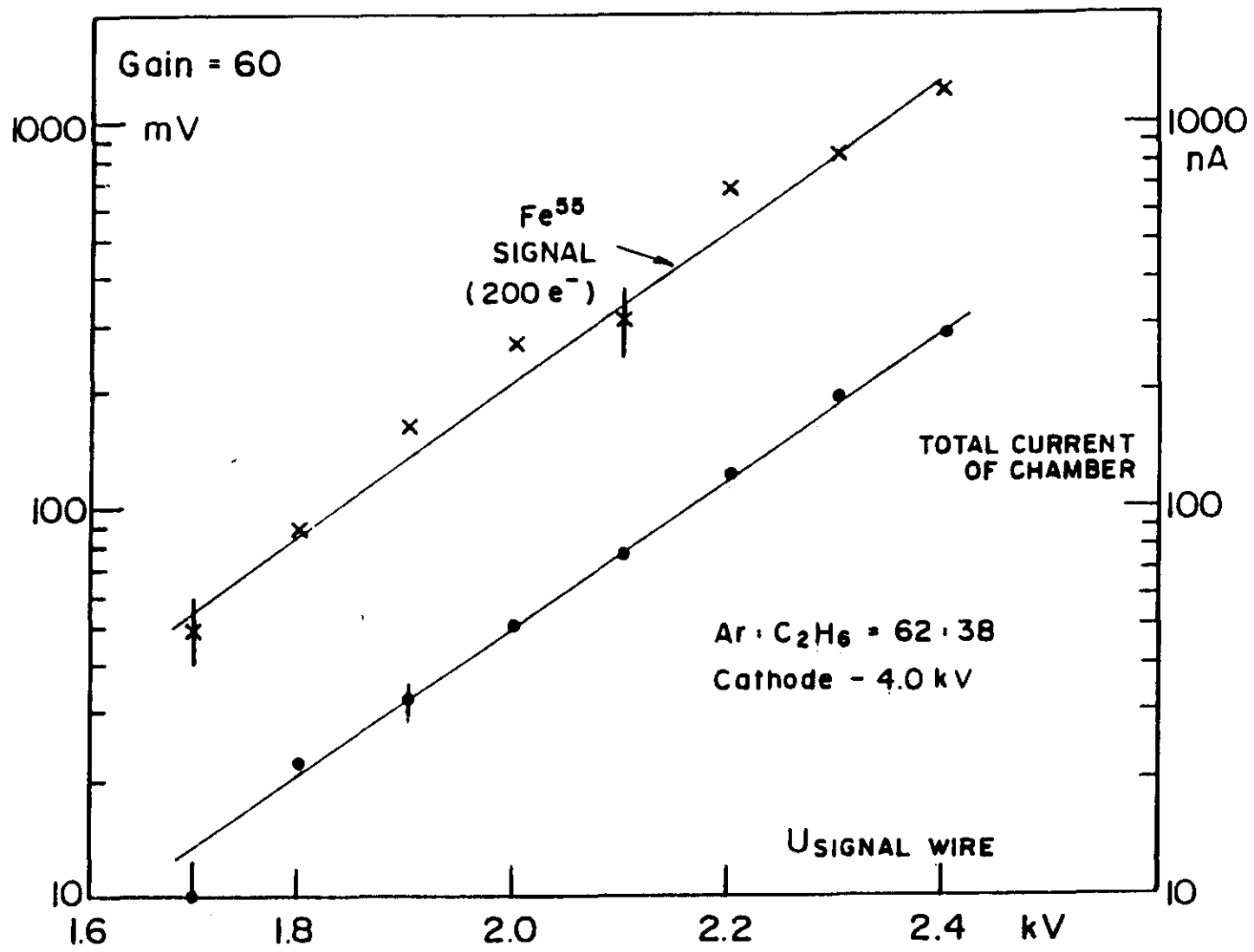
Gain = 60
1000
mV
100
10
1000
nA
100
10
Fe55
SIGNAL
(200 e−)
TOTAL CURRENT
OF CHAMBER
Ar : C2H6 = 62 : 38
Cathode − 4.0 kV
USIGNAL WIRE
1.6
1.8
2.0
2.2
2.4
kV

FIG. 4.10

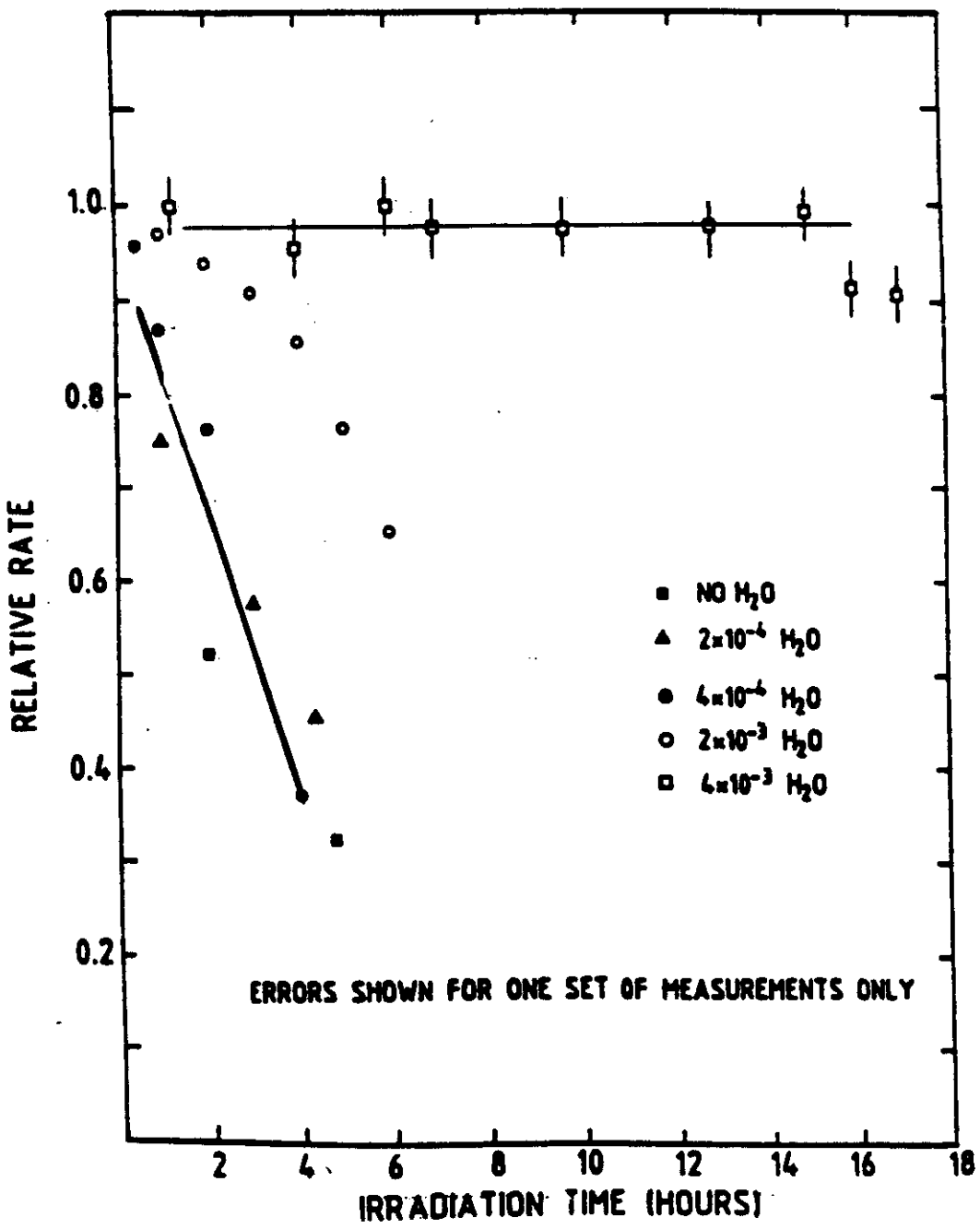
RELATIVE RATE
1.0
0.8
0.6
0.4
0.2
2
4
6
8
10
12
14
16
18
IRRADIATION TIME (HOURS)
NO H_2O
2×10^{-4} H_2O
4×10^{-4} H_2O
2×10^{-3} H_2O
4×10^{-3} H_2O
ERRORS SHOWN FOR ONE SET OF MEASUREMENTS ONLY

FIG. 4.11

L3 Muon Chambers P Gas System.

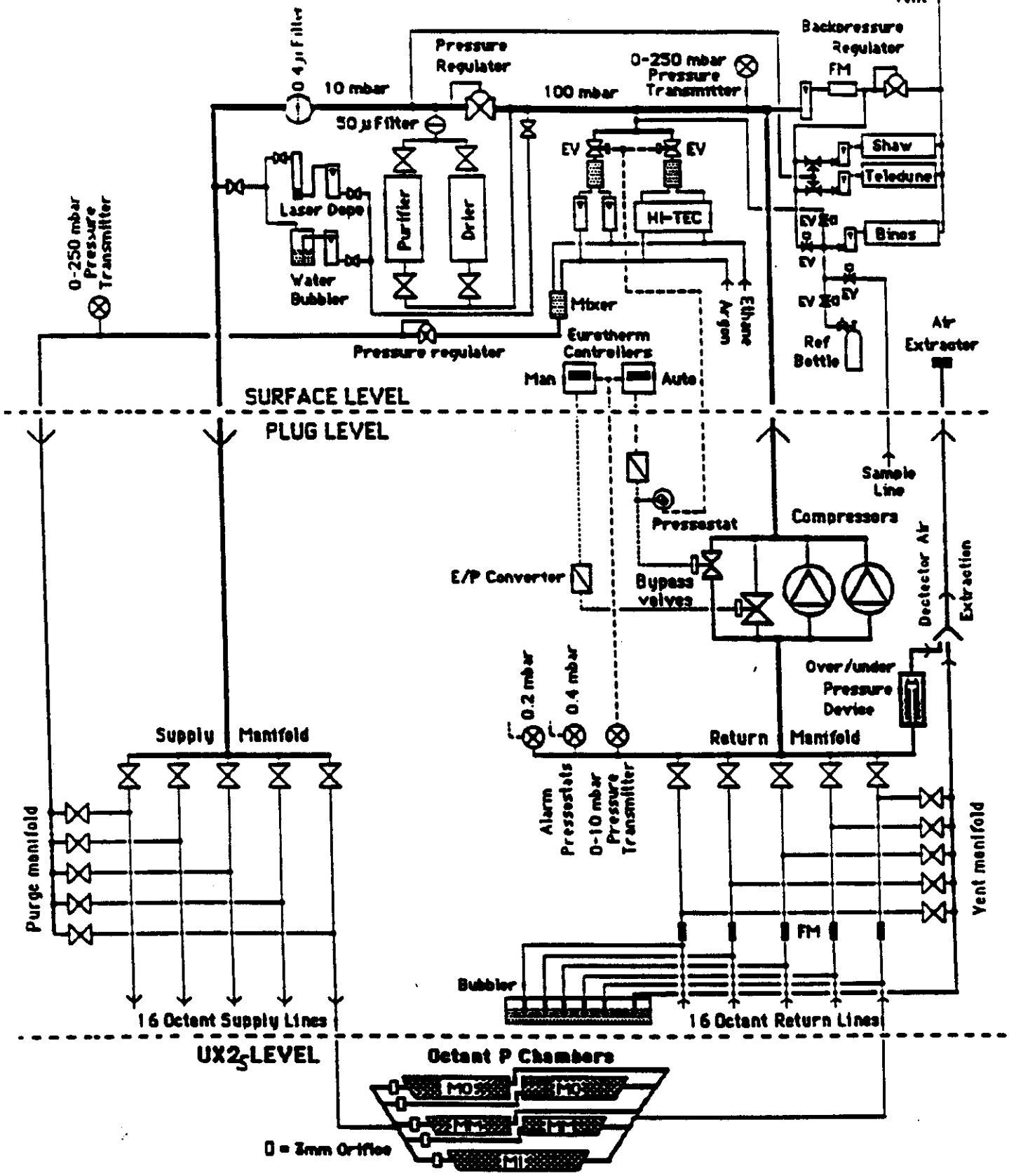

FIG. 4.12

STABILITY OF ARGON-ETHANE MIXTURE

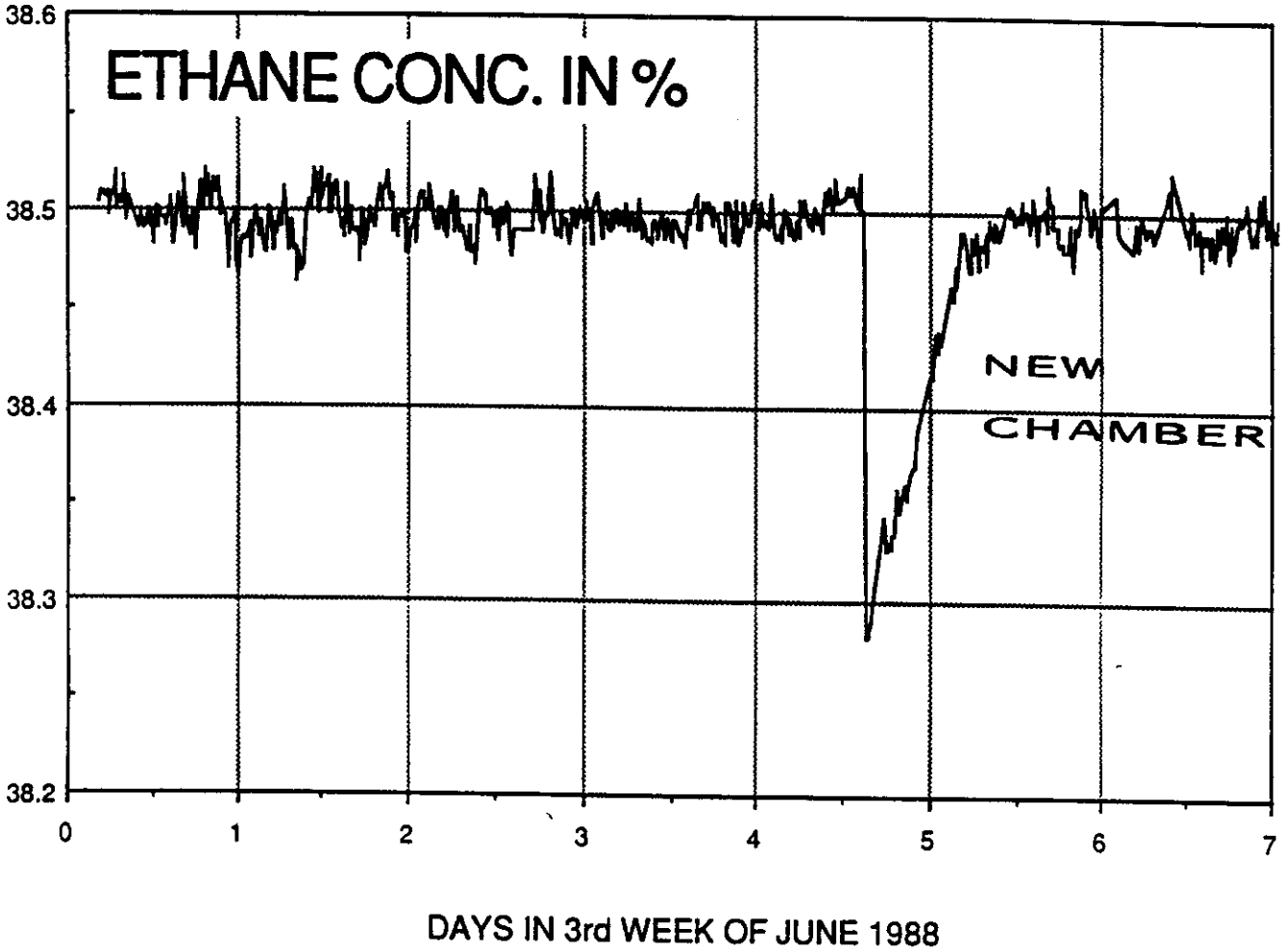

FIG. 4.13

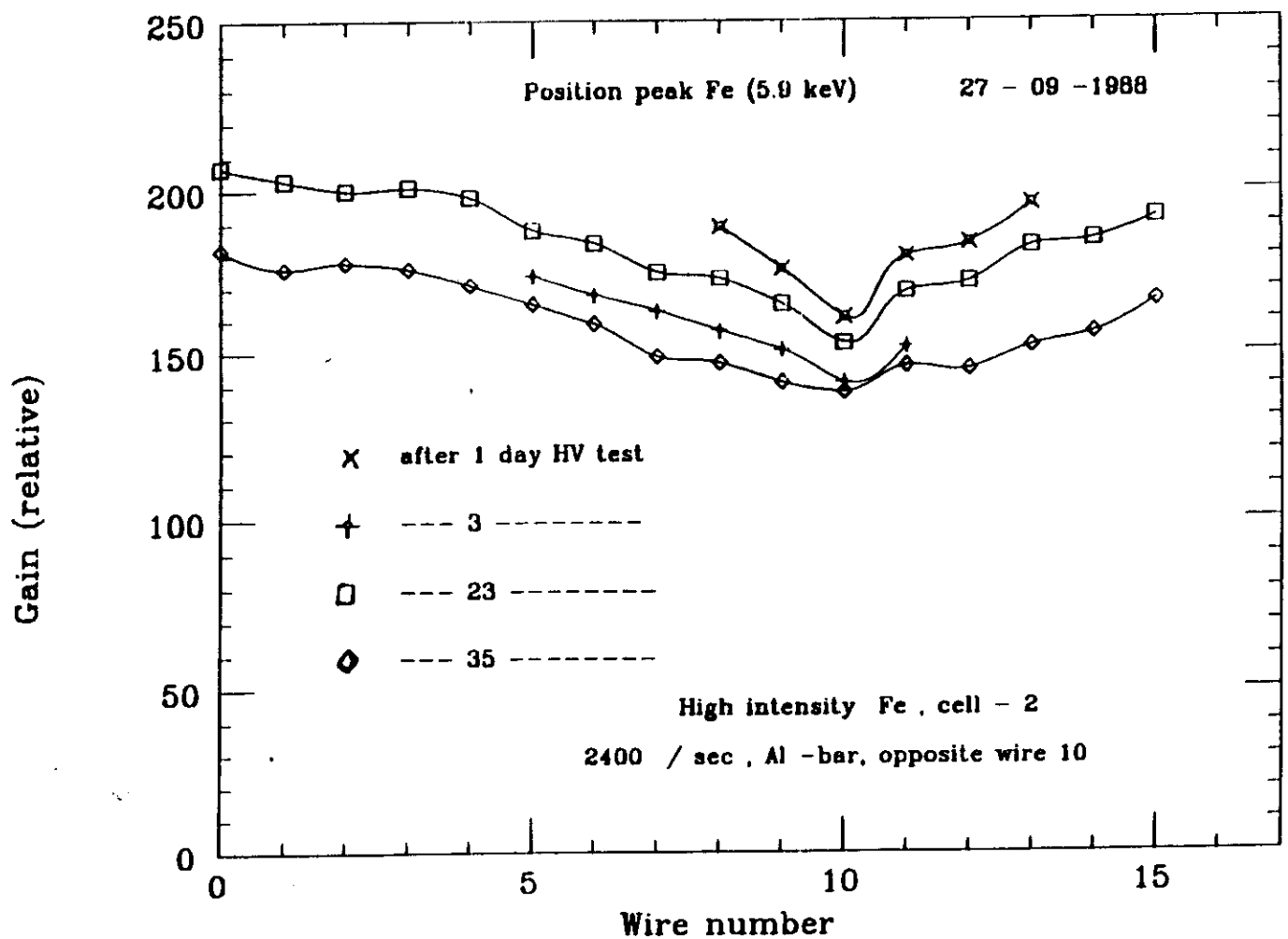
Position peak Fe (5.9 keV)
27 - 09 -1988
after 1 day HV test
--- 3 ---
--- 23 ---
--- 35 ---
High intensity Fe , cell - 2
2400 / sec , Al -bar, opposite wire 10
Gain (relative)
Wire number
250
200
150
100
50
0
0
5
10
15

FIG. 4.14

Marker = 1 μ

X 20000

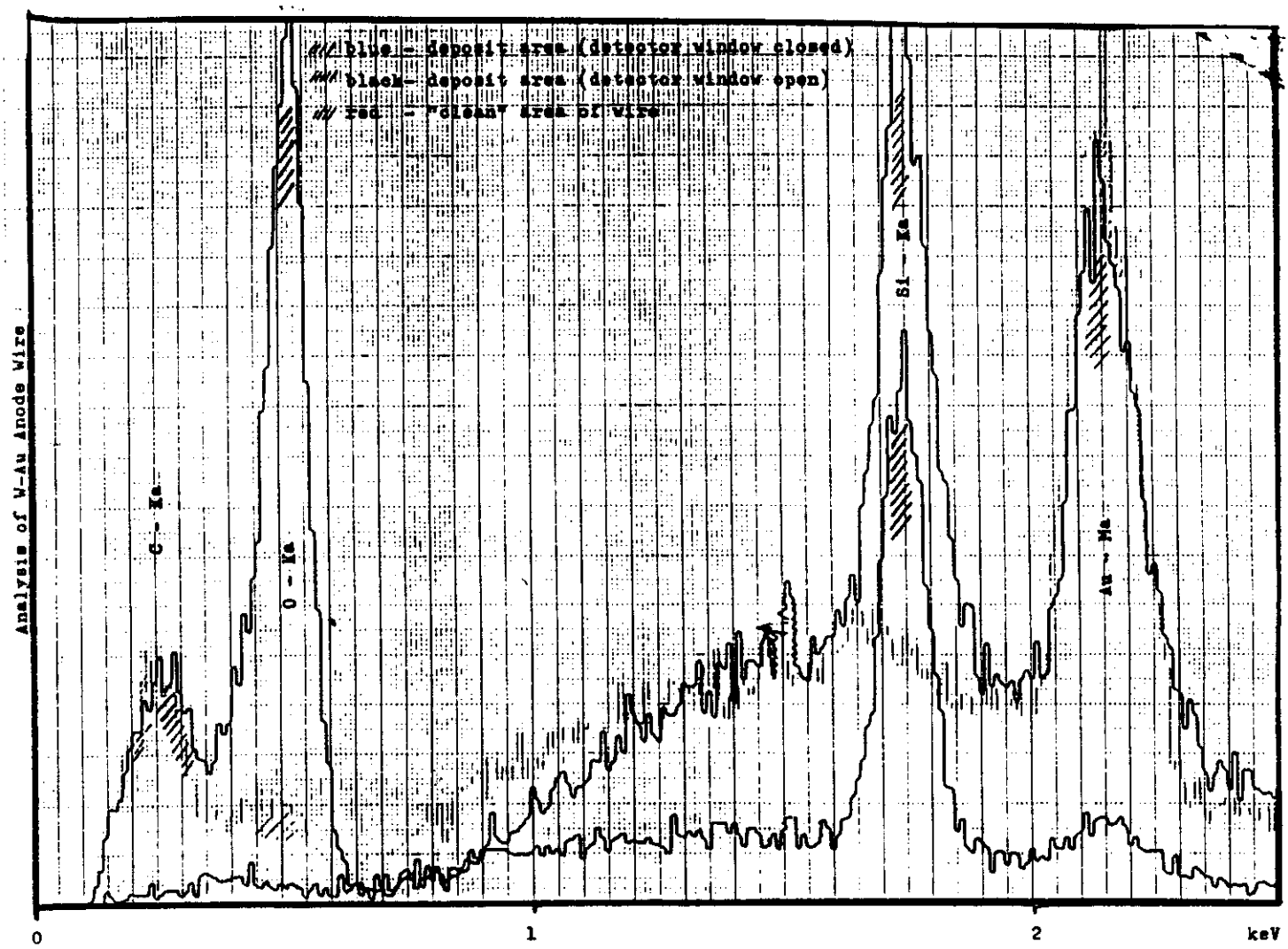

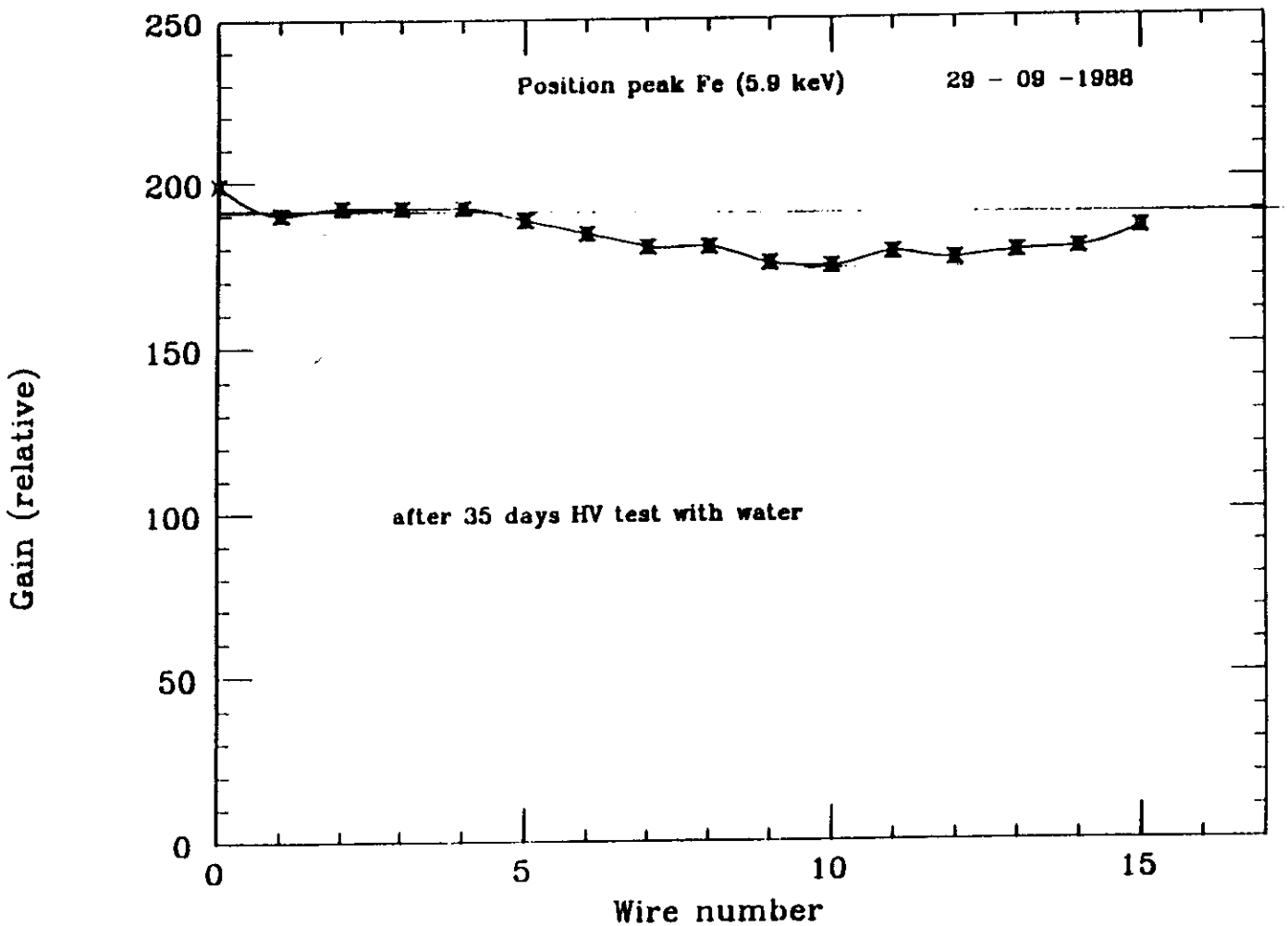
Position peak Fe (5.9 keV)
29 - 09 -1988
after 35 days HV test with water
Gain (relative)
Wire number
250
200
150
100
50
0
0
5
10
15

FIG. 4.16

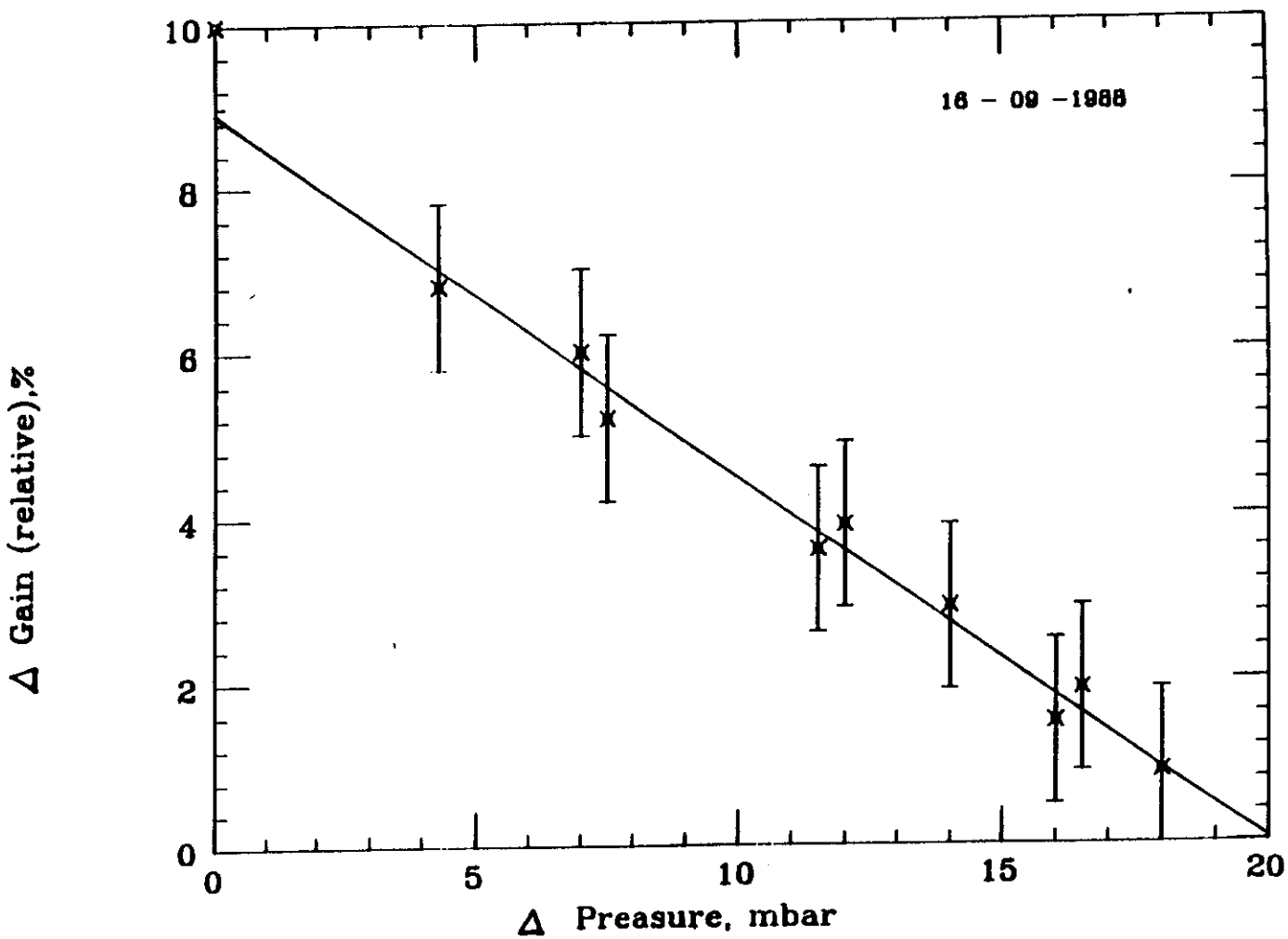

FIG. 4.17

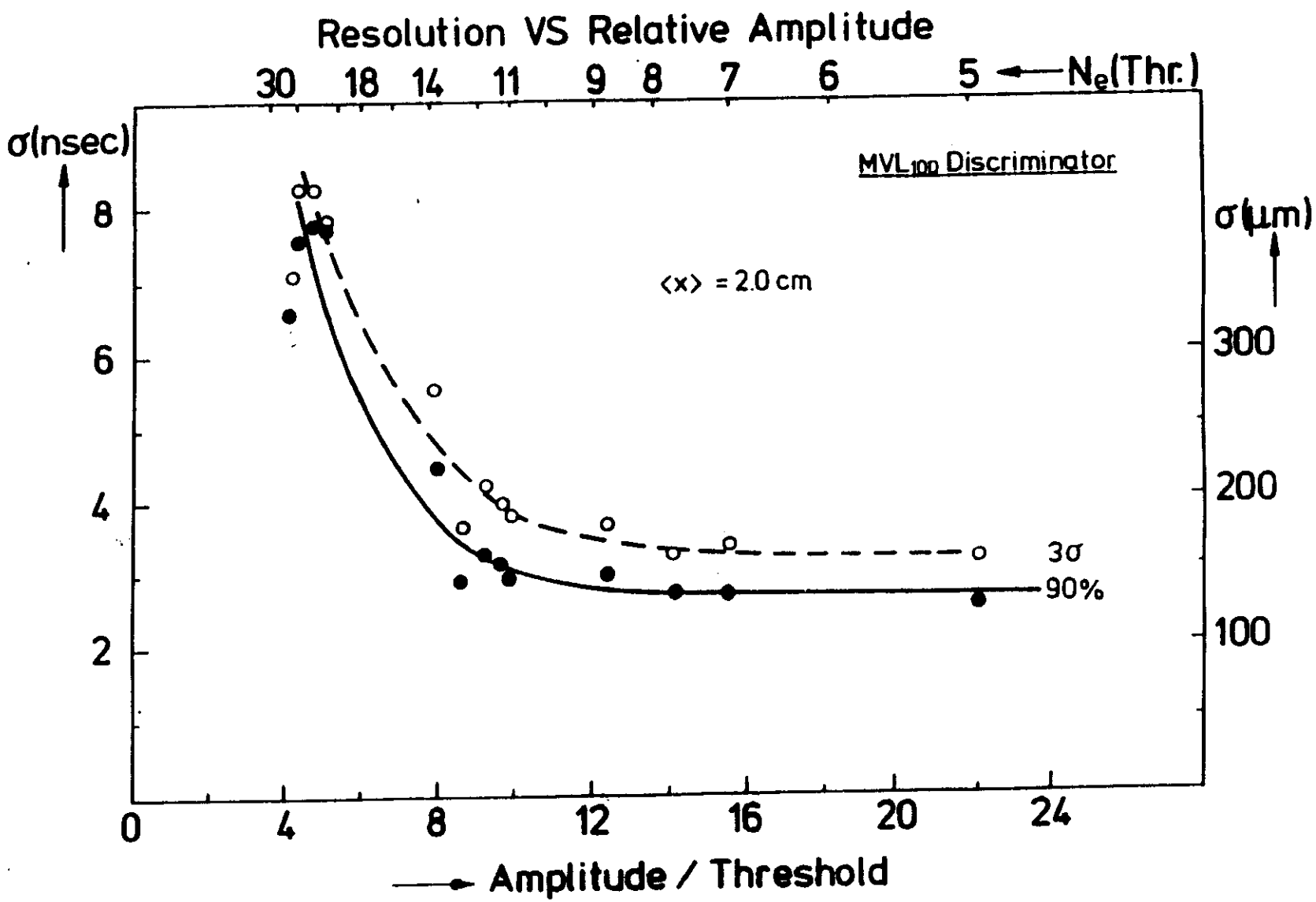
Resolution VS Relative Amplitude
30 18 14 11 9 8 7 6 5 ← Ne(Thr.)
σ(nsec)
8
6
4
2
MVL100 Discriminator
<x> = 2.0 cm
σ(μm)
300
200
100
3σ
90%
0 4 8 12 16 20 24
→ Amplitude / Threshold

FIG. 4.18

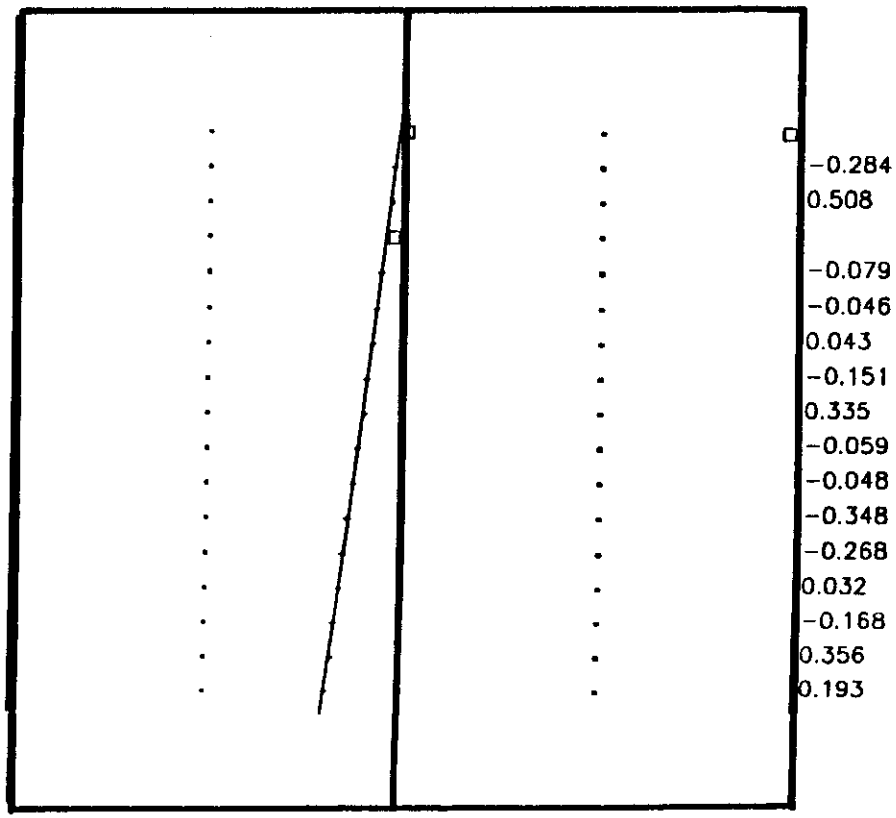
-0.284
0.508
-0.079
-0.046
0.043
-0.151
0.335
-0.059
-0.048
-0.348
-0.268
0.032
-0.168
0.356
0.193

FIG. 4.19

COSMIC MUON RESOLUTION

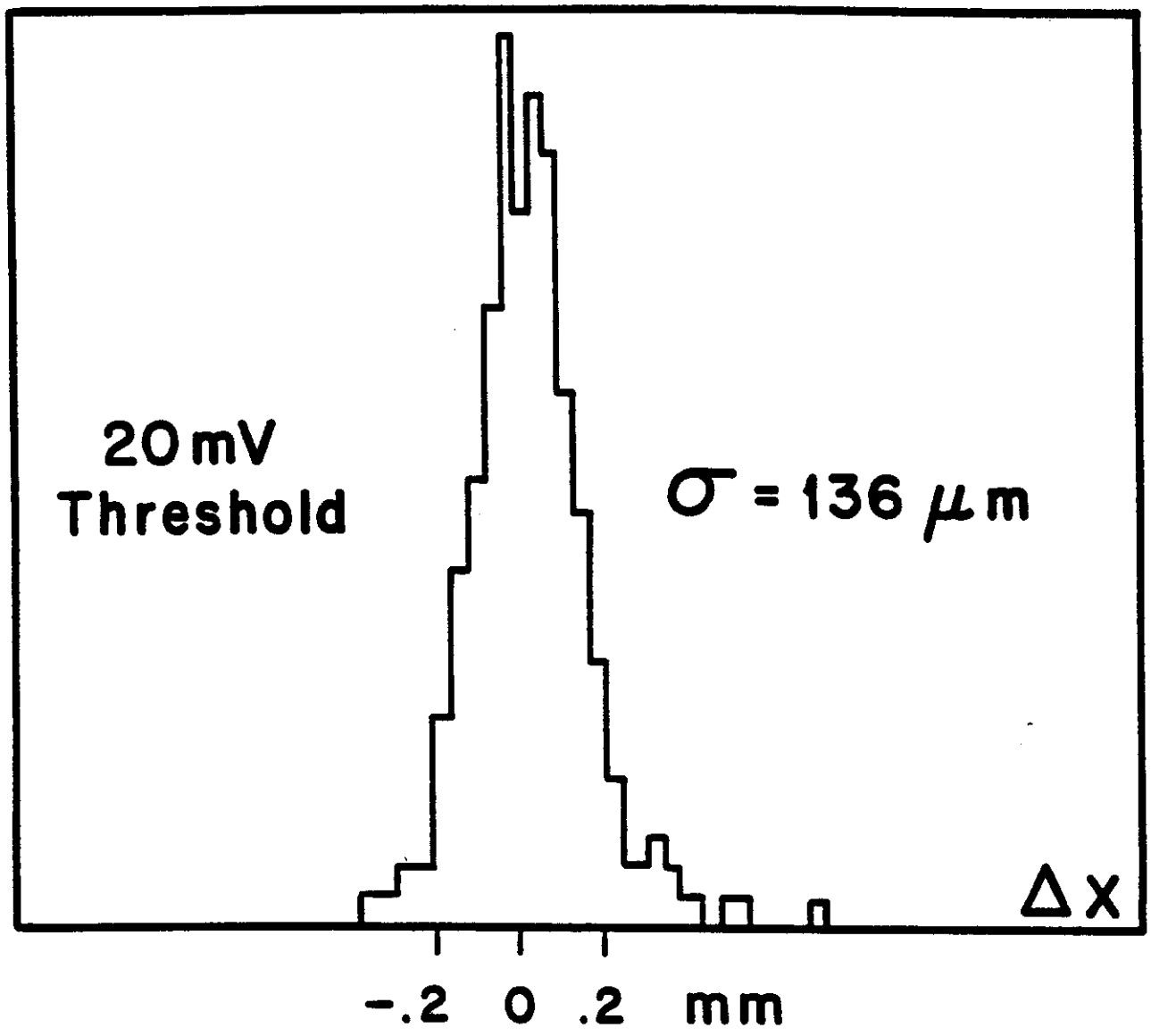

FIG. 4.20

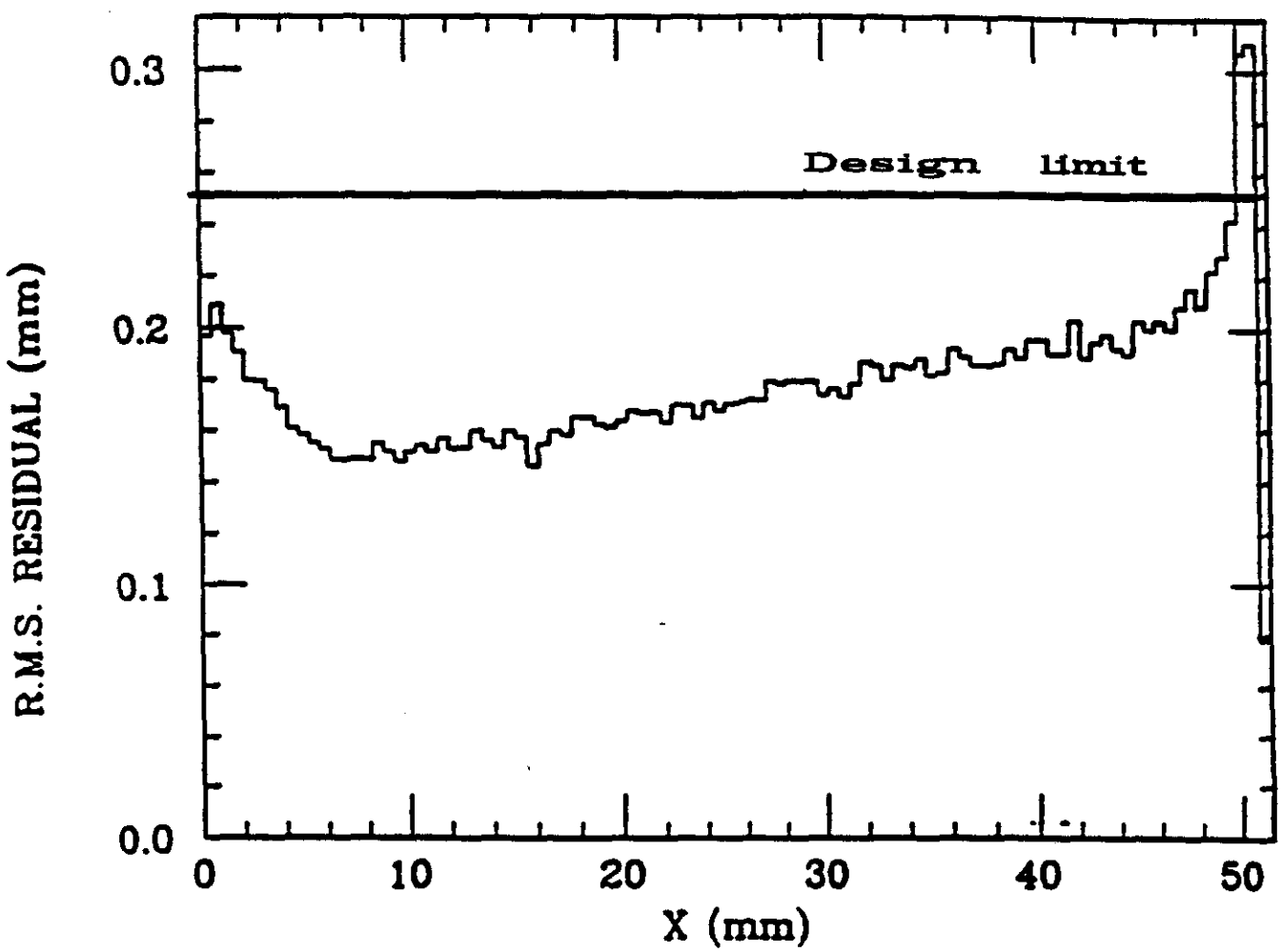

FIG. 4.21

Run #***** Event # 3003 Total Energy: 0.00 GeV

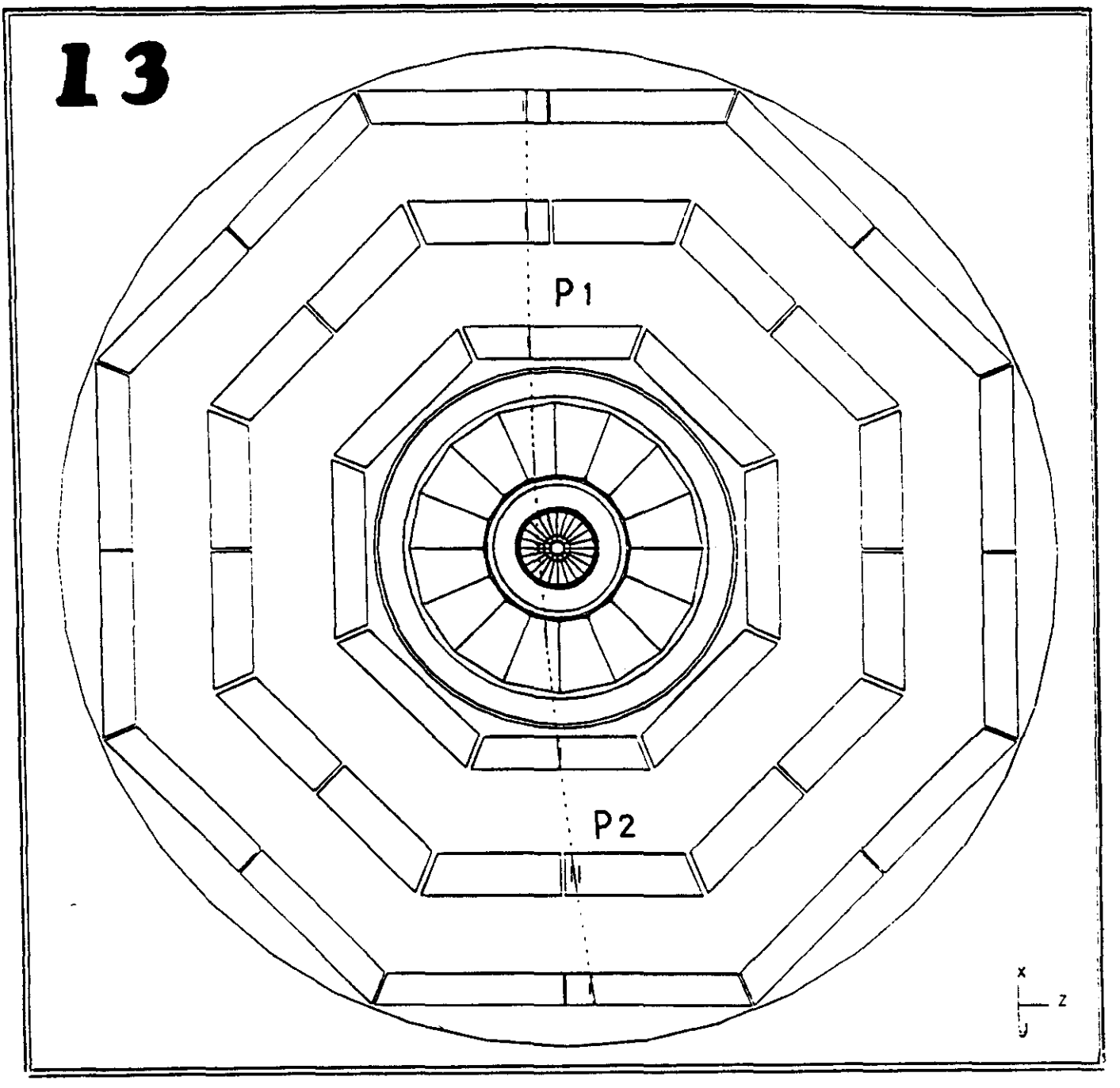

July 24th 1989

COSMIC

P1 = 14,5 GeV
− P2 = 9.1 GeV
= expected E Loss in U Calorimeter

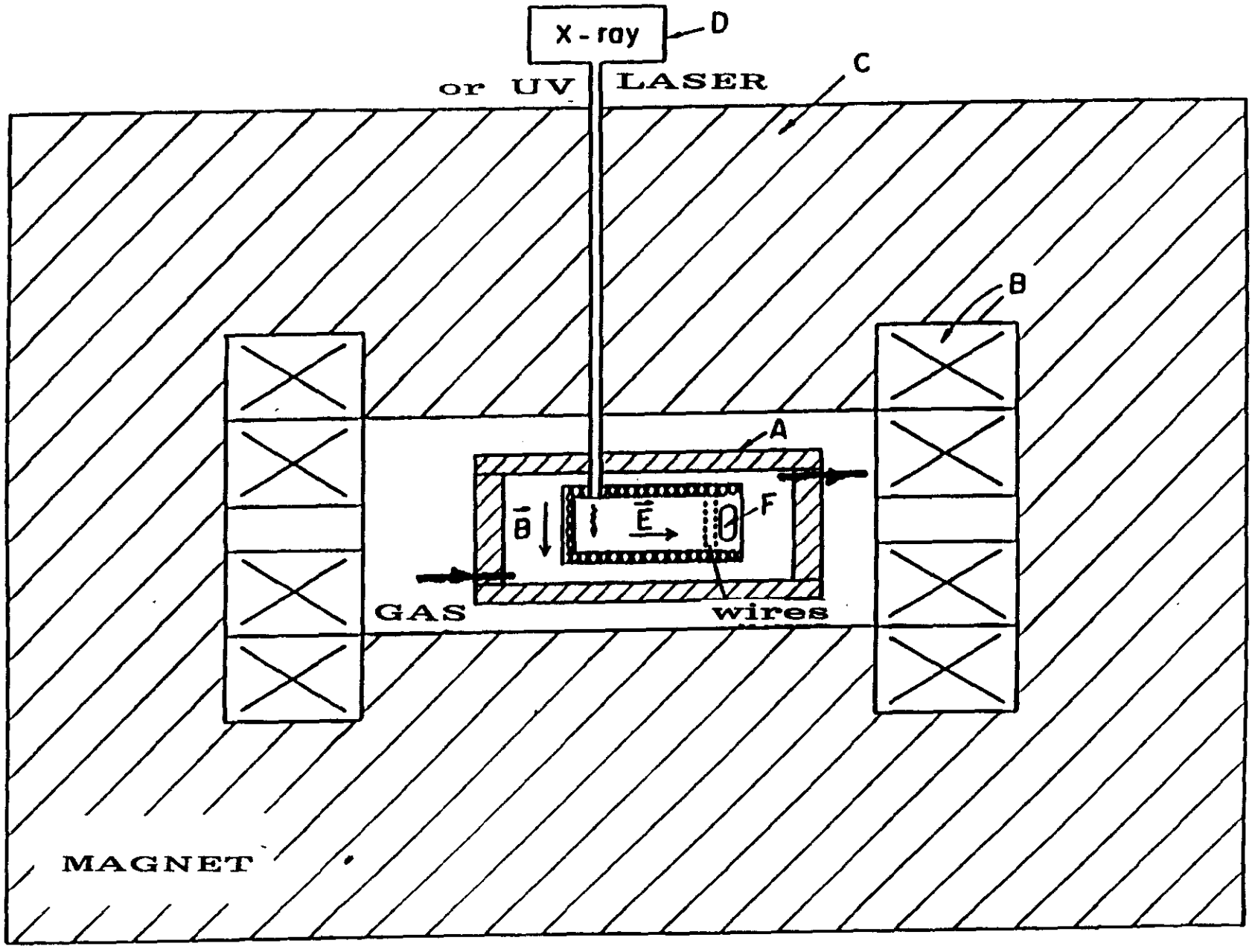

FIG. 4.23

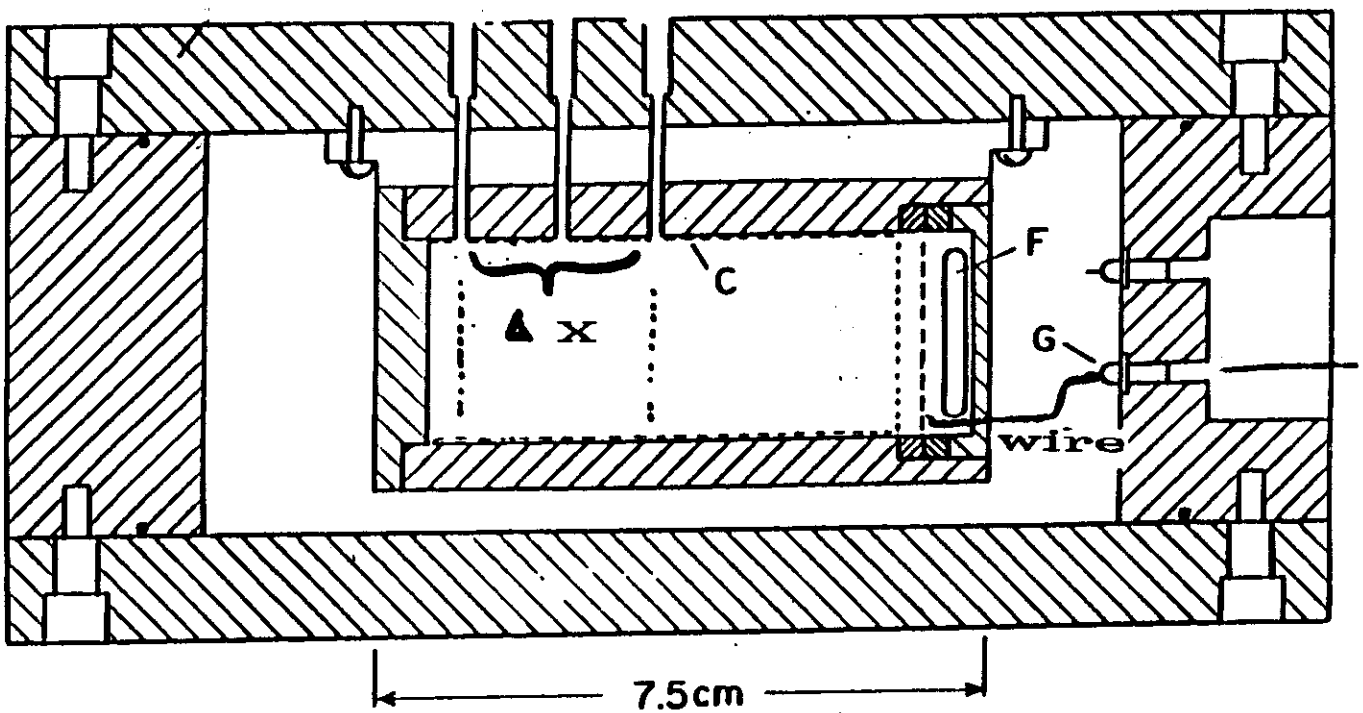

FIG. 4.24

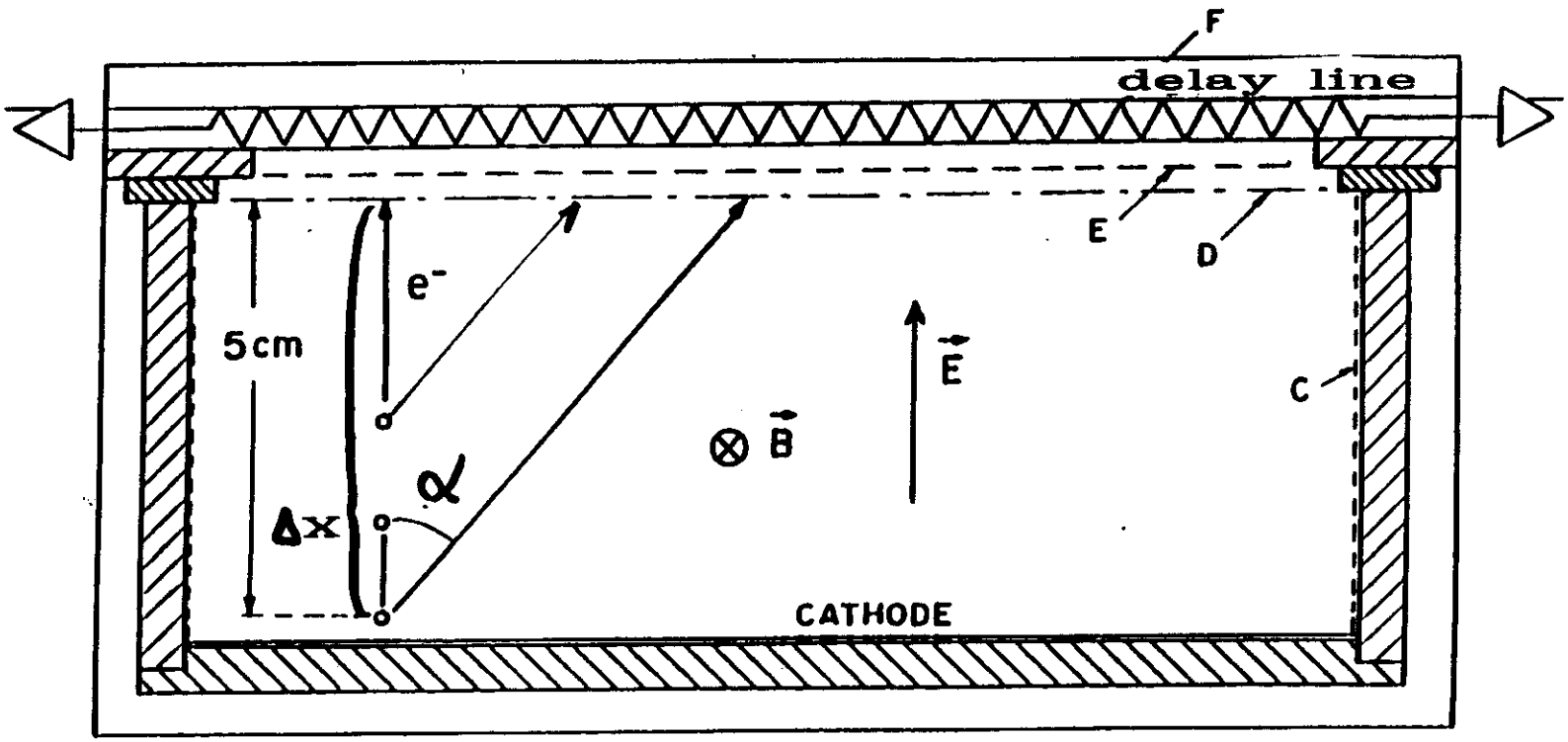

FIG. 4.25

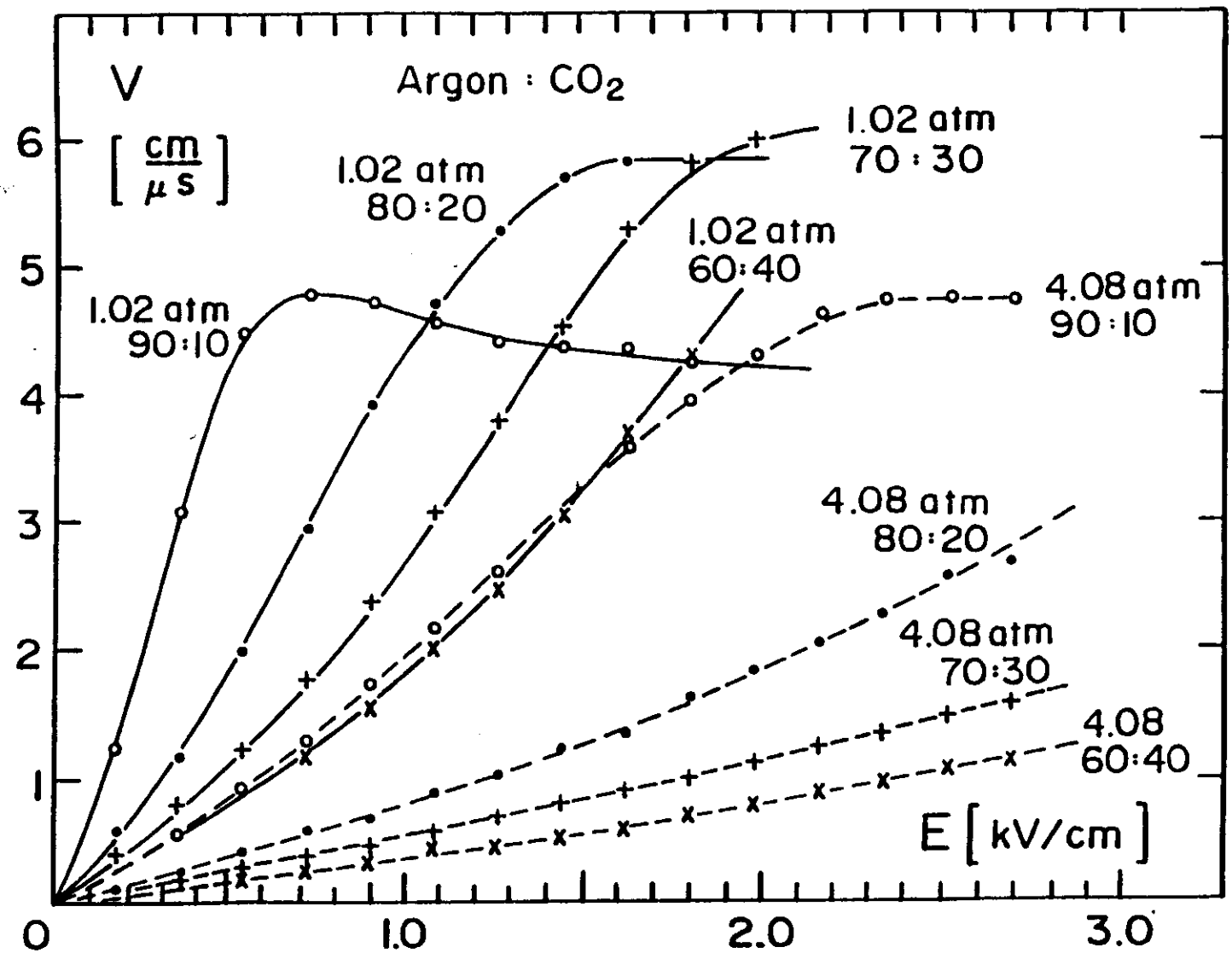

DRIFT VELOCITY vs ELECTRIC FIELD

FIG. 4.26

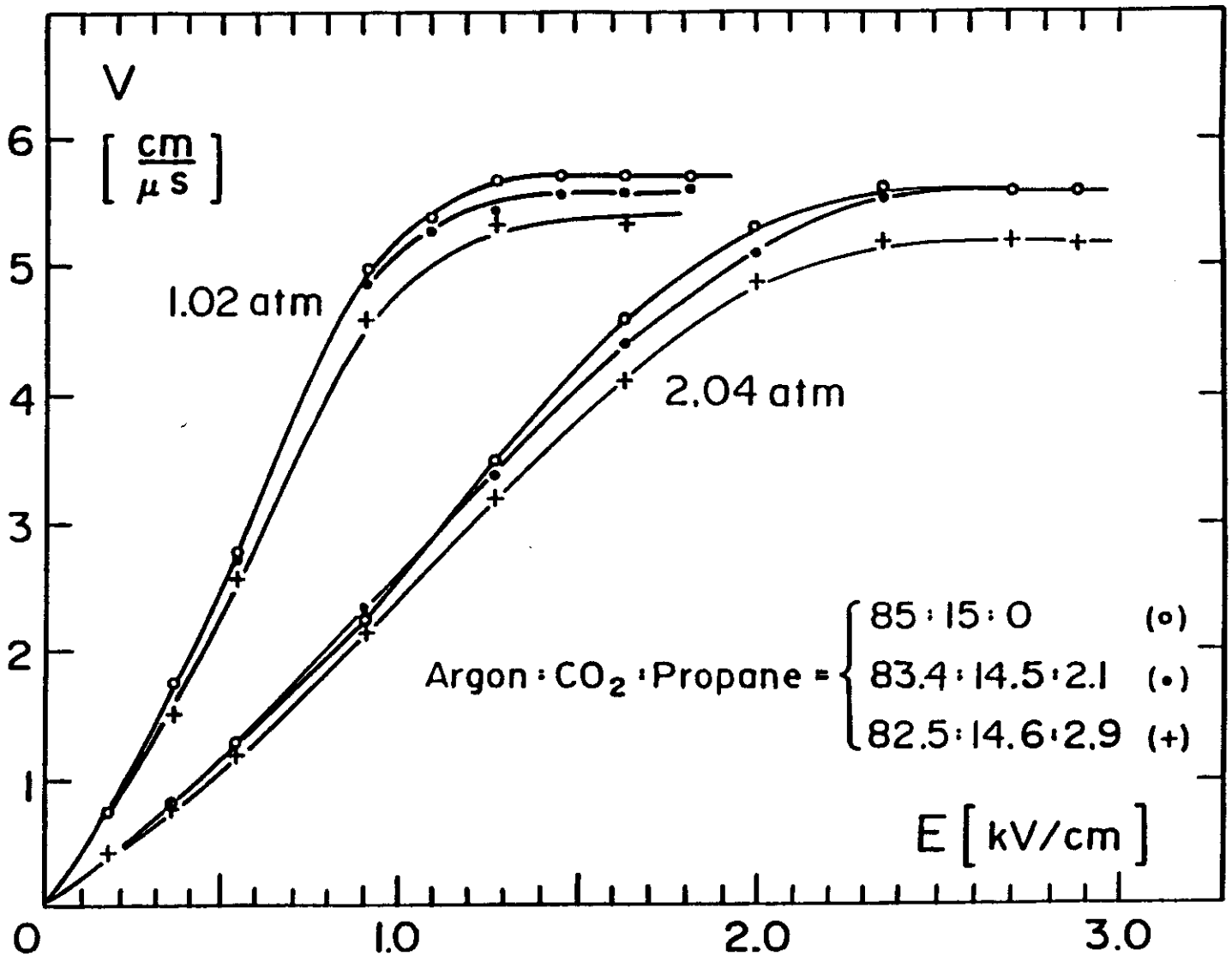

DRIFT VELOCITY vs ELECTRIC FIELD

FIG. 4.27

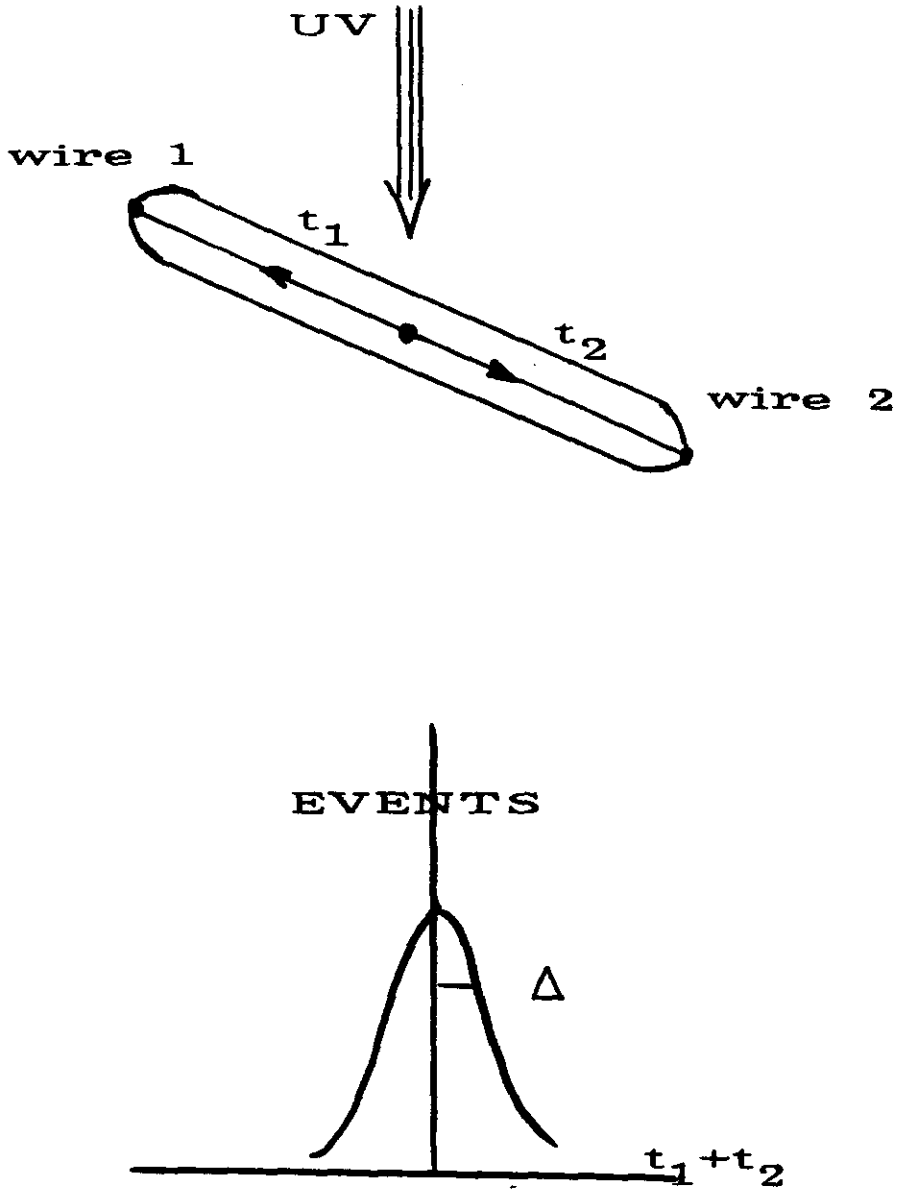

FIG. 4.28

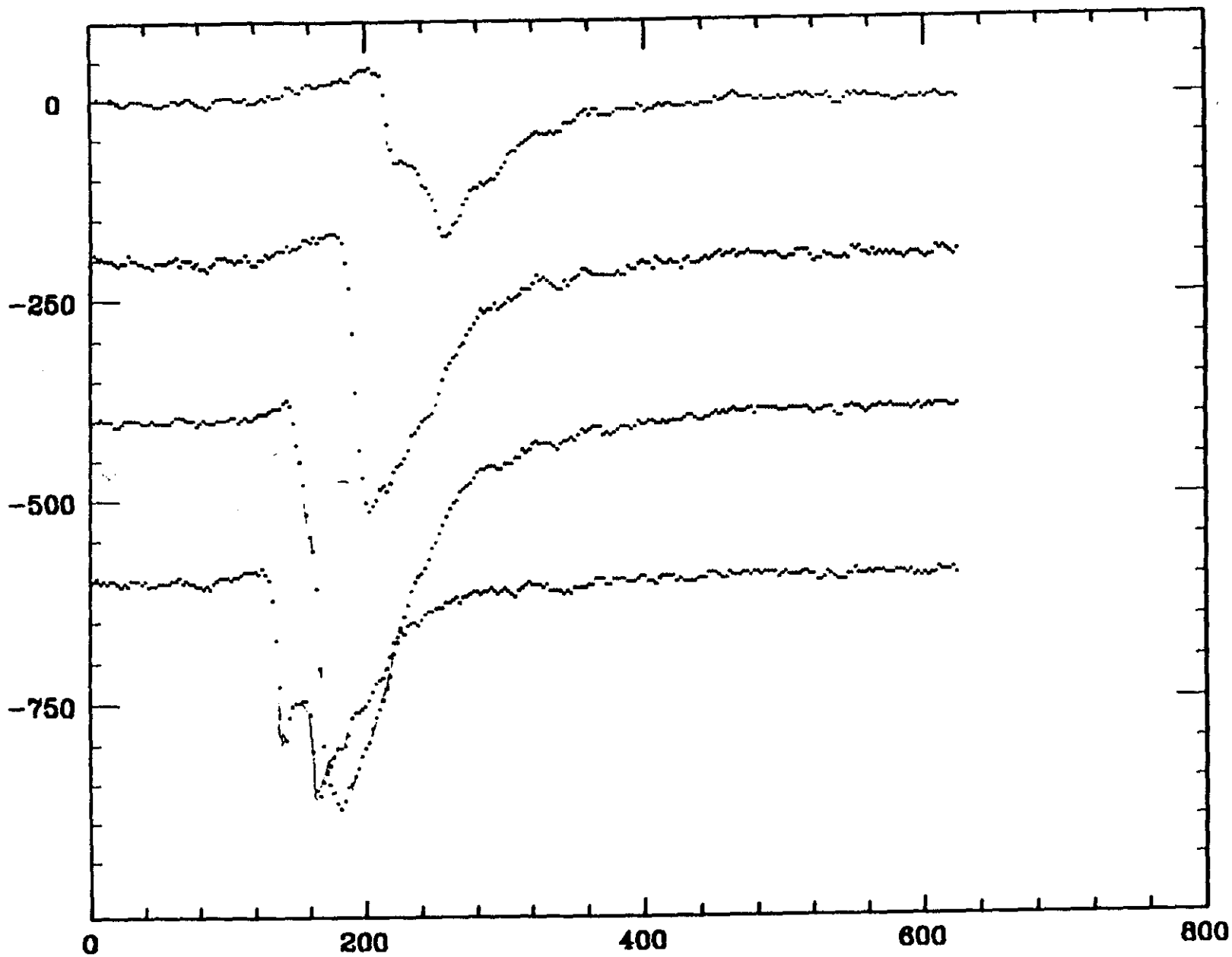

FIG. 4.29

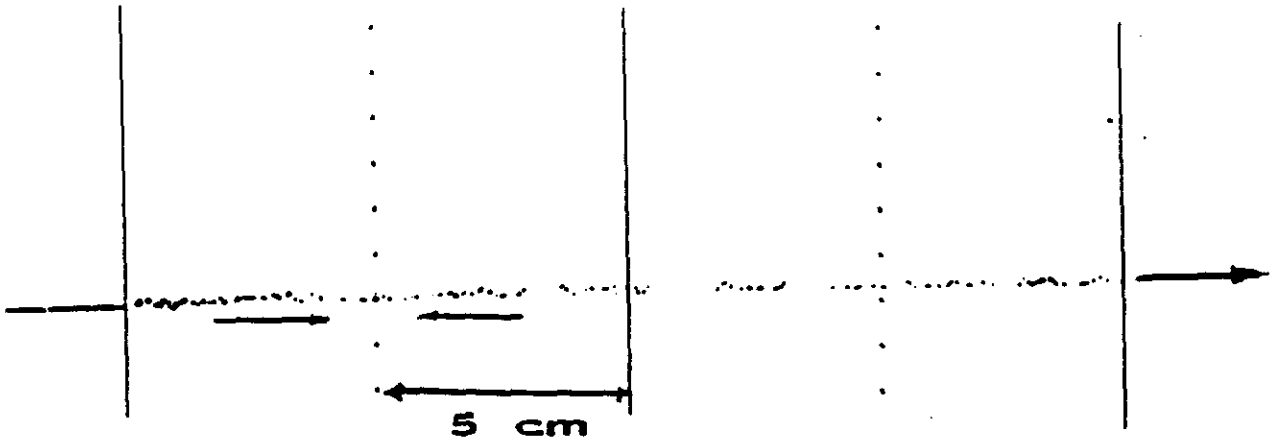

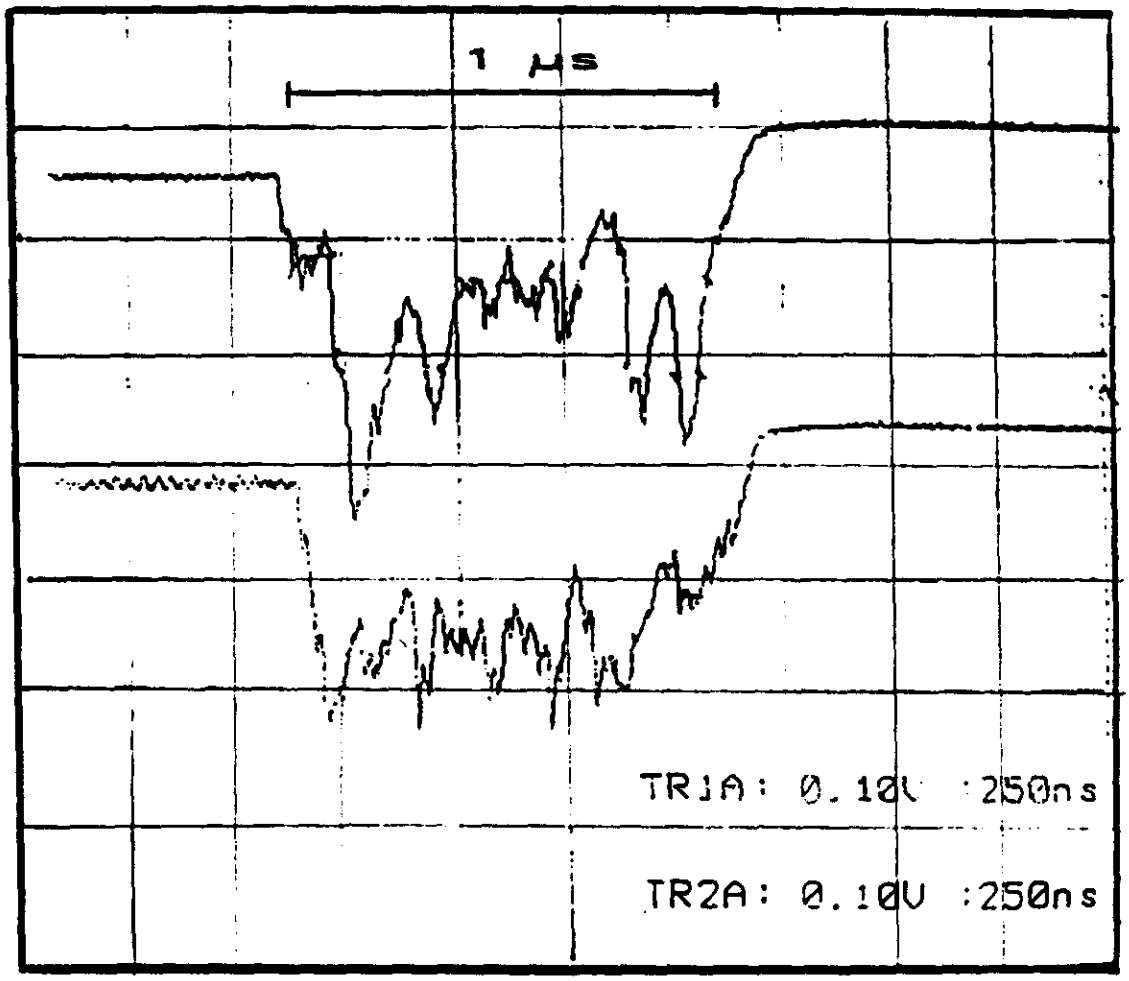

FIG. 4.30

CHAPTER V

RESEARCH AND DEVELOPMENT FOR THE SUPPORT AND ALIGNMENT OF MUON CHAMBERS AT THE SUPERCONDUCTING SUPER COLLIDER

G. Gratta, D. Kirkby, R. Mount, H. Newman
California Institute of Technology, Pasadena, CA
L. Wilk
Charles Stark Draper Laboratory, Cambridge, MA
D. Duchane, W. Kinnison, W. Miller, G. Sanders, H. Ziock
Los Alamos National Laboratory, Los Alamos, NM
J. Burger, D. Luckey, C. Grinnell, S.C.C. Ting
Massachusetts Institute of Technology, Cambridge, MA
R. Beckers, H. Cohn, A. Gabriel, J. Johnson
Oak Ridge National Laboratory, Oak Ridge, TN
J. Branson, I. Sheer.
University of California, San Diego, CA

Contact Person : C. Grinnell

A precision muon chamber is only useful if it can be supported and aligned precisely. This chapter is divided into three sections : structural design, structural analysis and alignment system. The support for the R & D on alignment system will be provided by the Swiss Commission for the Advancement of Scientific Research.

5.1 Structural design

a) The need for research and development in the structural design

The L3 structural designs were, in general, extremely satisfactory. The SSC muon detector is a necessary change of scale from our experience with L3 due to the substantially different environment at the SSC. Increased distances in the radial direction, needed to increase the track bending length, necessitate structural support over roughly twice the distance. Increased distances along the beam axis, needed for solid angle coverage in the forward direction, imply longer muon chambers and supporting structures. Finally, the overall increase in required precision of the alignment of the muon spectrometer equates to a higher degree of required structural stability.

Many complex problems arise with the substantial changes in dimensions and required precisions going from L3 to the SSC muon detector. Research into the feasibility of various conceptual designs will lead to a large, multifaceted, structural design development program.

b) Structural design considerations

The extreme mechanical accuracy required in positioning muon chamber sense wires is a primary, performance consideration for accurate muon momentum resolution. In order to meet performance goals, the following items of concern dictate the structural design of the muon chambers and the supporting structures :

1) The elastic nature of the structure
2) Stability against long term creep
3) Positioning accuracy and repeatability
4) Materials selection
5) Safety factors
6) Perturbations in the magnetic environment
7) Reliability and quality control
8) Construction and maintenance/repair
9) Cost Effectiveness

c) L3 structural design review

The L3 structural designs [5.1], and prototype support structure construction, were done by the Charles Stark Draper Laboratory (CSDL) of Cambridge, Massachusetts.

In L3, a single monolithic structure containing all eighty muon chambers was abandoned at an early stage. Considerations of cost effectiveness, fabrication, assembly, maintenance, and alignment adjustment requirements led to a modular design. The L3 muon barrel region structural design consists of the following three main structural elements as shown in App. I, Fig.10:

1) <u>A central "support tube"</u> is positioned along the longitudinal axis of the magnet and supported at its extremities on pillars mechanically isolated from the magnet. The support tube contains the calorimeters and vertex chamber on the inside, and supports externally the muon detector assembly.

2) Two "torque tubes" are mounted on rails on the outside of the support tube. These elements are the intermediate supports between the muon chamber modules and the support tube.
3) Sixteen high precision muon chamber modules, called "octants", are mounted on the two torque tubes. Each octant containing five muon chambers covering one eighth of the radial section and half of the distance along the beam axis.

The L3 structural design proved to be an extremely satisfactory solution to requirements of high precision and stability over large areas. The chamber mechanics successfully positioned the sense wires within each volume to meet the alignment specifications as verified by UV Laser and cosmic ray calibration (refer to Appendix I). Proper materials specification met all requirements for magnetic characteristics, safety requirements, and long term stability [5.1]. All octants were adjusted to meet alignment goals in a special fixture at their design orientation as shown in App.I, Fig.21. All octants were also verified in this fixture for elastic deformation characteristics (see App.I, Fig.22) and alignment repeatability. The flawless and efficient construction and installation of the octants in the experimental area attests to the success of the modular structural design.

Fig.29, Appendix I summarizes the success of the L3 structural designs. By meeting and exceeding all mechanical design specifications, muon chamber modules covering roughly $1000m^3$ ($35300\ ft^3$) of fiducial volume in the detector can resolve the sagitta of muons with an accuracy of 30μm (1mil.).

d) A proposed SSC muon chamber support structure design

The continuity of personnel involved in the development of L3, now turning their experience toward the SSC, is particularly beneficial in these initial stages of conceptualizing a successful detector. Referring to Chapter 2, and Figs.2.3 and 2.4, we find the SSC muon detector geometry. The following is a description of the structural support designs for this geometry.

We propose that the support of the muon chambers in both the central and forward regions consist of frames designed to minimize the volume of material. All proposed designs must be studied for compliance with the guidelines presented in section 5.1.b.

Fig.5.1 shows an elevation of the central region muon detecting module. The supporting frame consists of long bars, running the length of the chambers in Z, connected by diagonal members forming a truss. This structure covers both sides of the module, the two sides tied together by cross bars.

Fig.5.2 shows sections E-E and G-G of the central frame (see Fig.5.1). These sections show the structural elements which give the frame its rigidity in bending about the Z axis. The horizontal bars contain the attachment points of the muon chambers.

Fig.5.3 shows section F-F of the central frame (see Fig.5.1). Mid-way along the length of the chambers it is necessary to have no material infringing on the measuring volume of the chambers. The long supporting bars running the length of the chambers, and the truss members covering the sides of the module, must remain outside this volume.

The global support of each module in the central region is performed as shown in Fig.5.4. Large elements are rigidly attached to the magnet crown and the central calorimeter supporting plate. They take the load of the central region modules. These elements extend to the top four corners of the module between the outer chambers as shown in Fig.5.5.

The support structure for the forward muon chambers inside the solenoid is envisaged to be conceptually similar to the central region. The frame will be a truss structure which is supported at the magnet door end by the same supporting elements as the central region. The inner extremity of the module will be supported by the calorimeter support tube. Fig.5.6 is a preliminary sketch of the support structure of the muon chambers in the forward region inside the solenoid.

e) Scope, schedule and milestones of R & D for the structural design

Accurately estimating the amount of effort and time to realize a project of this scale is crucial to its success. Our projections for the SSC are based in our experience with L3.

The structural design of the SSC muon detector lends itself easily to a division into two basic areas of emphasis: the central and forward regions.

The central and forward regions are distinctly different structural design problems requiring two separate efforts closely coordinated for efficient communication and application of ideas and developed technologies.

The goal of the structural design R & D program is the comprehensive analysis and design of the muon chamber support structure in both the central and forward regions. In addition, support for the analysis and design of the muon chambers themselves is foreseen. The development of the structural design in the central and forward regions would involve three sections which must be advanced in parallel.

Section 1 : Module Definition

The first task in each of the two regions is to define the module boundaries based on stability, assembly, alignment, and maintenance/ repair considerations. At this point the basic structural form of the muon chambers (see muon chamber R & D, Chapter 3), the chamber support structures, the chamber to structure interface, and the alignment schemes (see alignment systems R & D, section 5.4) must be outlined. A first approximation of the module definition for the central region, and forward region inside the solenoid, has been completed and presented in Figs.2.3 and 2.4.

Section 2 : Muon Chambers

The development of the muon chamber structural design concentrates on the materials selection, enclosure geometry (see structural analysis, section 5.3), and wire supporting and adjusting systems. The development of the chamber structural design is in support of the general muon chamber research and development program outlined in Chapter 3.

Section 3 : Support Structures

The development of the muon chamber support structures concentrates on the materials selection, main structural element specification (see structural analysis, section 5.3), and the designs of the interfaces at the muon chambers/support structure, and global supporting elements/ support structure. Special attention must be given to the installation and maintenance/repair requirements of the muon chambers as well as the careful incorporation of alignment systems into the structure.

The structural design R & D program for the muon detector is directly linked to the structural analysis R & D program (section 5.3), the muon chamber R & D program (Chapter 3) and the alignment systems R & D program (section 5.4). Also, the structural design group must interact with many other groups working on the detector. An engineering coordinator (see Chapter 6) will be responsible for the interface between the structural design group and the following R & D efforts:

- Structural Analysis R & D
- Muon Chamber R & D
- Alignment Systems R & D
- Data Transfer R & D
- Magnet R & D

In addition, the engineering coordinator will be at the interface between the structural design group and any SSC Laboratory supported groups concerned with services and the experimental area.

The R & D on the structural design for the SSC muon detector is a three year program. The final product of this program will be full-scale, working prototypes which will verify the structural design in every detail before production. The first year will concentrate on feasibility studies of different structural design concepts. The milestone for the first year will be to freeze the designs with regard to major conceptual changes such that detailed designs can begin in the second year. The detailed designs will be completed in the first half of the second year. The milestone for the second year will be the fabrication of all hardware for the prototypes. The milestone in the third year will be the completion of assembly and rigorous assessment of the prototypes.

f) Request for support of the structural design R & D

The support of this program requires personnel experienced in the design of large area precision devices. The structural design research and development program will be carried out by the Charles Stark Draper Laboratory of Cambridge, Massachusetts under contract from MIT. Their success in the development of L3, coupled with their continued excellent reputation in the development of high precision mechanical systems, make them the unique choice.

The development of the detector structural designs must, above all, be consistent with our physics objectives. Support to this group in the way of critical physics input to guide the development of the designs will come from the following institute supported personnel :

California Institute of Technology : G. Gratta, R. Mount, H. Newman

Los Alamos National Laboratory : D. Duchane, W. Kinnison, W. Miller, G. Sanders, H. Ziock

M.I.T. : J. Burger, D. Luckey, S.C.C. Ting

Oak Ridge National Laboratory : H. Cohn, A. Gabriel

University of California, San Diego : J. Branson, I. Sheer

There will be additional engineering support in the development of the designs from Oak Ridge National Laboratory (ORNL) as their collaboration in the construction and assessment of prototypes is foreseen. The following engineers supported by ORNL will participate : R. Beckers, J. Johnson.

The financial request for the first year of the research and development program for the SSC muon detector structural designs is shown below. Chapter 7, Table V summarizes the estimates of the following years'requests. Partial times quoted for some personnel envisions the progressive formation of a group by the program manager.

Funding Request for FY90

(Estimate based on contract with Charles Stark Draper Laboratory)

	K$/M/yr*	Yrs.	Total K$
1 senior program manager (Len Wilk)	175	1.0	175
1 materials and fabrication specialist	150	0.75	113
1 structural design leader	150	0.9	135
2 designers	100	0.9	180
4 consultants	150	0.25	150
Travel			30
Total K$			**783**

* Personnel costs include all institute overhead charges

Funding request for FY91 and FY92 are summarized in Chapter 7.

5.2 Structural analysis

a) The need for structural analysis research and development

Any structural design of the scale and precision proposed necessitates the careful analysis of each mechanical element incorporated into the structure.

A detailed finite element analysis of the supporting structures, as well as the drift chambers themselves, is a necessary tool in prototype design and assessment. A proper analytical model using an industry standard program, such as NASTRAN (NAsa STRuctural ANalysis), yields critical information on mechanical performance, stress levels, deflection characteristics, and dynamic responses to transient loads.

After a final design has been fixed, additional detail can be added to the model in areas of particular structural interest. This makes the finite element model a very useful tool in the alignment of the modules. The results of the analysis can include effects of temperature changes and gradients on the alignment and alignment systems. An accurate knowledge of the deflections of the final system under different loading conditions allows substantial savings of time and manpower in the process of aligning the drift chambers.

It should be noted that a detailed structural analysis for detectors of this scale and precision will be necessary for nearly all SSC experiments.

b) L3 structural analysis review

The final computer model of a complete octant for L3 [5.1] is shown in Fig.5.7. The model contains all major structural components, the drift chambers, and all interfacing parts between the structure and chambers as well as between the structure and the external supports.

Before using the deflection information for L3 given by the program, a study was made to verify the accuracy of these predictions. One of the first of the production octants was placed in a fixture permitting its rotation to all of the final design orientations (see App.I, Fig.21). Extensive measurements of the deflections of the frame were made and compared with the program predictions. A sample of this comparison is shown graphically in Fig.5.8. The

deflections predicted by the NASTRAN agreed well with the measured values within the accuracy of the mechanical measurements which was ±25μm.

The alignment requirements for the chambers in L3 included their positioning at a precise radial position from the beam line with a specific degree of parallelism of the three layers. During initial assembly, the chambers were aligned within the octants in the radial direction at a vertical position using standard, gravity referenced, alignment tools. The accurate deflection information of the chambers in the radial direction at all orientations, given by the analysis, permitted us to properly pre-align each octant in the vertical position such that the chamber alignment specification would be met at the design orientation. Results confirmed the validity of this method thus greatly simplifying the difficult and time consuming task of alignment of the chambers in the radial direction at the design orientation.

c) Scope, schedule and milestones of R & D for the structural analysis

The proposed scale and nature of the SSC muon detector volume makes the application of a detailed structural analysis a necessity in the two basic regions: the central, and the forward/backward.

The configurations in the two muon detection regions are sufficiently different to require separate models to aid in the design of each region independently. It is proposed to initially develop four separate models to be merged into final design configurations in the two muon detecting regions. Two drift chamber and two support structure models will be as follows:

- The first model will be of the central region drift chambers, concentrating on the problems of stability at increased sizes.
- The second model will concentrate on the possibility of different chamber orientations in the forward/backward region.
- The third model will be of the central region support structure.
- The fourth model will be of the forward region support structure.

In the analysis of a mechanical system of this complexity, special techniques must be applied to model the structure accurately. The results of the analysis of the structures must be carefully validated by comparison with the real world. Evaluation of the validity of all analysis results will be an important task within this R & D program.

The finite element analyses of the structures are needed in three phases of the development of the muon detector :

Phase 1: Initial development of four relatively simple models will concentrate on feasibility of different configurations to arrive at a proposed prototype module in each region.

Phase 2: The second phase will develop one detailed model for each region to be used in the design detailing stage.

Phase 3: In the third phase the refinement of the models will be made to include details necessary for application as an alignment tool and the generation of necessary alignment information.

The structural analysis R & D program will run in parallel with the structural design R & D program, spanning the same time periods. It is foreseen that the three year structural analysis effort evolve from phase 1 to 3 following the progress of the structural designs. The milestone for the first year of the structural analysis R & D program will be completion of the models as outlined in phase 1 above. In the second year, the milestone of completing phase 2 outlined above must be consistent with activities in the structural design R & D program. The milestone of completing phase 3 outlined above could be realized at the end of the second or beginning of the third year.

A preliminary finite element model of the central region support structure is currently under study. Fig.5.9 shows the element diagram of the model.

d) Request for support of the structural analysis R & D

The support of this program requires personnel experienced in the analysis of complicated, large area devices with a deflection accuracy of ≈ 10 μm. The structural design research and development program will be carried out by the Charles Stark Draper Laboratory of Cambridge, Massachusetts, under contract from MIT. Their success in the development of the L3 structural analysis, coupled with their involvement in the structural design R & D program, make them the unique choice. The close coordination of the structural design and analysis R & D programs will be the responsibility of CSDL.

One engineer, experienced in the design of large area precision devices, will guide the development of the computer model and guarantee the validity of the results through careful evaluation. One programmer with a working knowledge of an industry standard, finite element analysis program will encode and run the computer models.

The financial request for the first year of the research and development program for the SSC muon detector structural analysis is shown below. Chapter 7, Table V summarizes the estimates of the following years'requests. Partial times quoted for personnel envisions the formation of the group after the structural design R & D program has developed a design concept.

Funding Request FY90 for Structure Analysis
(Estimate based on contract with Charles Stark Draper Laboratory)

	K$/M/yr*	Yrs.	Total K$
1 engineer	168	0.9	151
1 programmer	100	0.9	90
Computer time			20
Total K$			**261**

* Personnel costs include all institute overhead charges

The funding requests for FY91 and FY92 are summarized in Chapter 7.

5.3 Alignment systems

a) The need for research and development in alignment systems

The basis of muon momentum measurement is to determine the curvature of the particle tracks. This requires the alignment of measuring detectors to a high accuracy on a straight line with continuous monitoring. Continuous alignment monitoring is essential to correct the data for minute detector movements(eg. temperature induced) which are on the order of the required measurement resolution.

Our experience with L3 gives us unique expertise in the development and application of optical and mechanical alignment devices for the precise measurement of angles, linear distances, linearity, and planarity. The SSC muon detector foresees increased distances over which precise alignment is

required, and increases in the precision of the alignment. This new environment indicates a substantial level of research and development associated with the alignment of the muon chambers at the SSC.

b) L3 alignment systems review

The accurate measurement of angles, with respect to a gravity reference, became one of the foundations of the alignment process. For this purpose we developed an electronic bubble level [5.1] (see Fig.5.10) capable of absolute angular measurement accurate to 5μrads.

To reach the required precision of linear distance measurement between chambers in the radial direction special tools were developed [5.1] (see Fig.5.11) to measure absolute distances to 10μm. The devices were designed to minimize effects due to temperature and were calibrated using a laser interferometer accurate to <1μm [5.3].

One of the main alignment tasks is the accurate measurement of the linearity of three detector elements which are measuring the particle track. This principle is needed to align the three layers of chambers at both ends of the octant and also the wires within each chamber. The device which we developed (see Fig.5.12) consists of a modulated light source, a lens, and a 4-quadrant light sensitive cell. All elements of the device are referenced to an opto-mechanical 'zero' on an optical bench before incorporation into the octant. The 4-quadrant cell output gives the alignment status in two directions perpendicular to the optical line of sight to ≤10μm over a range of ±0.25mm.

Planarity of detector elements in L3 is measured with a device that creates a plane of laser light which is sensed by probes referenced to the sense wires within the muon chambers as shown in Fig.5.13. The laser beam is deflected by a rotating mirror to create a stable plane of light referenced through an electronic bubble level to vertical. The 'Laser Beacon'[5.2] permits the accurate measurement of the torsion in the muon chamber geometry to within 25μrads.

The alignment of the detector modules in L3 was verified with an ultraviolet laser system as shown in Fig.5.14. UV laser pulses are created in

the apparatus shown mounted on the end of the module. These pulses are directed by means of mirrors to eight paths across the top of the module and down through the drift chambers simulating infinite momentum particles. The system successfully verified the alignment of all sixteen octants in L3 to 30μm as described in Appendix I and shown in Fig.29.

c) A proposed SSC muon chamber alignment scheme

A preliminary alignment scheme for the central region muon detector, presented in Chapter 2, has been developed. It should be noted that the development of the alignment scheme was an integral part of the definition of the geometry and vice versa. As stated in Chapter 6, the development of an optimized, integrated, muon detecting system, is a function of many coordinated areas of effort.

Fig.5.15 is an elevation of the central region muon detector showing the muon chambers and the basic alignment scheme. The alignment scheme was developed with attention to three basic ideas :

1. Simplify the alignment process
2. Minimize the cost of the alignment systems
3. Maximize the intrinsic alignment accuracy of the system

The main alignment tool used is the opto-mechanical system used in L3, described in Appendix I and section 5.3.b, and shown in its L3 application in Fig.5.12. This system will align the bridges holding the wires within the muon chambers in a straight line for the three layers. There will be four of these 'optical lines of sight'(OLS), shown by dashed lines on Fig.5.15, running up each side of the module for a total of eight systems per module.

This configuration satisfies the parameters mentioned above. Choosing OLSs which form lines roughly coincident with the interaction point creates a geometry whose sagitta resolution is insensitive to torsion in the module. As these lines of sight are referenced to the ends of the bridges holding the wires and run at angles up the sides of the module, the system is also less sensitive to the radial position of the chambers. This system of alignment thus simplifies the alignment process and increases the intrinsic accuracy.

d) Scope and schedule of R & D for the alignment systems

The experience gained in the development of the alignment systems for L3 is applicable to all alignment problems foreseen in the SSC muon detector. The adaptation of existing systems and the elaboration of developed principles and technologies will satisfy most alignment measurement needs.

The first task in the development of a working system of alignment for the SSC muon detector is a clear definition of the alignment goals and a scheme to realize these goals. Once this alignment scheme has been developed, there are six different principles of alignment and associated areas of study. Each of the six alignment concepts requires the development of a working system for alignment of the muon chambers. The six systems needed are outlined below :

1. Linear distances

   The measurement of linear distances of 5m with an accuracy of 5μm is a possible extension of our current system. Temperature changes and gradients over these long distances require the development of a continuously monitored distance measuring system.

2. Colinearity

   The measurement of the colinearity of three detector elements over distances of 5m and longer requires refinement and upgrading of the current system or development of a new system. The development of a system which measures the colinearity of more than three points would afford many useful alignment solutions.

3. Planarity

   The L3 system for planarity measurements is conceptually applicable over the larger distance. Refinements of the current system and adaptation to a specific mechanical environment requires study.

4. Angles

   The precise measurement of angles and changes in angles is a basic task foreseeable in all schemes of alignment at the SSC. The electronic bubble level developed for L3 can measure more accurately than most needs but can not be used in the presence of a high magnetic field. Use of the bubble levels in a 7.5KGauss magnetic field requires study. Also, the study of the application of these very accurate angle measuring devices is needed.

5. Survey

The final element which brings the alignment information from all of the detector modules together into a global alignment network is a classic optical survey. The development of the global survey scheme at an early stage of the alignment systems development ensures an efficient incorporation of the global requirements into specific systems development.

6. Alignment verification

All alignment systems in general must be designed with redundancies to minimize the possibility of total system information loss. Redundancies in individual systems, however, does not yield an independent verification of the entire module's alignment status. The aim is to develop a system of independent, direct, complete verification of the alignment of the detector, from wire setup to the reconstruction software. The principles of the UV Laser system of L3 are particularly suited for this goal but this task requires substantial attention.

e) Support for the R & D on alignment systems

The R & D program on alignment systems for the SSC muon detector will be centered in Switzerland and supported by KWF(Swiss commission for the advancement of scientific research). In addition, the following groups will participate in the alignment systems development :

- Groupe Dixi, Lelocle, Switzerland
- E.T.H., Zurich, Switzerland
- University of Geneva, Geneva, Switzerland

The alignment systems R & D program for the SSC muon detector is directly linked to the structural design R & D program (section 5.1) and the muon chamber R & D program (Chapter 3). An Engineering Coordinator (see Chapter 6) will be responsible for the interface between these different groups.

References

[5.1] W.E. Toth, Charles S. Draper Report CSDL-R1885 (Oct. 1987) and SENER Report N.K. Chhabra, Charles S. Draper Report CSDL-R2011 (Sept.1987), P. Bowditch, Charles S. Draper Report CSDL-R1597 (Jan. 1983)

[5.2] P.G. Seiler, et al. "The Laser Beacon", L3 Muon Chamber Group Internal Note, 85-4, 1985, unpublished; H. Anderhub, M. Devereux, P.G. Seiler, "On a new method for testing and calibrating wire chambers", NIM 176, 323, (1980)
R.Fabbretti, et al., NIM A280(1989),13-24

[5.3] Hewlett Packard Interferometer 5526A

[5.4] F. Hartjes and J. Konijn, NIM 217, 311 (1983)
F. Hartjes, J. Konijn, and Y. Peng NIM A269, 544 (1988)
J.C. Guo, F. Hartjes, J. Konijn NIM 204, 77 (1982)
H. Anderhub, M. Devereux, and P. Seiler, NIM 176 (1980) 323

Figure Captions

Fig.5.1 A side view of the SSC muon detector central region support structure for the muon chambers.

Fig.5.2 An end view of the SSC muon detector central region support structure, at sections E-E and G-G from Fig.5.1, shows the geometry to support bending in the frame about the Z axis.

Fig.5.3 An end view of the central region support structure, at section F-F from Fig.5.1, shows the structure always outside the measuring volume of the muon chambers.

Fig.5.4 The central region module is supported by large elements fixed to the magnet crown and central calorimeter support plate as shown.

Fig.5.5 The central region module supporting elements from Fig.5.4 are shown between the outer chambers.

Fig.5.6 A preliminary support structure design is shown for the forward region inside the solenoid of the SSC muon detector.

Fig.5.7 The NASTRAN finite element model of the L3 octants contains virtually all mechanical parts as shown.

Fig.5.8 Verification of the NASTRAN deflection information was made by comparison to actual measurements.

Fig.5.9 Shown here is the element diagram from the preliminary finite element analysis of the SSC muon detector central region support structure.

Fig.5.10 The electronic bubble levels showns measure angles with an accuracy of 5μrads.

Fig.5.11 The top view shows linear distance measuring tools, developed at CSDL, for measuring distances of 100, 420, 630, and 700mm all with a range of ±15mm. In the bottom view, we see the calibration of a measuring tool with the HP interferometer.

Fig.5.12 Measurements of the alignment of the centers of the three chamber layers in L3 are made with this device.

Fig.5.13 The measurements of the deviation from a plane of all chamber centers in L3 is made with this device know as the 'Laser Beacon'.

Fig.5.14 The verification of the alignment status of the octants in L3 is made with the UV Laser system shown.

Fig.5.15 The SSC muon detector central region geometry with an alignment scheme is shown.

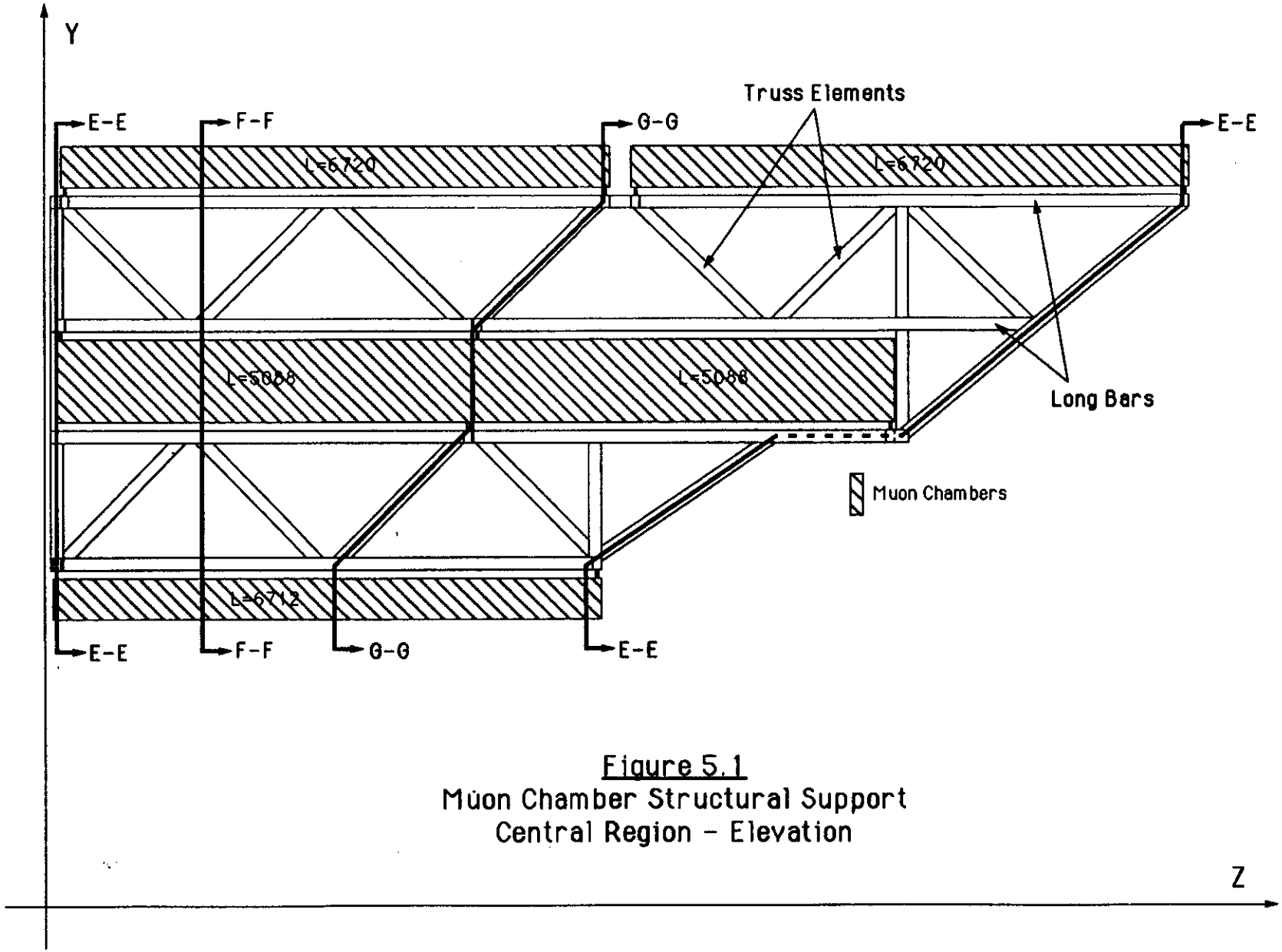

Figure 5.1
Muon Chamber Structural Support
Central Region - Elevation

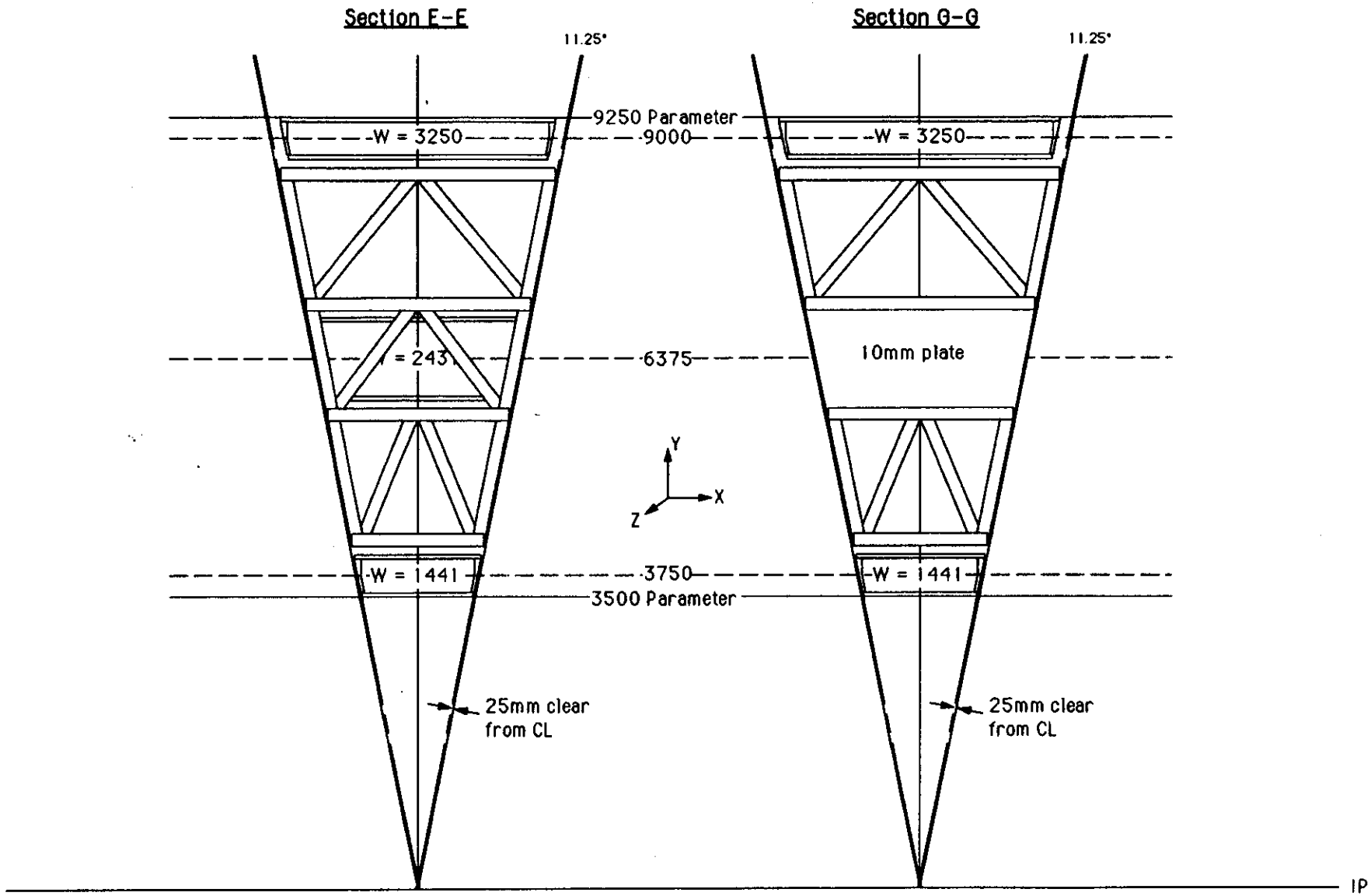

Figure 5.2
Sections E-E and G-G
from figure 5.1

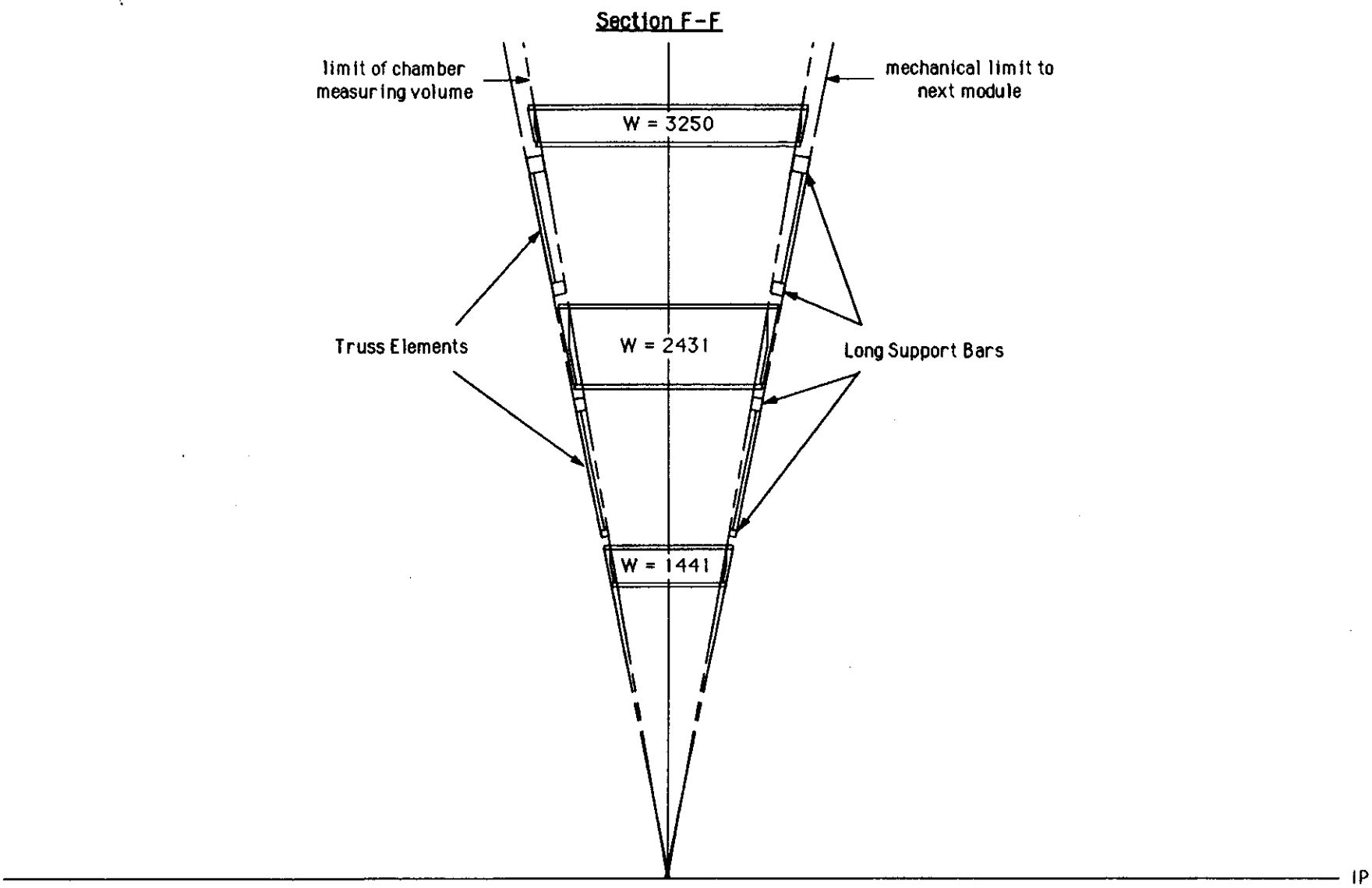

Figure 5.3
Section F-F
from figure 5.1

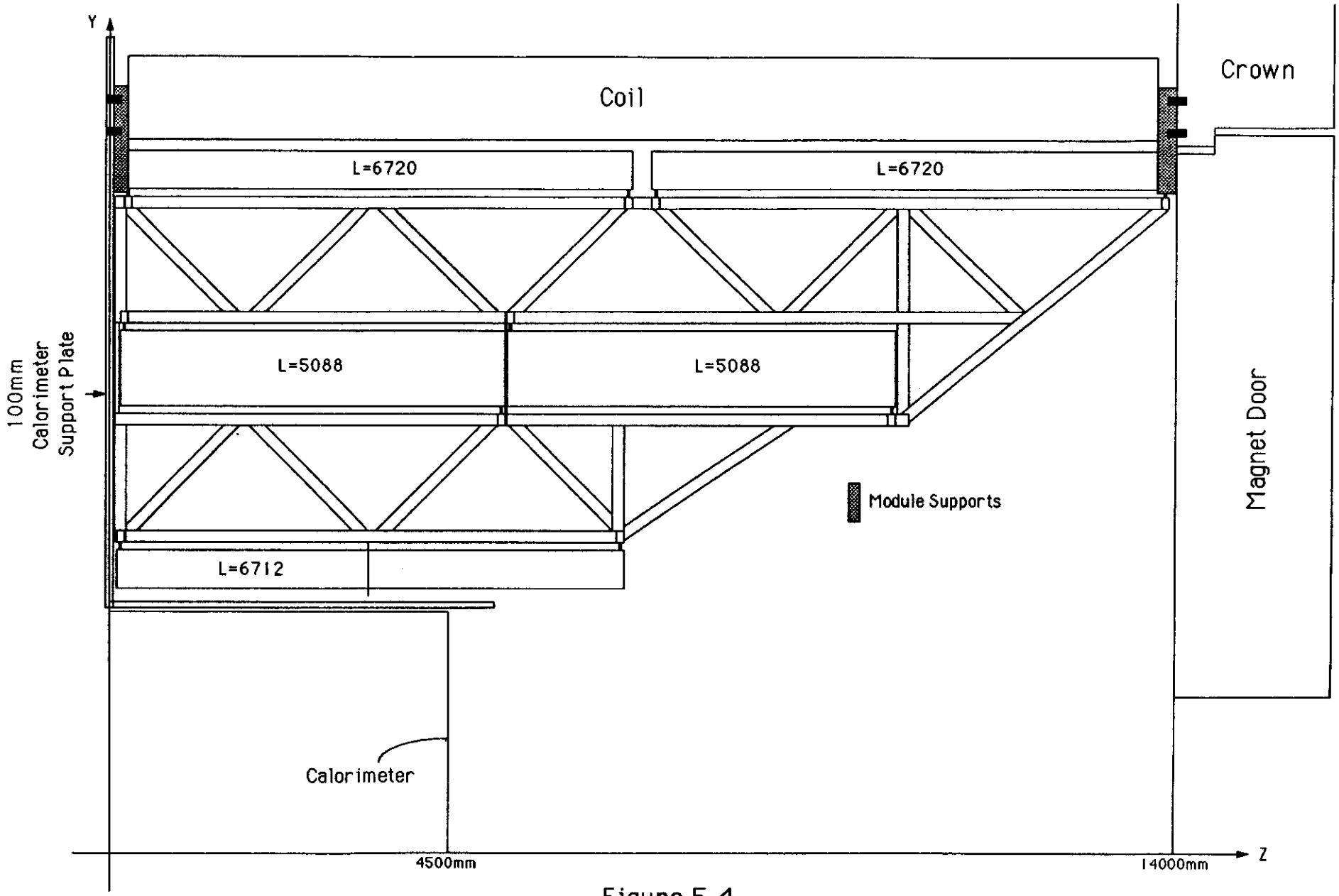

Figure 5.4
Global supporting elements
for the central region module

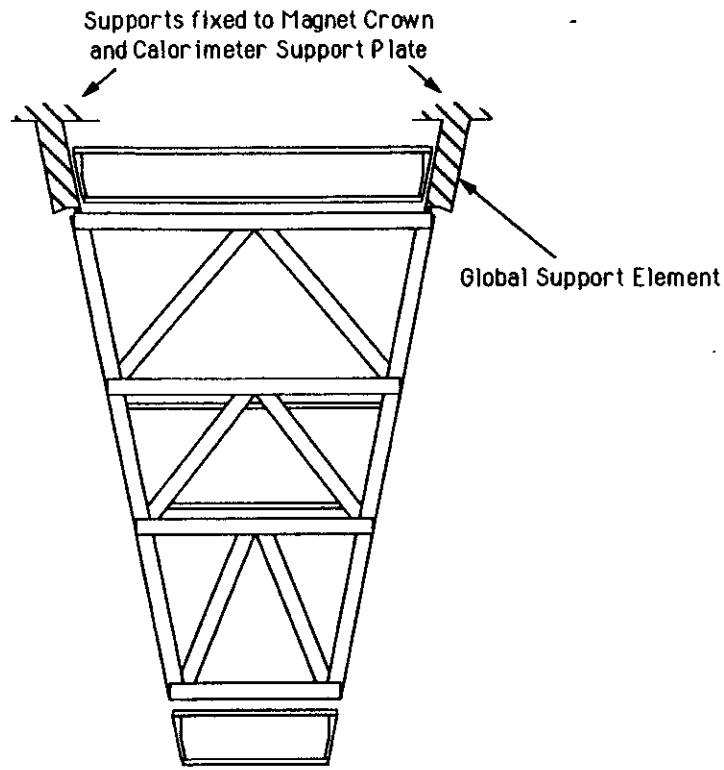

Figure5.5
Global Support of
Central Region Module

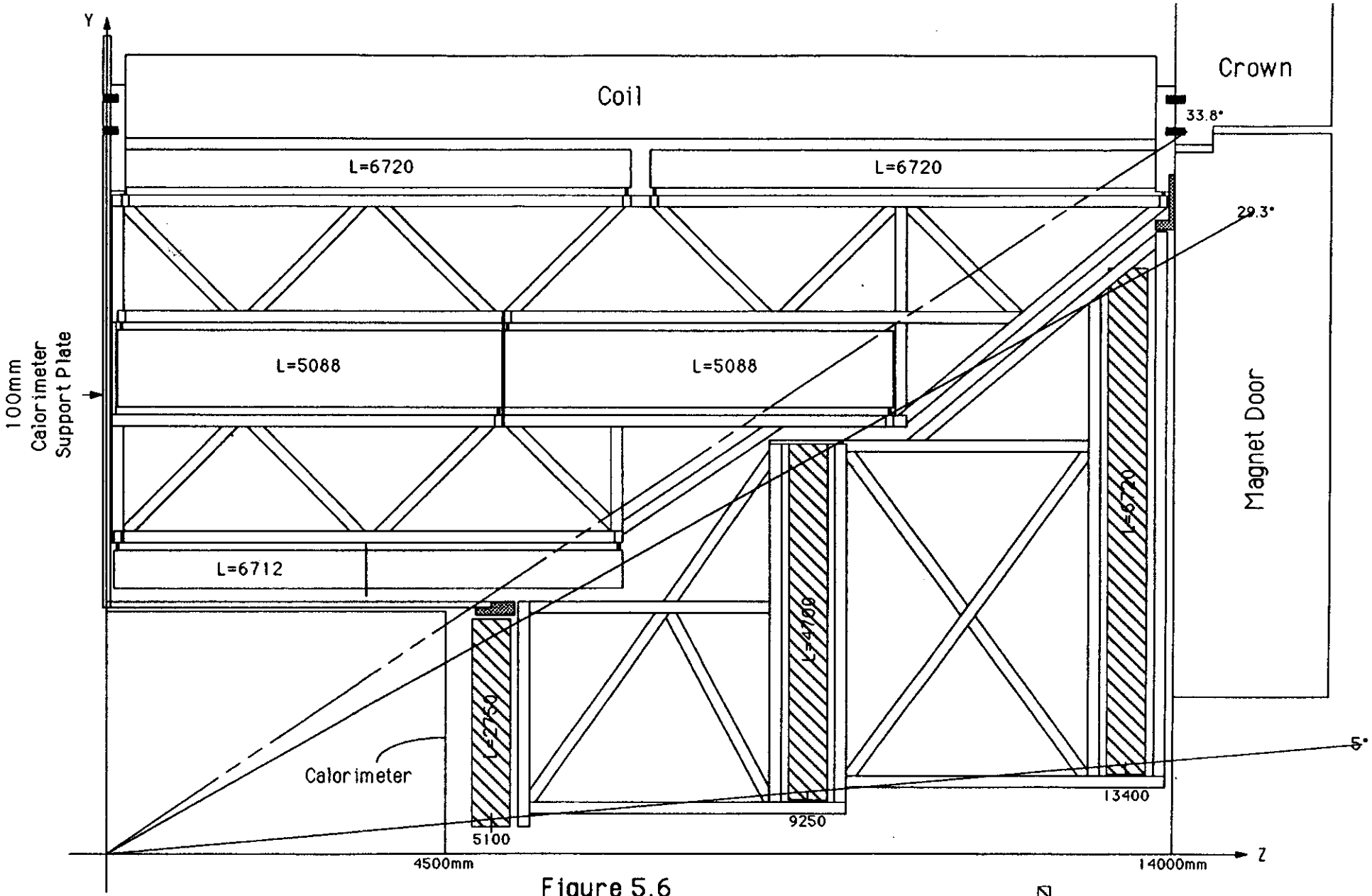

Figure 5.6
Structural design and support for the forward region inside the solenoid

Forward Muon Chambers

Global Supporting Elements

NASTRAN Analysis

- model contains all large structural members, chambers, and supporting hardware
- structure can be rotated to all design orientations for analysis
- analysis yields loads, stresses, and deflections at every node in the model

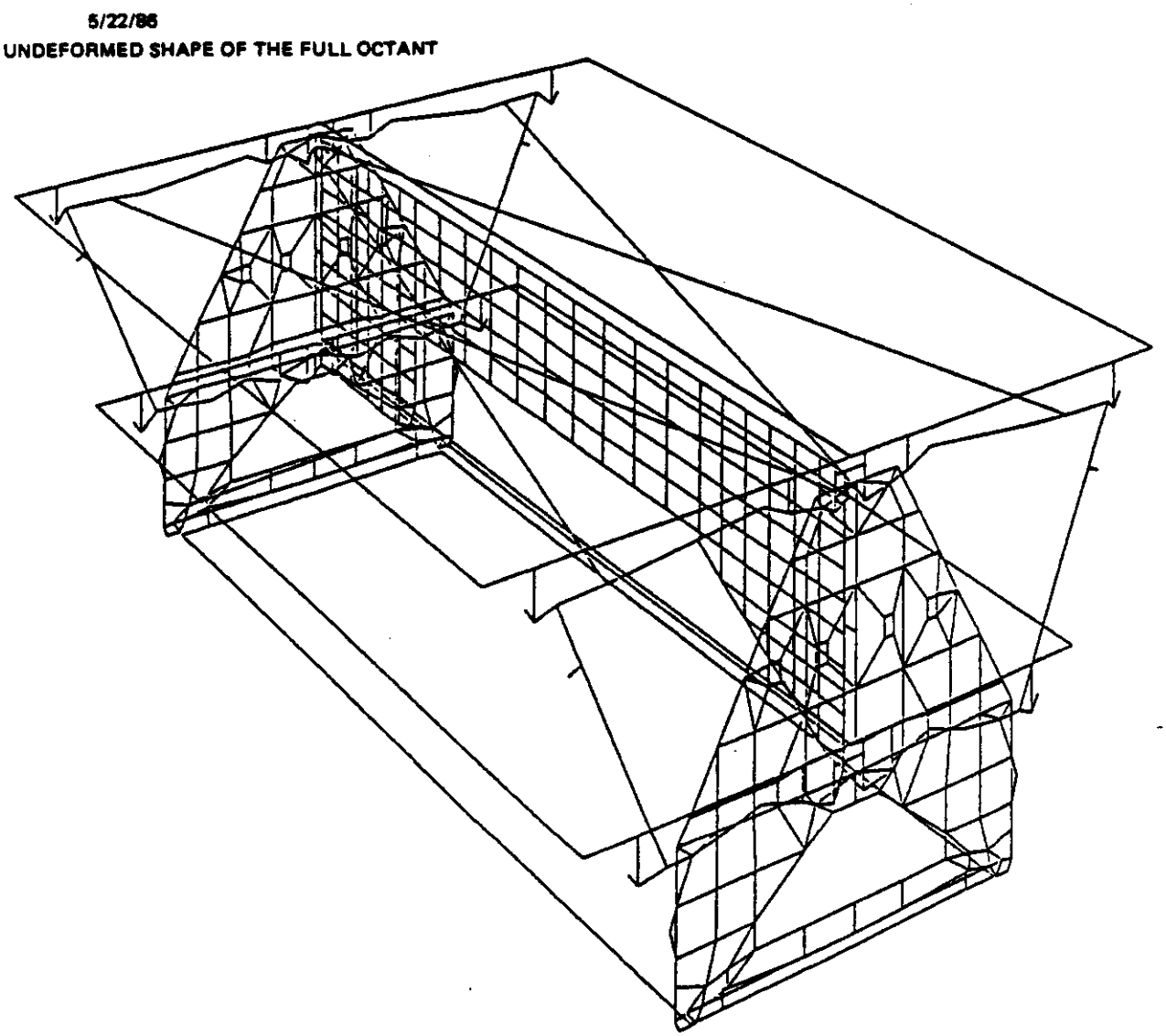

STATIC ANALYSIS OF A SIMPLY SUPPORTED OCTANT
ORIENTATION NO. 2
UNDEFORMED SHAPE

Figure 5.7
Element diagram from the finite element

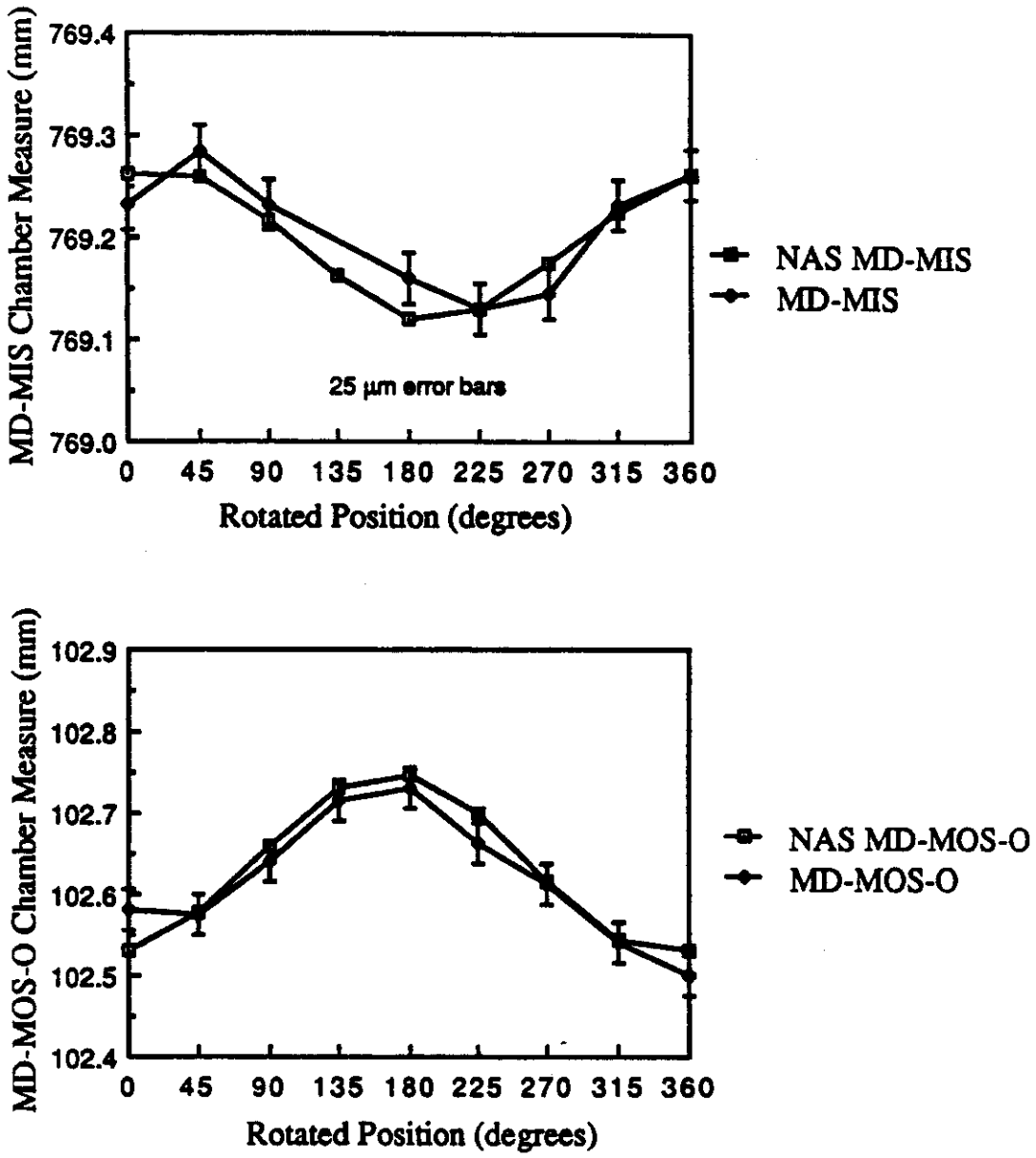

Figure 5.8
Verification of deflection information from the NASTRAN finite element analysis of the L3 octants

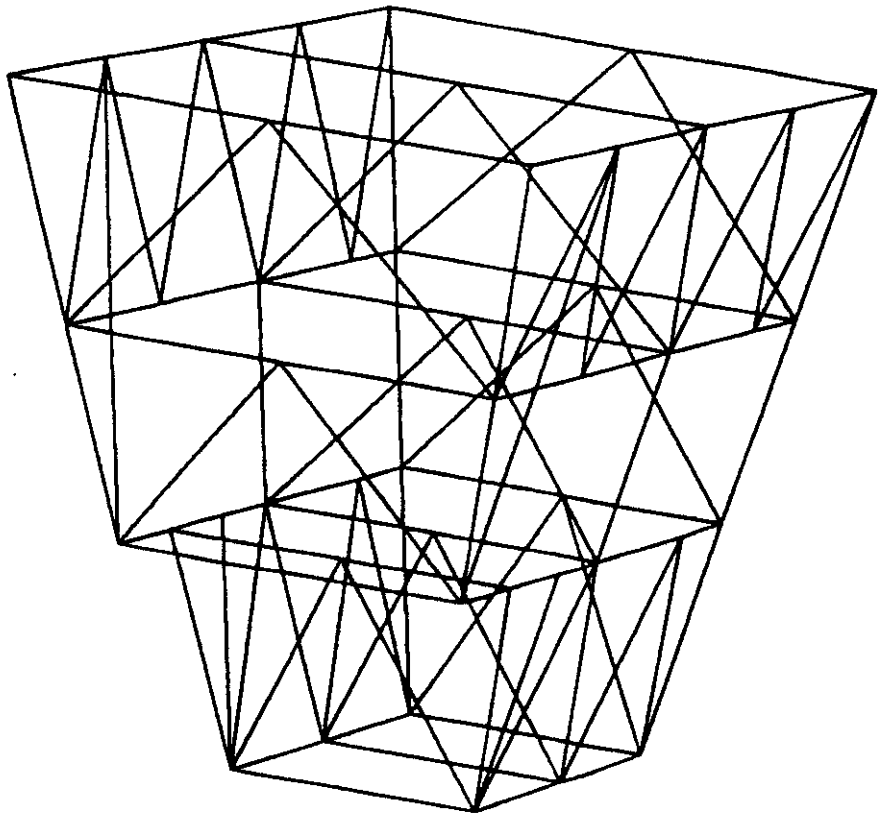

Figure 5.9
Element diagram from the preliminary finite element analysis of the central region support structure

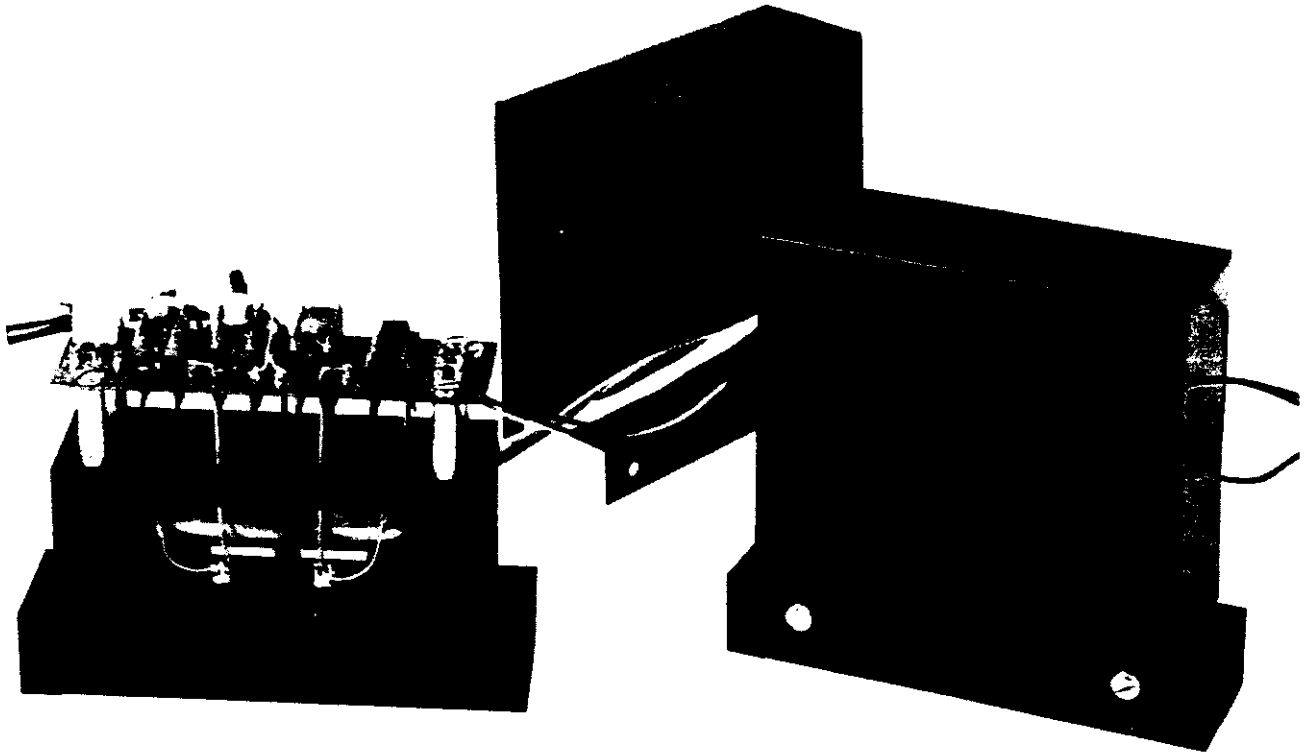

Figure 5.10
Measurement of angles in L3 using the 'Electronic Bubble Level'

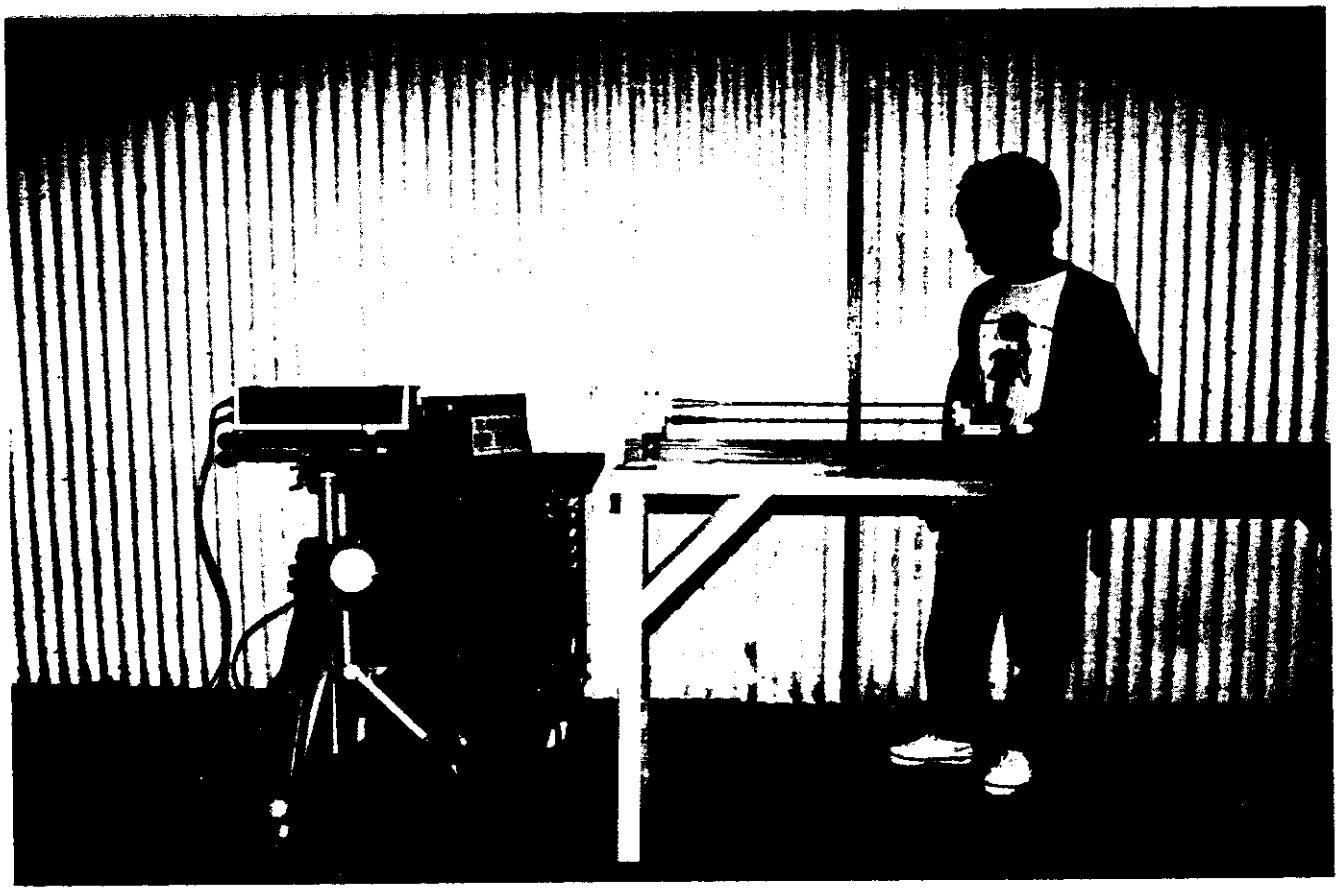

Figure 5.11
Linear distance measuring system for L3

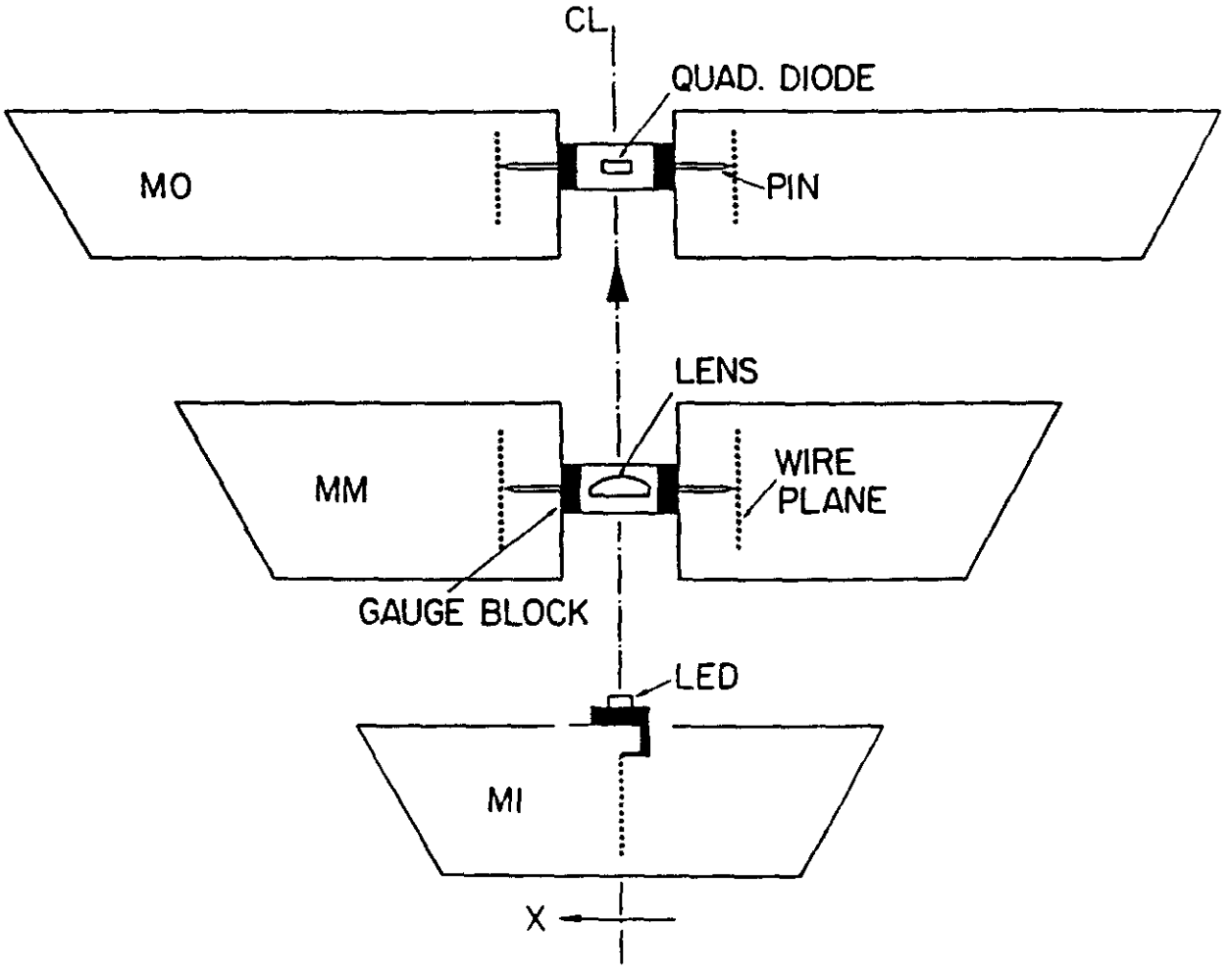

Figure 5.12

Colinearity measurements in L3

by an 'Optical Line of Sight'

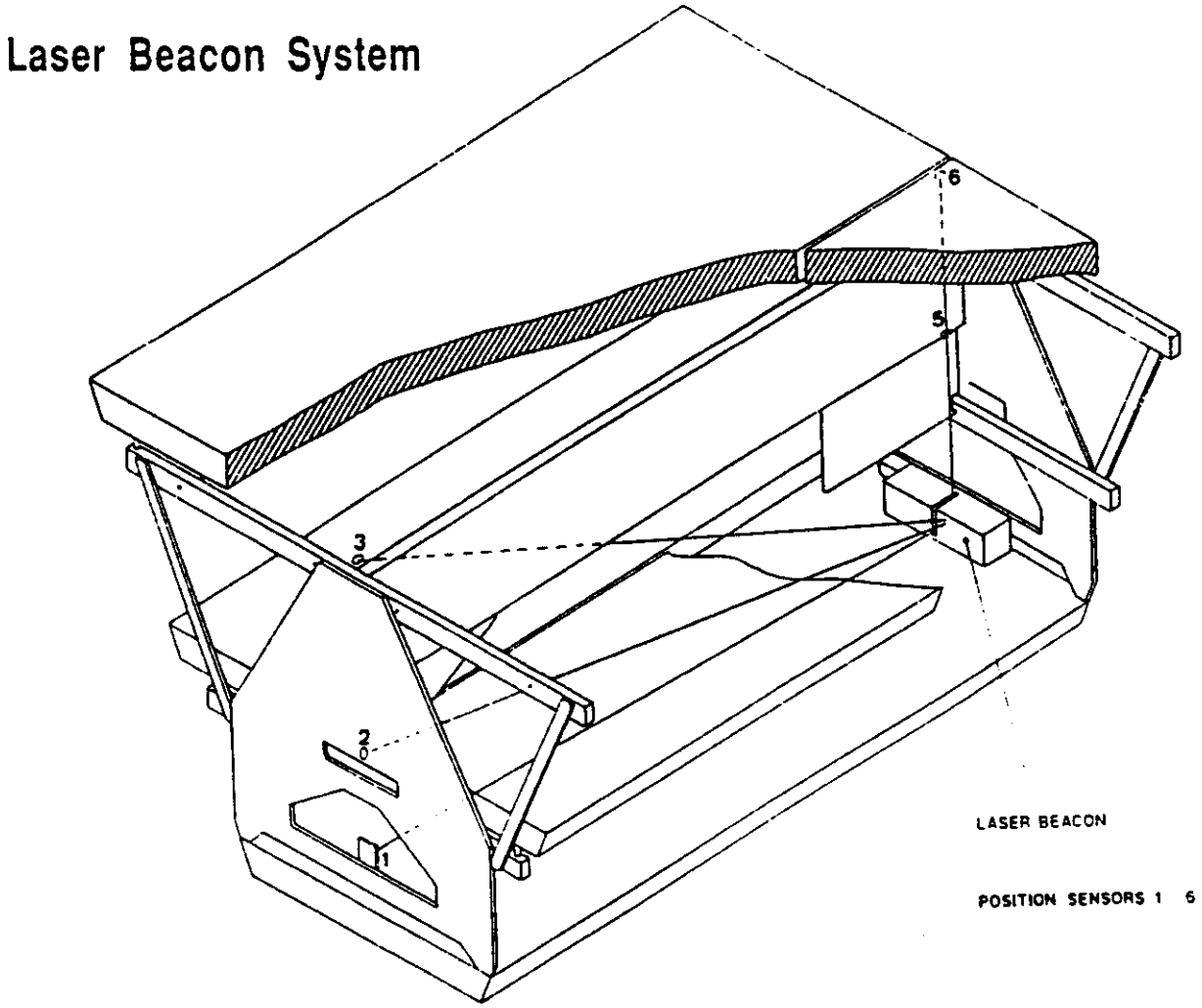

Figure 5.13

Planarity measurements in L3

using the 'Laser Beacon'

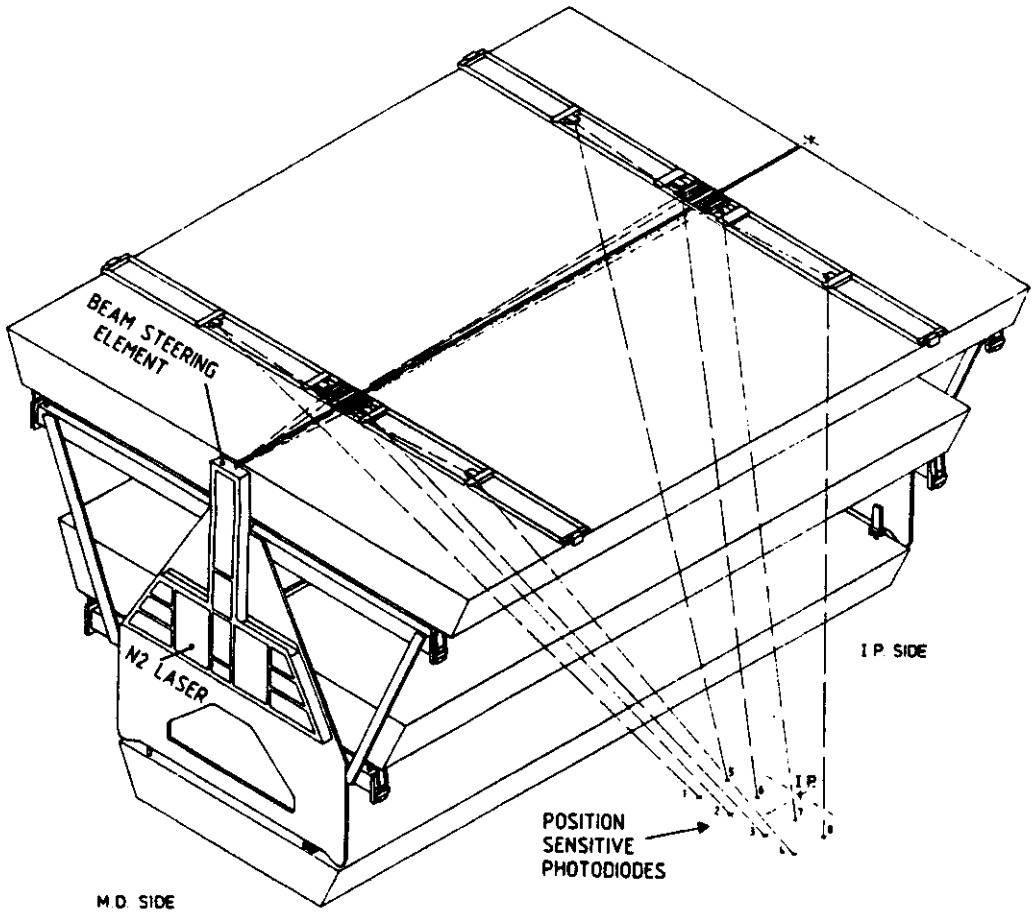

Figure 5.14
Alignment verification in L3 using the 'UV Laser'

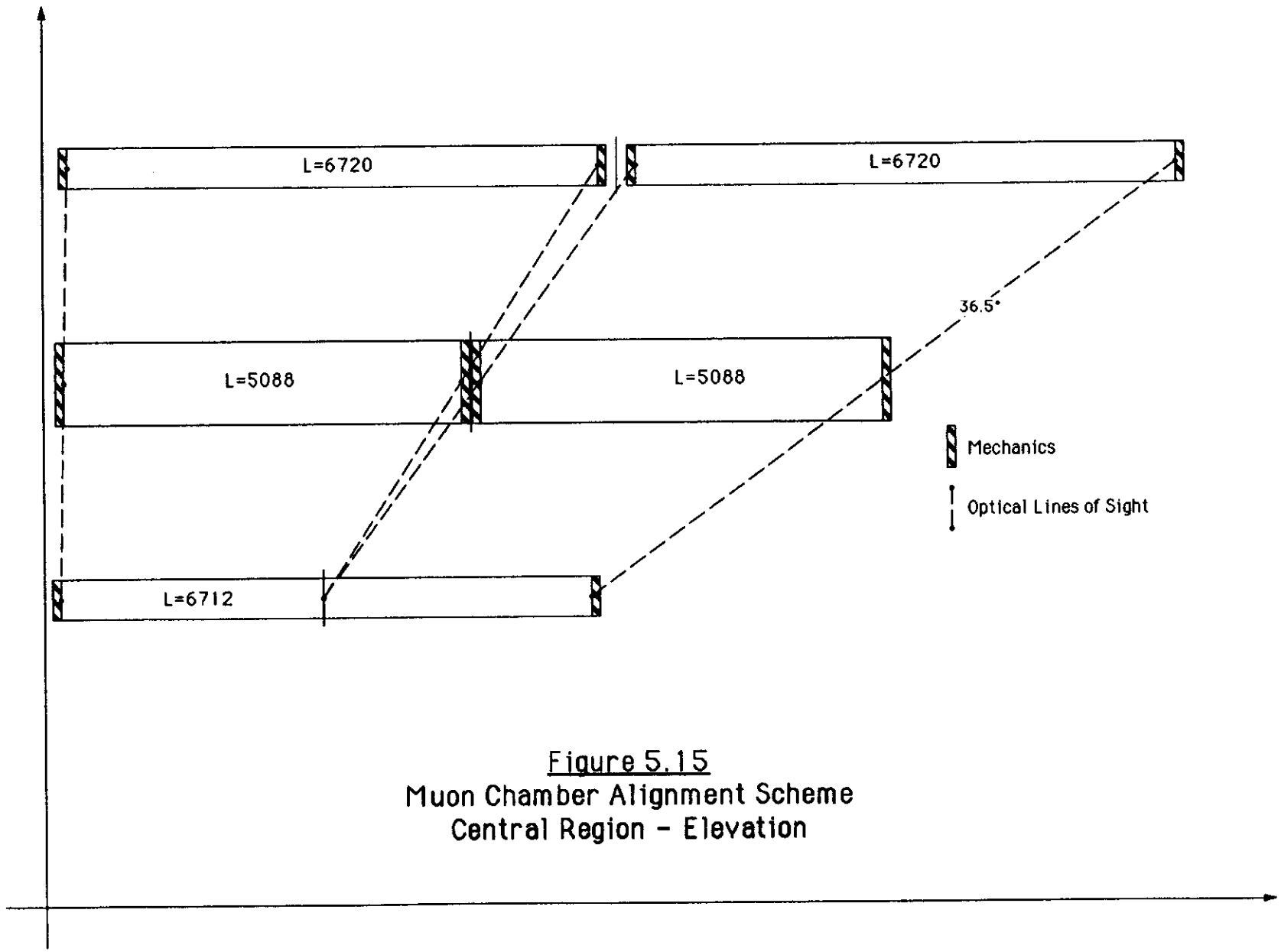

Figure 5.15
Muon Chamber Alignment Scheme
Central Region - Elevation

CHAPTER VI
COORDINATION OF ENGINEERING

C. Grinnell, S.C.C. Ting
Massachusetts Institute of Technology, Cambridge, MA

Contact person : C. Grinnell

6.1 The need for coordination of engineering support

The vast amount of engineering work necessary to support the research and development of a muon detector for the SSC requires a coordinating body to facilitate the effort. The size of the program makes division of the work into many subsections unavoidable, and even desirable. The main areas of development for the muon detector, which will each comprise a separate group, are :

Muon Chambers
Z Detectors
Structural Design
Structural Analysis
Alignment Systems
Gas
Gas Distribution System
Data Transfer
Electronics
Computers
Cables

As outlined in section 2.2, muon chamber R & D efforts must be coordinated with other groups developing the detector, such as magnet, experimental hall, calorimeter, vertex chamber and data acquisition and analysis.

These many groups necessary to support the large number of engineering tasks will be at least on two continents and most likely involve many different languages. This kind of a multinational collaboration in engineering support makes efficient coordination and communication essential.

6.2 Scope of engineering coordination

Generally stated, the main function of this group will be to ensure the consistency and quality of all engineering work and promote the flow of information and ideas between the various groups in the muon detector R & D program. In this capacity, this group will act as a communication interface, when concerning engineering needs. This will include communication between all groups within the SSC muon detector R & D program, and communications from inside the program to all outside groups.

Some specific areas of effort of this group will be to assist all SSC muon detector R & D programs in the definition of: consistent drawing standards, quality control programs, and standards of safety. The emphasis will be on the application of consistent engineering practices to promote the efficient development and integration of the various detector elements. The engineering coordination group will also assist all R & D programs in the definition of specific test and prototype assessment programs to ensure the engineering integrity of all elements of the detector.

Detailed assembly drawings incorporating all system components and defining the mechanical interfaces will be made. In addition, a continuous review of all designs for consistency with global objectives is foreseen. Coordination of the final, integrated, prototype module assessment program will be handled by this group. The group will compile and control all critical data from the various development groups for prototype assessment.

The engineering coordination group will be responsible for generating a global planning for all engineering tasks within the R & D programs. By reviewing the progress of the various programs and identifying problem areas, the coordinator will ensure the compliance of all groups with the global planning. Reports on the progress of all R & D programs will be compiled and made available.

6.3 Request for support of the engineering coordination

The position of coordinator of engineering support to the muon chamber R & D program will be offered to Charles Grinnell, an experienced engineer from L3. In the first year of the program the group will consist of a coordinator and the staff assistant. Shown below are estimates of financial support needed for the first year. Chapter 7, Table IV summarizes the estimates of the following years' requests.

Personnel	**K$/M/yr**	**Yrs.**	**Total K$**
1 coordinator	125	1.0	125
1 staff assistant	75	1.0	75
Travel			30
Total K$			**230**

CHAPTER VII

SUMMARY

7.1 Summary of activites for the SSC muon detector R & D program

The table I summarizes the activities for the muon detector R & D program.

Table I : Summary of Activities for the SSC Muon Detector R&D Program

	FY 90	FY 91	FY 92
Muon Chambers	-wire, foil and mesh plane studies of configuration, materials, tension, cost, fabrication, and alignment -design studies of bridges and actuators -conceptual studies of chamber structures and fabrication -study & test elec. field distortions	-produce models for verification -study fabrication with industry -continue electrostatic and wire plane studies -produce prototype wire tension by frequency device -structural stability studies	-integrate all components into chamber designs -wire tension by frequency device finalized -construct models to test alignment and signal calibration -construction methods finalized
Gas	-setup magnet laser and X-ray tube -construct small test chamber I -selection of first candidate gases	-continue research -construct small test chamber II -measure diffusion and reliability	-construct chamber prototype with accurate cell structure -aging tests and test beam measurements -final selection
Structural Design and Analysis	-support chamber designs -feasibility studies of structures -freeze drawings with respect to conceptual changes -structural analysis of chambers & structures for feasibility: 4 models	-continue support for structural designs of chambers -complete detailed designs of structures -fabricate prototype parts -refine finite element models for design details	-continue support for structural designs of chambers -complete assembly and assessment of all prototypes -refine finite element models for alignment process use
Coordination	-coordinate all R&D programs -plannings and progress reports -engineering quality and consistency verification -engineering interface to all other groups -drawing and design review	-coordinate all R&D programs -plannings and progress reports -engineering quality and consistency verification -engineering interface to all other groups -drawing and design review	-coordinate all R&D programs -plannings and progress reports -engineering quality and consistency verification -engineering interface to all other groups -drawing and design review
Alignment Systems	-system definitions -material studies -subsystem designs -construct subsystems	-subsystem design -construct subsystems -verification/test subsystems -system integration	-subsystem construction -verification/test subsystems -system integration -system testing
Electronics	-amplifier/discriminator -TDC integrated circuit	- amplifier/discriminator -TDC integrated circuit -TDC module -software package	-TDC module -software package -system construction -system testing
Data Transfer	-optoelectronic design -fiber/cable design -photodiode development -connector construction	-photodiode development -connector construction -optical switches -fiber/cable prototypes -connecting techniques	-connector construction -optical switches -fiber/cable prototypes -connecting techniques -packaging -system construction

7.2 Summary of milestones for the SSC detector muon R & D program

Table II summarizes the milestones for the SSC muon detector R & D program.

Table II : Summary of Milestones for the SSC Muon Detector R&D Program

	FY 90	FY 91	FY 92
Muon Chambers	-determine foil and mesh plane feasibility for manufacture and alignment -freeze chamber structural designs with regard to conceptual changes	-produce and evaluate a model of an endframe -produce and evaluate a model for cell verification -produce prototype wire alignment device -produce prototype tension device	-finalize chamber design and production methods -define wire and foil or mesh plane material, attachment, production and alignment methods -full length chamber model constructed and evaluated
Gas	-completion of setup for measurements	-measurements of diffusion and reliability for ten gas mixtures	-construct chamber prototype with accurate cell structure -test beam measurements at Bates Linear Accelerator or Harvard Cyclotron
Structural Design and Analysis	-complete structural designs without fine detail -freeze drawings with respect to conceptual changes -completion of models(4) of structures and chambers for feasibility studies	-complete detailed designs of structures -fabricate all prototype parts -complete finite element models(2) for design details	-complete assembly and assessment of all prototypes -complete finite element models for alignment process use

7.3 Summary of contributions by participating institutes in the SSC muon detector R & D program.

Table III summarizes the contribution by participating institutes in the SSC muon detector R & D program.

Table III : Summary of Contributions by Participating Institutes in the SSC Muon Detector R&D Program

Muon Chambers	Gas	Struct. Design and Analysis	Alignment Systems	Electronics	Data Transfer
Carnegie Mellon University I. Brock A. Engler T. Fergusen H. Vogel	Harvard University P. McBride K. Strauch I. Scott	Caltech G. Gratta R. Mount H. Newman	E.T.H. Zurich, Switz.	E.T.H. Zurich, Switz.	E.T.H. Zurich, Switz.
John's Hopkins University H. Akbari J.Z. Bao C. Spartlotis	M.I.T. U. Becker Y.H. Chang G. Herten T. Wenaus B. Wyslouch	Los Alamos Nat. Laboratory D. Duchane W. Kinnison W. Miller G. Sanders H. Ziock	University of Geneva Geneva, Switz.	University of Geneva Geneva, Switz.	University of Geneva Geneva, Switz.
M.I.T. P. Berges R. Clare T.S. Dai M. Fukushima Q. Li M. White		M.I.T. J. Burger D. Luckey S.C.C. Ting	Groupe Dixi Lelocle, Switz.	Le Croy SA Meyrin, Switz.	Asea Brown Boveri Ltd. Dättwil, Switz.
Oak Ridge National Lababoratory D. Kuban F. Plasil M. Rennich G. Young		Oak Ridge National Laboratory R. Beckers H. Cohen A. Gabriel J. Johnson			
Princeton University P. Denes P. Piroué D. Stickland		University of Cal. at San Diego J. Branson I. Sheer			
Purdue University A. Bujak T. McMahon B. Strinfellow					

7.4 Summary of requests for support of the SSC muon detector R & D program to the Swiss Government*.

Table IV summarizes the requests for support of the SSC muon detector R & D program to the Swiss Government (see Appendix III).

Table IV: Summary of Requests for Support of the SSC Muon Detector R&D Program to the Swiss Government

	FY 90		FY 91		FY 92	
Alignment Systems	-system definitions -material studies -subsystem designs -construct subsystems	2.1 MSF	-subsystem design -construct subsystems -verification/test subsystems -system integration	2.5 MSF	-subsystem construction -verification/test subsystems -system integration -system testing	2.4 MSF
Electronics	-amplifier/discriminator -TDC integrated circuit	2.2 MSF	- amplifier/discriminator -TDC integrated circuit -TDC module -software package	3.2 MSF	-TDC module -software package -system construction -system testing	3.6 MSF
Data Transfer	-optoelectronic design -fiber/cable design -photodiode development -connector construction	1.7 MSF	-photodiode development -connector construction -optical switches -fiber/cable prototypes -connecting technique	1.9 MSF	-connector construction -optical switches -fiber/cable prototypes -connecting technique -packaging -system construction -system testing	2.4 MSF

---

* The Swiss participation represents a significant research enterprise which is to be strictly carried out in cooperation with major Swiss universities and industries. In this specific framework, funding can neither be increased nor transferred to other areas.

7.5 Summary of requests for support of the SSC muon detector R & D program to D.O.E.

Table V summarizes the requests for support of the SSC muon detector R & D program for FY90 and estimates requests for FY91 and FY92.

Table V : Summary of Requests for Support of the SSC Muon Detector R&D Program to D.O.E.

	FY 90		FY 91		FY 92	
Muon Chambers	2 technicians 1 designer 205K$ equipment 60K$ mat. & serv. 100K$ travel 15K$	380 K$	manpower 220K$ equipment 30K$ mat. & serv. 140K$ travel 20K$	410 K$	manpower 230K$ equipment 35K$ mat. & serv. 150K$ travel 20K$	435 K$
Gas	1 post doc 2 students 0.5 elec. tech. 188K$ equipment 118K$ mat. & serv. 124K$ travel 13K$	443 K$	manpower 197K$ equipment 22K$ mat. & serv. 130K$ travel 14K$	363 K$	manpower 205K$ equipment 25K$ mat. & serv. 136K$ travel 16K$	382 K$
Structural Design and Analysis	1 program manager 4 engineers 2 designers 1 programmer 994K$ CPU time 20K$ travel 30K$	1044 K$	manpower 1110K$ materials 1400K$ CPU time 10K$ travel 30K$	2550 K$	manpower 1110K$ materials 600K$ CPU time 20K$ travel 20K$	1750 K$
Coordination	1 program manager 1 staff assistant 200K$ travel 30K$	230 K$	manpower 200K$ travel 30K$	230 K$	manpower 200K$ travel 30K$	230 K$

As seen from Table IV and V, the requests from D.O.E. and from the Swiss government are :

	SSC Laboratory	Swiss Government
FY90	2097K$	6.0MSF (3750K$)
FY91	3553K$	7.6MSF (4750K$)
FY92	2797K$	8.4MSF (5250K$)

This funding is based on our many years of experiences. We are confident that we will be able to construct the first working prototype of a precision instrument to measure TeV muons to 1 to 2% accuracy. Therefore, this R & D program will ensure that a precision muon detector at the SSC can be constructed in time.

* * * * * * *

APPENDIX I

DESCRIPTION OF THE L3 MUON CHAMBER SYSTEM

1. The L3 experiment

In 1982, based on the experience we gained at DESY, Brookhaven, ISR-CERN and PETRA, we began to build the L3 detector [1]. It is designed to study e^+e^- collisions in the 100 GeV range with emphasis on high resolution energy measurement of electrons, photons, and muons. It is an effort involving a worldwide collaboration of 460 physicists belonging to 33 institutions from 13 countries. Preparation of the experiment from its conception to the beginning of data taking in summer 1989 took 8 years and 1100 technical man years of effort. The L3 detector as shown in Fig.1 has the following components :

a) Magnet:

Since the momentum resolution $\frac{\Delta p}{p}$ of charged particles following a path of length L in a magnetic field behaves as

$$\frac{\Delta p}{p} \propto \frac{1}{BL^2}$$

we have chosen a relatively low field in a large volume to optimize muon momentum resolution. The magnet has an inner radius of 6 meters and it provides a BL^2 = 180 kGauss·m^2. The BL^2 is two to ten times larger than other detectors in high energy physics today. Fig.2 shows one of the coil packages, and Fig.3 shows the finished magnet with one of the doors open. Fig.4 is the result of the survey of the centers of the coil packages, and shows that the 1000 ton coil is aligned to ± 1mm.

b) Muon Detector:

The momentum of muons P_μ is measured very precisely in free space with three layers of drift chambers. To obtain a momentum resolution $\frac{\Delta p}{p}$ of approximately 2%, nearly ten years of effort from 1976 to 1986 were devoted to conceptual research, concept proving tests, to the construction of the chambers and of their support system, as well as to the alignment system. The muon detector system covers a volume of 1000m^3 and operates in a 5 kGauss field. There are a total of 80 large drift chambers, each with an approximate area of 20m^2. The muon chambers are supported by a specially

designed structure which monitors the chamber positions to ± 30μm. Each chamber measures the muon coordinate to 50μm and measures the angle to 1 to 2 mrad. This system enables us to measure a 100 GeV particle decaying into a pair of muons with a mass resolution:

$$\frac{\Delta m}{m} \approx 1\%$$

c) Hadron Calorimeter:

The hadron calorimeter measures hadron energies with a resolution of $(55/\sqrt{E}+5)\%$ and $\Delta\Theta = 2.5°$, $\Delta\Phi = 3.5°$ for jets. This provides a clean muon sample by absorbing hadrons close to the e^+e^- interaction point to minimize in-flight pion decays, and by tracking muons through the uranium absorber. The calorimeter also measures muon energy loss. Fig.5 shows the assembled hadron calorimeter inside the magnet. The calorimeter is made of 8000 proportional chamber planes sandwiched with 300 tons of U_{238} absorber. Fig.6 shows the measured energy resolution of the hadron calorimeter.

d) Electromagnetic Calorimeter:

The electromagnetic calorimeter, which uses a new type of crystals (BGO), is shown in Fig.7. It measures photon and electron energies with an accuracy of better than 1% above 2 GeV and of 5% at 100 MeV. The measured position resolution for photons is ± 1mm. The measured BGO resolution is shown in Fig.8. It is nearly a factor of 10 better than the more commonly used electromagnetic calorimeters.

e) Vertex Detector:

A central detector tracks charged particles with a 40μm average single wire accuracy in the bending plane and 450μm double track resolution. In the non-bending plane, the Z coordinates are measured by four additional wire chambers providing 300μm single track resolution and 7mm double track resolution. Fig.9 shows the measured single track resolution.

The L3 detector provides good hadron rejection. The muon momentum is measured twice: first in the vertex chamber as p_v, and second, by the precision muon chambers as p_μ. The muon energy loss ΔE is measured by the sampling calorimeter which also monitors large angle photon radiation. The energy balance:

$$p_\nu = \Delta E + p_\mu$$

allows us to eliminate hadron decays and hadron punch throughs from muon signals. These properties of L3 make it well adaptable for use at the LEP Hadron Collider (LHC).

2. The L3 muon chamber system

L3 is designed to measure muons to an accuracy of $\frac{\Delta p}{p} = 2\%$ at 50 GeV, thus providing a 1.4% dimuon mass resolution at 100 GeV. This is achieved using a configuration of three layers of drift chambers which very precisely measure the curvature of the muon trajectory in the region between the support tube and the magnet coil. In this region, the 5 kGauss magnetic field makes a 45 GeV muon track deviate from a straight line by a sagitta

$$"s" = 3.7\text{mm}.$$

The 1000m^3 modular muon detector is made of two ferris wheels, each having eight independent units or "octants", as shown in Fig.10. Air pads on the support tube allow rotation during the installation phase. Rails are used to roll the assembled ferris wheel inside the magnet.

Each octant consists of a special mechanical structure supporting five precision or "P" chambers which measure the momentum. There are two chambers (MO) in the outer layer, two chambers (MM) in the middle layer, and one inner (MI) chamber, all of which measure track coordinates in the bending plane. In addition, the top and bottom covers of the MI and MO chambers are drift chambers. They measure the Z coordinate along the beam, and thus the Θ angle. There are six Z chambers per octant. Fig.11 shows a complete octant with five momentum measuring chambers, six Θ measuring chambers, amplifiers, UV alignment system, and gas tubing attached to the torque tube.

In order to obtain $\frac{\Delta p}{p} = 2\%$, we have to measure $\frac{\Delta s}{s}$ to 2%, i.e. $\Delta s = 74\mu\text{m}$. This means that systematic errors in the drift chambers, in the octant structures, and in the internal octant alignment must be kept below 30μm. Such accuracy required precise optical and mechanical measurements, as well as verification by UV laser and cosmic rays.

3. Principles of accuracy for the L3 muon chamber system

Prime consideration was given to the accuracy of the sagitta determination. The major contributions to sagitta measurement errors are:

a) intrinsic drift chamber resolution
b) multiple scattering
c) accuracy of alignment of chambers belonging to different layers.

We have minimized contributions from each of these areas, as is described below.

An intrinsic accuracy of 250μm per wire is sufficient to reach the design resolution. Careful chamber optimization studies have led to smaller values [2]. We average over n wires to obtain the final tracking accuracy. The principle is shown in Fig.12a. Multiple sampling improves chamber resolution by a factor $\frac{1}{\sqrt{n}}$ over single wire resolution. MI, MM and MO sample the muon track n = 16, 24, and 16 times respectively. The resulting measurement error is:

$$(\varepsilon_1^2/2 + \varepsilon_2^2)^{1/2}$$

Thin aluminum honeycomb material with an average of 0.9% of a radiation length per two layers encloses the middle chambers as shown in Fig.12b. Using this design, multiple scattering introduces an error of approximately 1% in $\frac{\Delta p}{p}$ at 50 GeV. Since the sagitta values are small, muons more energetic than 3 GeV will be essentially confined to one octant. Therefore, as schematically shown in Fig.13, alignment is only critical between chambers of the same octant.

Alignment errors <30μm were achieved in all production octants.

4. Chambers

a) Precision Chambers

The momentum measuring chambers in L3 are constructed of 2 aluminum end frames, cast and machined, and 2 extruded aluminum side panels. The inner and outer chambers are closed on the top and bottom by Z chambers. The middle chambers are closed by honeycomb panels as mentioned above, to avoid

degradation of the resolution due to multiple scattering. An exploded view of the mechanical structure of one MO (MI) chamber is shown in Fig.14. Also shown in Fig.14 is the Z layer double plane configuration. Fig.15 is a photograph of a chamber during assembly in the clean room. It shows bridges positioning the 5.6 meter long wire planes inside the gas tight mechanical box of end frames and side panels.

Each momentum measuring chamber contains about 320 signal wires, 620 field and guard wires, and 2000 cathode wires making a total of 3000 wires. The signal and field shaping wires are positioned by precision Pyrex glass and carbon fiber bridges to within 10μm in the magnetic bending direction (Fig.14). These bridges have very small thermal expansion coefficients (1.5ppm/°C) thus temperature effects on the wire positions are negligible.

The Pyrex glass pieces were glued to carbon fiber supporting bars on a very precise Invar template. Bridges thus produced have a surface to surface spacing of 101.500mm. All bridges were measured using an HP laser interferometer system [3] with an accuracy of 2μm. The measured RMS absolute position accuracy for all 255 bridges produced was 5.2μm as shown in Fig.16a.

There are 3 bridges per chamber. One bridge at each extremity precisely positions the wires, and one bridge in the middle both positions the wires and reduces sag by a factor of 1/4 (Fig.16b). The two end bridges are positioned with respect to external reference surfaces. Wire planes were put into position in the chamber and tension was adjusted so that for signal wires, the vibration frequency of the first harmonic was 27.85 Hz to within 2%. This ensures that the gravitational sag for all signal wires is 95μm and known to 2%.

Internal alignment systems are integrated into the structure of the bridges. They allow us to position the middle bridges to an accuracy of 10μm and ensures straight wires. The middle bridge is moved by actuators in x and y (perpendicular to the beam direction) as shown in Fig.16b.

The threefold alignment system consists of LED's, lenses, and quadrant photodiodes. Each set of three elements was individually calibrated on an optical bench. Light from an LED mounted on one end bridge is focused by the

lens in the middle bridge onto the quadrant photodiode at the opposite end bridge. The system is aligned when all four quadrants of the photodiode receive equal amounts of light. Wires were positioned along the Pyrex surfaces of the 3 bridges by means of a template and were then attached with an insulating wax. Fig.17a depicts a chamber cell with 16 signal wires showing the computed drift paths in a 5.0 kGauss magnetic field and for an Argon:Ethane (62:38) gas mixture.

The chamber cell has a uniform electric field throughout the active region. Sense wires are spaced 9mm apart and are interspersed with field wires. Eight additional wires beyond the last sense wire equalize the drift time behavior of all sense wires to within 0.2 nsec (10μm). A plane of cathode wires, spaced 2.25mm apart, is at a distance of 50.75mm from the sense wire plane. Four different high voltages are applied to the sense, field, cathode and guard wires. These voltages allow us to control the drift field, the gas amplification and the zero potential position. At nominal voltage settings, in a 5.0 kGauss magnetic field and at 740 mm Hg pressure, the gas gain is 5×10^4. The electric field is 1140 V/cm in the drift region, and the drift angle due to the Lorentz force is 18.8 degrees.

Fig.17b shows the computed drift velocity for constant pressure, temperature, and magnetic field. The time-to-distance conversion function $x(t) = v(\Phi,B,P) \cdot t$ in the drift cell has been mapped in test beam runs and its dependence on the track slope Φ, magnetic field, and barometric pressure measured. Without magnetic field, the measured cosmic ray residuals of a chamber with a threshold equivalent to the 10th-12th drifting electron reaching the wire, and using 14 of the 16 measurements is 136μm (Fig.18a).

Chamber resolution in a magnetic field depends on the distance from the wire plane and on the slope of the track. Resolution across the cell varies from about 120μm to a maximum of 200μm very close to the sense wire. Fig.18b shows the RMS resolution as a function of the distance from the sense wire. The best resolution is attained for tracks roughly perpendicular to the electron drift in the magnetic field. Calculations based on our test beam data indicate that the overall RMS chamber resolution is 168μm. This averages over all positions and slopes which we can expect for high momentum tracks.

b) Z Chambers

A Z chamber [4] consists of 2 layers of drift cells. Cells of the upper plane are shifted by one half cell with respect to the lower ones, thus helping to resolve left-right ambiguities. Each cell has two parallel aluminum I Beams (Fig.19) connected to -2.4 kV and a single anode wire of gold plated molybdenum with 50μm diameter at +2.1 kV in the center. The cell is closed by two aluminum sheets at ground potential and is isolated from the I Beam profiles by fiber glass strips.

The Z chamber gas mixture is 91:9 Argon:Methane. It was chosen because it is nonexplosive. The drift velocity averaged over the cell is 30μm per nsec. Measured resolution, both in a test beam with a prototype, and with cosmic rays in production chambers is typically 500μm (Fig.19). These chambers are the covering elements of inner and outer precision chambers.

5. Supporting structure

The supporting structure [5] was designed by the Charles Stark Draper Laboratory.

Octant stands are precision structures supporting the chambers and maintaining chamber alignment to ≤ 30μm over long time periods. They have been designed to avoid tensor force transmission, thus octant behavior is fully predictable under all conditions of stress, load and temperature.

The main elements of the octant support structure are the "A Frames" (Fig.20a). They support each P chamber at four points, two in each A Frame. The inner chamber is mounted directly onto the A Frame, while the other chambers are mounted on special support bars. A combination of support points with zero, one, or two degrees of freedom ensures that chambers can move following temperature variations without introducing unwanted mechanical stresses. A longeron connecting the two A Frames provides mechanical stiffness in the Z direction.

In addition to the large aluminum structural components, there are approximately 300 small precision parts per octant. Design, fabrication, quality control, and assembly of all octant stand parts have been performed with a view toward our ultimate alignment goals. Materials were carefully

chosen for strength, thermal characteristics, and long term stability. Special materials, such as titanium and copper beryllium, have been used for chamber support feet, chamber tie plates, torque tube joints and other highly stressed areas.

Each octant has undergone detailed dimension and referencing checks during its assembly phase; some of the design tolerances are listed in Fig.20b. Four support feet on the floor were positioned in a plane to 50μm, which simulates the torque tube attachment. Critical distances between reference surfaces were measured to 10μm by means of special tools calibrated with a laser interferometer. Angles were measured with electronic bubble levels [6] which have intrinsic resolutions of better than 5 μrad.

After chamber loading, preliminary alignment, and functionality tests, each octant was rotated to the angle corresponding to its final position in the ferris wheel. Final alignment was then performed.

The elastic nature of the structure, with little or no hysteresis allows us to assume reproducibility if the octant is rotated back and forth. This was extremely important in view of the installation scheme on the torque tube. For this reason, each octant was rotated through 360° as shown in Fig.21, after which its alignment was rechecked. All octants were checked in this way, and showed full reproducibility, hence elastic behavior. Fig.22 shows the measurement of the middle chamber position during such a rotation. The initial and final chamber positions were reproduced to within 6μm, which was our measurement accuracy.

Structures of such accuracy are crucial to the success of this experiment. This was achieved after many years of collaboration with the Charles Stark Draper Laboratory. The experience gained in designing and building the L3 muon chambers with unprecedented precision permits us to design high resolution muon detectors for use at the SSC.

6. Electronics

The signals from 27,648 P chamber wires are connected via 82Ω decoupling resistors to 13,824 amplifiers [7] in corresponding pairs of

wires from both detector wheels. Amplifiers are located in the median plane of the detector. The amplifiers convert incoming currents to voltages with a conversion factor of 25mV/μA. The differential output (typically 200 mV for a muon) is connected via 30m of twisted pair cable to discriminators [8] set to 20 mV threshold. The logical "time over threshold" signal is conducted through 14m of twisted pair cable to 500 MHz Time Digitizers [9] which continuously record until the common stop from the beam crossing arrives. The TDC's cover a range of 1100 nsec with 1.1 nsec least hit accuracy, and do not contribute significantly to the resolution.

The system has proved stable to 0.2 nsec (corresponding to 10μm) when checked by our standard "T_0" calibration system which electronically induces pulses onto the wires (Fig.23). In a similar fashion, all wires of the Z chambers are processed by 7,680 time recording channels, which are also read out by FASTBUS TDC's. Parallel outputs without time processing are used to form fast road triggers.

7. Alignment systems

a) Alignment within the chambers

The accuracy of the bridges inside the momentum measuring chambers and of the internal alignment systems built into them (Fig.16) assures that wires within a chamber are precisely positioned with respect to each other, as described in section 4.

b) Alignment of the three chamber layers

A dual straightness monitor (Fig.24) forms one part of the octant alignment system. A precision piece containing two LED's is attached to each end frame of an inner chamber. Similar pieces are mounted between the two middle and the two outer chambers. The assembly between the middle chambers contains a lens, and that between the outer chambers contains two quadrant diodes. An insulated brass pin, referenced to the LED's, lens, or quadrant photodiodes touches one wire of a signal plane. The end bridge can be moved to allow the wire to just make or break electrical contact with the pin. These pieces, and thus the wire planes of opposing chambers, are kept at precise separations of 101.500mm by means of gauge blocks. In this way, the end bridge positions are known to within a few microns. Each end of the octant has a dual set of straightness monitors.

Light from the LED's is focused by the lens onto the quadrant diodes. The system is aligned when all quadrants receive equal amounts of light. The middle chamber layer can be moved on its titanium flexure feet based on the readout of these systems to bring the chamber centers into a straight line. These sets of three elements were calibrated on an optical bench, and the readout defines the center line through the three chamber layers to $\leq$ 10μm.

c) Torque measurement

The vertical alignment systems guarantee that the chambers line up at each end of the octant, but the two octant center lines must also be parallel to each other. We use a rotating laser beacon [10] to measure the extent to which the two ends of the octant are parallel. A He-Ne laser beam is reflected 90° by a highly accurate rotating pentaprismatic mirror assembly which sweeps out a plane to an accuracy better than 30μm. The deviation of the octant center lines from this reference plane is measured by six position sensors (photodiode arrays) attached directly to the three elements of each straightness monitor. The laser beacon can measure the angle between the two octant center lines to less than 25μrad. The corresponding error induced in the sagitta is less than 10μm. The outer and middle chambers are adjusted such that this measured angle is zero (Fig.25).

d) UV laser alignment verification

Each of the 16 octants contains a two stage nitrogen ultraviolet laser [11], which is operated under computer control. The laser beam is directed up and across the top of the outer chamber layer by means of an addressable beam steering element (Fig.26). Mirrors direct the beam down through a quartz window into the drift cells of all layers of the octant which are connected by tubes pointing roughly to the interaction point. Photodiodes at the bottom of the inner chamber measure the position of the beam centroid. Each octant has eight laser beam trajectories, which simulate infinite momentum particles going toward the interaction point.

The sagitta of laser events should be zero, and thus is used to verify the alignment. Two of the laser beams have movable mirrors and can produce parallel trajectories of accurately known separation. This allows us to measure and constantly monitor the electron drift velocity, thus also monitoring chamber behavior.

8. Verification

Prior to verification, each of the octants was adjusted to within the alignment specifications using the double set of straightness sensors and the laser beacon. All octants were then tested prior to installation in L3.

UV laser runs of 100 events were taken using the eight different laser beam paths in each octant. Reconstruction of the laser trajectories (Fig.27a) should show straight lines. The sagitta, which is a measure of our alignment accuracy, is defined as:

$$s = (x_{mi} + x_{mo})/2 - x_{mm}$$

where x_{mi}, x_{mm}, and x_{mo} are the coordinates measured in the inner, middle, and outer chambers, respectively.

Fig.27b shows the results of 42 different laser runs as an example of the verification of one octant. Errors on the points are derived from the residuals of 100 event runs. The resulting average of all runs, -26±10μm, is within the design limit of 30μm. The 10μm error is derived from the scatter of run results, thus taking systematic errors of the laser into account.

Fig.28 show an independent way of checking octant alignment in the absence of a magnetic field by using cosmic muons. Scintillation counter hodoscopes are positioned above and below the octant. The resulting coincidence trigger is used as a TDC stop. Tracks were reconstructed from the chamber segments (Fig.28a). Accepting all cosmic rays, we obtain the wide histogram in Fig.28b which has an RMS of 1.3mm. This large width is due to multiple scattering from the predominantly low energy of cosmic muons.

The L3 muon chambers are unique in that they also measure the local slope of the particle trajectory to an accuracy of ≈ 1 mrad. Demanding that the local slope in a chamber agree with the overall particle trajectory to within 2 mrad eliminates multiple scattered events. Indeed, a 400μm wide distribution of 760 events is obtained in Fig.28b (shaded) which confirms that this octant is aligned to:

$$s = 2 \pm 400\mu m/\sqrt{760} = 2 \pm 14.5\mu m$$

Fig.29 summarizes the results for all 16 octants. The s = 0 value is given by the setting of the two independent straightness monitors. The black squares show verification of the geometry by UV laser measurements. The cosmic ray data are shown in circles as a third independent measurement.

We see excellent agreement between all three alignment methods:

opto-mechanical
cosmic
UV laser

and find our octants to be well within the range of specification of ± 30μm.

L3 was installed at LEP by June 1989. The LEP ring was closed in mid-July of 1989, and machine studies began. The first collisions occurred at around midnight of August 13th. Fig.30 and 31 show the first inclusive muon event from Z° decay at LEP as recorded by the L3 Detector. The first $Z^\circ \rightarrow \mu^+\mu^-$ decay at LEP is shown in Fig.32 (end view), and 33 (side view). The LEP center of mass energy was 91 GeV, and the measured momenta in the dimuon event are 40 and 44 GeV. There was a dE/dx loss of 4 GeV, and a photon of 3 GeV was emitted in the BGO. The event emerges from the nominal intersection point to within 3mm.

This measurement is of unprecedented accuracy. It shows the full potential of this approach to exploit muon physics at SSC energies.

References

[1] L3 Collaboration, Letter of Intent (January 1982)
L3 Collaboration, "The L3 Technical Proposal" CERN LEPC (March 1983)

[2] U. Becker, et al., NIM 180 (1981), 61;
P. Duinker, et al. NIM 201 (1982), 351

[3] Hewlett Packard Interferometer 5526A

[4] U. Becker et al., NIM 128 (1975) 593; C. Willmott. NIM A263 (10) 1988

[5] W.E.Toth, C.S. Draper Report CSDL-R1885 (Oct.1987) and SENER Report
N.K. Chhabra, C.S. Draper Report CSDL-R2011 (Sept.1987),
P. Bowditch, C.S. Draper Report CSDL-R1597 (Jan.1983)

[6] M.G. Dix, et al., NASA Technical Briefs, 1981, p319

[7] P.Rewiersma, NIKHEF-H, Amsterdam Feb. 1986 internal note "L3 wire amplifier" The hybrid (NH19-6112) was made by Philips.

[8] P.Rewiersma, NIKHEF-H, Internal Note DISC.DOC27.03.87PR Unpublished.

[9] LeCroy LRS 1879 Fastbus TDC

[10] P.G.Seiler, et al. "The Laser Beacon", L3 Muon Chamber Group Internal Note, 85-4, 1985, unpublished; H. Anderhub, M. Devereux, P.G. Seiler, "On a new method for testing and calibrating wire chambers", NIM 176, 323, (1980); R.Fabbretti, et al., NIM A280(1989),13-24

[11] F.Hartjes and J.Konijn, NIM 217, 311 (1983)
F.Hartjes, J.Konijn, and Y.Peng NIM A269, 544 (1988)
J.C.Guo, F.Hartjes, J.Konijn NIM 204, 77 (1982)
H.Anderhub, M.Devereux, and P.Seiler, NIM 176 (1980) 323

Figure Captions

Fig.1 A perspective view of the L3 Detector.

Fig.2 One section of the L3 1000 ton aluminum coil is shown.

Fig.3 The completed magnet shown with doors open.

Fig.4 Results of survey show that the coil is aligned to 1mm.

Fig.5 The hadron calorimeter during installation in the support tube.

Fig.6 Energy resolution of the hadron calorimeter.

Fig.7 A BGO crystal along with its microprocessor card.

Fig.8 The BGO energy resolution.

Fig.9 The excellent TEC single wire resolution.

Fig.10 A perspective view of the assembled muon detector.

Fig.11 An octant module is attached to the supporting torque tube. Precision chambers, Z chambers, octant support stand, electronics, gas system, and the UV laser calibration system are indicated.

Fig.12 a) A curved muon trajectory is drawn. The figure indicates how measurement errors of the sagitta are defined.
b) A detail of the middle chamber showing the arrangement of wires in a chamber.

Fig.13 An end view of the three chamber layers in one octant, with a schematic view of the alignment system is shown.

Fig.14 Exploded view of an Outer (MO) precision chamber. Endframes, side panels, two of the three bridges, wire planes, and covering Z chambers can be seen.

Fig.15 Chamber in the clean room during the assembly phase. Two bridges are visible.

Fig.16 a) The bridge accuracy can be seen from this distribution of errors in the equidistant locations of the Pyrex glass pieces.

b) Three bridges which support the wires, and three straightness monitors and actuators used for bridge alignment are shown. The side sketch shows the principle of the straightness monitor systems.

Fig.17 a) Electric field lines in a drift cell of an inner or outer chamber are shown with a 5.1 kGauss magnetic field parallel to the wires. Drift times refer to a muon track 45mm from the signal wires.

b) Drift velocity is computed as a function of the drift field.

Fig.18 a) Distribution of residuals for cosmic muon tracks fitted to 14 of 16 wire measurements.

b) Resolution of a 5 cell test chamber in a 5 kGauss magnetic field has been plotted as a function of drift distance.

Fig.19 Z Chamber resolution, and the double cell structure of the Z chamber are shown.

Fig.20 a) Octant stand structure. Frames, longerons, as well as many of the smaller parts are shown. Feet aligned in a plane to 50μm attach the octant to the floor, simulating the actual attachment to the torque tube in the detector.

b) Some of the alignment tolerances for chambers in assembled octants. The alignment tolerance on the chamber center lines is only 25μm.

Fig.21 An octant in the rotation cradle.

Fig.22 The middle chamber position was recorded during rotation of the octant through 360°. After a complete rotation, it returned to the initial position to within our measuring accuracy (about 6μm).

Fig.23 The stability of the time zero calibration system is better than 0.2 nsec and satisfies our requirements.

Fig.24 The principle of referencing the octant center line directly to the wires of the three chamber layers is shown. The straightness monitor is mounted on the inner chamber, and between the two middle or outer chambers.

Fig.25 The laser beacon references six points in the center plane. The laser beam rotates in a plane and is detected by photodiode arrays which are attached to the straightness monitors.

Fig.26 Basics of UV laser alignment are schematically shown in this figure. The laser beam from an N_2 laser is directed by a beam directional element into eight trajectories essentially limiting the fiducial volume. Position sensitive photodiodes measure the beam location at the bottom of the inner chamber and are schematically indicated.

Fig.27
a) A computer reconstructed laser event.
b) Plotted results of a series of 42 runs of 100 laser shots each to measure the sagitta.

Fig.28
a) A cosmic ray track is reconstructed in the middle chamber.
b) Sagitta distributions are plotted without any cuts (white area), and with 2 mradian cuts (shaded area).

Fig.29 This is a compilation of alignment results for all 16 octants. The zero sagitta prediction is the result of the opto-mechanical measurement. UV laser verification results are shown as squares and circles indicate the center of cosmic ray distribution measurements. This shows that all sixteen octants are aligned to the design value of 30μm.

Fig.30 End view of the first L3 inclusive muon event from Z° decay

Fig.31 The same event as Fig.30 is shown from the side.

Fig.32 A $Z^\circ \rightarrow \mu^+\mu^-$ decay in L3, recorded in August 1989 at LEP. The muon momenta are 40 and 44 GeV. Data from the hadron calorimeter proved the particles to be minimum ionizing.

Fig.33 The same $Z^\circ \rightarrow \mu^+\mu^-$ event from Fig.32 is shown in the side, or non-bending view. A 3 GeV photon, emitted into the lower BGO barrel is clearly visible.

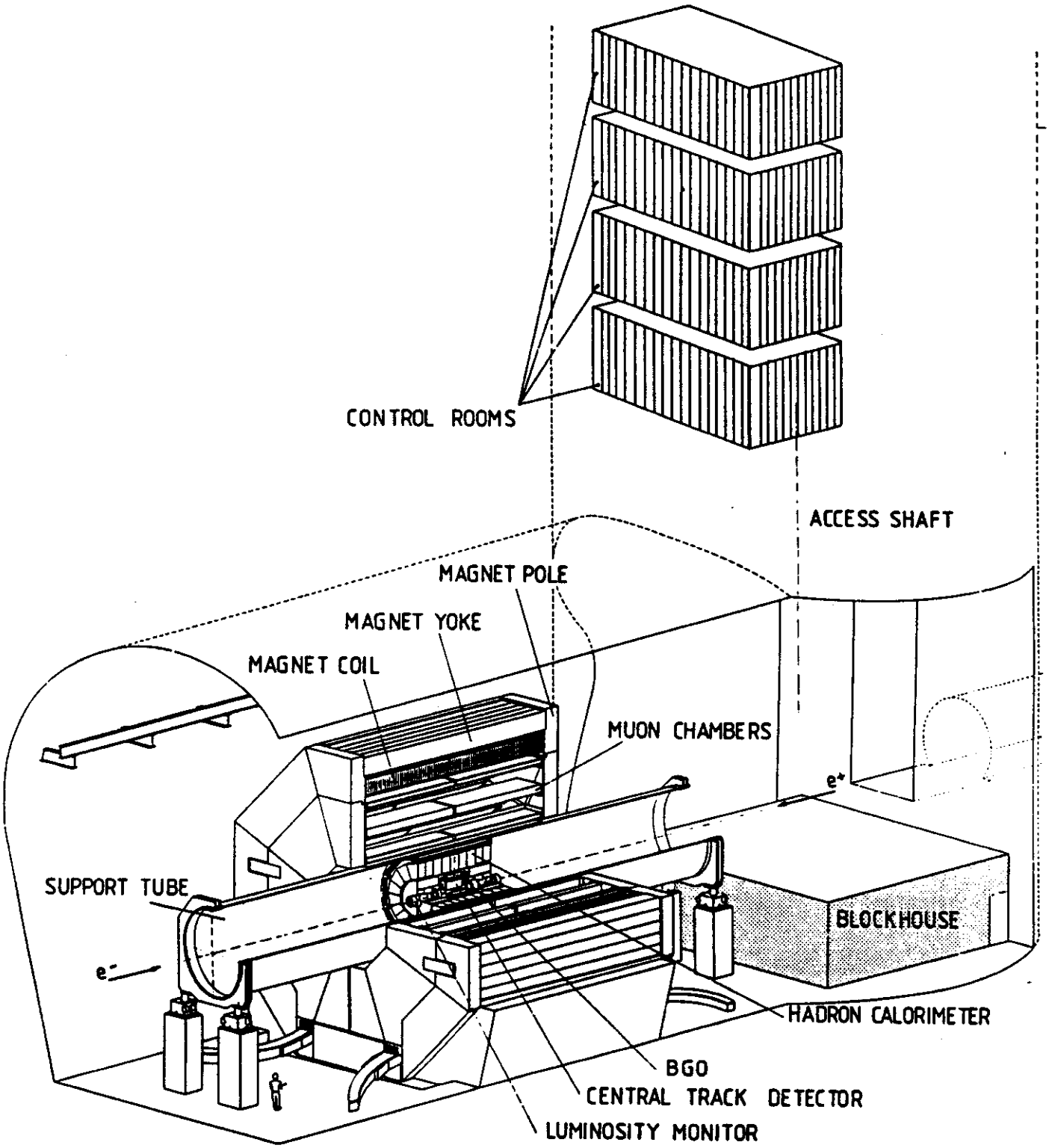
CONTROL ROOMS
ACCESS SHAFT
MAGNET POLE
MAGNET YOKE
MAGNET COIL
MUON CHAMBERS
e+
SUPPORT TUBE
e-
BLOCKHOUSE
HADRON CALORIMETER
BGO
CENTRAL TRACK DETECTOR
LUMINOSITY MONITOR

Fig.1

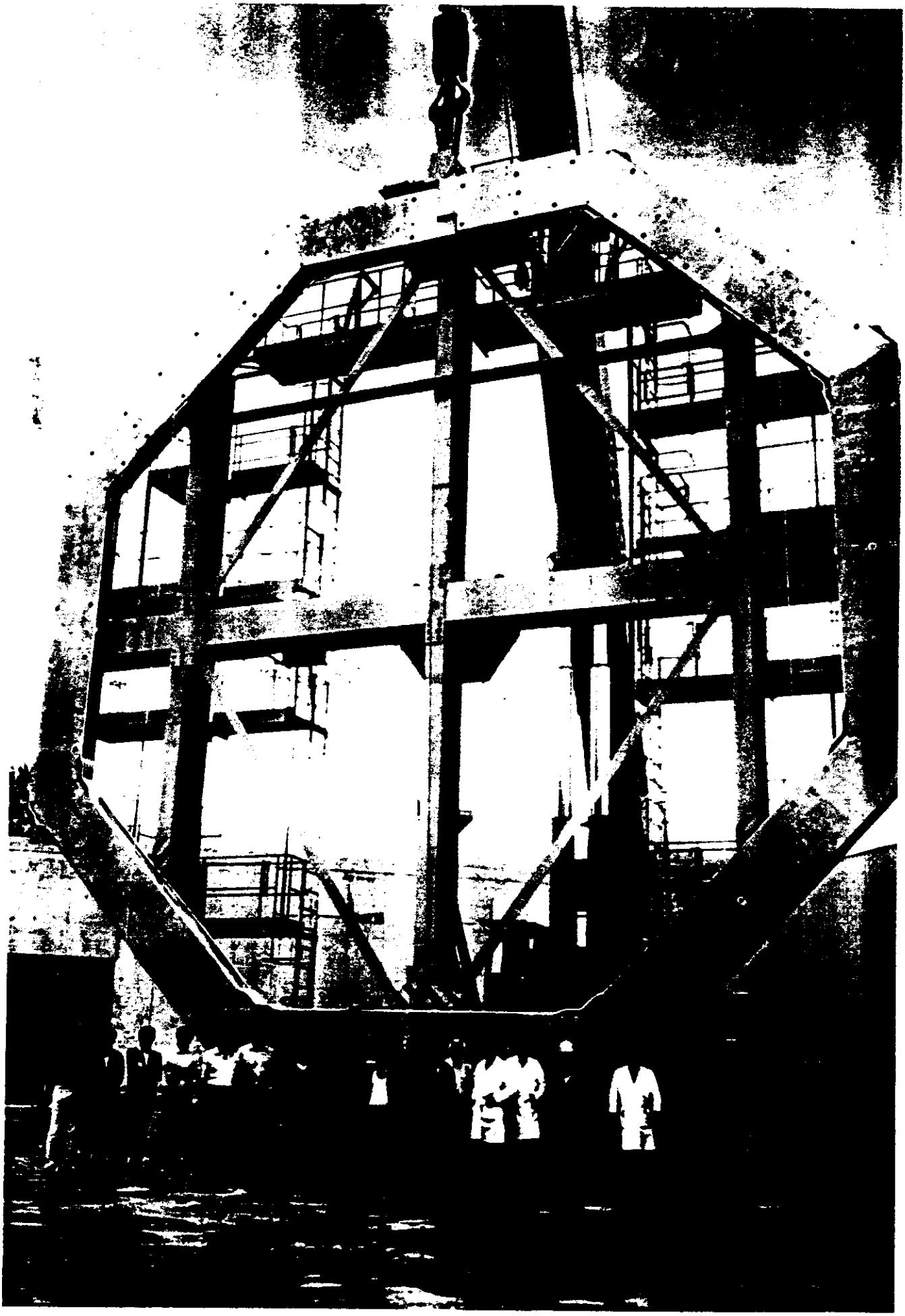

Fig 2

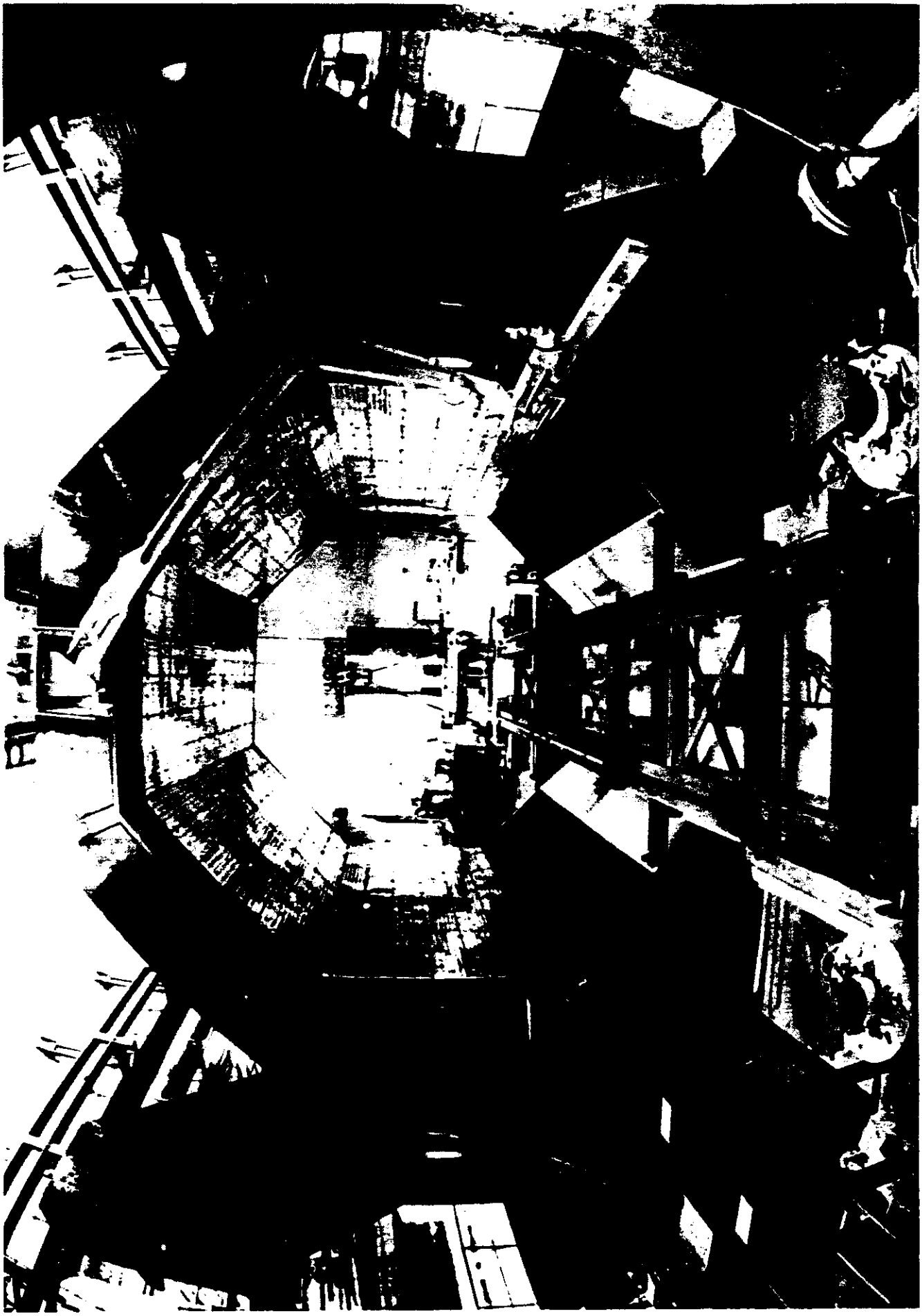

Fig.3

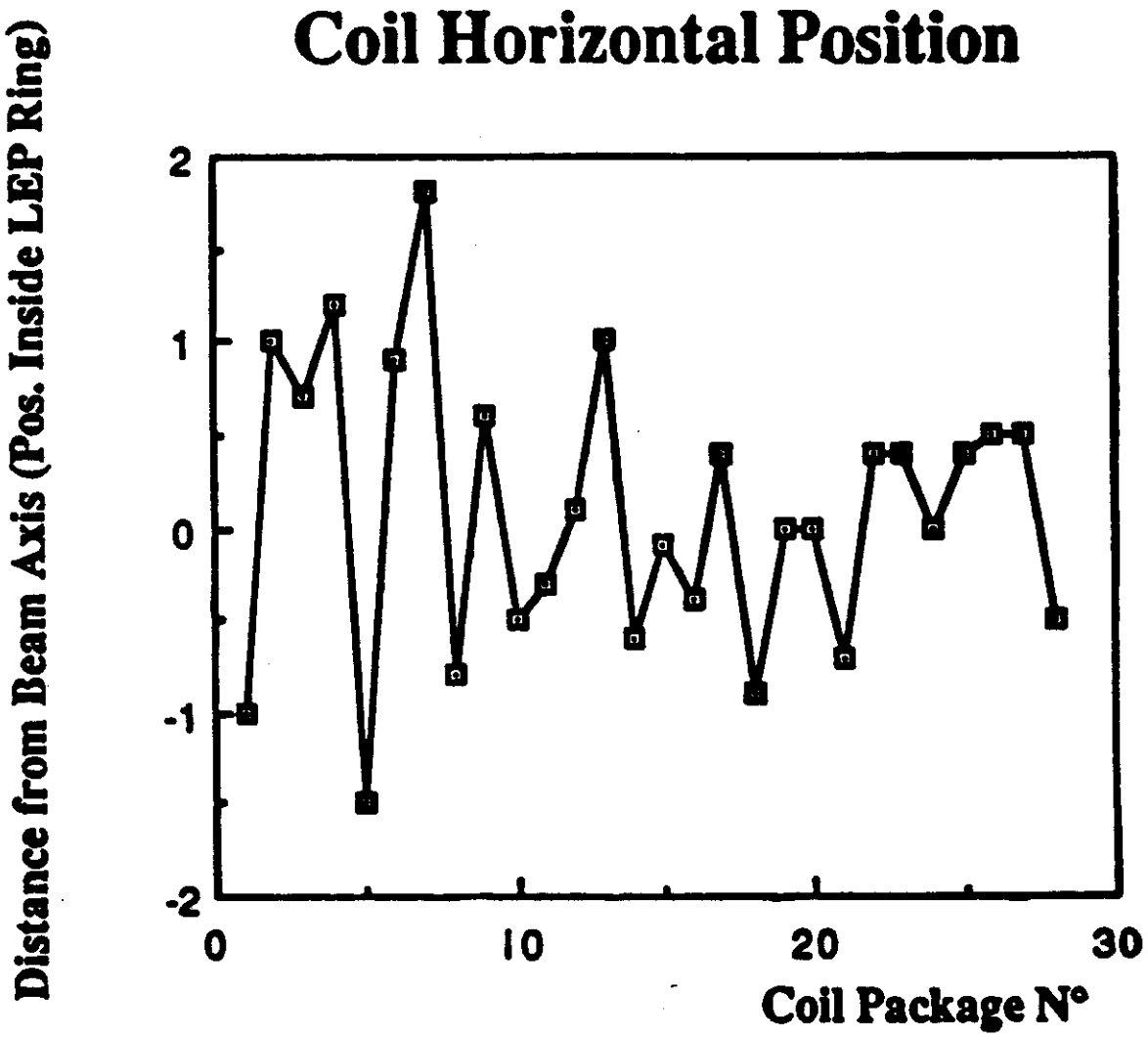
Coil Horizontal Position
Distance from Beam Axis (Pos. Inside LEP Ring)
2
1
0
-1
-2
0
10
20
30
Coil Package N°

Fig.4

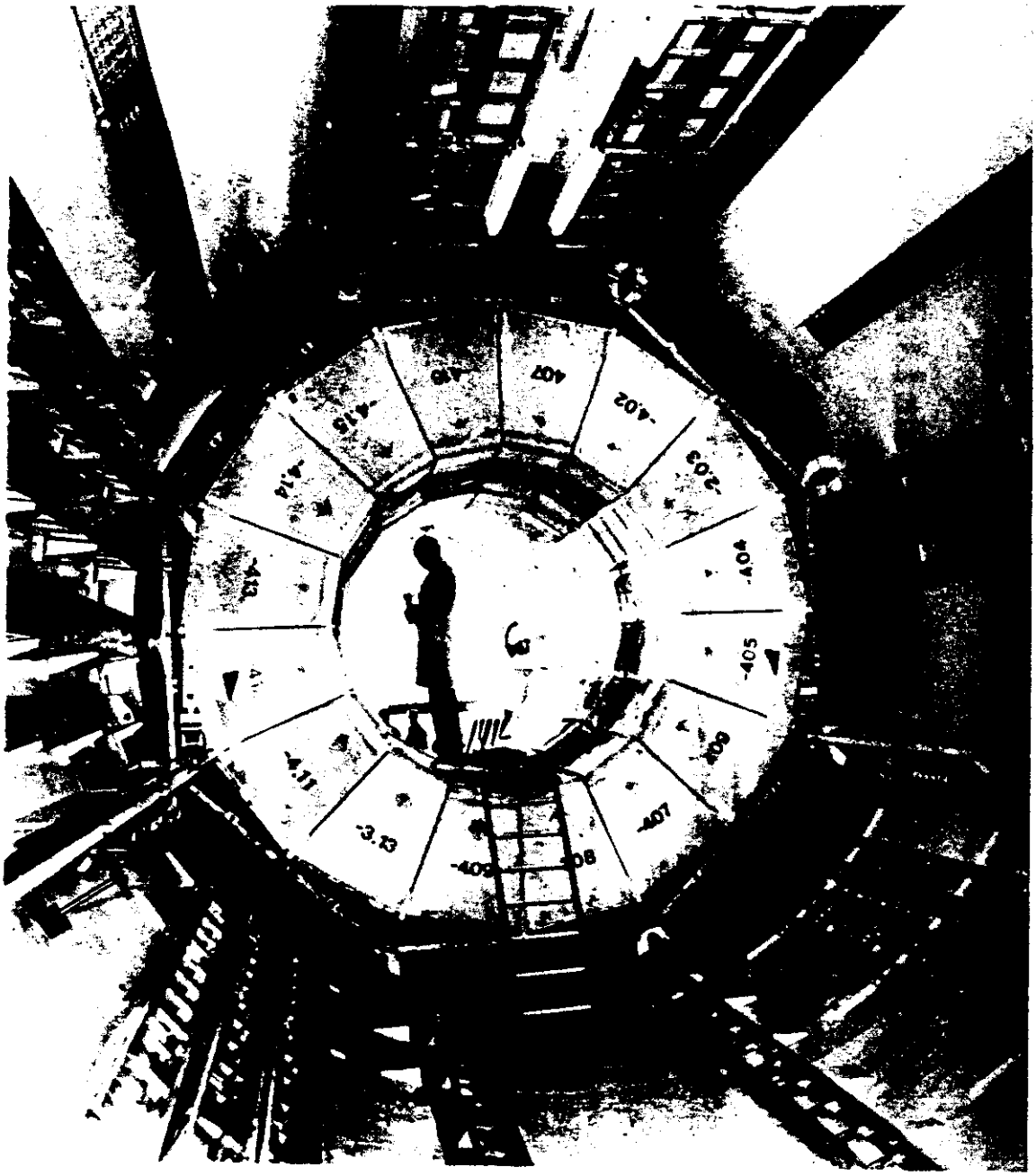

Fig.5

L3 Hadron Calorimeter Resolution

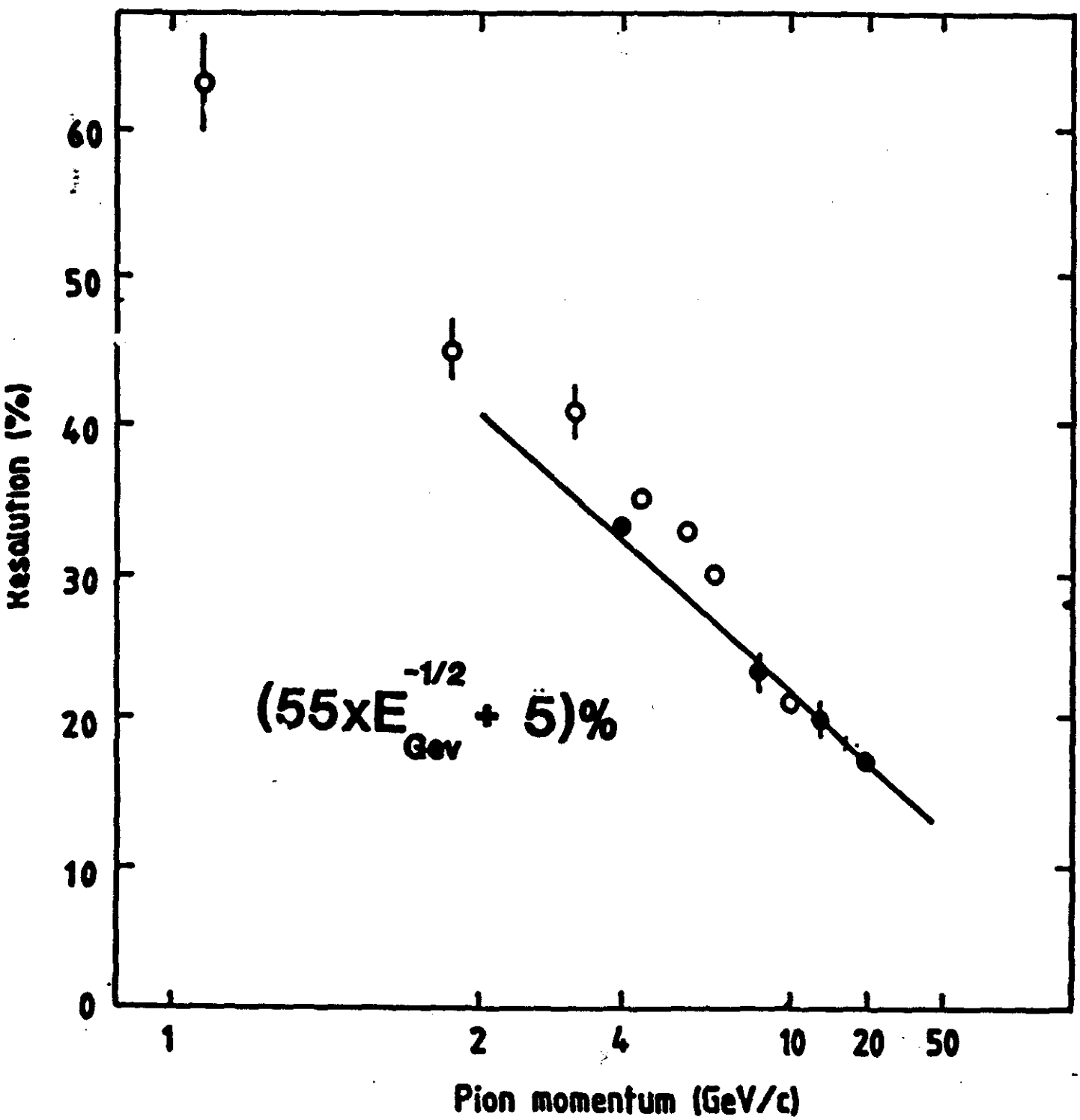

Fig.6

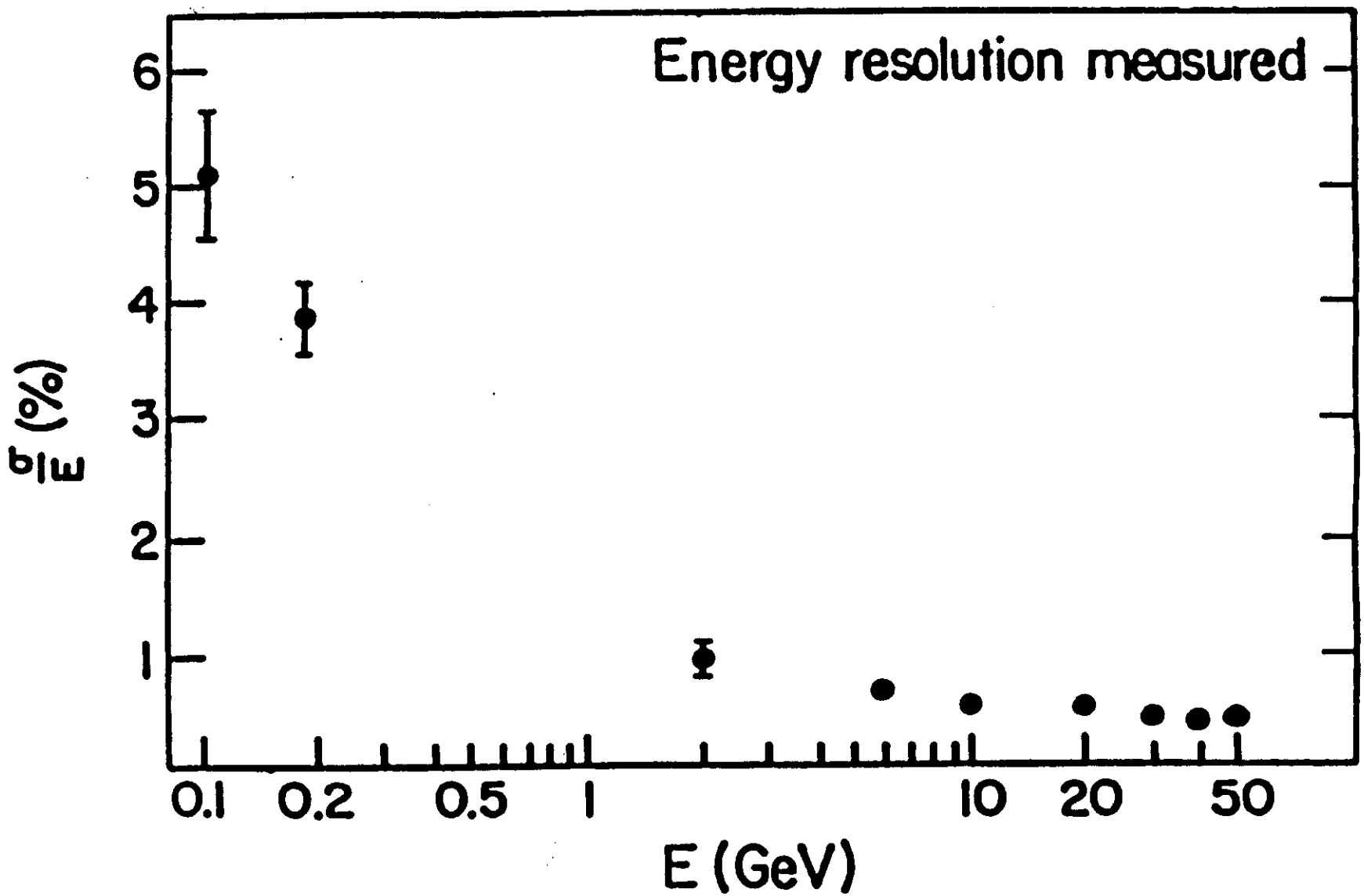

Fig.8

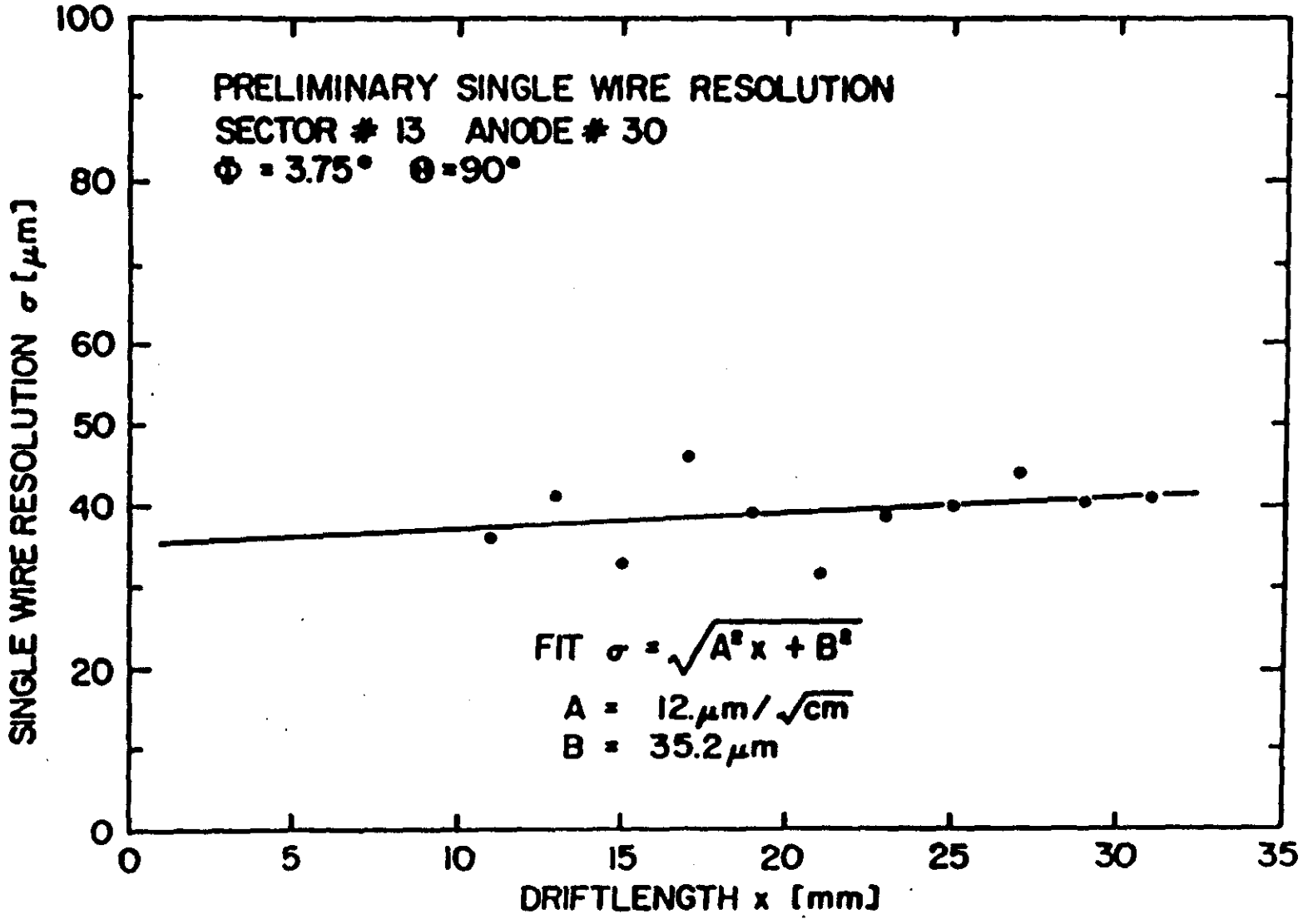
PRELIMINARY SINGLE WIRE RESOLUTION
SECTOR # 13 ANODE # 30
Φ = 3.75° Θ = 90°
FIT σ = √(A² x + B²)
A = 12.μm/√cm
B = 35.2μm
SINGLE WIRE RESOLUTION σ [μm]
DRIFTLENGTH x [mm]
0
20
40
50
60
80
100
0
5
10
15
20
25
30
35

Fig.9

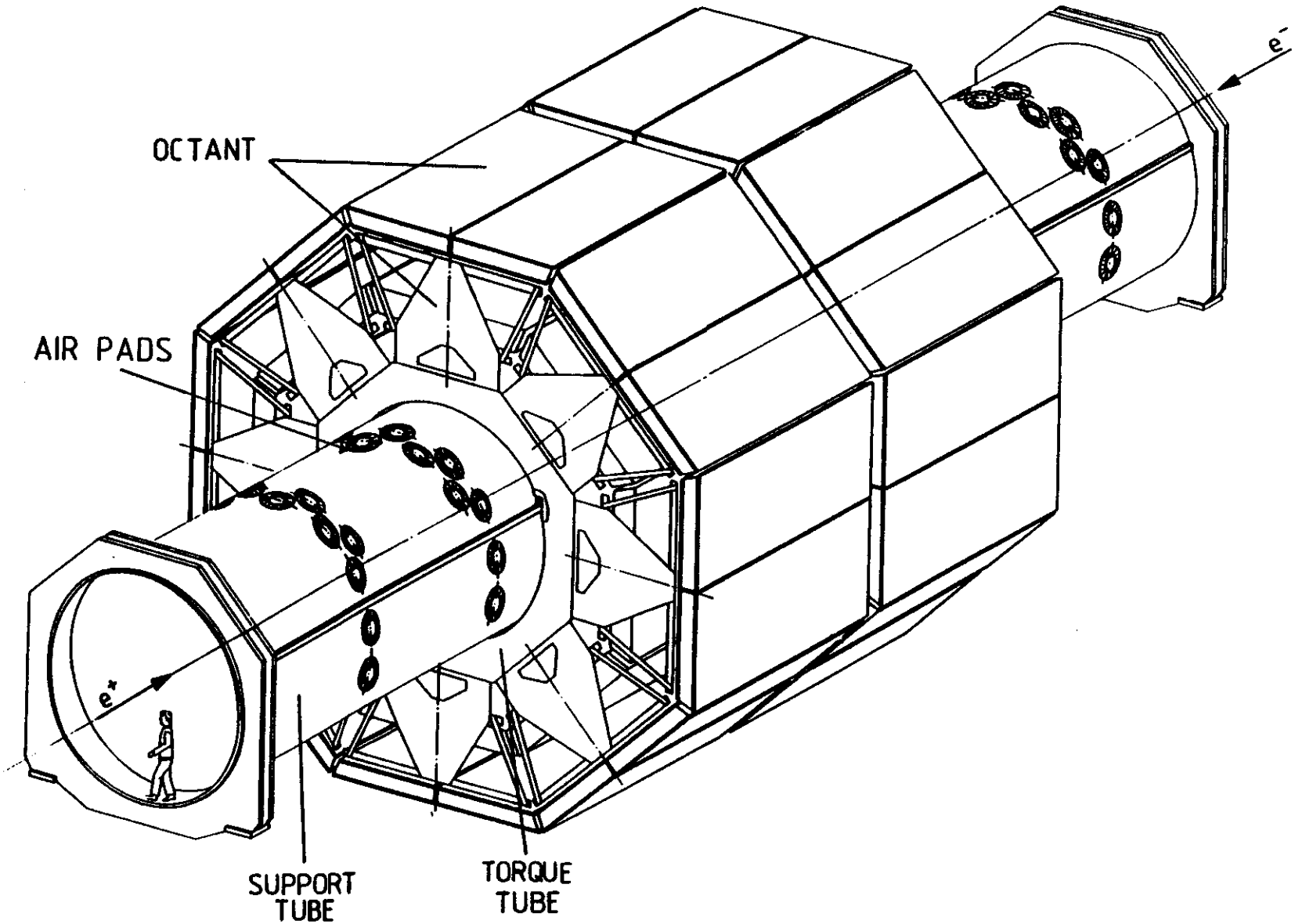

Fig.10

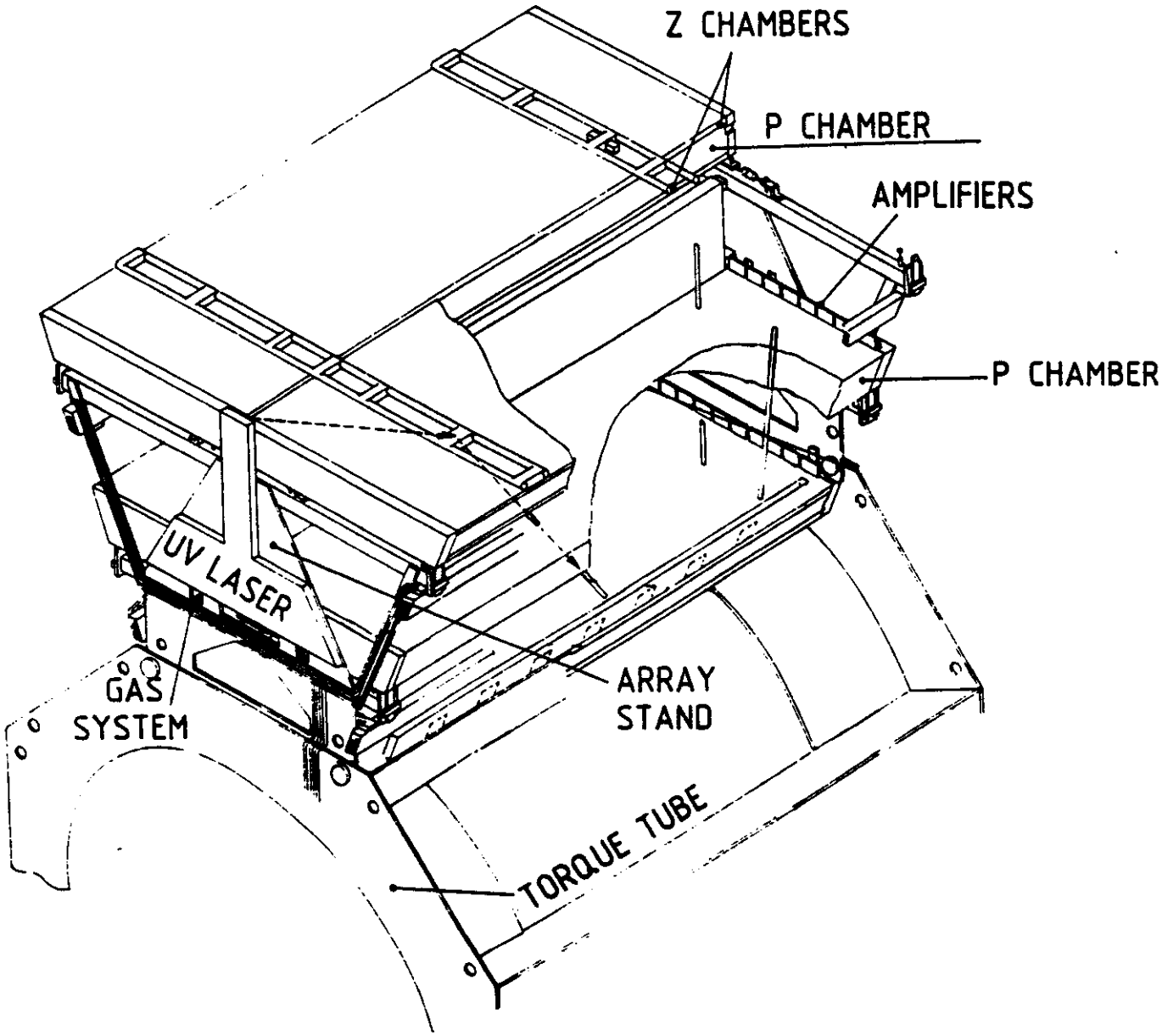
Z CHAMBERS
P CHAMBER
AMPLIFIERS
P CHAMBER
UV LASER
GAS
SYSTEM
ARRAY
STAND
TORQUE TUBE

Fig.11

PRINCIPLE OF ACCURACY

a)

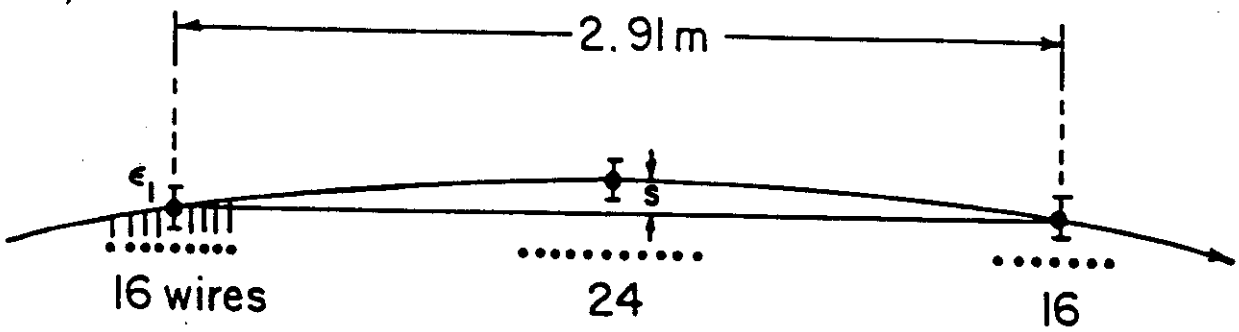

$$\epsilon_1 = \frac{250\mu m}{\sqrt{N_1}} \qquad \epsilon_2 \qquad \epsilon_3 = \epsilon_1$$

b)

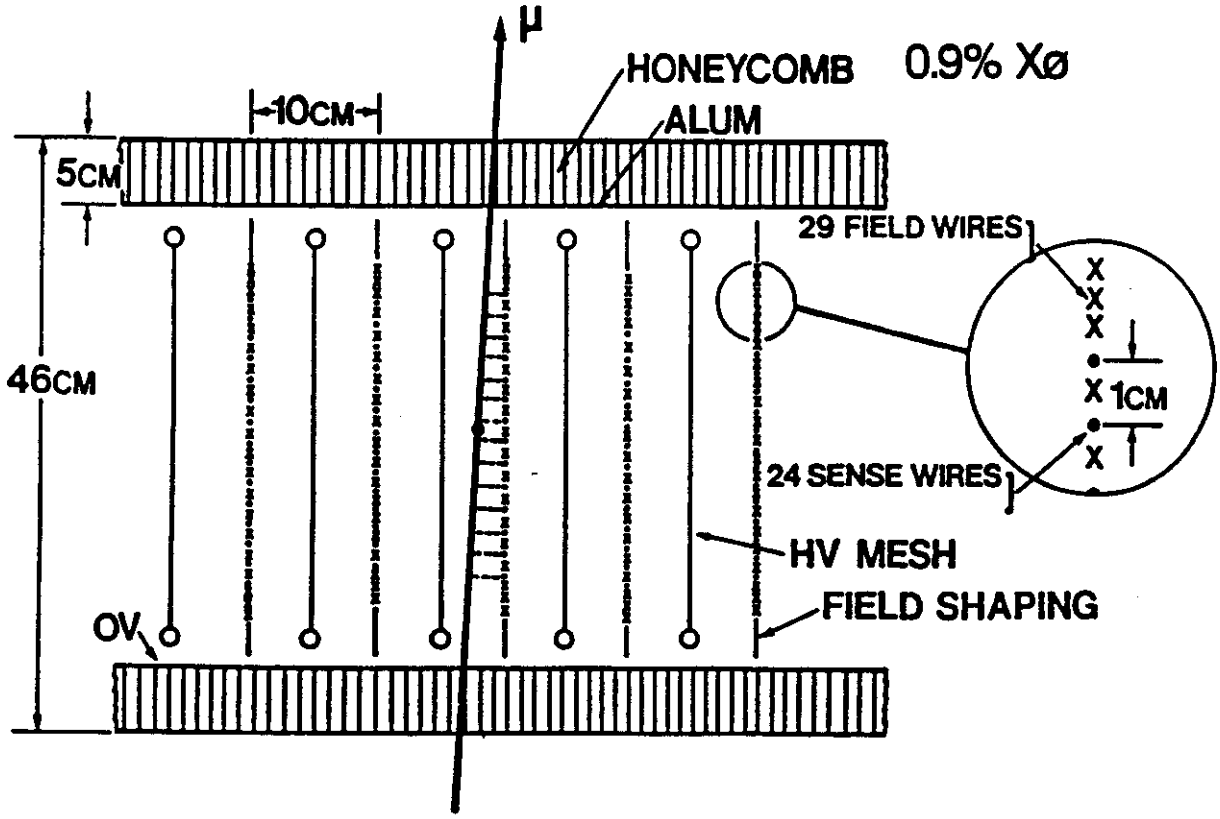

Fig.12

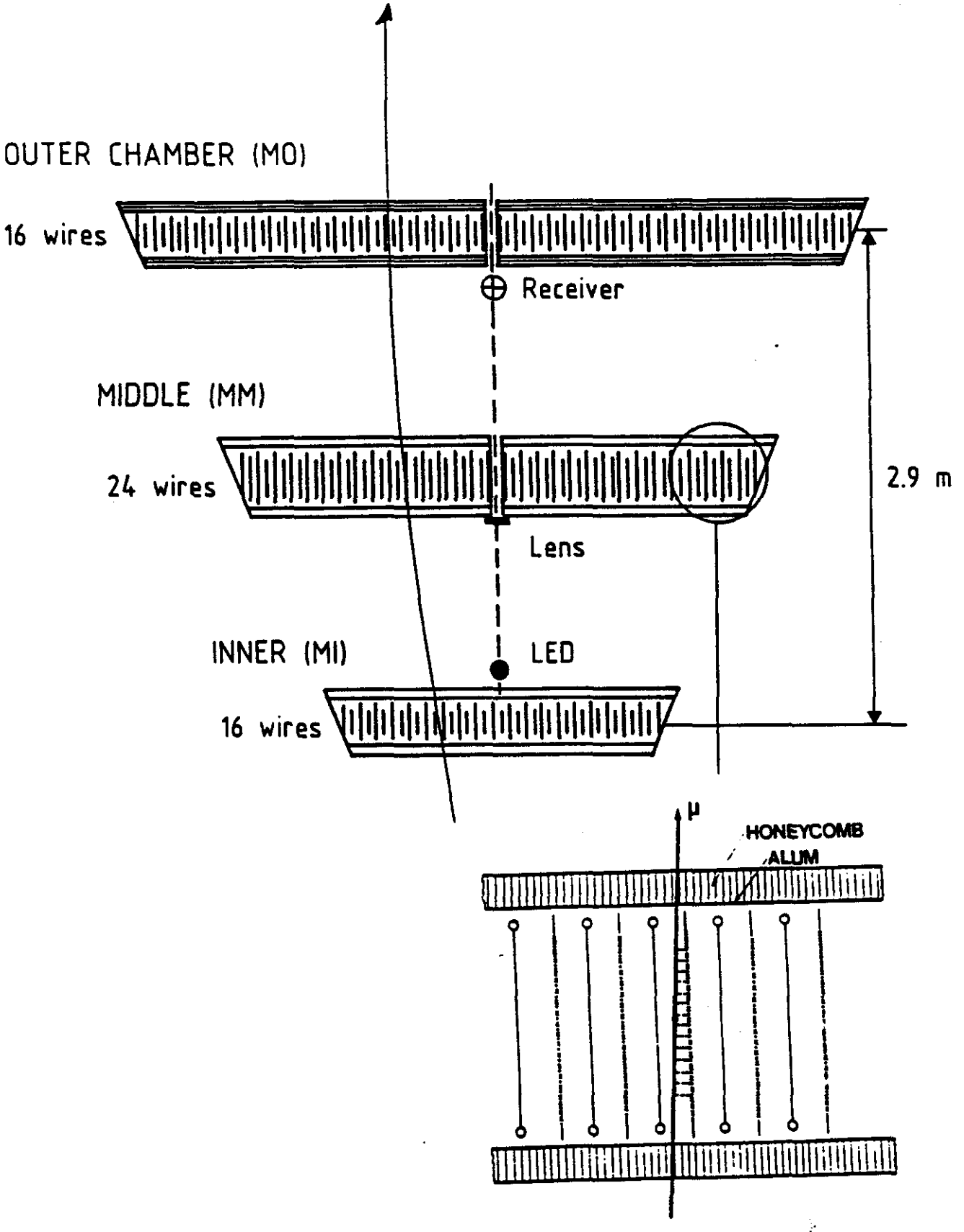
OUTER CHAMBER (MO)
16 wires
Receiver
MIDDLE (MM)
24 wires
Lens
INNER (MI)
LED
16 wires
2.9 m
μ
HONEYCOMB
ALUM

Fig.13

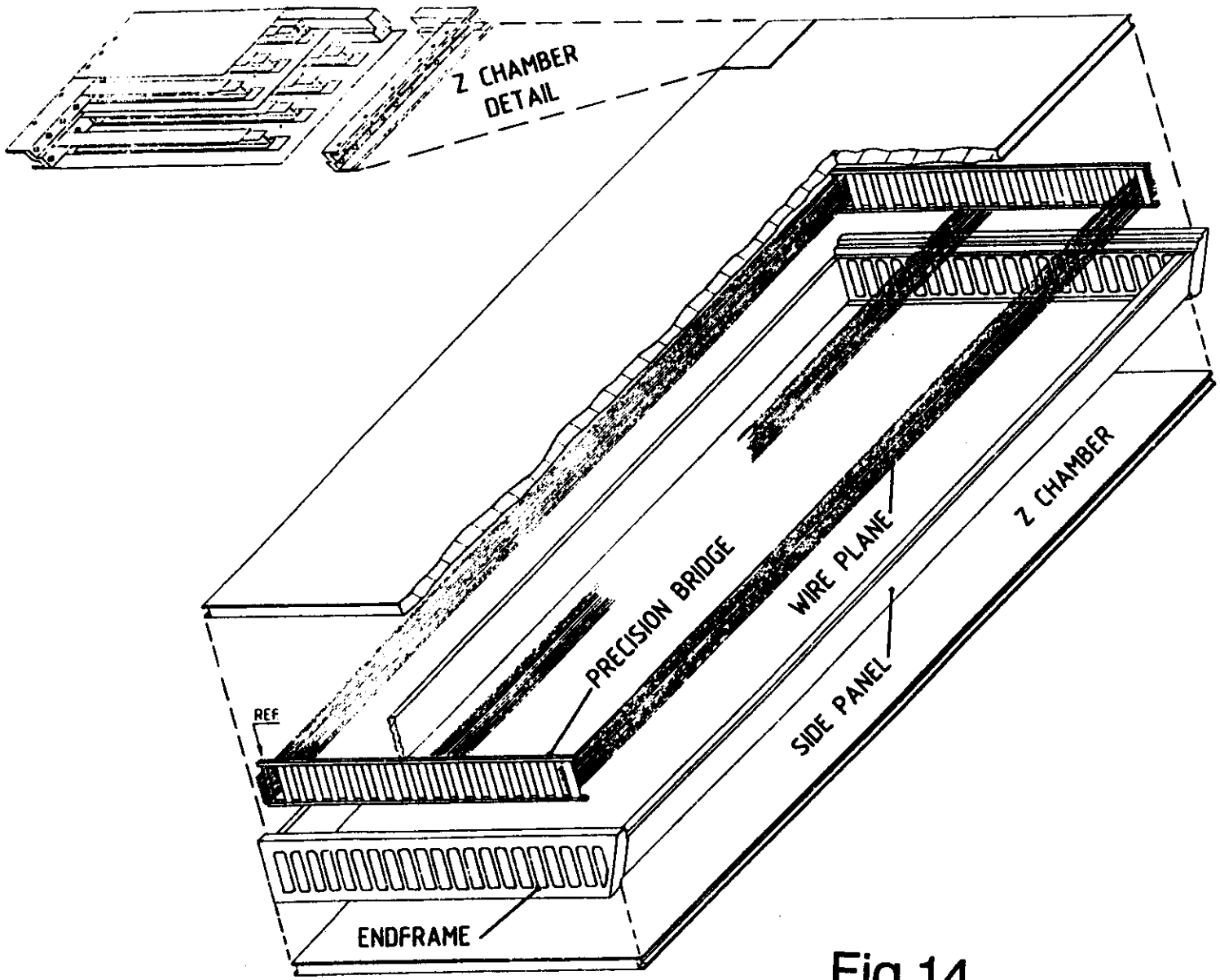
Z CHAMBER
DETAIL
REF
PRECISION BRIDGE
WIRE PLANE
Z CHAMBER
SIDE PANEL
ENDFRAME

Fig.14

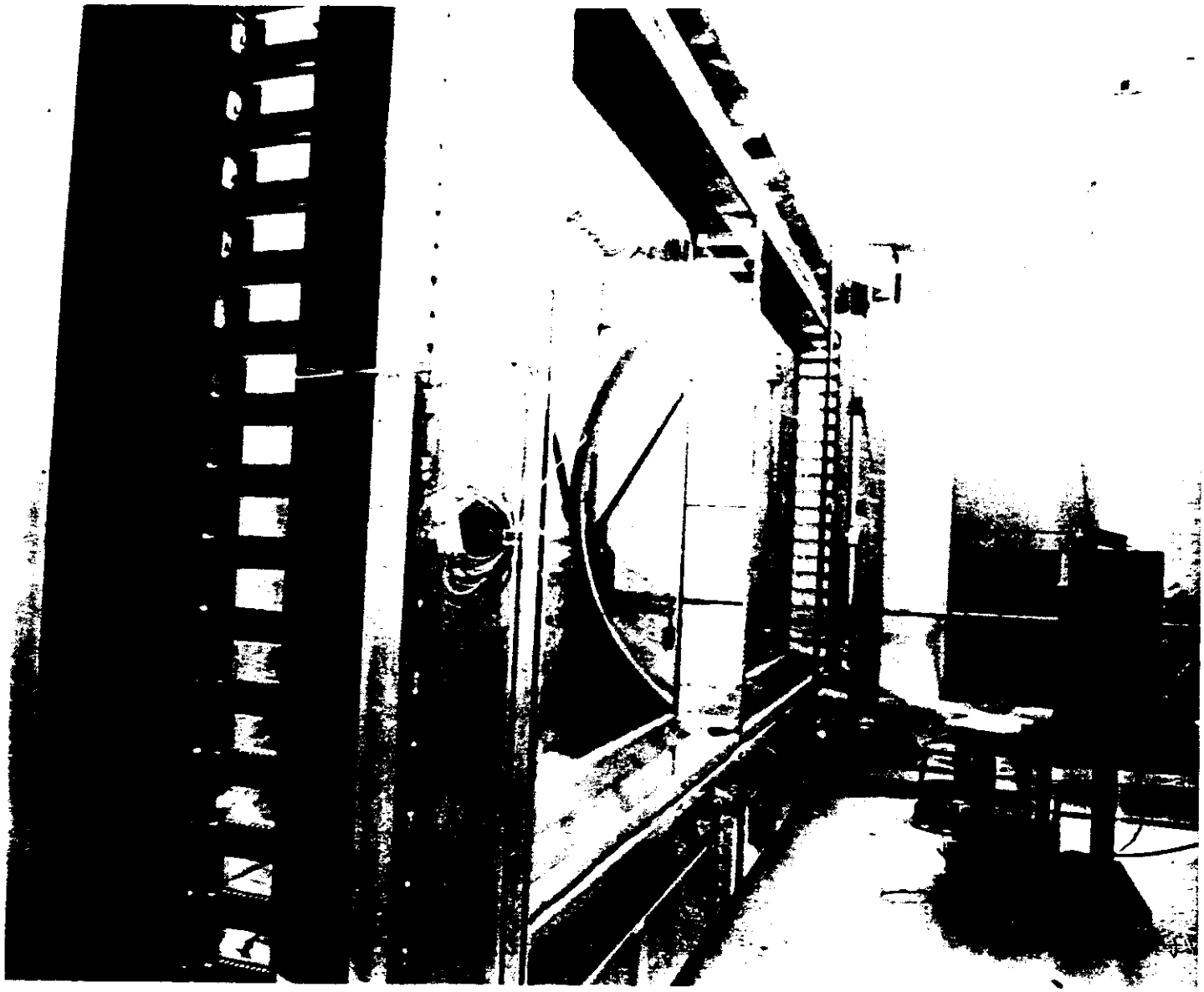

Fig.15

a)

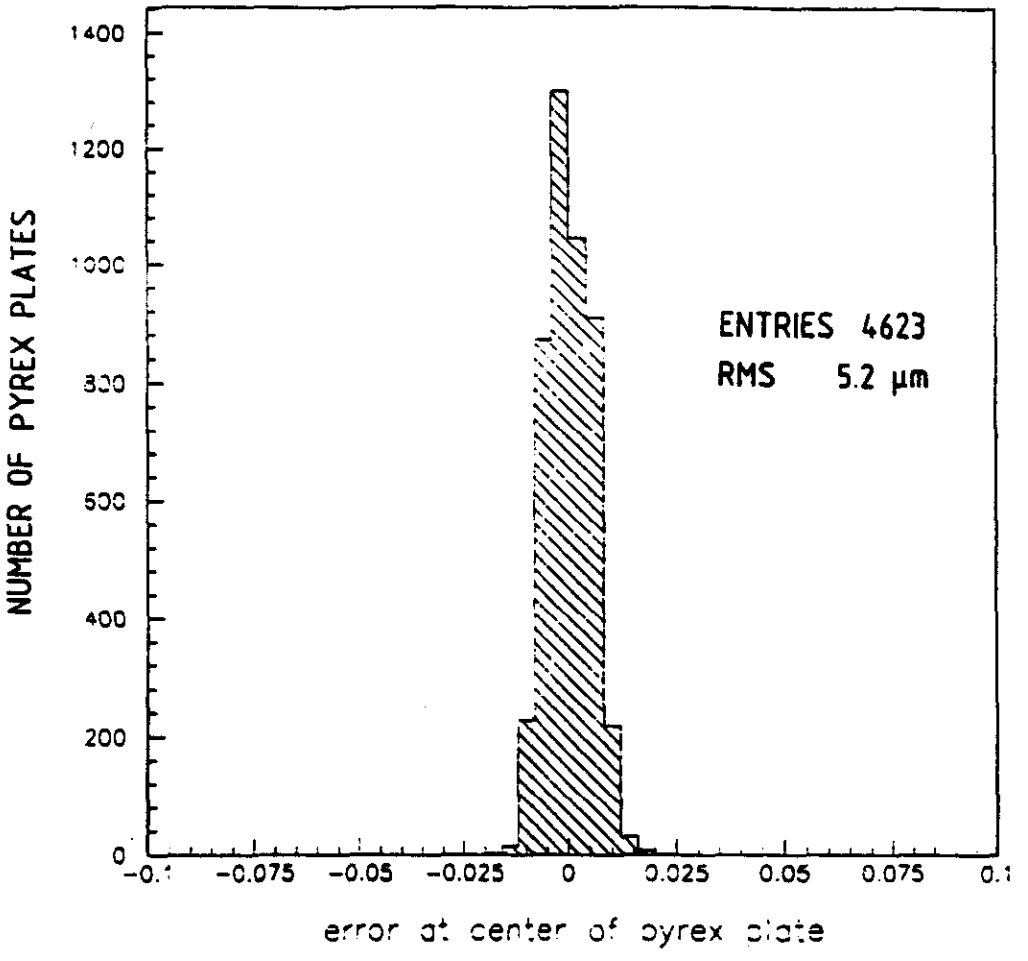
NUMBER OF PYREX PLATES
1400
1200
1000
800
600
400
200
0
ENTRIES 4623
RMS 5.2 μm
-0.1
-0.075
-0.05
-0.025
0
0.025
0.05
0.075
0.1
error at center of pyrex plate

b)

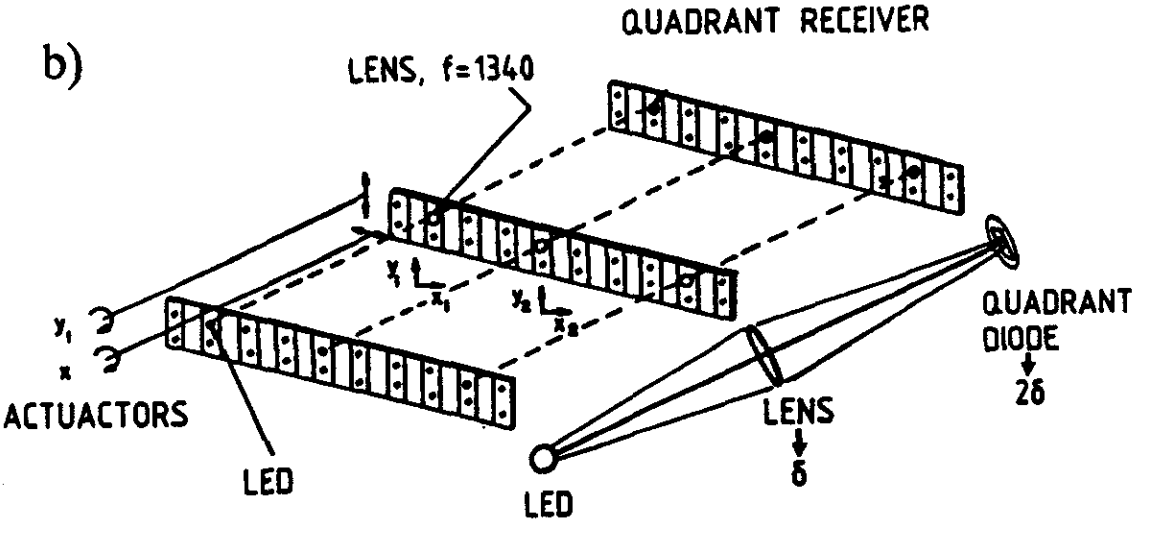
QUADRANT RECEIVER
LENS, f=1340
ACTUACTORS
LED
LED
LENS
δ
QUADRANT
DIODE
2δ

Fig.16

a)

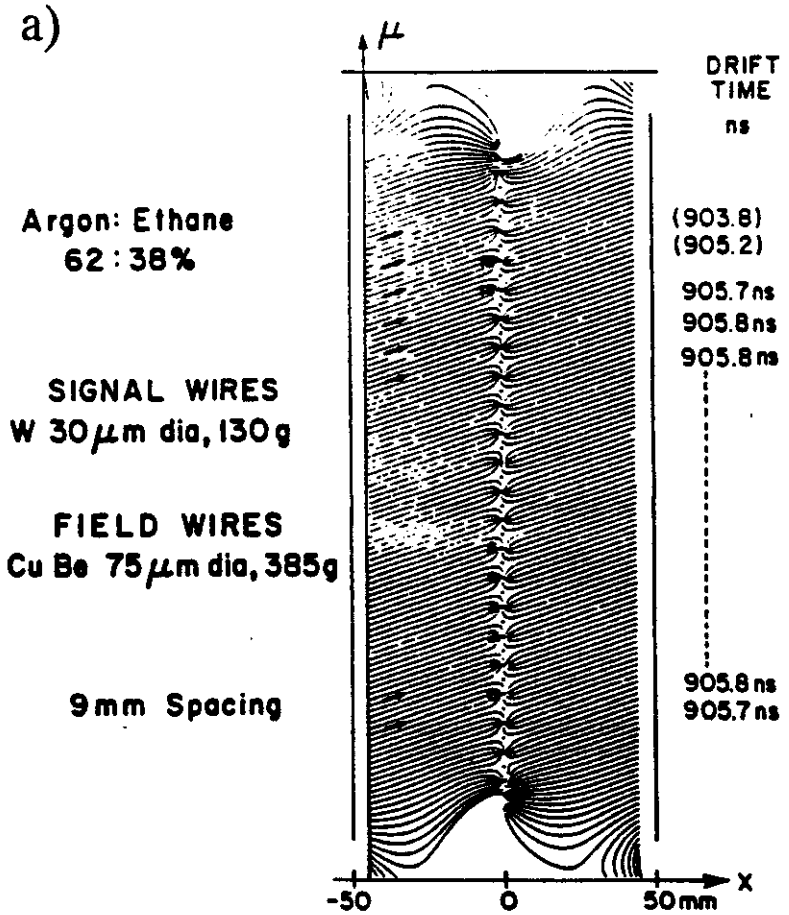
μ
DRIFT TIME ns
Argon: Ethane
62 : 38%
(903.8)
(905.2)
905.7ns
905.8ns
905.8ns
SIGNAL WIRES
W 30μm dia, 130g
FIELD WIRES
Cu Be 75μm dia, 385g
9mm Spacing
905.8ns
905.7ns
-50
0
50mm
X

a)

b)

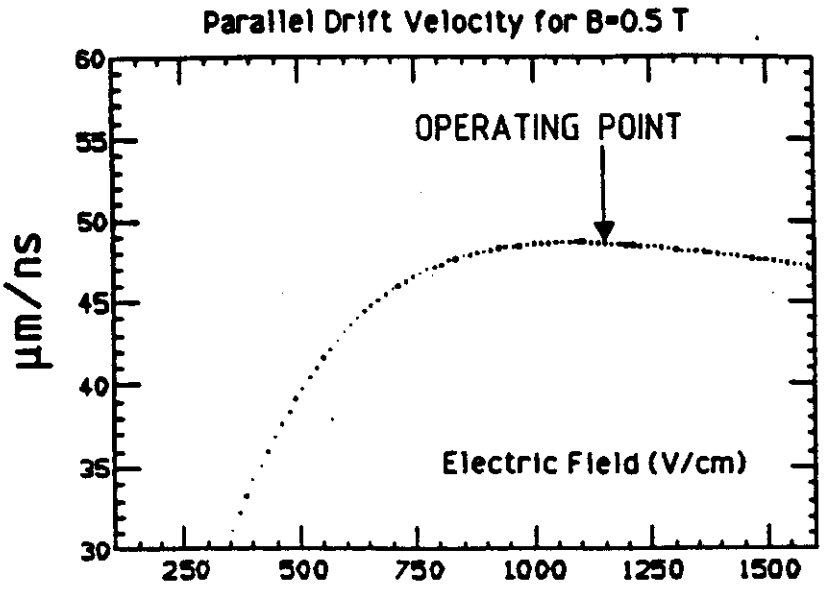
Parallel Drift Velocity for B=0.5 T
OPERATING POINT
μm/ns
Electric Field (V/cm)
60
55
50
45
40
35
30
250
500
750
1000
1250
1500

b)

Fig.17

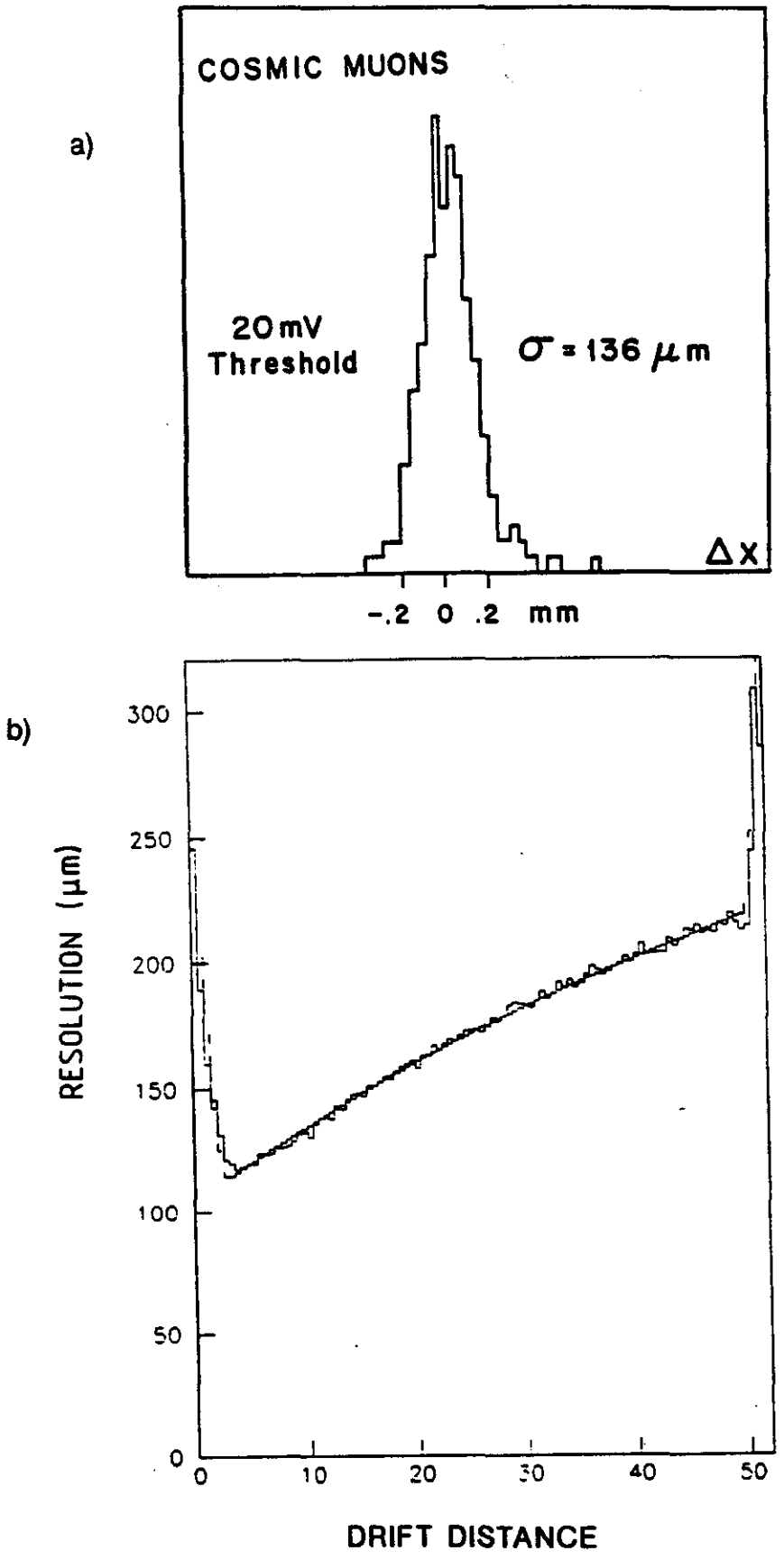
a)
COSMIC MUONS
20 mV
Threshold
σ = 136 μm
ΔX
-.2 0 .2 mm
b)
RESOLUTION (μm)
300
250
200
150
100
50
0
0 10 20 30 40 50
DRIFT DISTANCE

Fig. 18

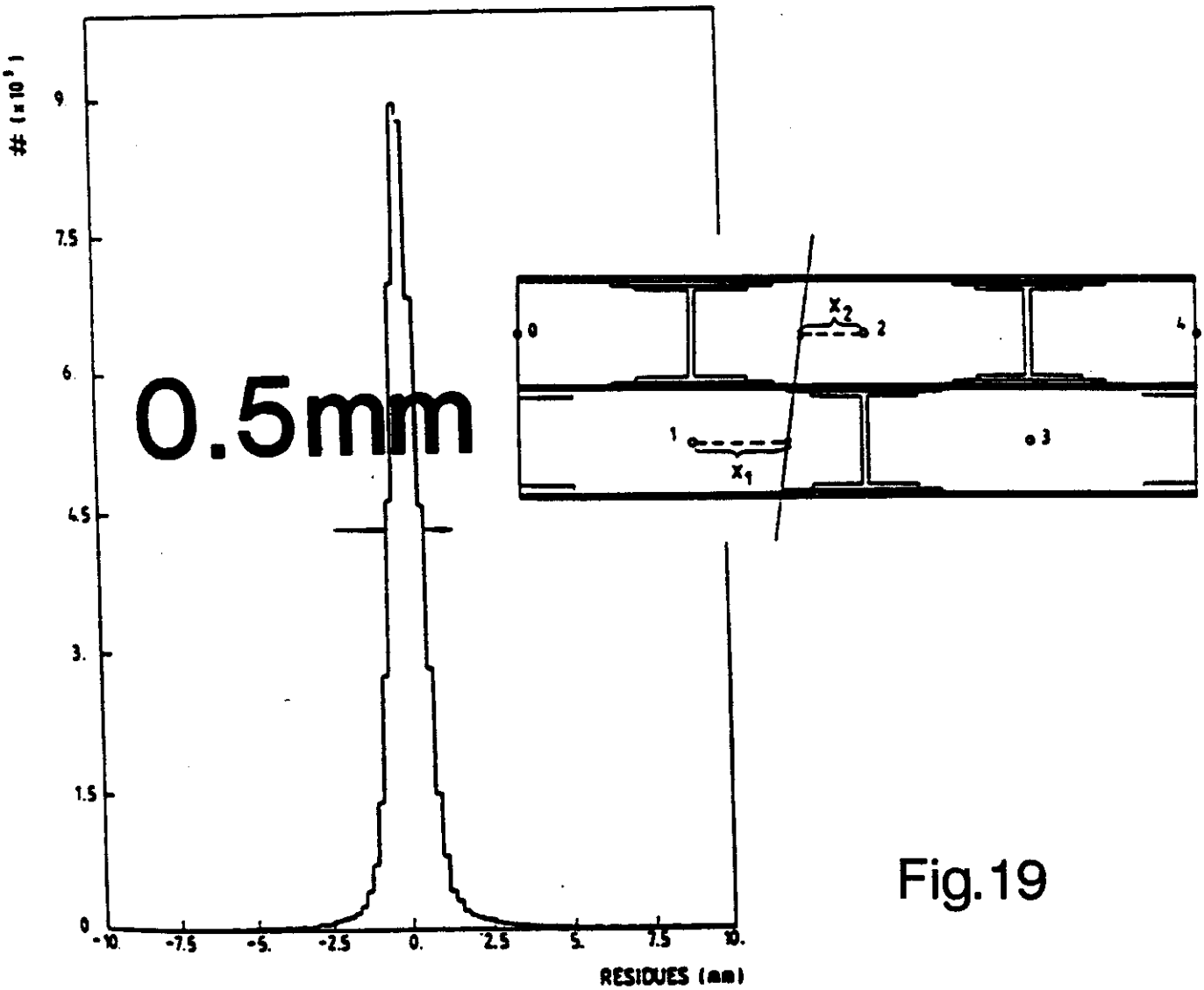
0.5mm
(x10³)
9.
7.5
6.
4.5
3.
1.5
0
-10.
-7.5
-5.
-2.5
0.
2.5
5.
7.5
10.
RESIDUES (mm)
0
1
2
3
4
X1
X2

Fig.19

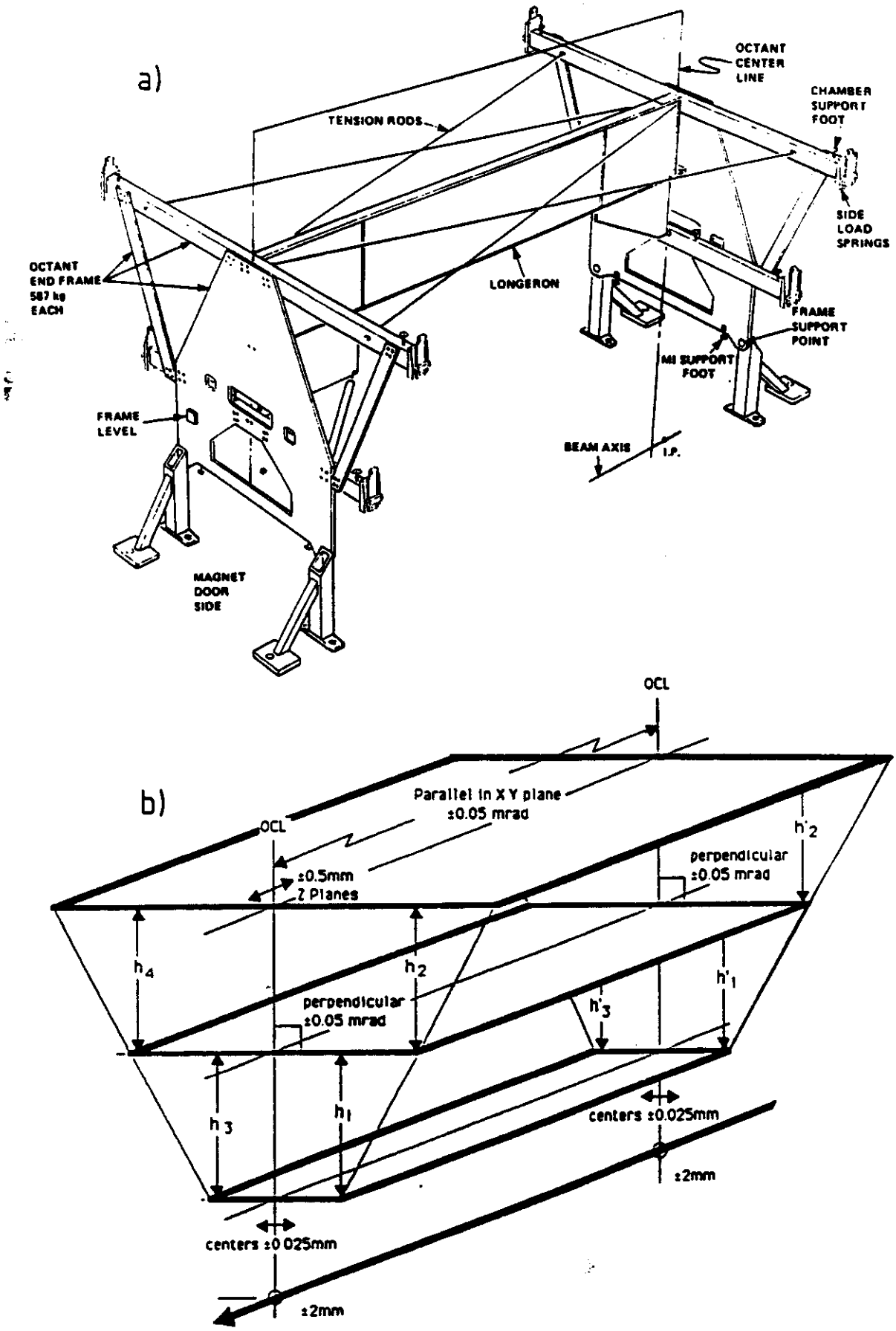
a)
OCTANT CENTER LINE
CHAMBER SUPPORT FOOT
TENSION RODS
SIDE LOAD SPRINGS
OCTANT END FRAME 587 kg EACH
LONGERON
FRAME SUPPORT POINT
MI SUPPORT FOOT
FRAME LEVEL
BEAM AXIS
I.P.
MAGNET DOOR SIDE
b)
OCL
Parallel in X Y plane ±0.05 mrad
OCL
h'2
perpendicular ±0.05 mrad
±0.5mm Z Planes
h4
h2
h'1
perpendicular ±0.05 mrad
h'3
h3
h1
centers ±0.025mm
±2mm
centers ±0.025mm
±2mm

Fig.20

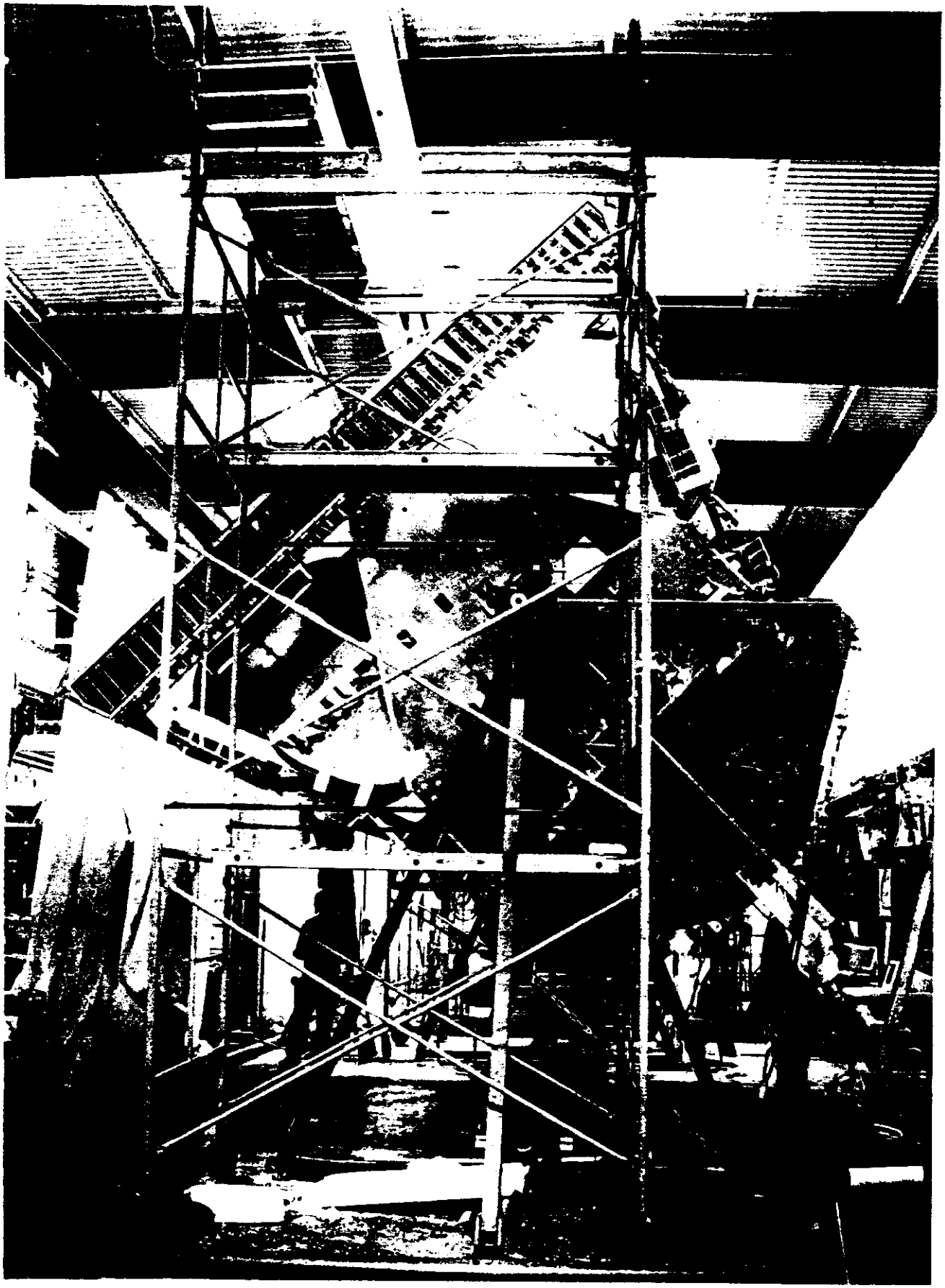

Fig 21

Performance Achieved
Reproducibility during Rotation
Middle Chamber

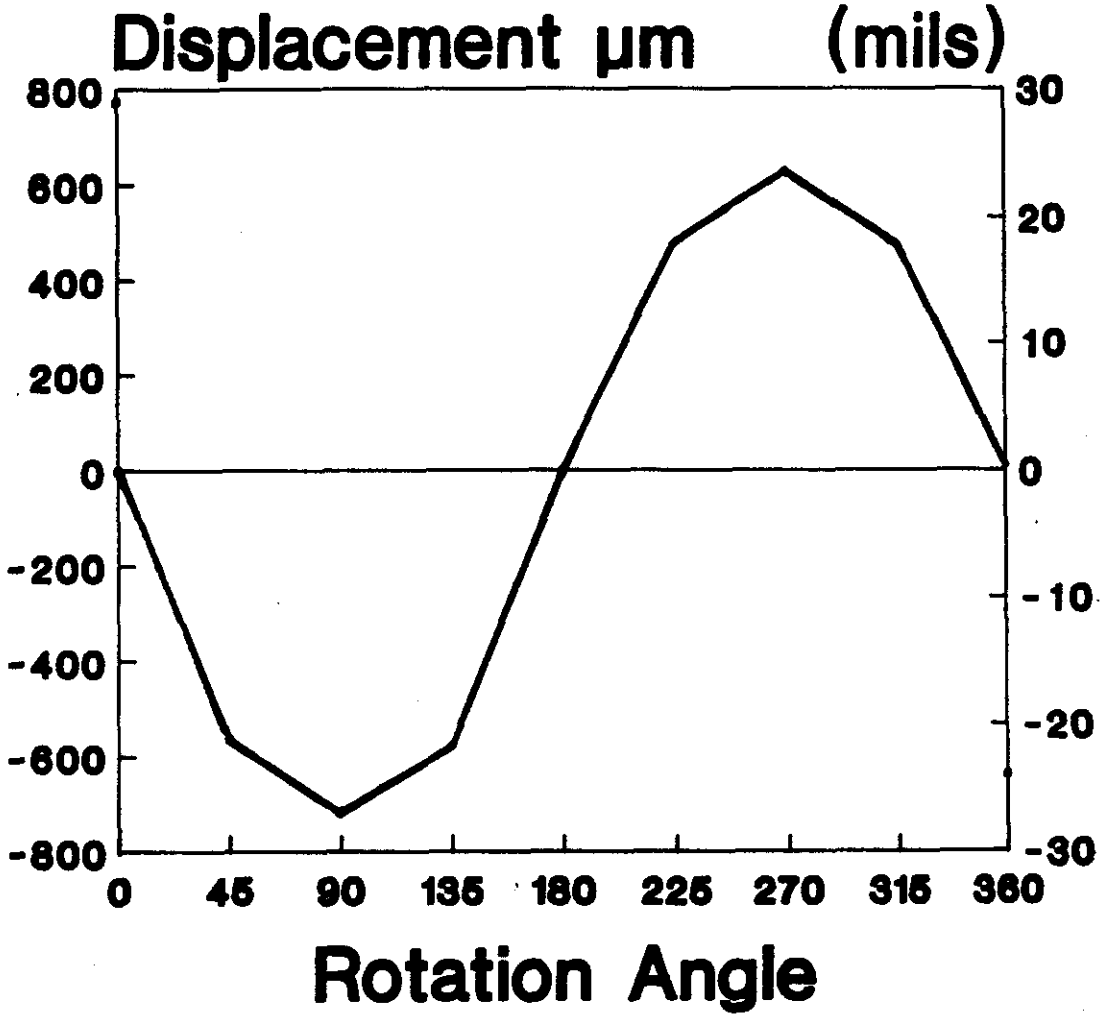

0 to 360 degree rotation
Reproduces to 6 µm = 1/4 mil !

Fig.22

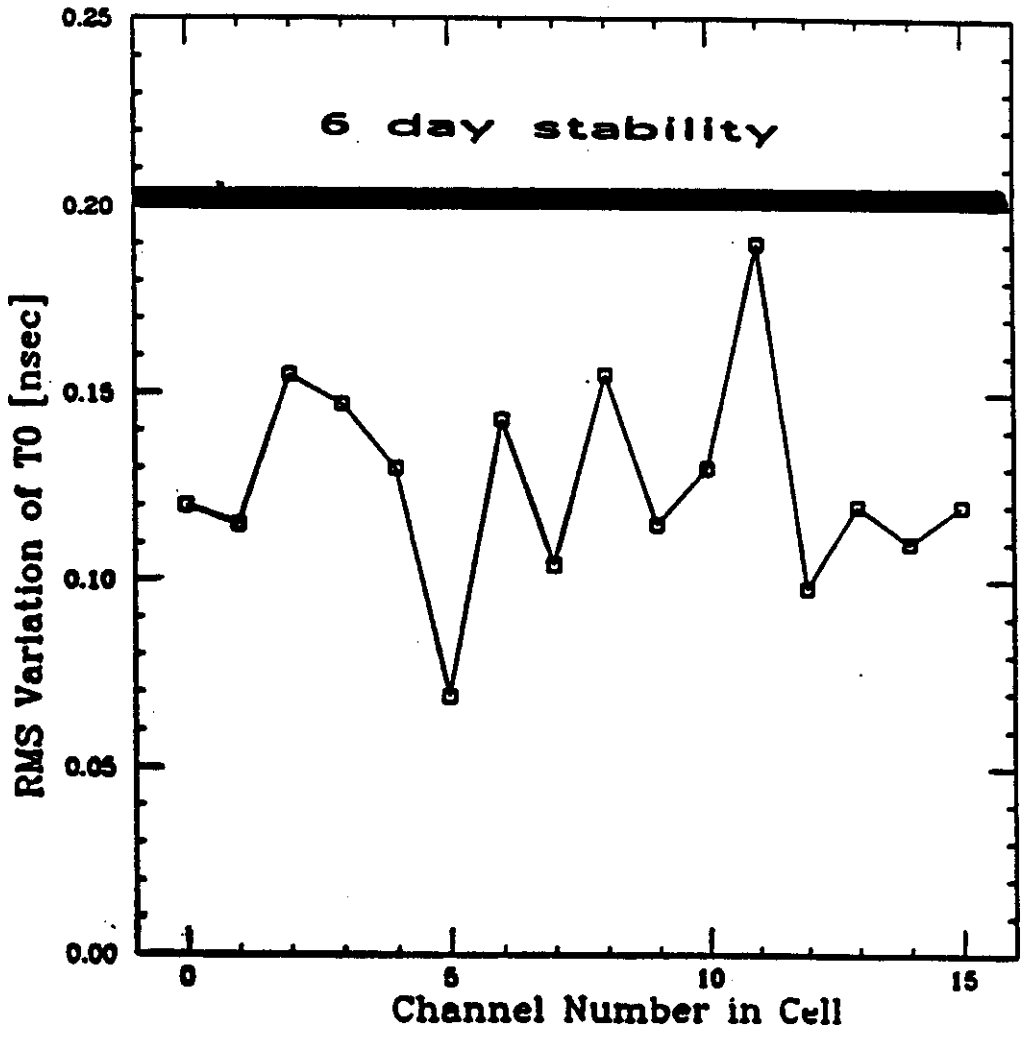
6 day stability
RMS Variation of T0 [nsec]
0.25
0.20
0.15
0.10
0.05
0.00
0
5
10
15
Channel Number in Cell

Fig.23

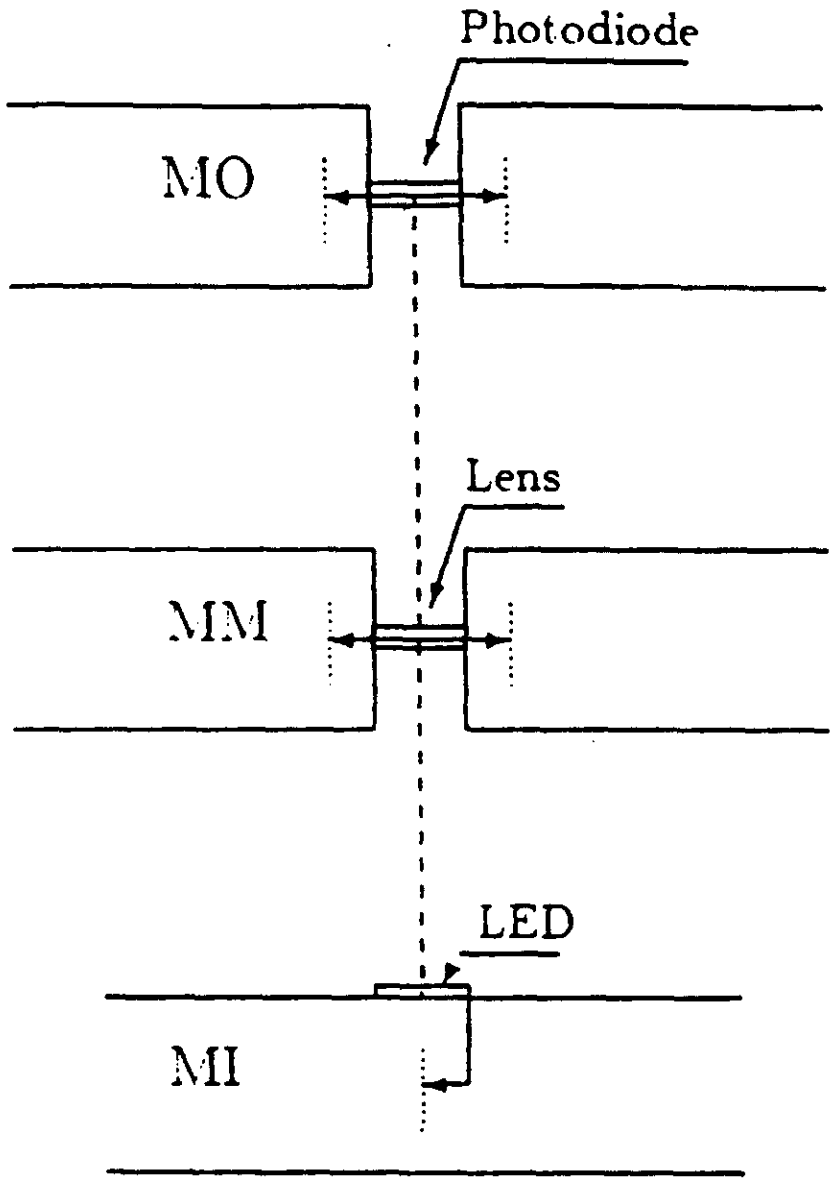

Fig.24

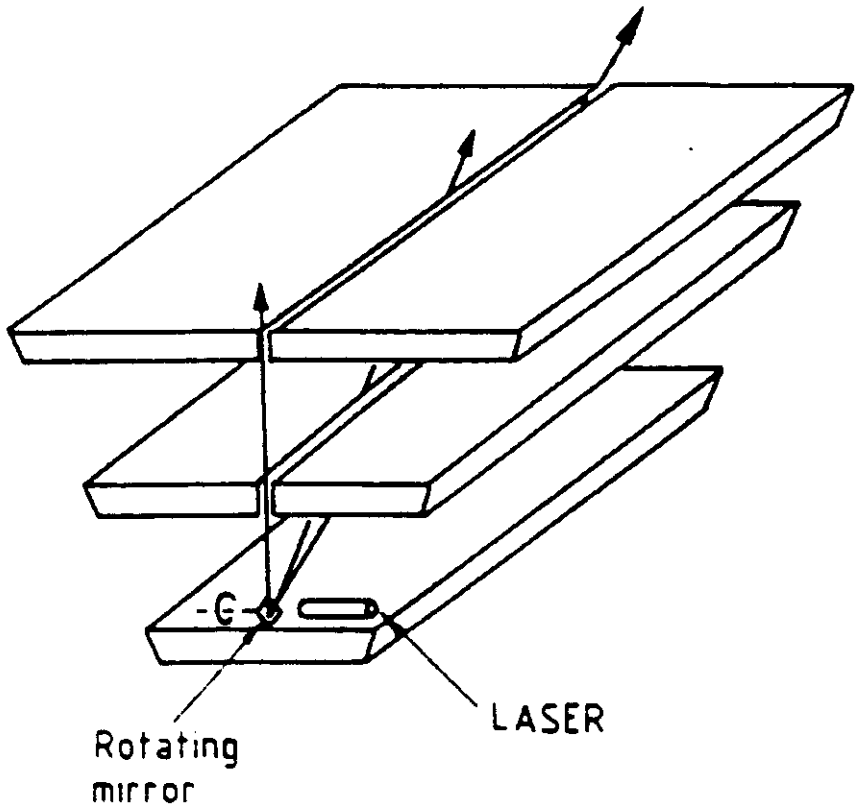

Fig.25

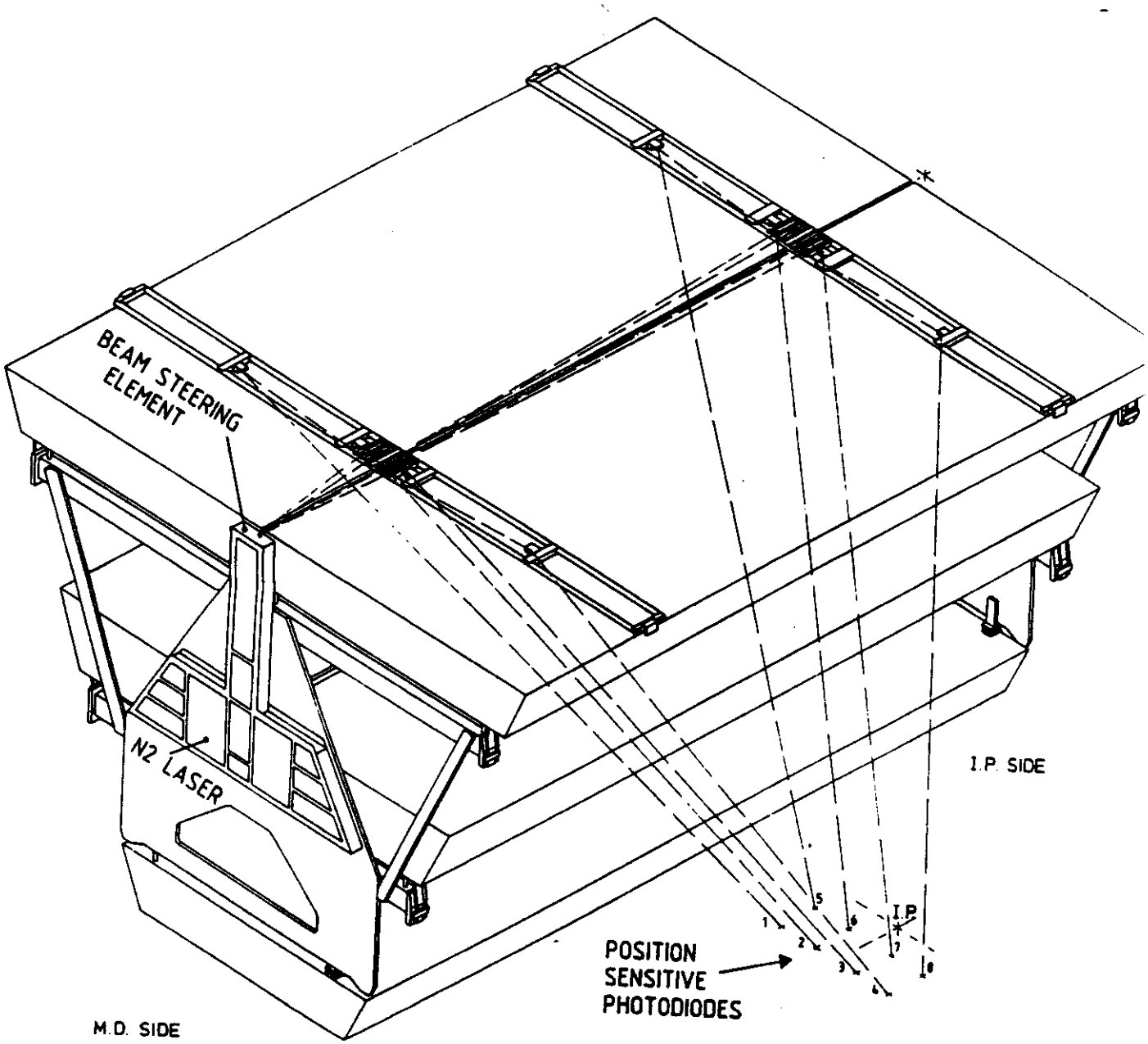
BEAM STEERING ELEMENT
N2 LASER
I.P. SIDE
M.D. SIDE
POSITION SENSITIVE PHOTODIODES
I.P.
1
2
3
4
5
6
7
8

Fig.26

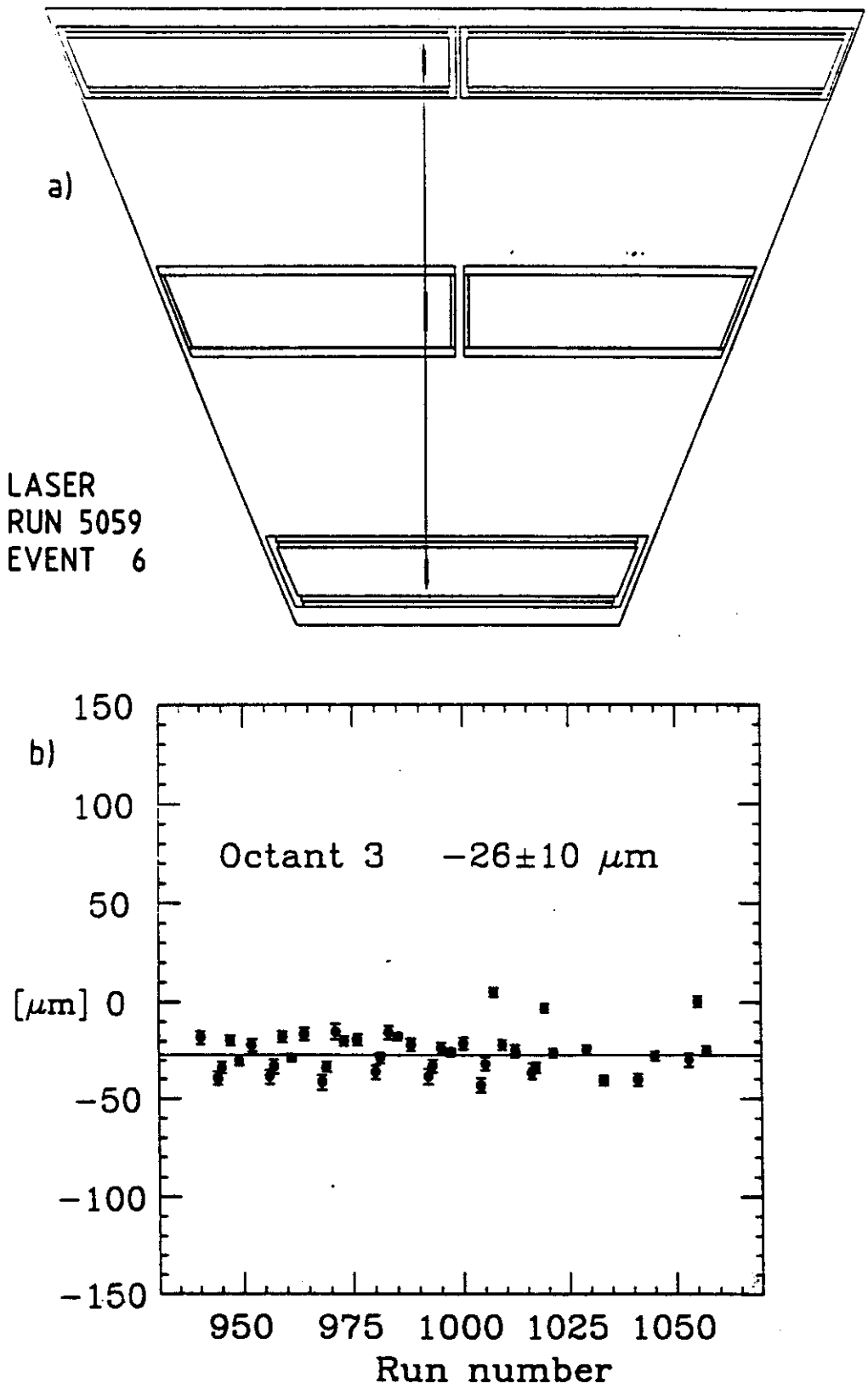
a)
LASER
RUN 5059
EVENT 6
b)
Octant 3 −26±10 μm
[μm]
150
100
50
0
−50
−100
−150
950
975
1000
1025
1050
Run number

Fig.27

a)

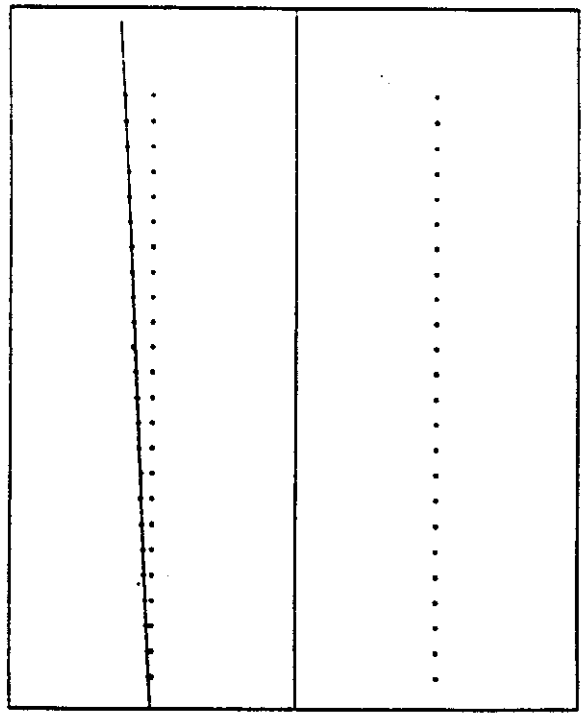

(a)

b)

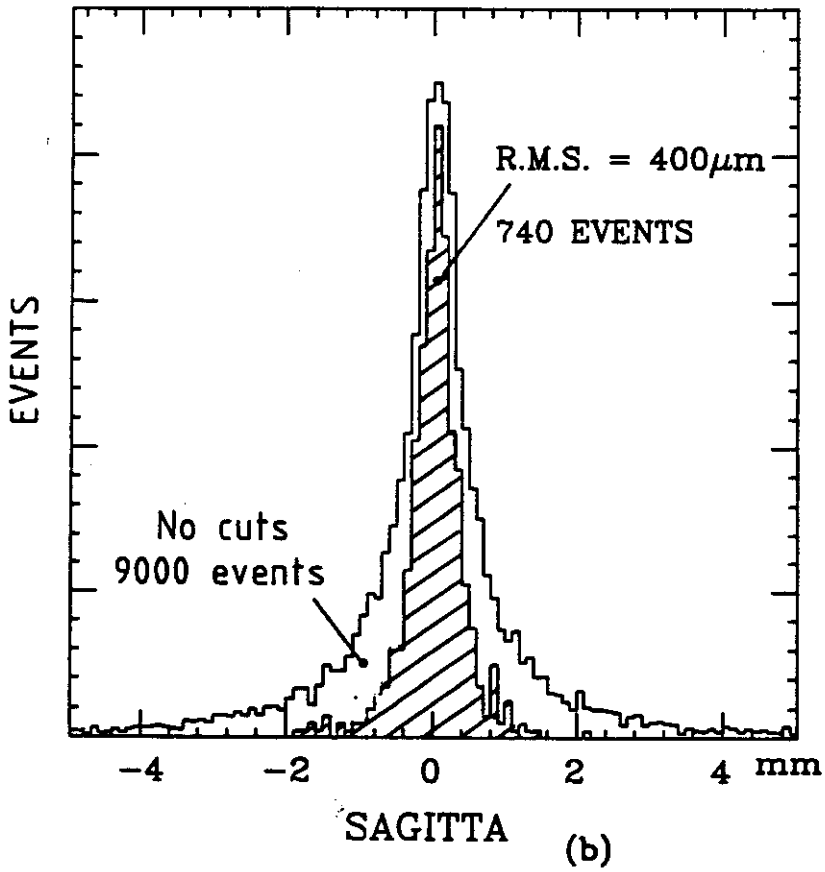
R.M.S. = 400μm
740 EVENTS
EVENTS
No cuts
9000 events
−4
−2
0
2
4
mm
SAGITTA

(b)

Fig.28

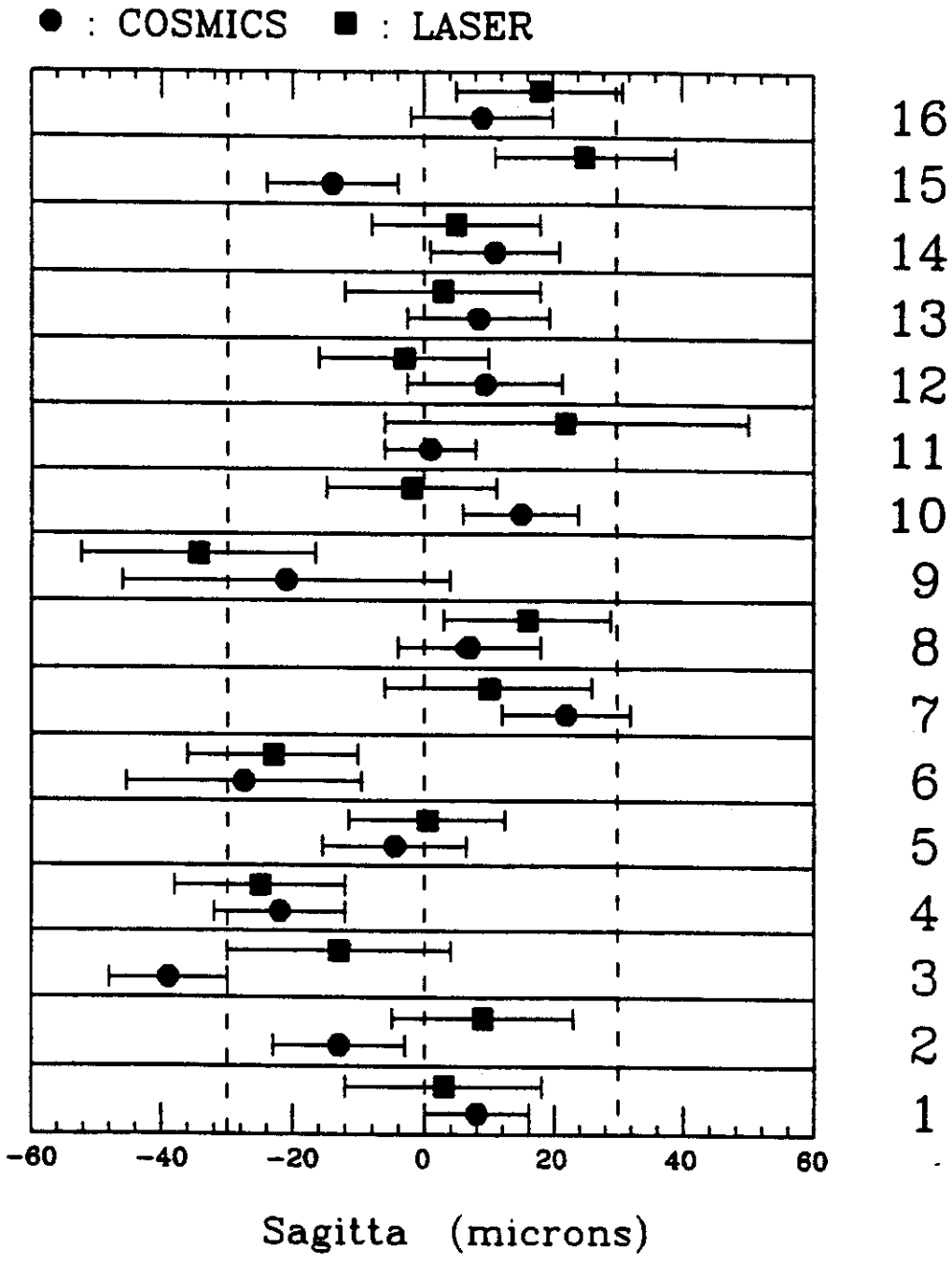
● : COSMICS ■ : LASER
16
15
14
13
12
11
10
9
8
7
6
5
4
3
2
1
-60
-40
-20
0
20
40
60
Sagitta (microns)

Fig.29

FIRST MUON EVENT FROM Z DECAY AT LEP

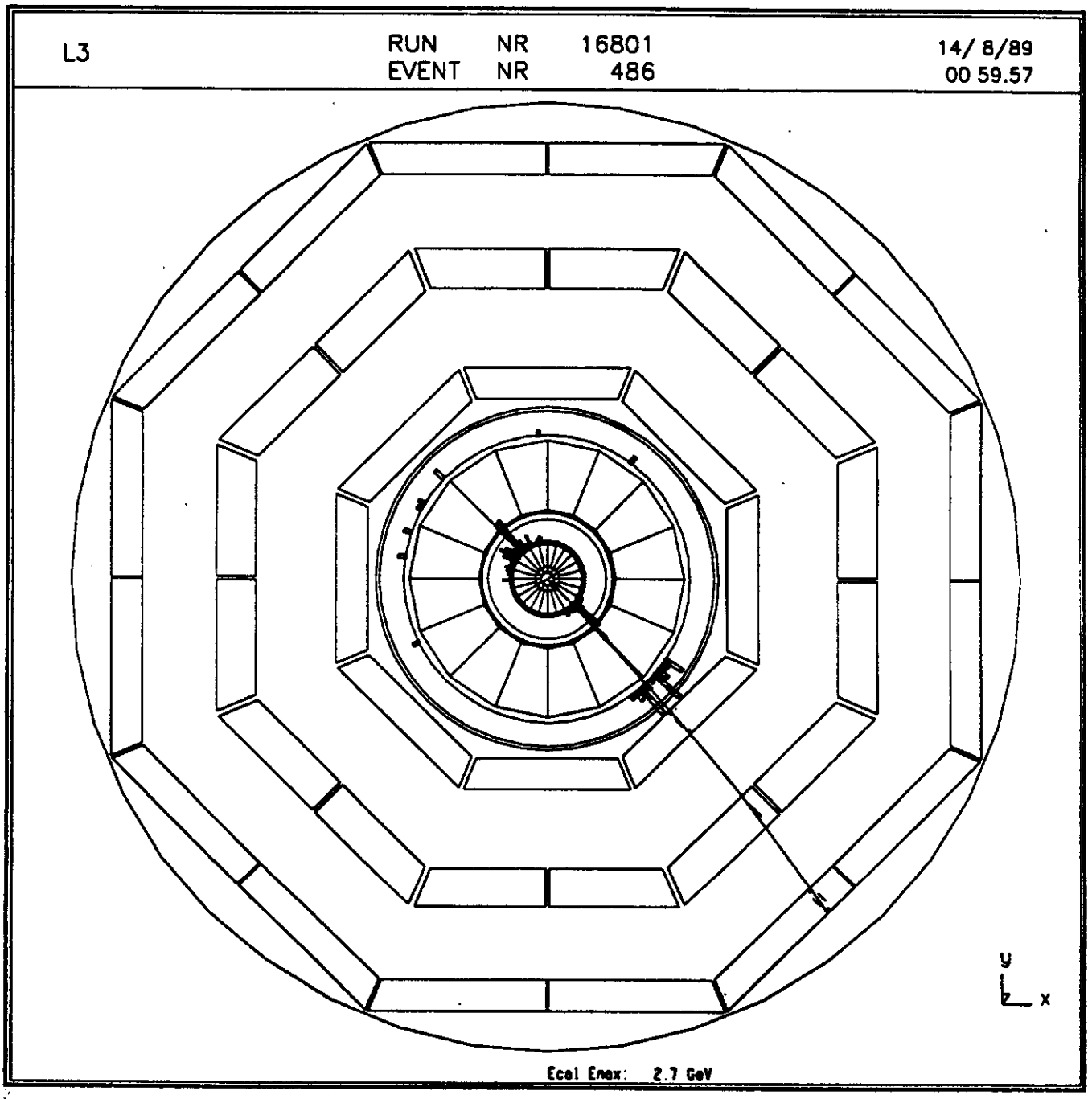

Fig.30

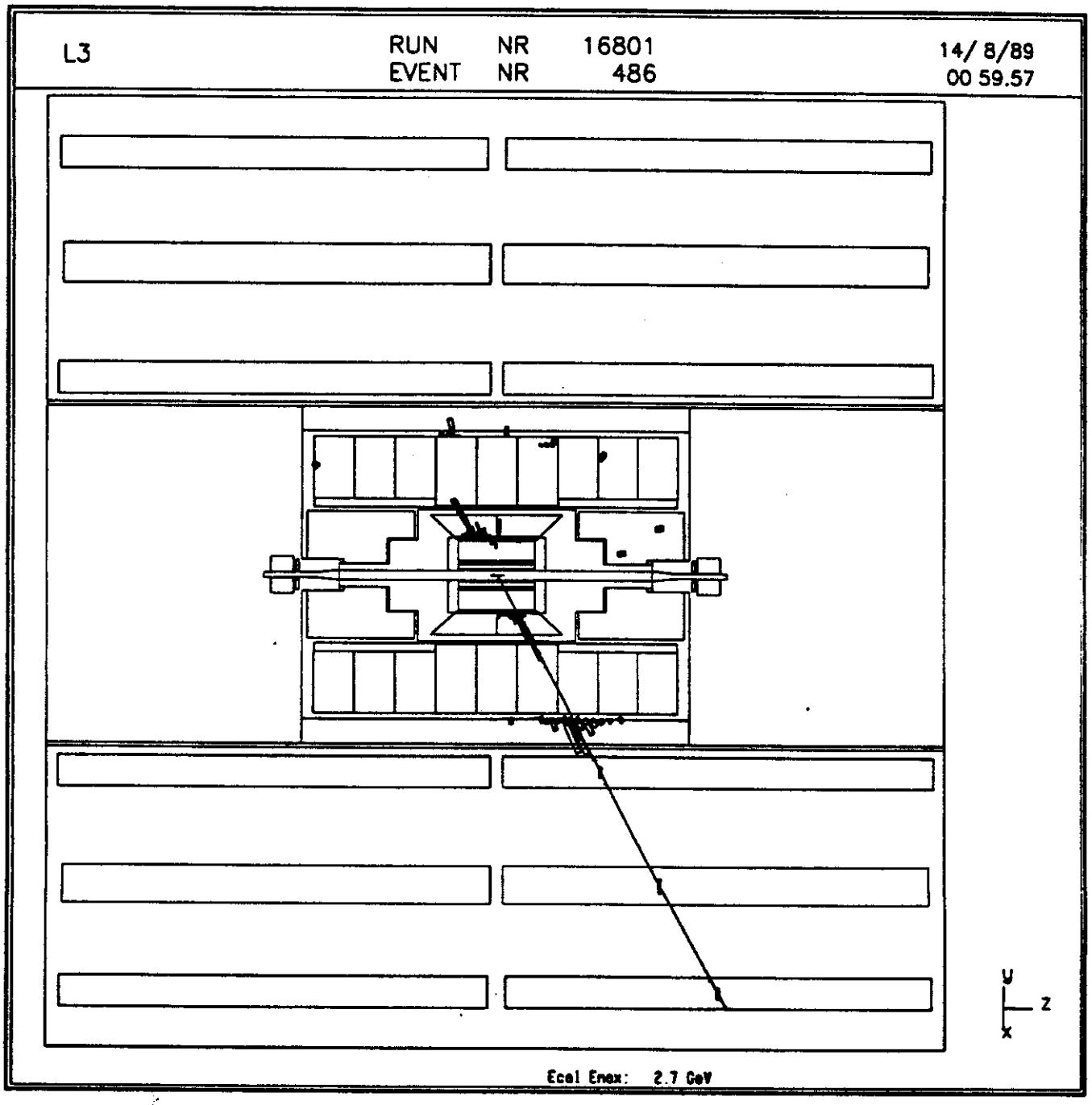

Fig.31

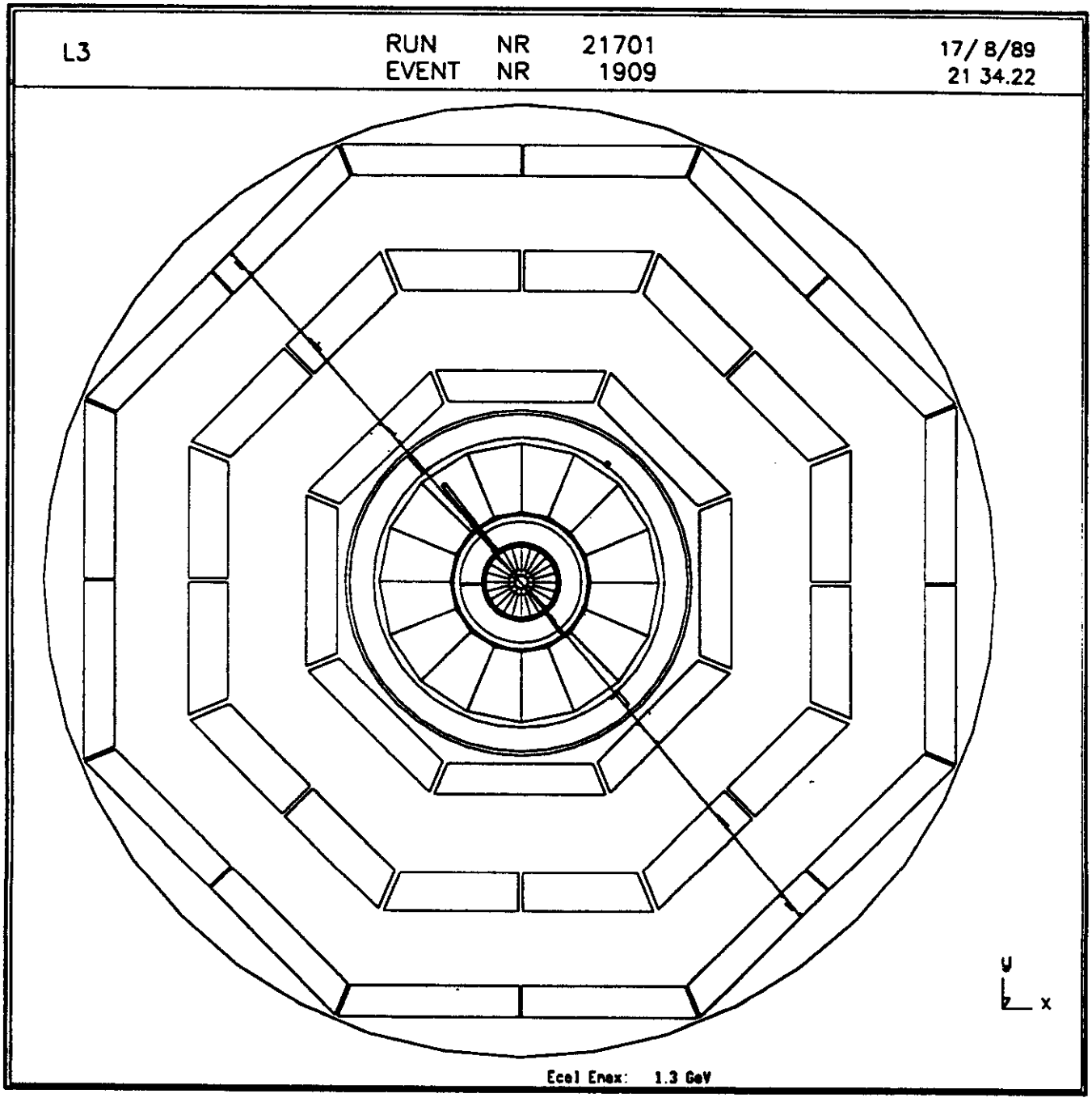

Fig.32

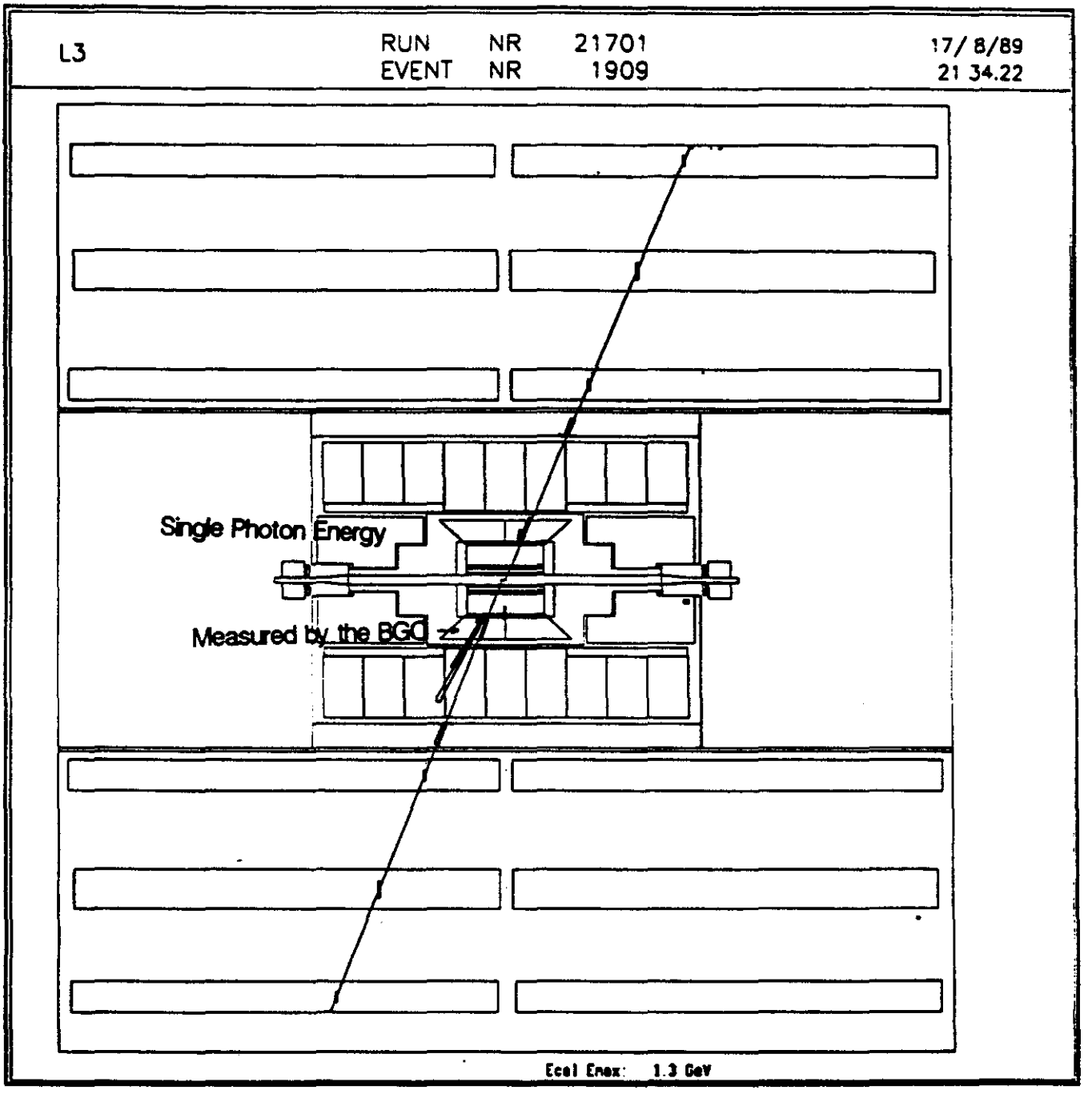
L3
RUN NR 21701
EVENT NR 1909
17/ 8/89
21 34.22
Single Photon Energy
Measured by the BGO
Ecal Emax: 1.3 GeV

Fig.33

APPENDIX II

DEVELOPMENT OF LARGE AREA PRECISION MUON DETECTORS

The detection [1] of $J \rightarrow e^+e^-$ was possible because the detector had a sophisticated system of proportional chambers providing 0.1% mass resolution. This was possible because the small solid angle in the laboratory corresponded to a large fraction in the relevant center of mass system. Therefore, with 8 chambers [2] of less than 2 by 1 m^2 area having 6800 electronic channels total this could be achieved.

Subsequent experiments looking for vector bosons decaying into lepton pairs according to

$$V \rightarrow \mu^+ \mu^-$$

needed much higher energies ($\sqrt{s}$). These could only be provided by storage rings and by hadron collisions. Copious π° production overshadows the $V \rightarrow e^+e^-$ decays with background, therefore the $V \rightarrow \mu^+\mu^-$ mode - relying on filtering out all background by heavy material - provides a much cleaner signal. Fig.1 shows a detector [3] based on these considerations. It was set up in 1977 at the ISR which provided energies up to $\sqrt{s}$=63GeV, which at that time was the highest center of mass energy available. The intersection point was surrounded by magnetized iron toroids of 350 ton weight interleaved with large drift chambers in order to

a) absorb hadrons and
b) measure the momentum of all the penetrating muons

1. Development of large area drift chambers.

We notice from Fig.1 that the outer two chamber layers constitute a large detection area of

$$400m^2.$$

Covering this area by conventional proportional chambers with one wire every 2mm would have required more than one hundred thousand electronic channels and was out of the question.

That was the time when drift chambers were discovered. We developed a special drift chamber [4] covering 50mm/wire instead of 2mm/wire used previously, thus reducing the number of channels by a factor 25.

The chamber structure is shown in Fig.2. It consists of two layers with signal wires spaced by 100mm. The second layer is shifted by 50mm. This resolves the left-right ambiguity inherent to drift chambers. For 90° incident particles the measured distances $x_1 + x_2$ must add up to 50mm. This is the very important feature of **self calibration.**

Mechanically the chambers are made of aluminum sheets with I beams glued onto them, separated by insulating strips. This forms a light and extremely strong structure enabling economic construction of self supporting units up to

6.5m (20') length.

This type of chamber was developed in 1975 and it has been very successful and used in many experiments. Fig.3 gives a view of the chambers [5] used now in the LEP L3 experiment [6] showing essentially the same structure.

Fig.4 shows how the ionization electrons drift from a particle track along the electrical field lines to the wire. Deliberately, the geometry of the I beam has been chosen to make the field along direction a-a as uniform as possible in order to have a constant drift velocity and good resolution. Therefore the I beam solves the mechanical and electrical requirements simultaneously in an elegant way, saving material and labor. This enabled the construction of large area detectors in an affordable way.

In Ref.4, it was realized and demonstrated by measurements for the first time that one indeed can apply "drift electron optics" as seen in Fig.4. Subsequent similar designs for muon detectors [7] used this method to design more sophisticated profiles modelling a good electrical cell. Today, the method is used as an analytical tool [8].

The ISR experiment [3] detected the J and T resonances and measured scaling down to smallest values of the scaling variable, see Fig.5. The

resolution of the experiment was limited by multiple scattering in the iron to about 12%. The chambers could have done much better. Filled with Argon:Isobutane (70:30% in volume) the chambers reach 350μm resolution.

The same type of chambers were used in 1979 in the MARK J experiment [9] to detect the important forward-backward asymmetry in the process

$$e^+e^- \rightarrow \mu^+\mu^- \qquad \text{at } \sqrt{s}=45\text{GeV}$$

heralding the advent of the neutral force carrier Z° through interference. Fig.6 gives a side view of an event detected by these chambers, which were inserted into a magnetized iron toroid.

The chambers measure the momentum from the deflection in the toroids and accurately determine the relevant angle to the beam axis, hence enabling the asymmetry measurement. The chambers must have high and uniform efficiency in order not to introduce a bias into the measurement. This was verified in Fig.7 where cosmic rays were shown not to contribute to the measurement. The result of the measured asymmetry is given in Fig.8 and predicted the Z° at about 90 GeV.

96 chambers of the same type are used in L3. They measure the coordinates in the nonbending plane as shown in Fig.9 for an event displaying the decay $Z \rightarrow \mu^+\mu^-$.

2. Development for high rates

The proportional chambers used in the BNL experiment were subject to extremely high particle fluxes (10^{13} ppp on a 0.1 λ target). Using an unusual mixture of Argon and Methylal vapor (88:12% in volume), the chambers operated properly for more than 3 years. This is the highest dose we are aware of in a regular experiment.

At the ISR and PETRA intersection regions, high instantaneous rates occurred. Proportional chambers could have been used for vertex detection, however the necessary bulky frames and high number of signal cables cause complications and dead areas if used as a vertex detector. More important,

their resolution is about 2mm, and thus is not adequate. We therefore developed thin walled drift tubes of small diameter in array form.

At the ISR they were used to measure extremely small angle scattering of α particles, correctly determining the first and second diffraction minima, thus demonstrating good resolution at high rates.

At PETRA we used an array of 2616 tubes (Fig.10). There they determined the interaction vertex (Fig.11) in a high background environment of synchrotron radiation.

This idea has been picked up by the MAC Collaboration, and the concept is widely known now as "straw chambers".

3. Studies for high accuracies by high magnetic field or slow gas

In view of the high momenta of particles from future colliders, we studied the behavior of tracking devices in extremely high magnetic fields [10] (up to 105 kGauss) and very high electrical fields (up to 10kV/cm). Although in general the operation of drift chambers is possible, the drift angles at moderate electrical fields in normal drift gases are uncomfortably high for good reconstruction. This stimulated a search for a gas having a low deflection angle.

Indeed a special gas mixture with very small drift angle at low velocities was found [11]. These measurements showed that it has small (<5°) deflections in magnetic fields up to 10kGauss field at 2.4kV/cm. This gas is now used in the time expansion chamber (TEC) of L3 which tracks vertices with 40μm accuracy.

4. Development of large precision drift chambers

This development started in 1978 for ISABELLE as a DOE sponsored research program to find suitable gases and precision chambers to work in the environment of a high intensity hadron collider.

Extensive R&D on gases was started in the relatively new field of drift chambers, by evaluating 300 mixture and pressure combinations as given in Appendix III.

In order to match the high resolution of the drift chambers, we also developed optical alignment systems to monitor the mechanical stability required in the large structures. We demonstrated that dynamic compensation of small mechanical deformations is possible [12] using CCD sensors with actuator feedback. We achieved a dynamic stability of

$$<13\mu m$$

for a frame of 2m by 6m size, when subject to load and temperature variation.

The results of this research and development were applied to the L3 experiment at LEP after the discontinuation of the ISABELLE project.

The magnetic bend of 50GeV particles in the biggest magnet planned for L3 at LEP only provides a 3.4mm deflection. A 2% measurement then requires 70μm of positioning accuracy from the chamber, which is typically 5.4m long.

In order to keep multiple scattering reasonable, thin material had to be chosen for the chambers, and therefore only atmospheric pressure gas could be used. For 1 atmosphere, the intrinsic resolution of normal gases as given by primary ionization and diffusion could be expected to be between σ=200 and 250μm.

To increase accuracy, the concept of multiple sampling chambers was developed, relying on the principle that the average coordinate measured by N wires is determined to higher accuracy by

$$\sigma/\sqrt{N}$$

provided the N measurements are independent and unbiased. This was verified using an array of 32 thin walled drift tubes [13]. We allowed high energy particles to traverse all of the tubes (fig. 12a), and then studied whether averaging of N ($\leq$ 32) wires indeed improved the resolution proportionally to

$1/\sqrt{N}$. Fig.12b shows that this was the case, as we expected from these tubes, being independent units.

Whether or not there would be correlations if all wires share the same gas volume was investigated to high accuracy with a 96 wire chamber [14] in the Brookhaven test beam (Fig.13a). The result of comparing up to 36 wires to the track which was determined by the 48 outer wires is shown in Fig.13b. This confirms the basic $1/\sqrt{N}$ dependence [15] and shows that chambers with 16 and 24 wire sampling could reach the required accuracies.

In parallel research, the study concentrated on minimizing σ by the choice of gas as well as the operating conditions for a large detector. This is described in chapter 5.

For wires that are as long as 5.4 meters, the mechanical and the electrical properties can easily result in degraded resolution σ.

A four years R&D program was carried out between 1978 and 1982 at the BNL test beam, and developed a 5.4 meter long drift chamber module capable of performing without notable loss of resolution compared to short chambers (See Fig.14a).

In fact, we developed electronics to intercept the pulse from the wire at 8% level (approximately the 8th drifting electron), which resulted in a very good resolution of $\sigma = 127\mu m$ at 1cm in a 5kG magnetic field as shown in Fig.14b.

The development of the L3 detector with multisampling chambers and optomechanical alignment as shown in Fig.15 was based on our previous extensive R&D. It included the dynamic compensation of small mechanical deformations as a design ingredient. As described in chapter 2, this muon detector has begun operation, and has indeed reached

an alignment accuracy of 30μm

which is at least **one order of magnitude better** than achieved in any previous detector.

References

[1] J.J. Aubert, et al. PRL 33, (1974) 1404

[2] shown in exhibitions in the Smithsonian Museum, Washington DC, and at the main building at FNAL 7th floor.

[3] D. Antreasyan PRL 45 (1980) 863

[4] U. Becker, et al. NIM 128 (1975) 593

[5] C. Willmott, NIM A263 (1988) 10

[6] L3 Collaboration, Letter of Intent (January 1982)
L3 Collaboration, "The L3 Technical Proposal" CERN LEPC (March 1983)

[7] UA1 muon detector, K.Eggert et al. NIM 176 (1980) 217

[8] Design program WIRCHA, ETH

[9] D.Barber et al. Phys. Rep. 63 (7) (1982) 333

[10] U.Becker, et al., NIM 205 (1983) 137

[11] U.Becker, et al., NIM 214 (1983) 525

[12] U.Becker, J.A.Paradiso NIM 196 (1982) 381

[13] U.Becker, et al., CERN-EP 80-154 (1980), NIM 180 (1981) 61

[14] P.Duinker et al., NIM 201 (1982) 351

[15] knock on electrons cause a small correlation which can be eliminated by dropping the worst 6% of the measurements.

Figure Captions

Fig. 1) Cut-away view of the detector at the CERN intersecting storage rings. The magnetized iron toroids are labelled (4) and the muon drift chambers (F). Superimposed is a reconstruction of a observed dimuon event with 24.5 GeV mass.

Fig. 2) Structure of a drift chamber is shown. The 50μm signal wires are enclosed by I beams at negative potential, which generates the drift field. X_1 and X_2 are coordinates from a track.

Fig. 3) Schematic view of the structure of the multicell drift chamber.

Fig. 4) Electric field configuration in a drift cell (the wire and I beam potentials are 2150 and -2500V respectively).

Fig. 5) The scaling function $F(\tau)$ is plotted as a function of $\sqrt{\tau}$.

Fig. 6) An $e^+e^- \rightarrow \mu^+\mu^-$ event in the MARK J detector is shown.

Fig. 7) A measurement of the detector asymmetry is shown using cosmic ray muons with energy more than 10GeV.

Fig. 8) The forward-backward asymmetry measured by MARK J is shown.

Fig. 9) A side view of L3 is shown with a $Z^\circ \rightarrow \mu^+\mu^-$ event as recorded by I beam type drift chambers.

Fig. 10) A section of the vertex chamber parallel to the beam is shown.

Fig. 11) Vertex reconstruction by the MARK J drift tubes is shown.

Fig. 12a) Drift tube array

Fig. 12b) This measurement shows that the accuracy improves with $1/\sqrt{N}$, where N is the number of wires.

Fig. 13a) The chamber with 96 wires is shown.

Fig. 13b) Experimental results from the BNL test beam check the $1/\sqrt{N}$ law.

Fig. 14a) A one cell, 5.4 meter long, multisampling chamber is shown.

Fig. 14b) The measured resolution of the 5.4 meter long wires in a test beam is shown.

Fig. 15) Principal structure of the L3 octants, with schematic indication of optomechanical alignment is shown. The 24 wire middle chambers can be moved by a servo motor until LED, lens and receiver form a straight line.

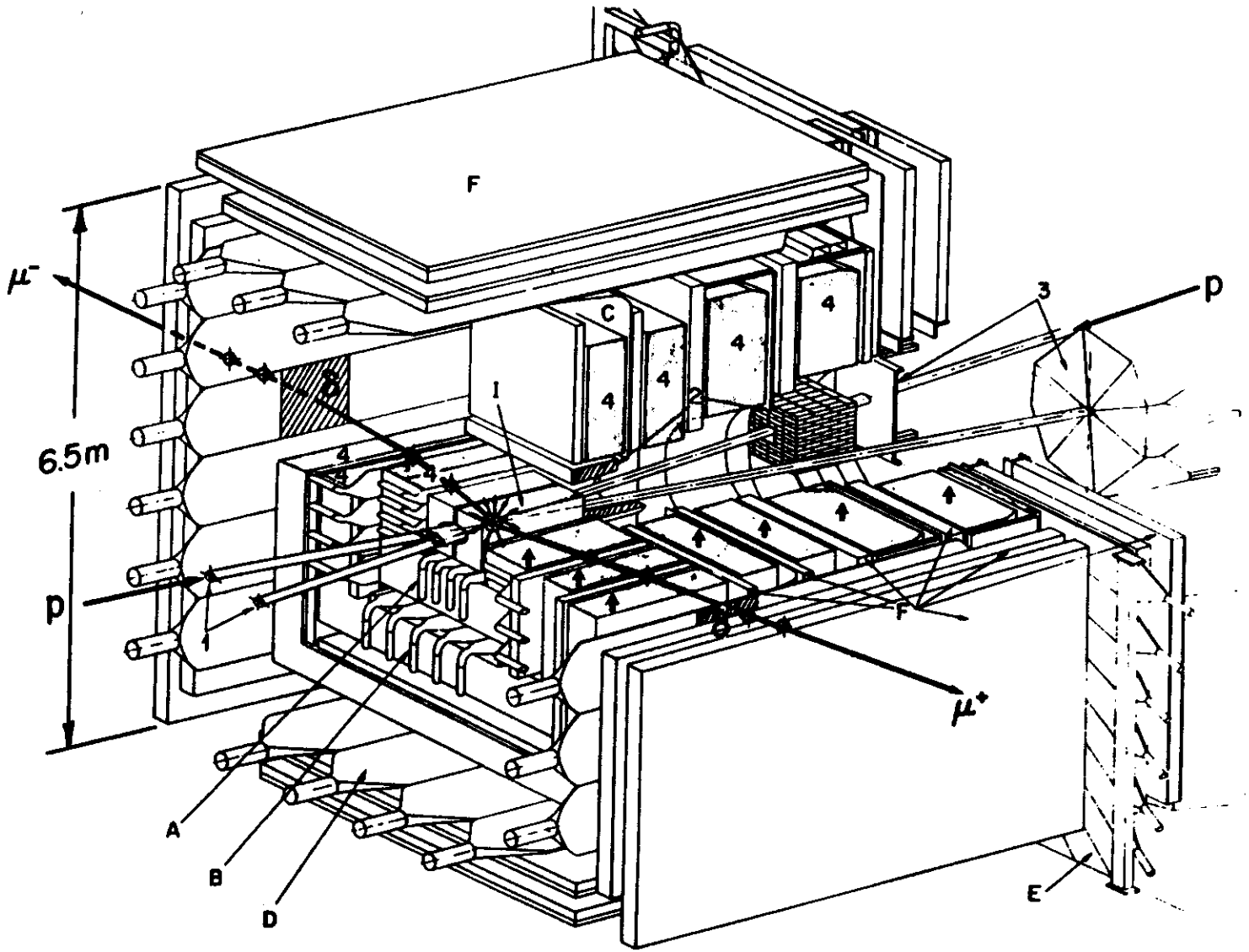

FIG.1

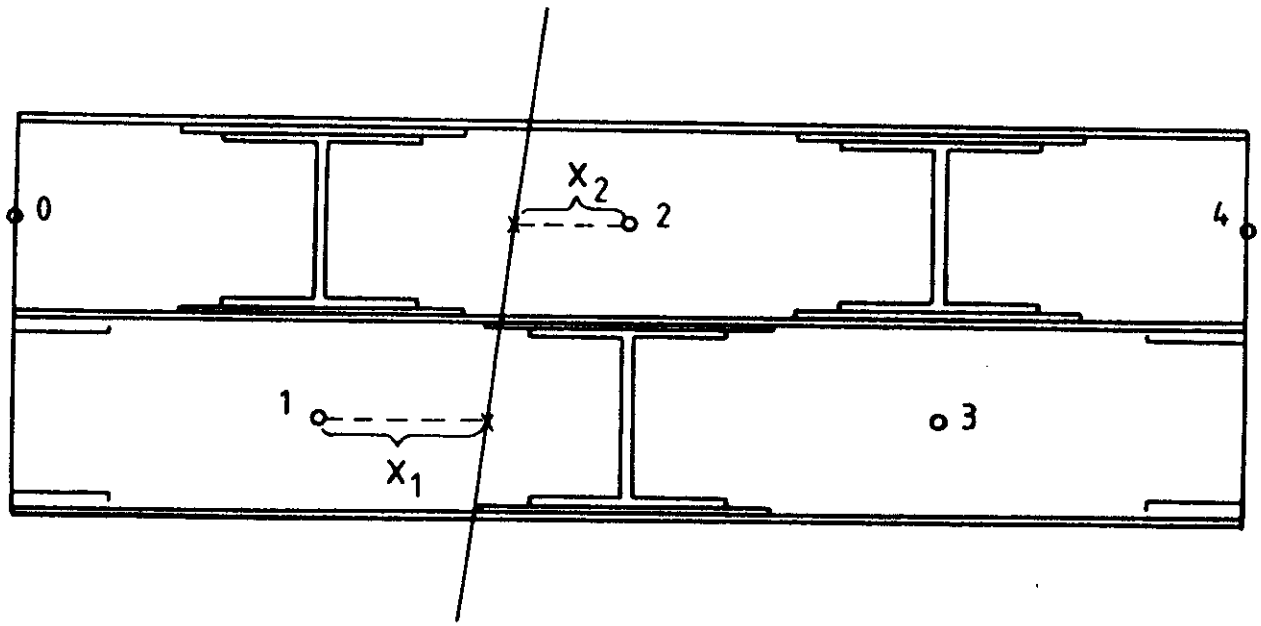

FIG.2

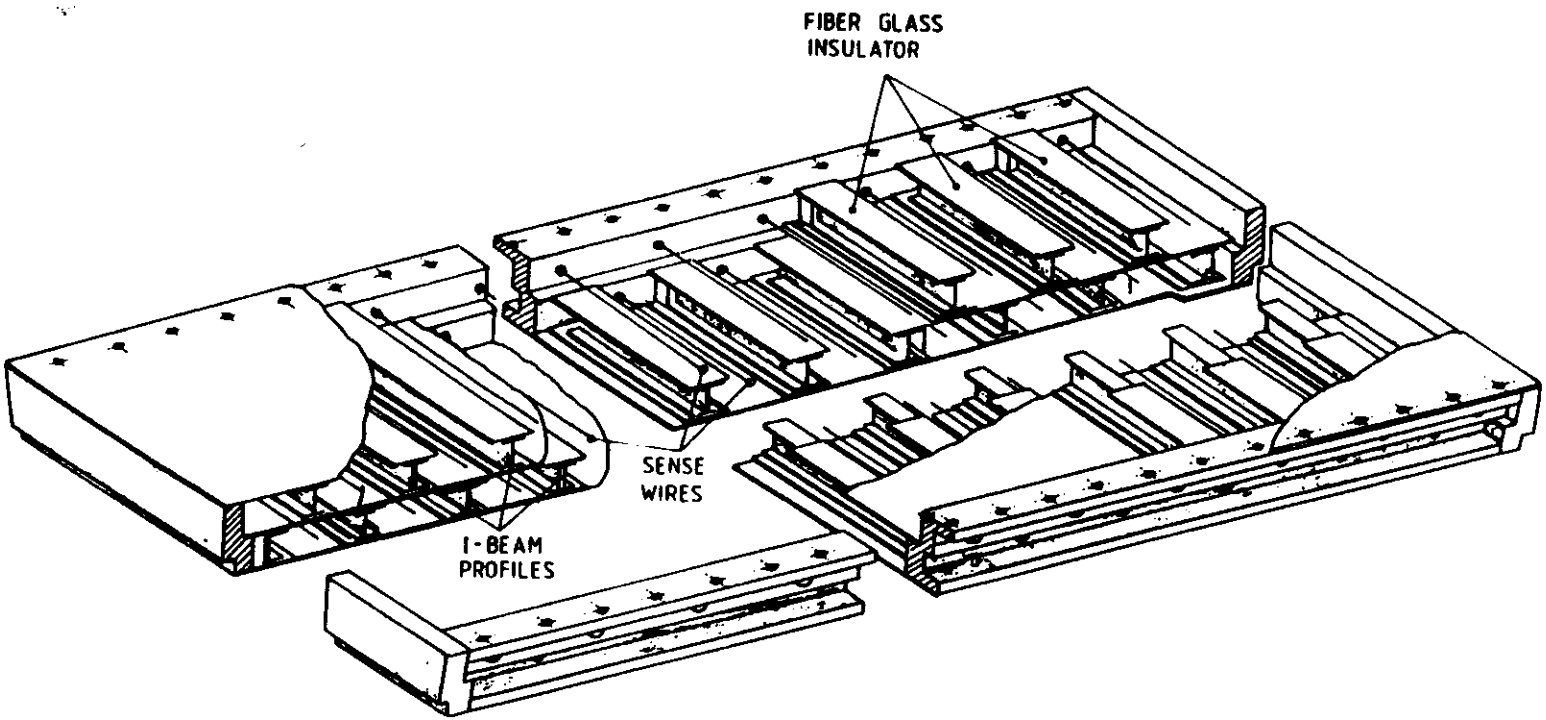

FIG.3

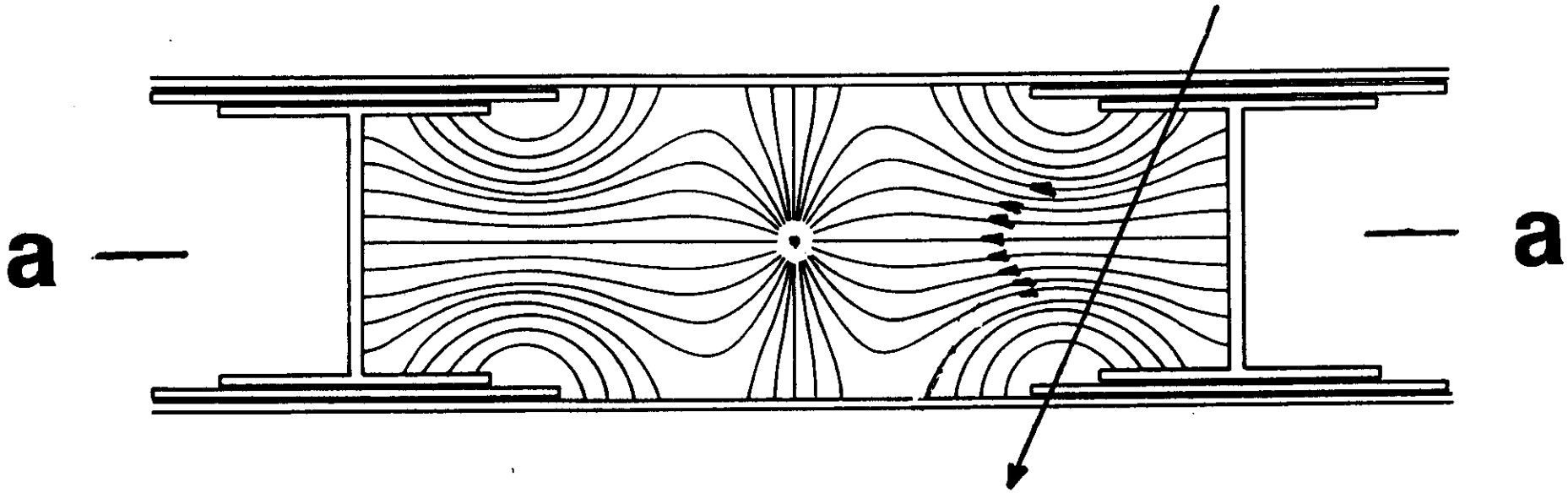

FIG.4

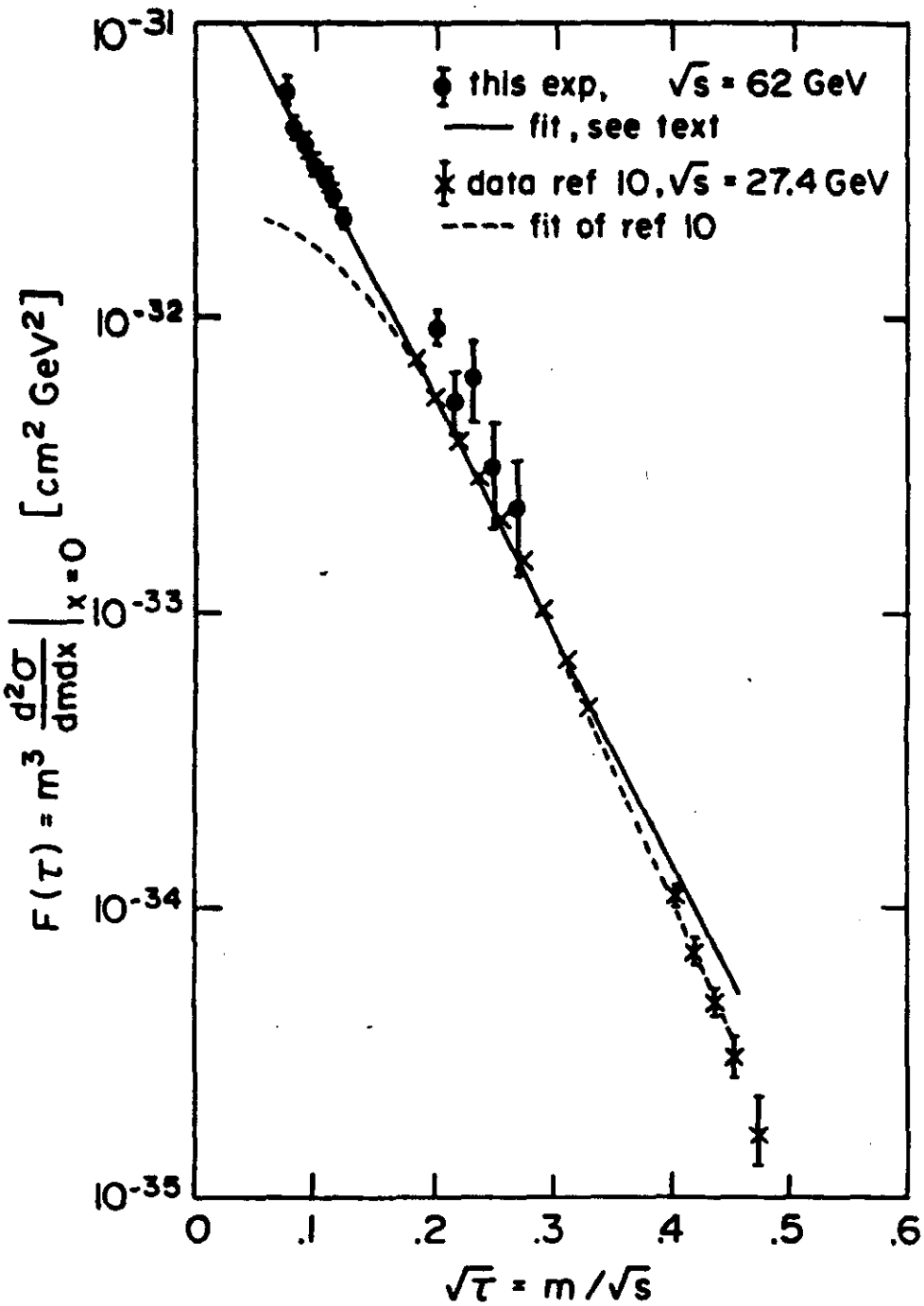
this exp, $\sqrt{s}$ = 62 GeV
fit, see text
data ref 10, $\sqrt{s}$ = 27.4 GeV
fit of ref 10
10^{-31}
10^{-32}
10^{-33}
10^{-34}
10^{-35}
$F(\tau) = m^3 \frac{d^2\sigma}{dm\,dx}\Big|_{x=0}$ [cm^2 GeV^2]
0
.1
.2
.3
.4
.5
.6
$\sqrt{\tau} = m/\sqrt{s}$

FIG.5

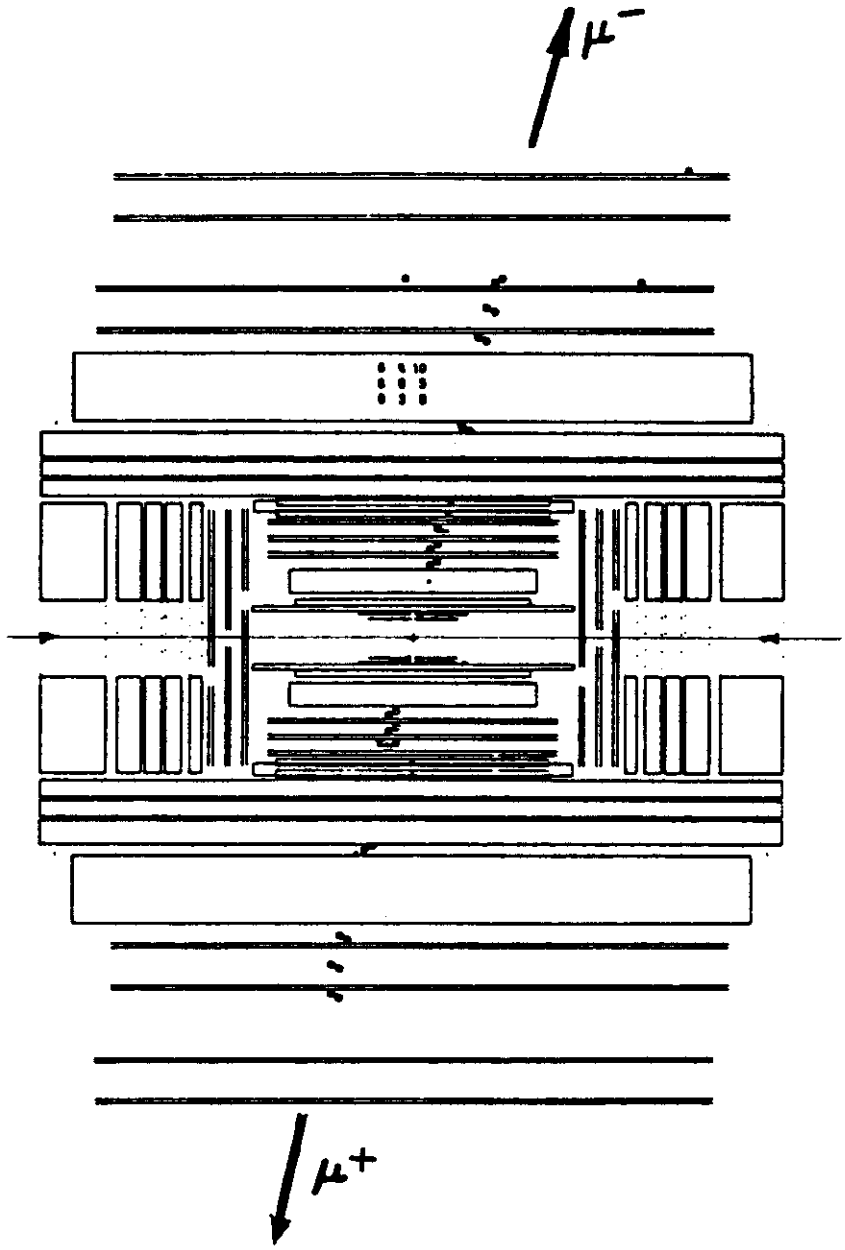

FIG.6

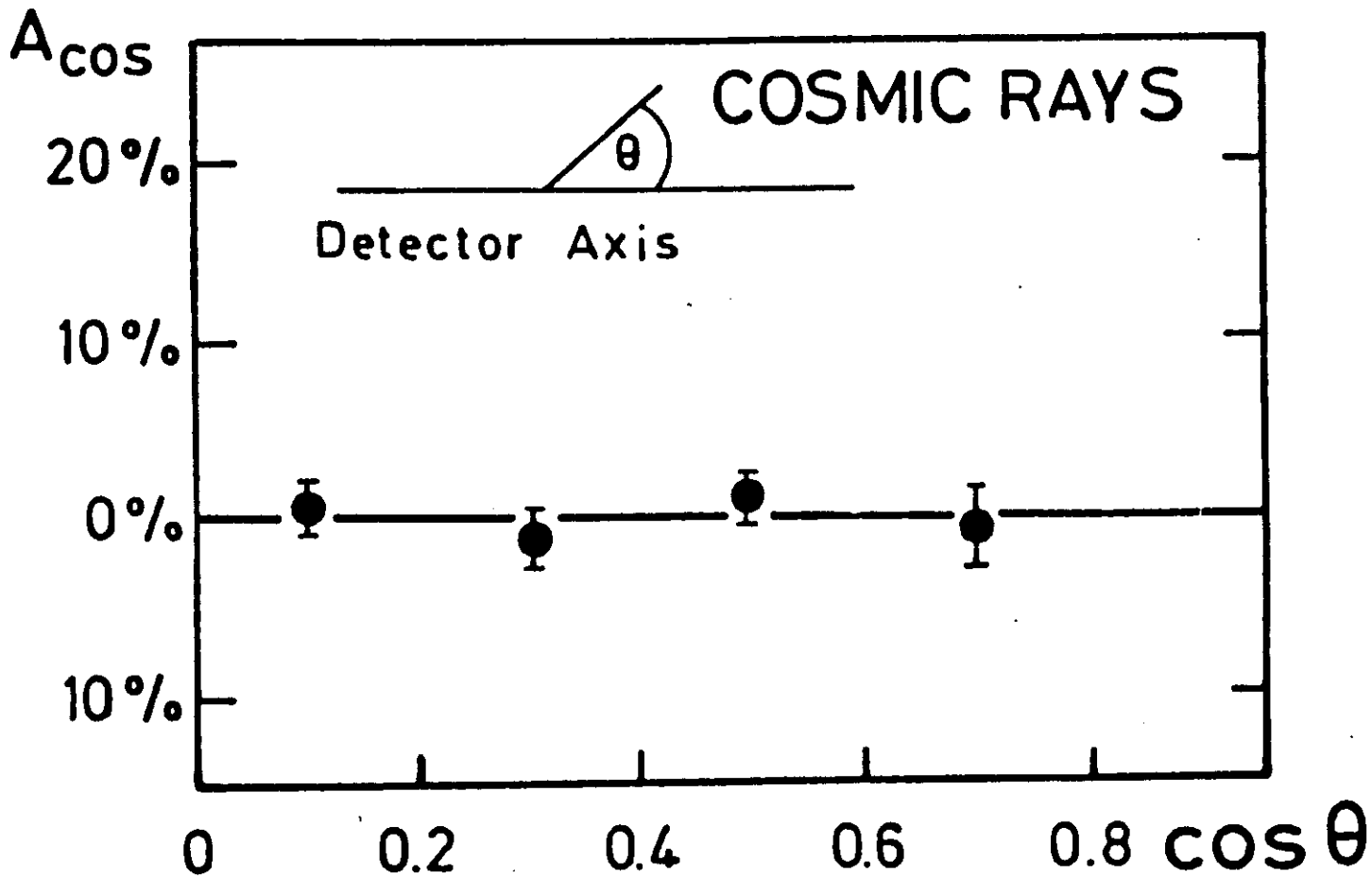

FIG.7

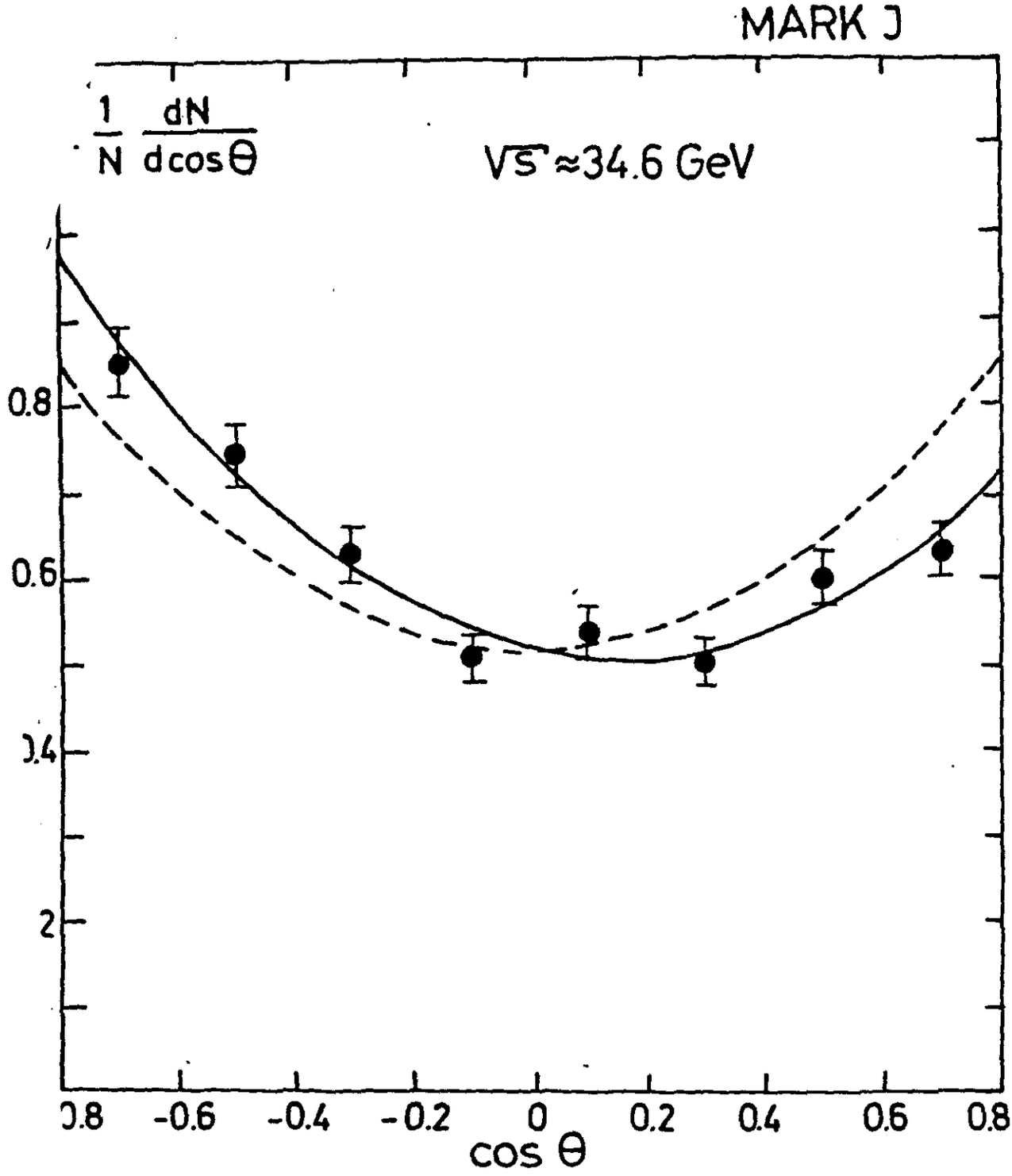
MARK J
$\frac{1}{N}\frac{dN}{d\cos\theta}$
$\sqrt{s} \approx 34.6$ GeV
0.8
0.6
0.4
0.2
-0.8
-0.6
-0.4
-0.2
0
0.2
0.4
0.6
0.8
cos θ

FIG.8

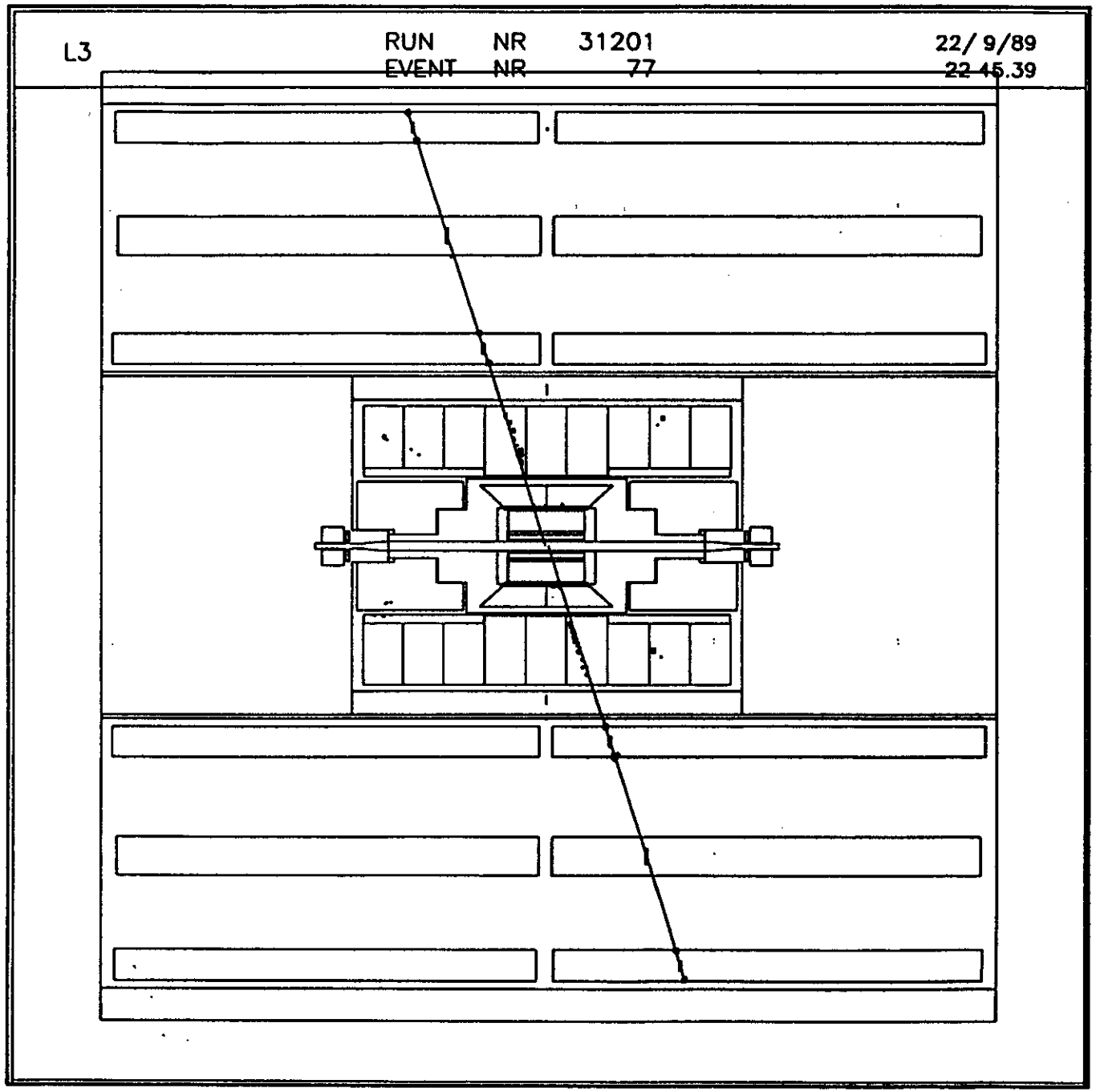

FIG.9

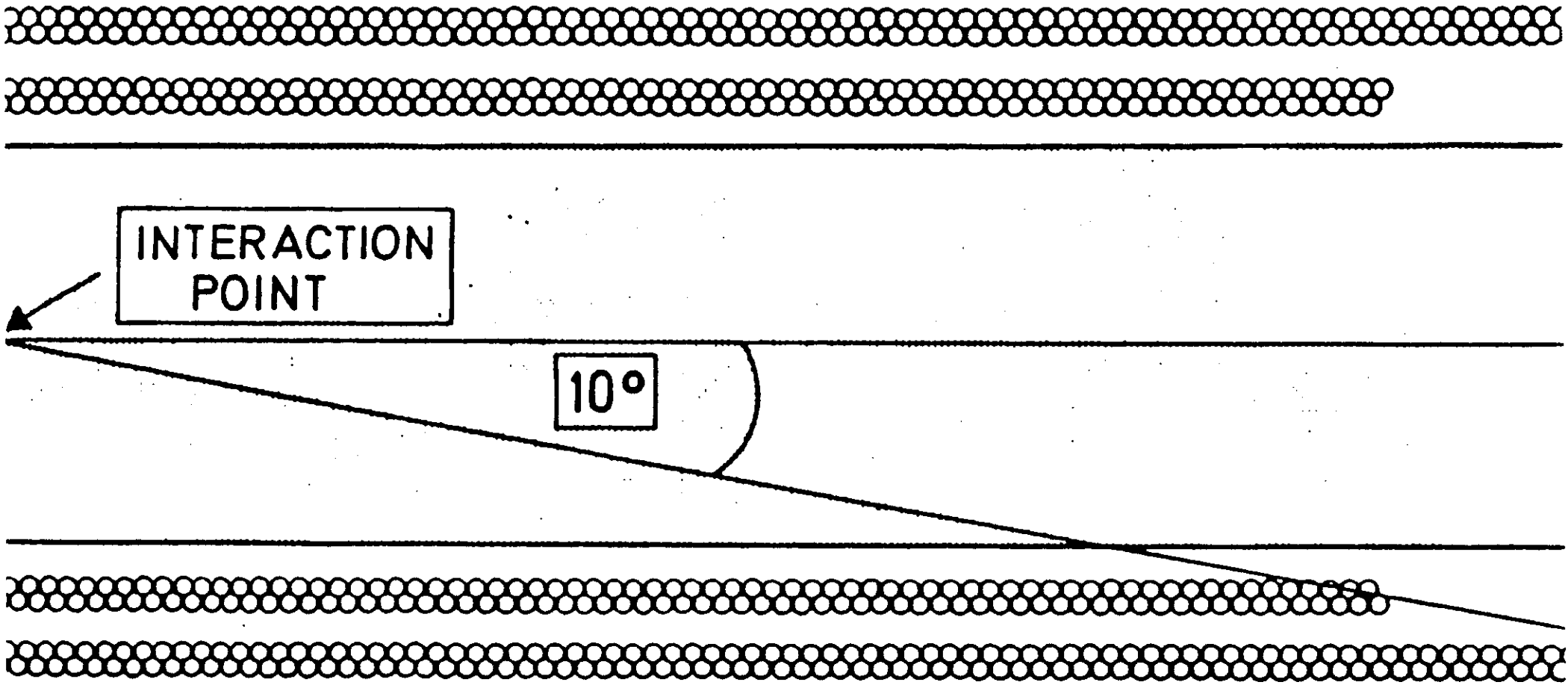

TOTAL ARRAY CONSISTS OF 2616 TUBES

FIG.10

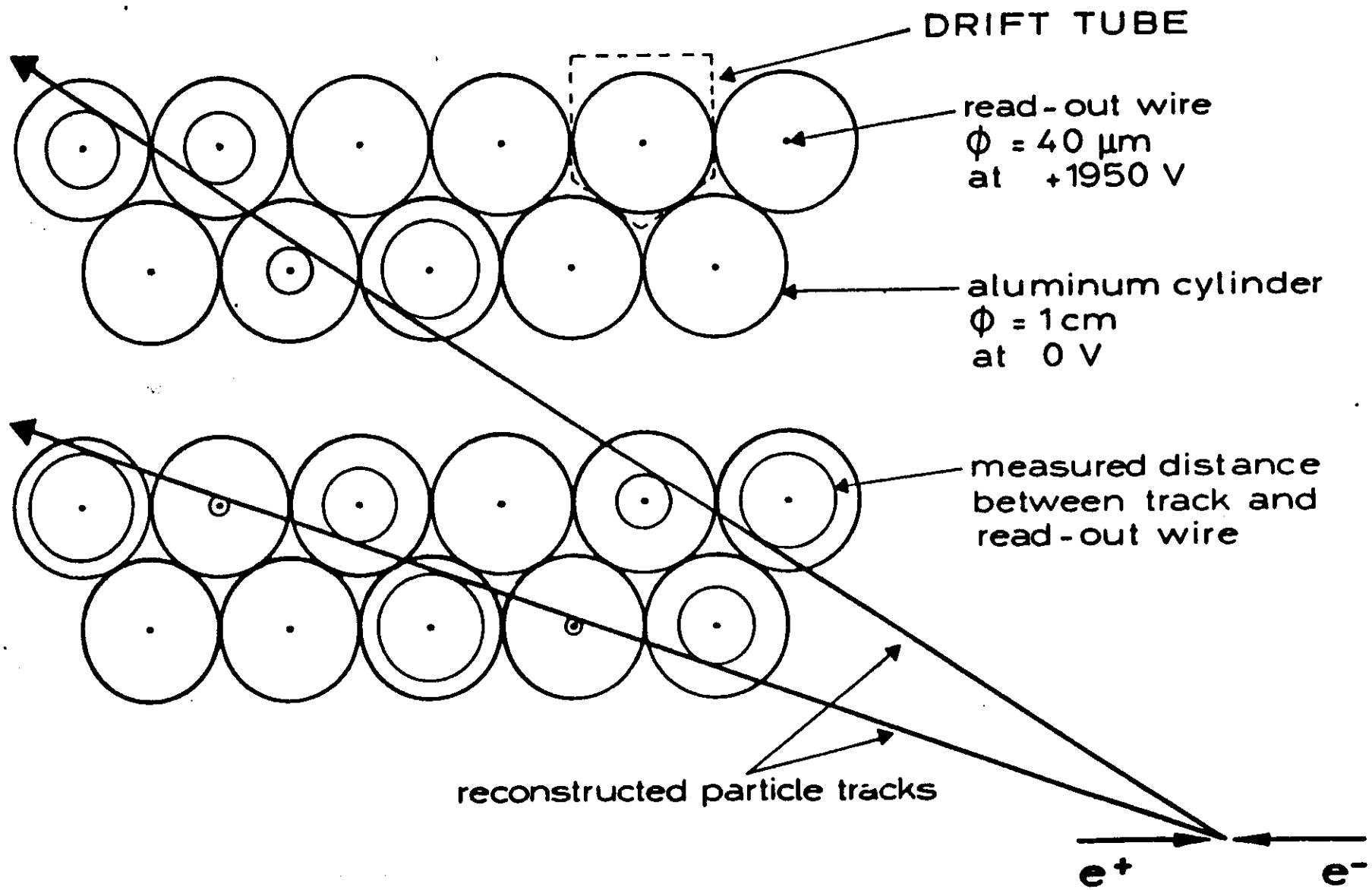
DRIFT TUBE
read-out wire
Φ = 40 μm
at +1950 V
aluminum cylinder
Φ = 1 cm
at 0 V
measured distance
between track and
read-out wire
reconstructed particle tracks
e+
e−

FIG.11

a)

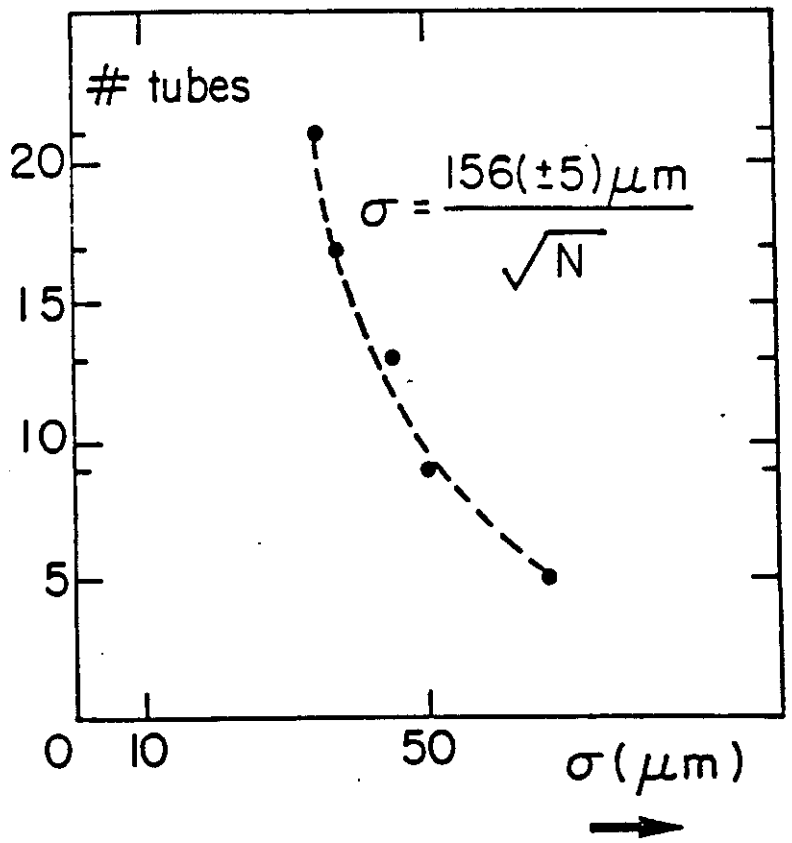

b)

FIG. 4a

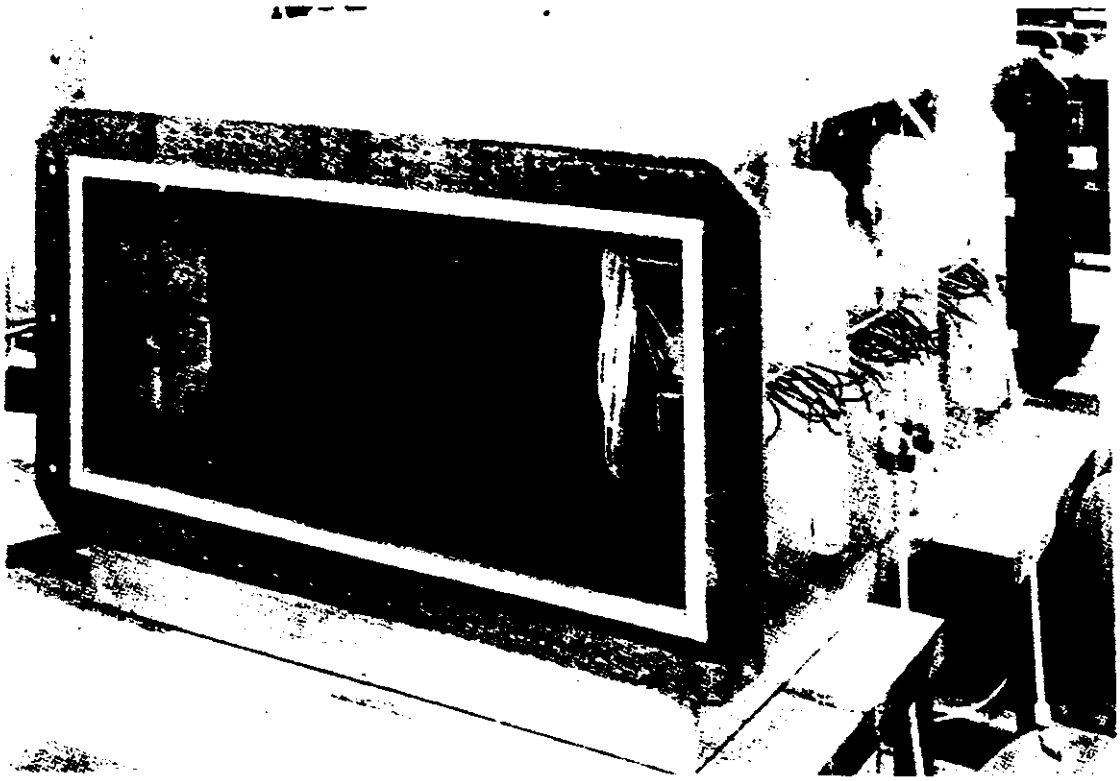

A)

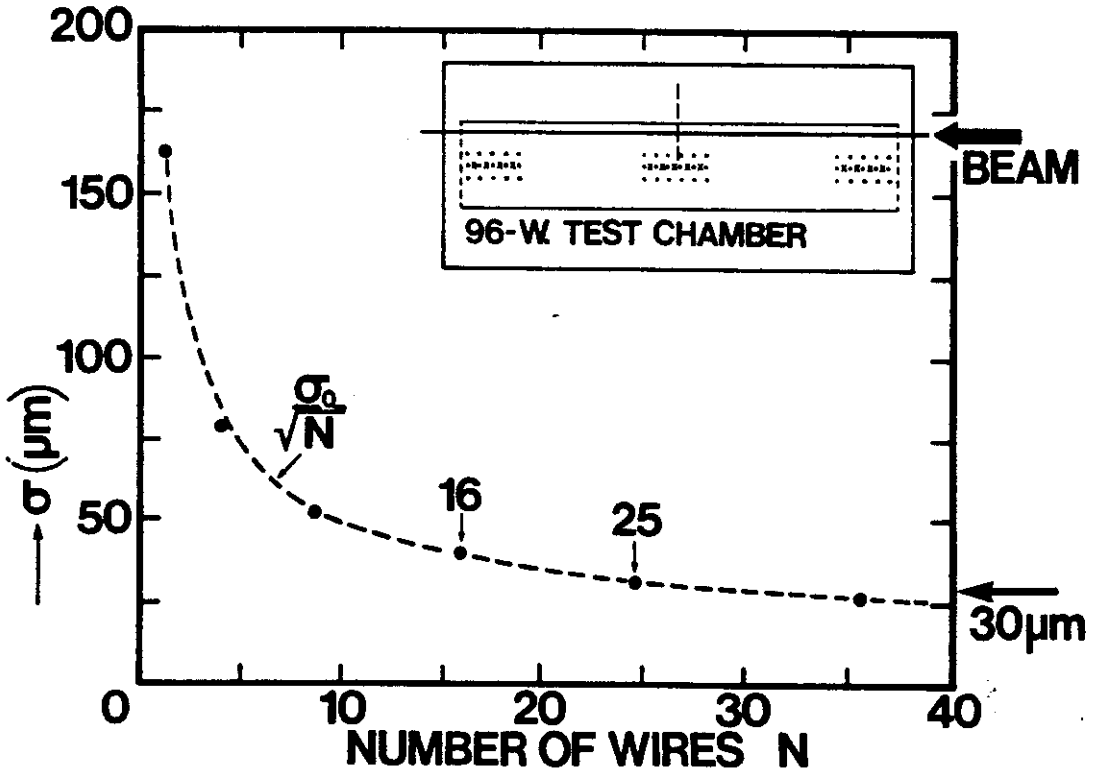
200
150
100
50
0
10
20
30
40
σ (μm)
NUMBER OF WIRES N
96-W. TEST CHAMBER
BEAM
σ0/√N
16
25
30μm

B)

FIG.13

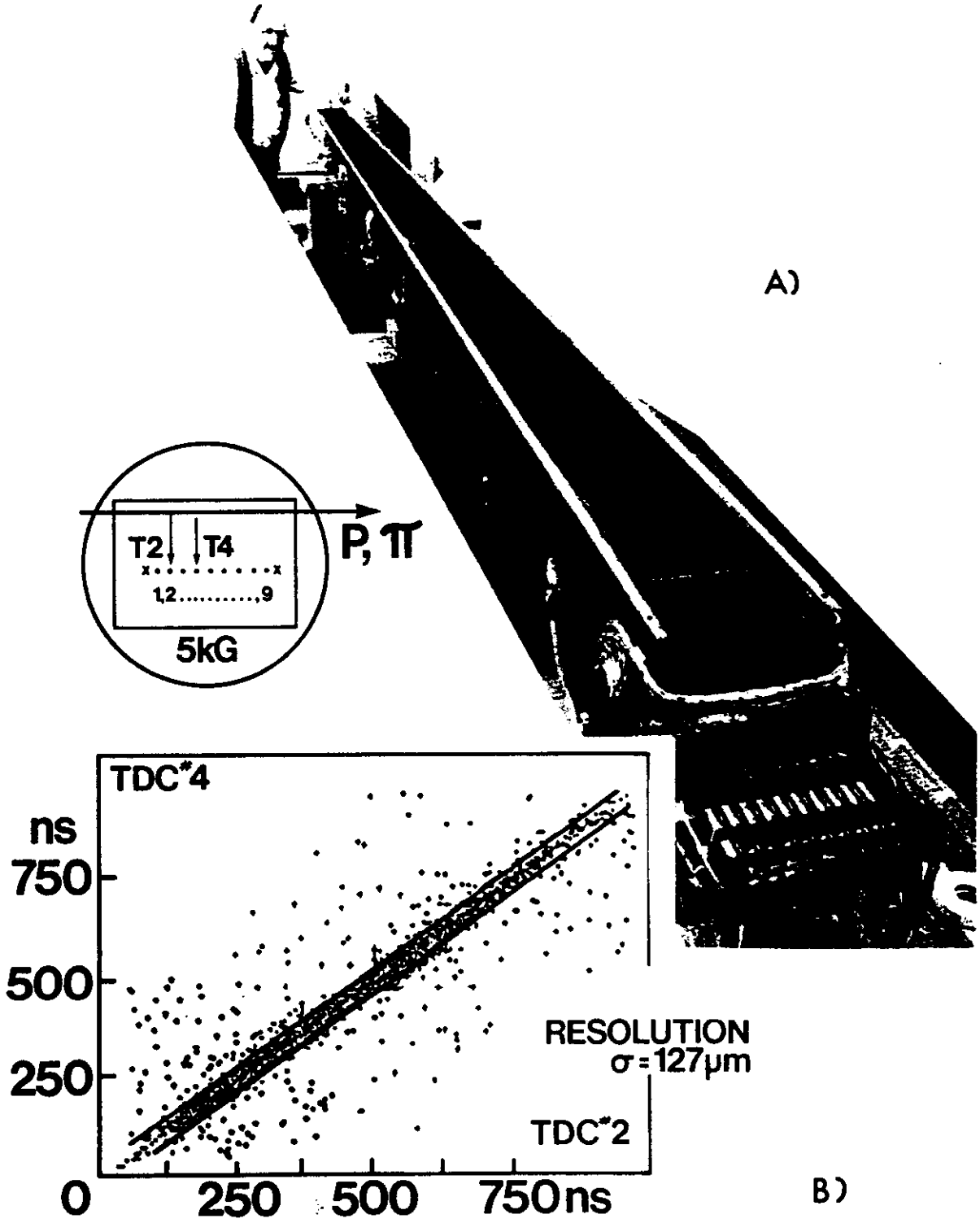
A)
T2
T4
1,2.....,9
5kG
P, π
TDC#4
ns
750
500
250
0
250
500
750ns
RESOLUTION
σ = 127μm
TDC#2
B)

FIG.14

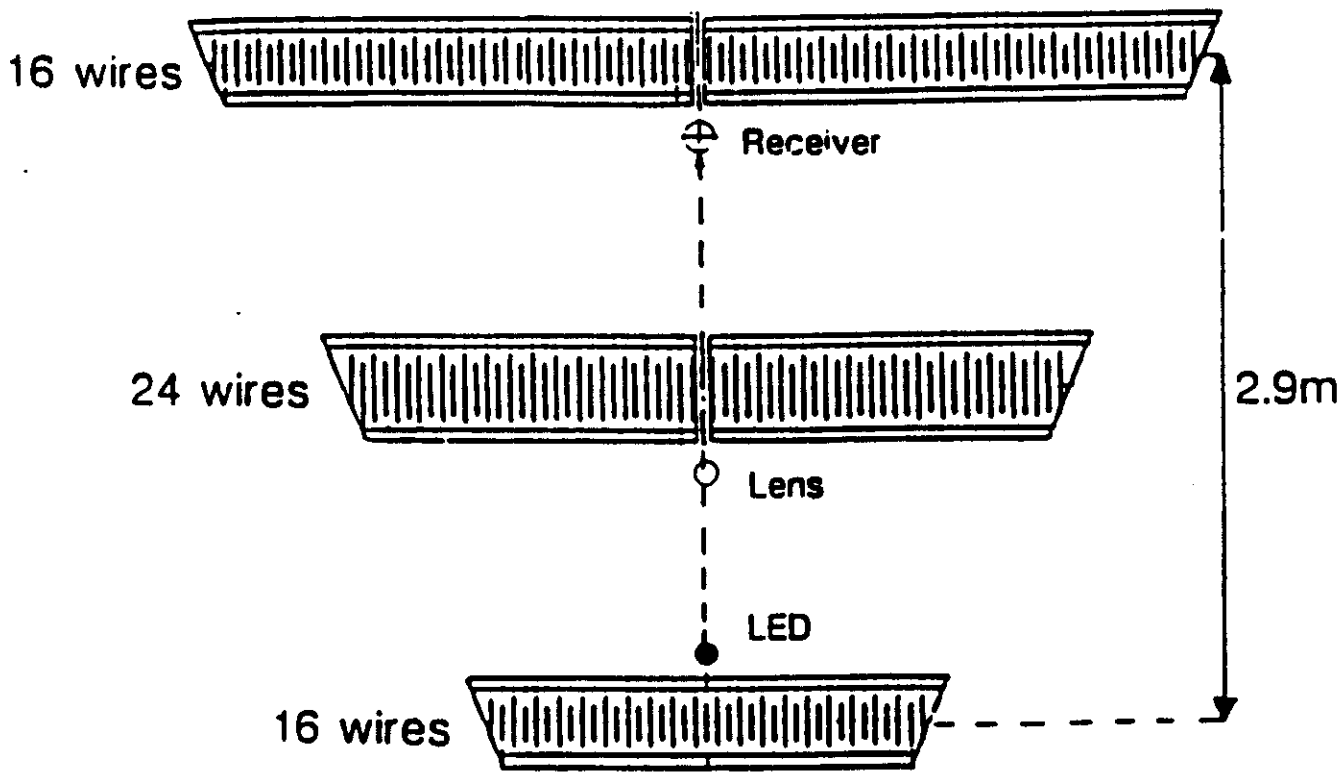

FIG.15

APPENDIX III

ABSTRACT

SYNERGY BETWEEN INDUSTRY AND HIGH ENERGY PHYSICS FOR MARKET RELEVANT NEW METHODS IN HIGH PRECISION LASER SURVEY TECHNIQUES, HIGH RESOLUTION TIME MEASUREMENT AND PARALLEL OPTICAL DATA TRANSMISSION

RESEARCH AND DEVELOPMENT PROGRAMME FOR A PRECISION SSC MUON SPECTROMETER

The Institutes for High Energy Physics of the Swiss Federal Institute of Technology Zurich (ETH Zurich) and of the University of Geneva have submitted a research and development programme for a SSC Muon Spectrometer to the Swiss Authorities. It is complimentary to the Programme submitted to SSC on October 2, 1989. All efforts will be combined in collaboration with leading Swiss industry. Funding will be provided through Swiss Authorities, namely the Committee for the Promotion of Applied Scientific Research, and the Swiss industry involved in the research and development programme. The programme shall start January 1, 1990 for a duration of three years. The total cost of the programme is 22 MSF (see also Table I).

The entire programme consists of three sub projects: Muon Spectrometer Alignment Systems, Readout Electronics and Data Transfer.

I. Muon Spectrometer Alignment Systems (defined in the proposal to SSC)

Alignment systems to be integrated in the SSC Muon Spectrometer will be developed together with the Swiss company DIXI S.A. with headquarters and production in Le Locle (about 100 km from Geneva) and additional high technology manufacturing facilities in Meyrin near CERN. DIXI S.A. is subdivided into eight different branches (Defense Division, High Precision Machine Tools, Screw Machines, High Precision Tooling, Industrial Refrigeration, ZENITH Watches, Training Devices for Police and Army etc.). DIXI delivers their high precision products, among others, to Oak Ridge, Lawrence Livermore National Laboratory, Charles Stark Draper Laboratory, GEC, Rolls Royce, Boeing, ROF Cardiff, Daimler Benz, ZF, Aerospatiale, Peugeot, Fiat etc.

Close collaboration with the department constructing high precision machine tools is foreseen. The technical demands for high precision production, permanent monitoring and fast corrections to eventual deformations is for the large precision machine tools produced by DIXI of same magnitude as for the L* Muon Spectrometer. The newest machine tools constructed by DIXI have a total weight of about 70 tons, overall dimensions of about six meters by six meters by two meters and must be kept in position with an accuracy of about three microns in all operating conditions.

The common efforts between DIXI and Swiss universities and the engagement of the Charles Stark Draper Laboratory in Cambridge (USA) will result in the development of alignment systems and methods which will be used for the SSC Muon Spectrometer.

II. Readout Electronics

The enormous number of channels to be read out for the L* Muon Spectrometer calls for a change in the basic concept of the readout system. Together with LeCroy S.A. in Meyrin Swiss institutes will develop a high performance, high density readout system with the potential to operate under the experimental conditions at SSC. With the integration of fiber optics for the signal transmission into the readout system it will become possible to develop new low power, high density amplifier/discriminator units which, because of their low heat dissipation, can be mounted directly on the chambers. In the frame of this project we will also work on the improvement of the time digitizing units thus, for example, to achieve a time resolution better than one nanosecond. Major attention will be given to the development of electronic components with high reliability, simple system integration and resistance to radiation effects at the level as expected at SSC.

III. Data Transfer

The third R and D Project investigated by Swiss collaborators in the SSC Muon Spectrometer will attack the general problem transmitting large volumes of data with highest speed over long distances. The project will be carried out together with the Asea Brown Boveri (ABB) Research Center in Dattwil near Zurich.

We will develop a multi-line (64 or 128) fiber optical system transmitting the signals from the discriminator's output, mounted on the chambers, over a distance of eventually up to 150 meters to the TDC's input.

Advantages of such a system are obvious and overcome many serious technical and engineering problems:

1. No attenuation of signals over the entire transfer lines.
2. No noise pickup.
3. High density of signal lines per given cross-section. This reduces dead space as well as the number of cables and connections. As a consequence, installation time will be drastically reduced.
4. Considerable reduction of weight of cables. Forces pulling on the mechanical structures of the Muon Spectrometer, and which must be compensated, are reduced.

TABLE I
COST ESTIMATE
SWISS RESEARCH AND DEVELOPMENT PROGRAMME
FOR THE SSC MUON SPECTROMETER

Project	Total Cost (MSF)
Muon Spectrometer Alignment Systems	7.0
Readout Electronics	9.0
Data Transfer	6.0
TOTAL	22.0

As attachment to this document we include the cover page of the respective application ("Beitragsgesuch") to the Swiss Government.

1990

Activity	COST
I. Muon Spectrometer Alignment Systems	
System Definitions	0.8 MSF
Material Studies	0.4 MSF
Subsystem Design	0.6 MSF
Subsystem Construction	0.3 MSF
TOTAL PROJECT	2.1 MSF
II. Readout Electronics	
Amplifier/Discriminator	1.5 MSF
TDC Integrated Circuit	0.7 MSF
TOTAL PROJECT	2.2 MSF
III. Data Transfer	
Optoelectronic Design	0.9 MSF
Fiber/Cable Design	0.3 MSF
Photodiode Development	0.3 MSF
Connector Construction	0.2 MSF
TOTAL PROJECT	1.7 MSF

1991

Activity	COST
I. Muon Spectrometer Alignment Systems	
Subsystem Design	0.5 MSF
Subsystem Construction	1.0 MSF
Verification/Tests Substystems	0.8 MSF
System Integration	0.2 MSF
TOTAL PROJECT	2.5 MSF
II. Readout Electronics	
Amplifier/Discriminator	0.7 MSF
TDC Integrated Circuit	0.8 MSF
TDC Module	1.4 MSF
Software Package	0.3 MSF
TOTAL PROJECT	3.2 MSF
III. Data Transfer	
Photodiode Development	0.3 MSF
Connector Construction	0.3 MSF
Optical Switches	0.5 MSF
Fiber/Cable Prototypes	0.5 MSF
Connecting Techniques	0.3 MSF
TOTAL PROJECT	1.9 MSF

1992

Activity	COST
I. Muon Spectrometer Alignment Systems	
Subsystem Construction	0.8 MSF
Verification/Tests Subsystems	0.3 MSF
System Integration	0.8 MSF
System Testing	0.5 MSF
TOTAL PROJECT	2.4 MSF
II. Readout Electronics	
TDC Module	0.8 MSF
Software Package	0.5 MSF
System Construction	1.7 MSF
System Testing	0.6 MSF
TOTAL PROJECT	3.6 MSF
III. Data Transfer	
Connector Construction	0.3 MSF
Optical Switches	0.3 MSF
Fiber/Cable Prototypes	0.2 MSF
Connecting Techniques	0.2 MSF
Packaging	0.4 MSF
System Construction	0.5 MSF
System Testing	0.5 MSF
TOTAL PROJECT	2.4 MSF

Eidg. Volkswirtschaftsdepartement

KOMMISSION ZUR FÖRDERUNG
DER WISSENSCHAFTLICHEN FORSCHUNG

Wildhainweg 21
Postfach 2338
3001 Bern

Telefon 031 61 21 43/46/49

Bitte leer lassen

Projekt Nr. _____

Referent: _____

Eingereicht auf Stichtag

31. März ____ ☐

30. September ____ ☐

Beitragsgesuch

Titel des Projektes (1–2 Zeilen zur Veröffentlichung bestimmt, z.B. im Tätigkeitsbericht der Kommission zur Förderung der wissenschaftlichen Forschung / KWF *)

Synergie zwischen Industrie und Hochenergiephysik für die marktrelevante Entwicklung neuartiger Methoden in höchstpräziser Laser-Vermessungstechnik, hochauflösender elektronischer Zeitmessung und paraller optischer Datenübertragung.

1. Zusammenfassende Angaben

	Name	Institut/Firma
1.1. Hauptgesuchsteller	Professor Dr. Hans HOFER	Institut für Hochenergiephysik ETH Zürich
1.2. Mitgesuchsteller	Professor Dr. Maurice BOURQUIN	Université de Genevé Dept. de Physique Nucl. et Corpus.

1.3. Projektpartner

Groupe DIXI; 42 av. de Technicum, 2400 Le Locle
LeCroy S.A.; 101 Route du Nant-d'Avril, 1217 Meyrin 1
Asea Brown Boveri Ltd; 5405 Baden Dättwil

1.4. Neues Projekt [X] Fortsetzung des KWF-Projektes Nr. ____

1.5. Beginn: 01.01.1990 Dauer: 3 Years

1.6. Gesamtkosten des Projektes Fr. 22 MSF

Beiträge Dritter / Eigenleistungen (VO Art. 11 **) Fr. 11 MSF

Gewünschter Bundesbeitrag Fr. 11 MSF

Abkürzungen

* KWF: Kommission zur Förderung der wissenschaftlichen Forschung

** VO: Verordnung des Eidgenössischen Volkswirtschaftsdepartementes über Bundesbeiträge für die Förderung der praxisorientierten Forschung und Entwicklung vom 17. Dezember 1982

APPENDIX IV

MASSACHUSETTS INSTITUTE OF TECHNOLOGY

LABORATORY FOR NUCLEAR SCIENCE REPORT

Technical Report Number 129 October 22, 1982

Drift Velocity and Drift Angle Measurements[§]

C. M. Ma[1*)], U. Becker[1)], D. A. Ma[1*)] A. H. Walenta[2**)]

1) Laboratory for Nuclear Science, Massachusetts Institute of Technology Cambridge, Massachusetts, USA

2) Brookhaven National Laboratory, Upton, New York, U.S.A.

Abstract

Drift velocities as function of electrical field have been measured for 95 drift chamber gas mixtures and pressures. The drift angles in magnetic fields up to 20 kgauss are presented.

[§]Work supported by the Laboratory for Nuclear Science and the U.S. Department of Energy, DE-AC02-76ER03069.

*) Visitor from Institute of High Energy Physics, Beijing

**) Now University of Siegen, West Germany

I. Introduction

Because of the inhomogeneous field in multiwire drift chambers[1] satisfactory position resolution can be obtained only with a gas whose drift velocity does not depend on the electrical field strength over an appropriate range. A number of gases which have a "saturated drift velocity" have been found, but no systematic study has been performed to obtain optimum behavior. We present a series of drift velocity measurements carried out at Brookhaven National Laboratory. Many gases were investigated which carried promise of being usable as drift chamber gases. Attention was paid to those gases with constant saturated drift velocity, and their mixture sensitivity was studied. The magnetic deflection angles of drifting electrons in most gases were measured for magnetic fields up to 20 kgauss. The ranges measured cover many of the applications for track detectors for present-day storage ring experiments.

II. Apparatus and Measurement Technique

The drift velocities were measured in a chamber containing 5 parallel wires (see Fig. 1). The primary ionization was induced by X-rays injected from a Kevex X-ray tube being pulsed with 8 ns FWHM at ~100 kHz. The copper target emitted characteristic X-rays of 8.1 KeV. The thick brass wall of the chamber had three holes serving as a first set of collimators for X-ray injection. Taking differential measurements between collimating holes 2.278 cm apart on the chamber enabled the determination of the drift velocity. A flat high voltage electrode and a screen at ground potential define the drift space of maximally 5 cm. The G10 walls of the chamber carried field shaping copper strips held at the appropriate potentials.

Fig. 2 gives a top view of the chamber showing the operation in magnetic field. The magnetic field lines are orthogonal to the paper plane. On the side

propagation time of 10.5 ns/cm. Measuring the difference in pulse arrival time from both ends of the delay line determines the position of the electrons arriving at the anode. The difference between the magnetic field "on" and "off" allows the determination of the deflection angle.

The chamber was located in a standard Brookhaven D36 dipole magnet capable of producing homogeneous magnetic fields up to 25 kgauss with an inhomogeneity $\Delta B/B < 1\%$. The X-rays were injected through a channel drilled through the pole piece of the magnet (see Fig. 3). This channel guided the X-rays into the chamber parallel to the magnetic field lines. In this way the X-ray tube, which is sensitive to magnetic field, could operate properly.

III. Drift velocity measurements

In the following, we list a series of graphs showing the drift velocity measurements for various gas mixtures, which are given in volume percentages. The pressures indicated correspond to 15, 30, 45, and 60 psi. Before each gas filling, the chamber was evacuated to 10^{-3} Torr. Therefore, residual impurities are negligible. The mixtures were obtained by filling with partial pressures. The reading accuracy was ~1%.

Corrections have not been made for systematic error due to temperature effects, which can affect the drift velocity at low E/p.[4] The measurements were performed at ambient temperature (15-30°). Gas purity also influences the measurements in the low electrical field region. Technical grade purity was used for hydrocarbon gases, i.e., 99.5%, as in most high energy physics experiments.

The measurements are in reasonable agreement with older measurements[2] and agree very well with recent data[3] wherever a comparison is available.

The curves drawn on the graphs are to guide the eye only.

In general, mixtures with very low concentrations of hydrocarbons were found to lead to sparking behavior at higher drift fields. This is apparent from the graphs in Chapter III, showing only the measurements which were not affected. Whereas the absolute value of the sparking is chamber-dependent, the relative comparison indicates the usefulness of the gases in this respect.

IV. Measurement of drift angle in magnetic field

We present measurements done with gases which correspond in part to the drift velocity measurements given in Chapter III. Not shown is a systematic uncertainty of about 1°. We notice the very different behavior of mixtures containing CO_2. A more detailed study of these mixtures has been performed recently.[5)]

V. Acknowledgements

It is our pleasure to thank Drs. D. Lowenstein, G. Danby, V. Radeka for support and G. von Aachen, G. W. Rowe, and E. Scheidker for technical help.

REFERENCES

1) A. H. Walenta et al., NIM 92, 373 (1971).

2) For a compilation see S. C. Brown, Basic Data of Plasma Physics, John Wiley & Sons; R. H. Healey and J. W. Reed, "The Behavior of Slow Electrons in Gases," Amalgamated Wireless Ltd., Sydney, 1941.

3) I. Lehraus et al., CERN-EF 82-1; Daum et al., NIM 152, 541 (1978); Farr et al., NIM 54, 175 (1978).

4) C. R. Bowman, D. E. Gordon, Journal of Chem. Physics 46, 1878 (1967).

5) U. Becker et al., MIT-LNS Report 130, November 5, 1982, submitted to NIM.

FIGURE CAPTIONS

Fig. 1 Side view of the test chamber made of brass walls A. X-ray injection holes B. C is field shaping of the drift chamber. D is the grid enclosing the proportional wires E, with the delay line F forming the back wall.

Fig. 2 Top view of the chamber with direction of E and B fields. Symbol explanation as in Fig. 1.

Fig. 3 Test setup in the dipole magnet with coil B and return yoke C. X-rays were injected through a long channel.

DRIFT VELOCITY MEASUREMENTS

Gas Mixture	Ratio	Pressure (atm)				Figure #
Argon/Ethane	50/50	1.02	2.04	3.06	4.08	4
	44/56	1.02	2.04	3.06	4.08	5
	56/44	1.02	2.04	3.06	4.08	6
	All mixtures	1.02			4.08	7
Argon/Propane	95/5	1.02	2.04	3.06	4.08	8
	90/10	1.02	2.04	3.06	4.08	9
	80/20	1.02	2.04	3.06	4.08	10
	All mixtures	1.02				11
Argon/Isobutane	80/20	1.02				12
	75/25	1.02	2.04	3.06		13
	70/30	1.02	2.04			14
	All mixtures	1.02				15
Argon/Ethylene	90/10	1.02				16
	80/20	1.02	2.04	3.06	4.08	17
	70/30	1.02		3.06	4.08	18
	All mixtures	1.02				19
Argon/CO_2	90/10	1.02	2.04	3.06	4.08	20
	85/15	1.02	2.04	3.06	4.08	21
	80/20	1.02	2.04	3.06	4.08	22
	70/30	1.02	2.04	3.06	4.08	23
	60/40	1.02	2.04	3.06	4.08	24
	All mixtures	1.02			4.08	25
Argon/CO_2/Propane	83.5/14.5/2	1.02	2.04	3.06	4.08	26
	82.5/14.5/3	1.02	2.04	3.06	4.08	27
	All mixtures	1.02	2.04			28
Argon/Isobutane/Propane	70/15/15	1.02	2.04	3.06		29
Argon/Isobutane/Ethylene	70/15/15	1.02	2.04	3.06		30
Argon, Ethane, Propane	pure	1.02				31

MEASUREMENT OF DRIFT ANGLE IN MAGNETIC FIELD

Gas Mixture	Ratio	Pressure (atm)				Figure(s)
Argon/Ethane	50/50	1.02	2.04	3.06	4.08	32-35
	44/56	1.02	2.04	3.06	4.08	36-39
Argon/Propane	80/20	1.02	2.04	3.06	4.08	40-43
Argon/Isobutane	75/25	1.02	2.04			44, 45
Argon/CO_2	90/10	1.02	2.04	3.06	4.08	46-49
	80/20	1.02	2.04	3.06	4.08	50-53
	85/15	1.02	2.04	3.06	4.08	54-57
Argon/Isobutane/Propane	70/15/15	1.02	2.04	3.06		58-60
Argon/Isobutane/Ethylene	70/15/15		2.04			61
Xenon/Ethane	50/50	1.02	2.04			62, 63
Argon/Methane	90/10	1.02				64

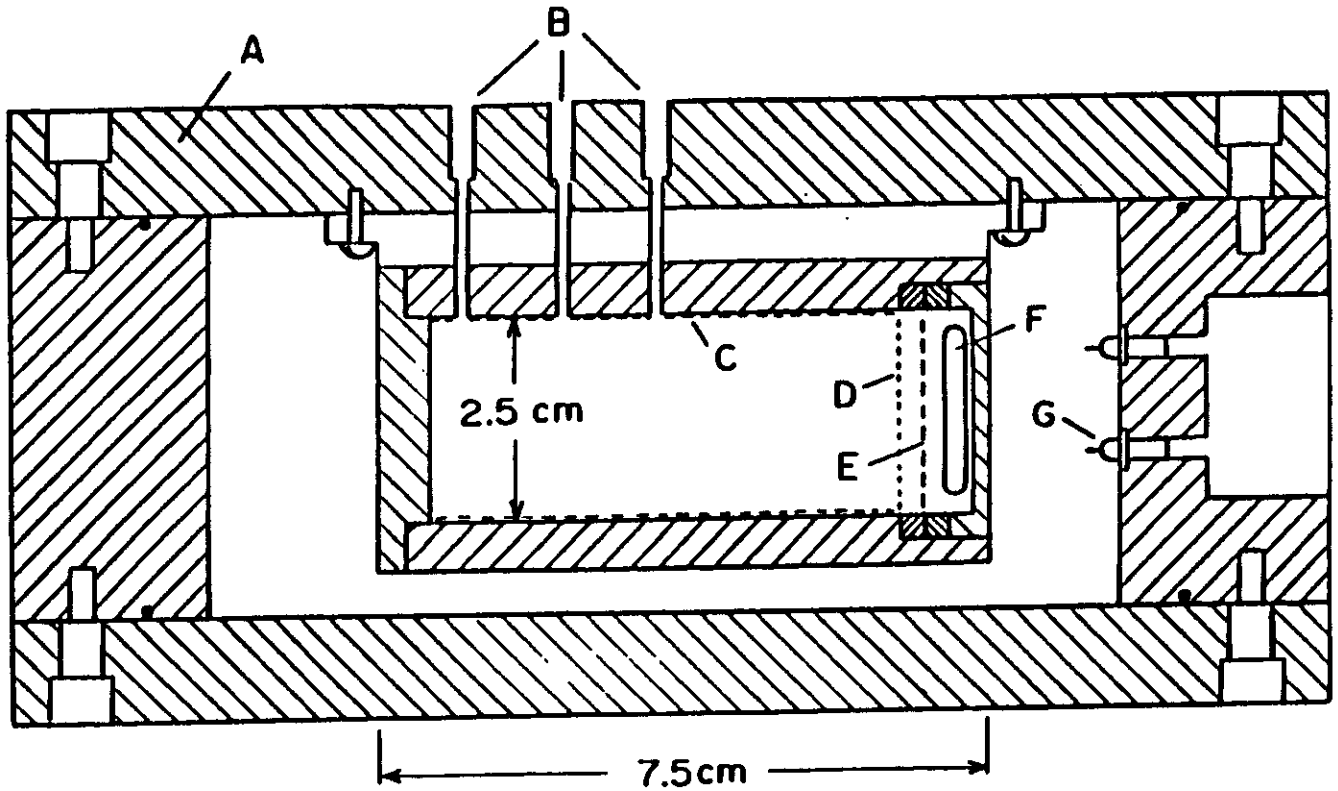

Figure 1

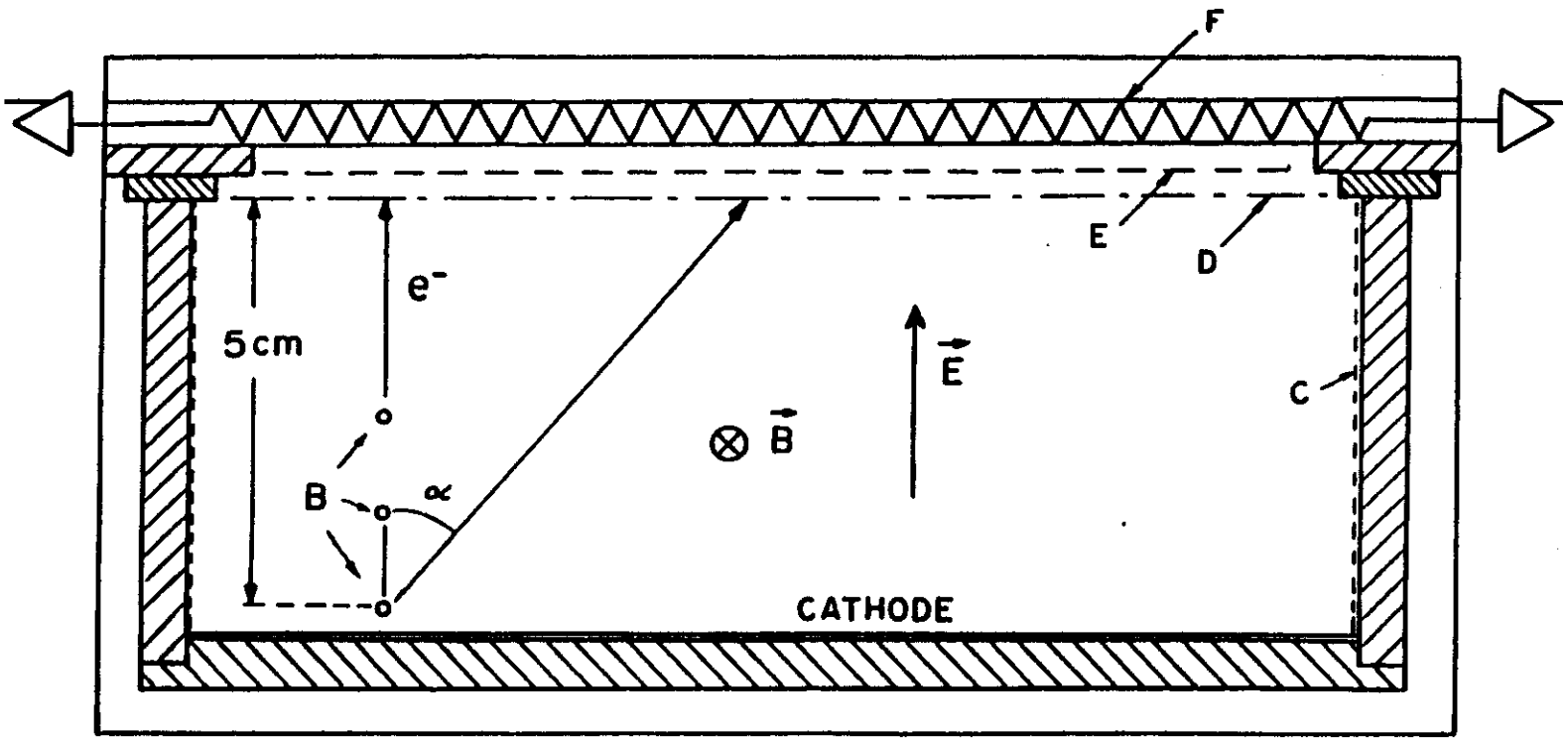

Figure 2

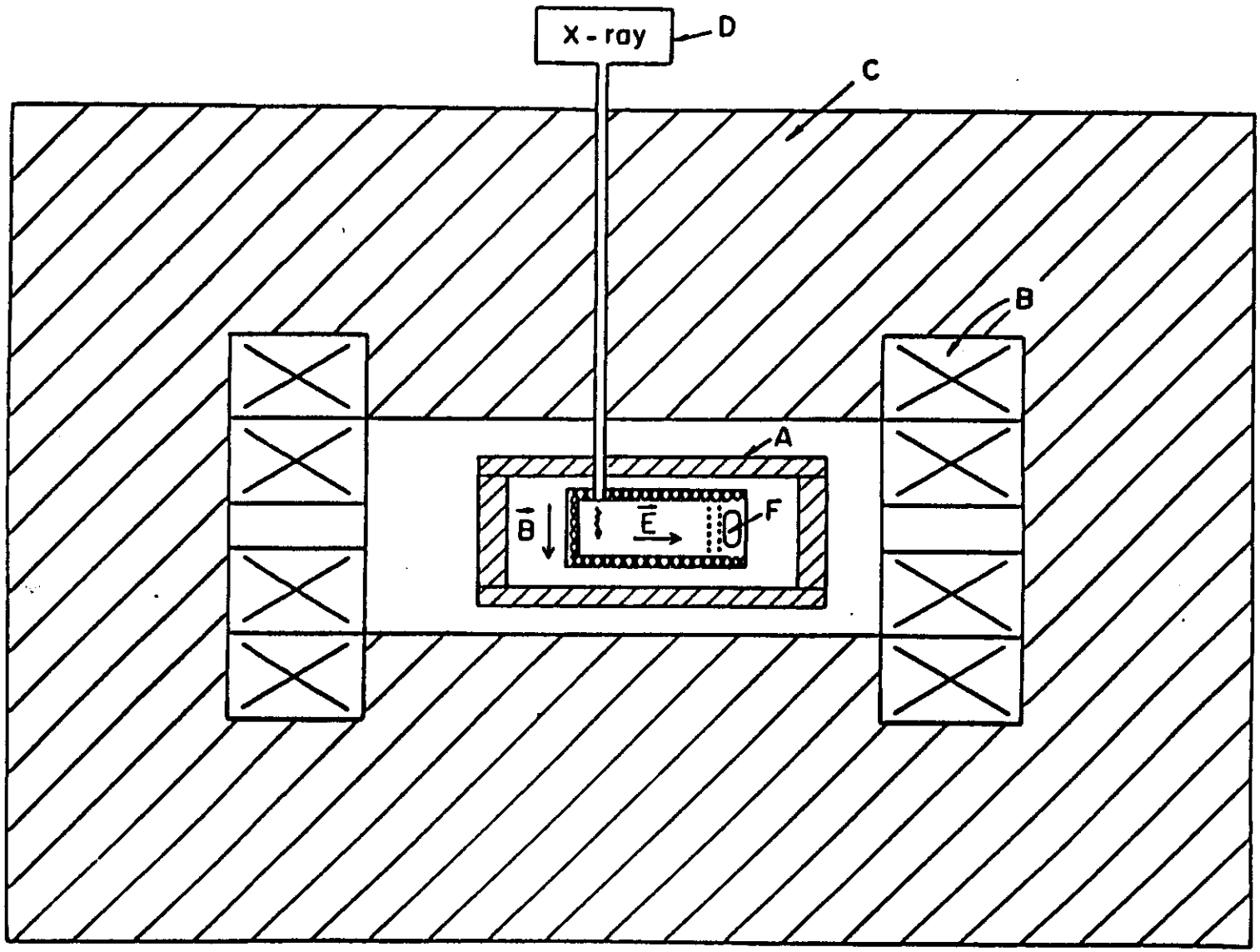

Figure 3

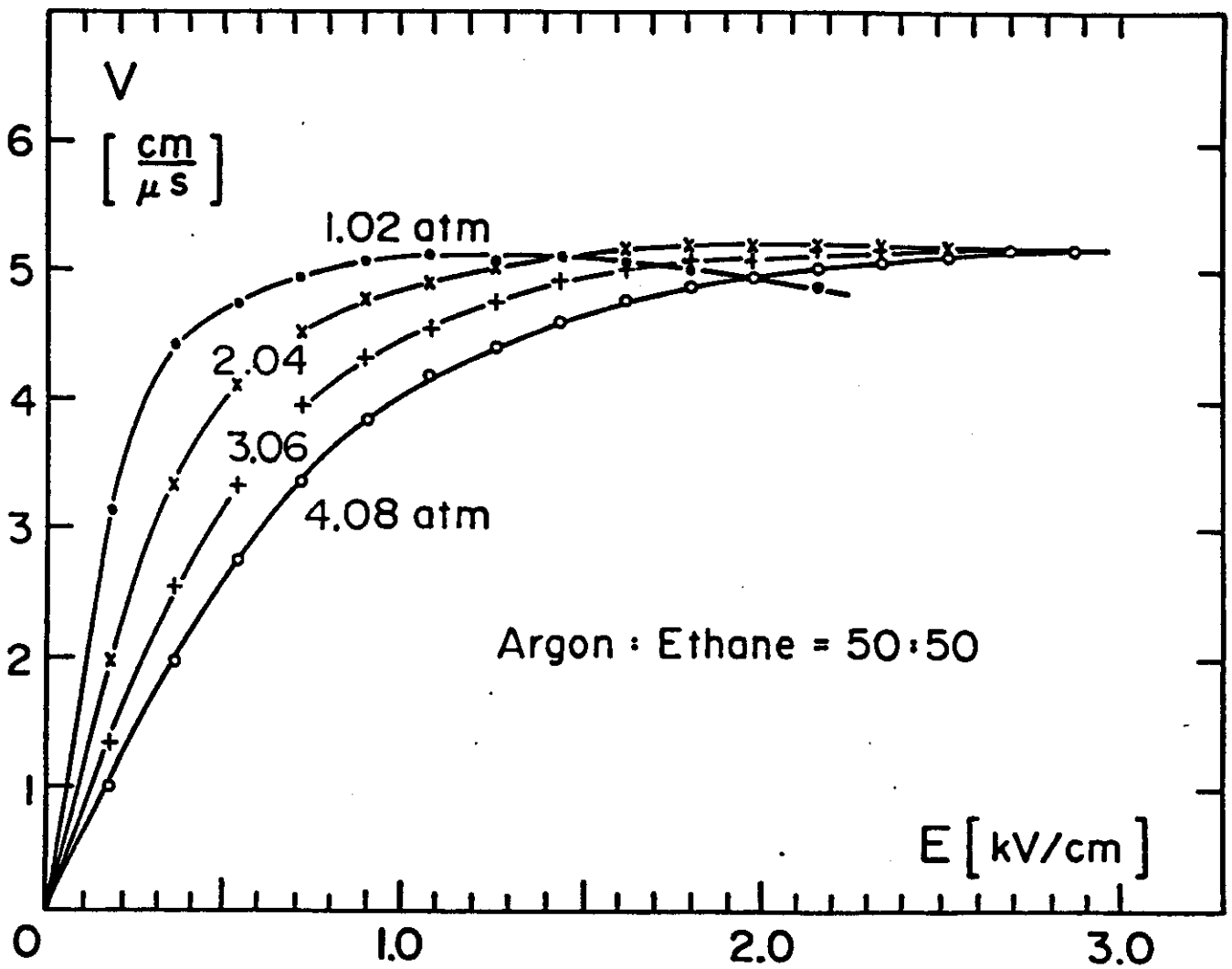

Figure 4 DRIFT VELOCITY vs ELECTRIC FIELD

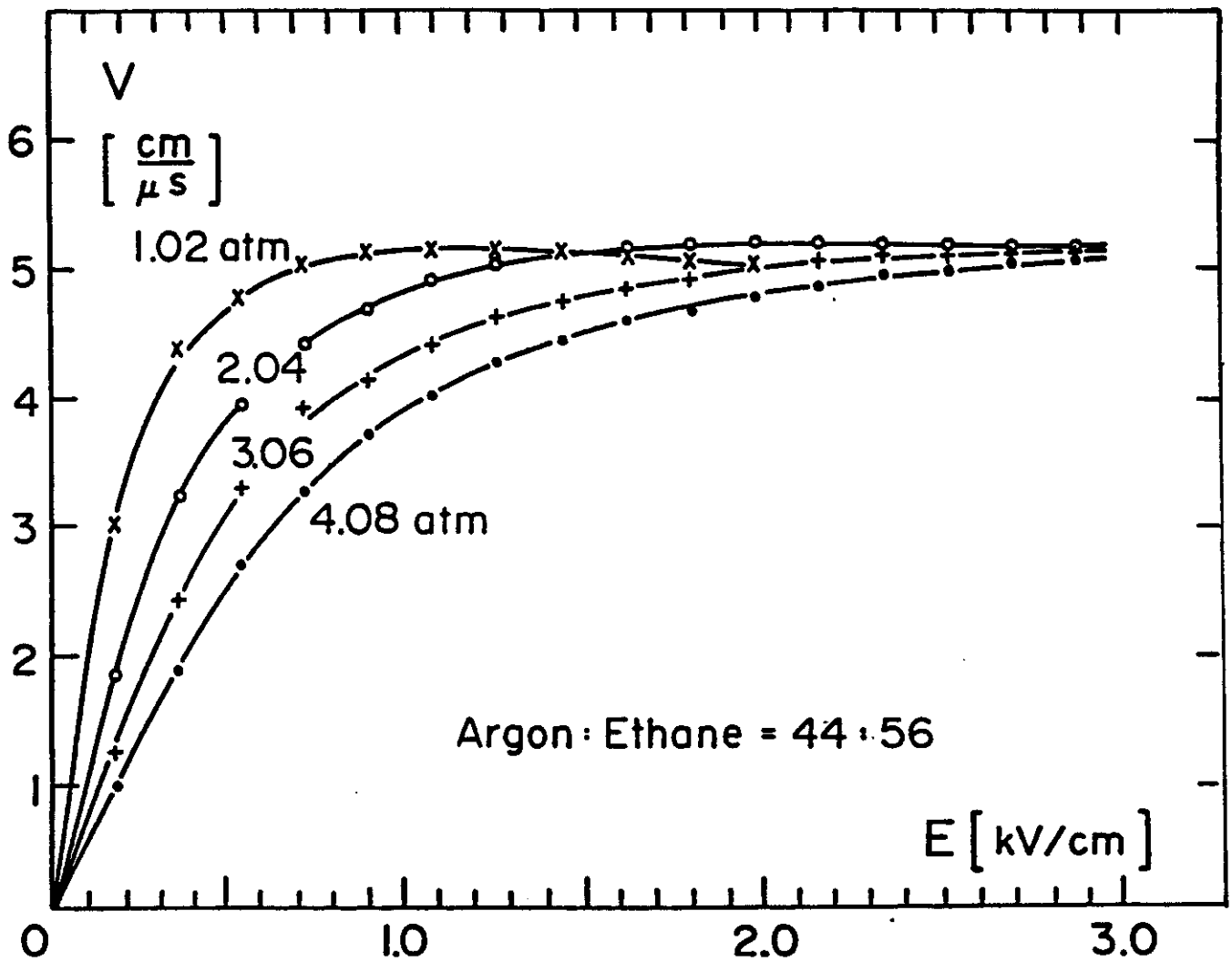

Figure 5 DRIFT VELOCITY vs ELECTRIC FIELD

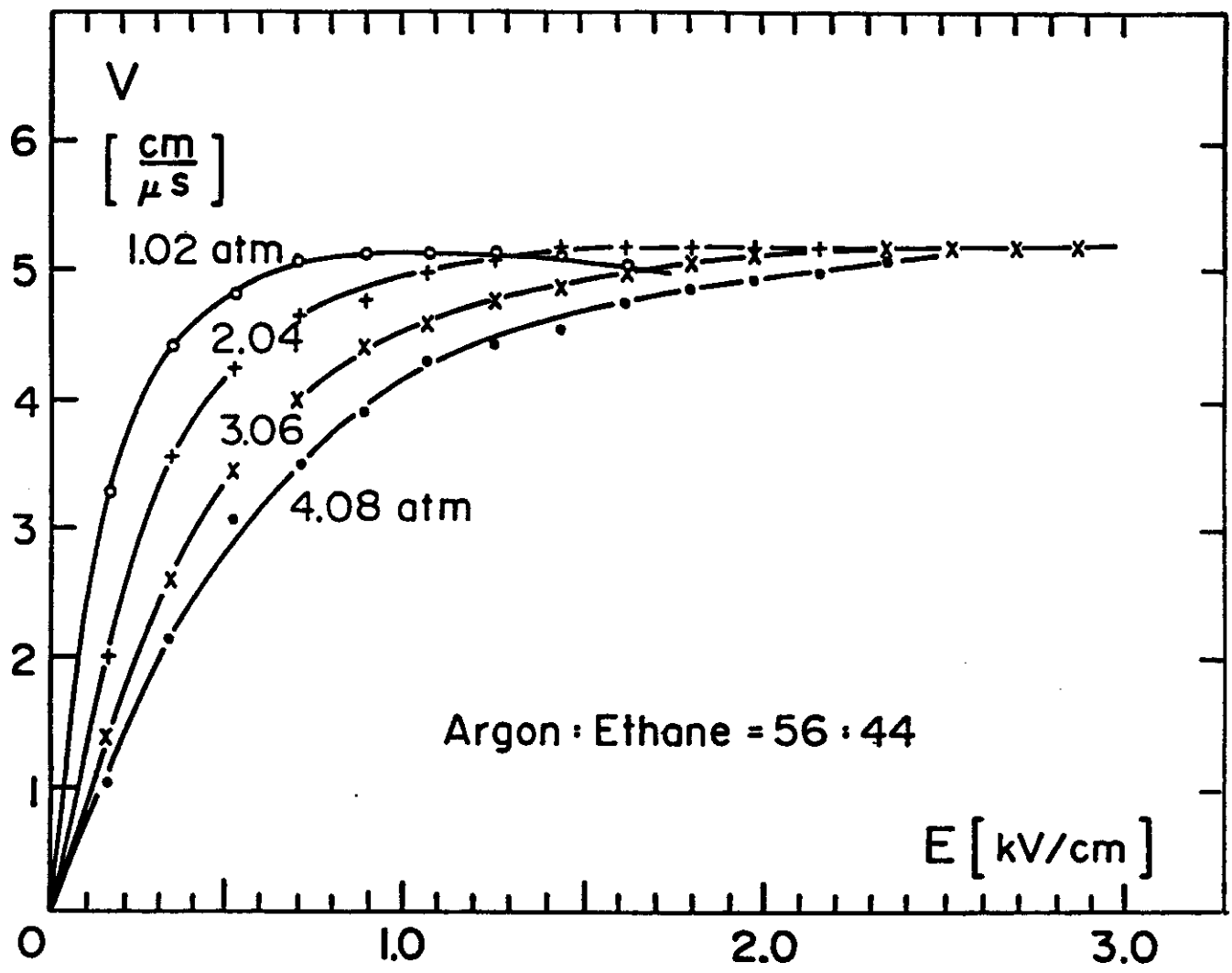

Figure 6 DRIFT VELOCITY vs ELECTRIC FIELD

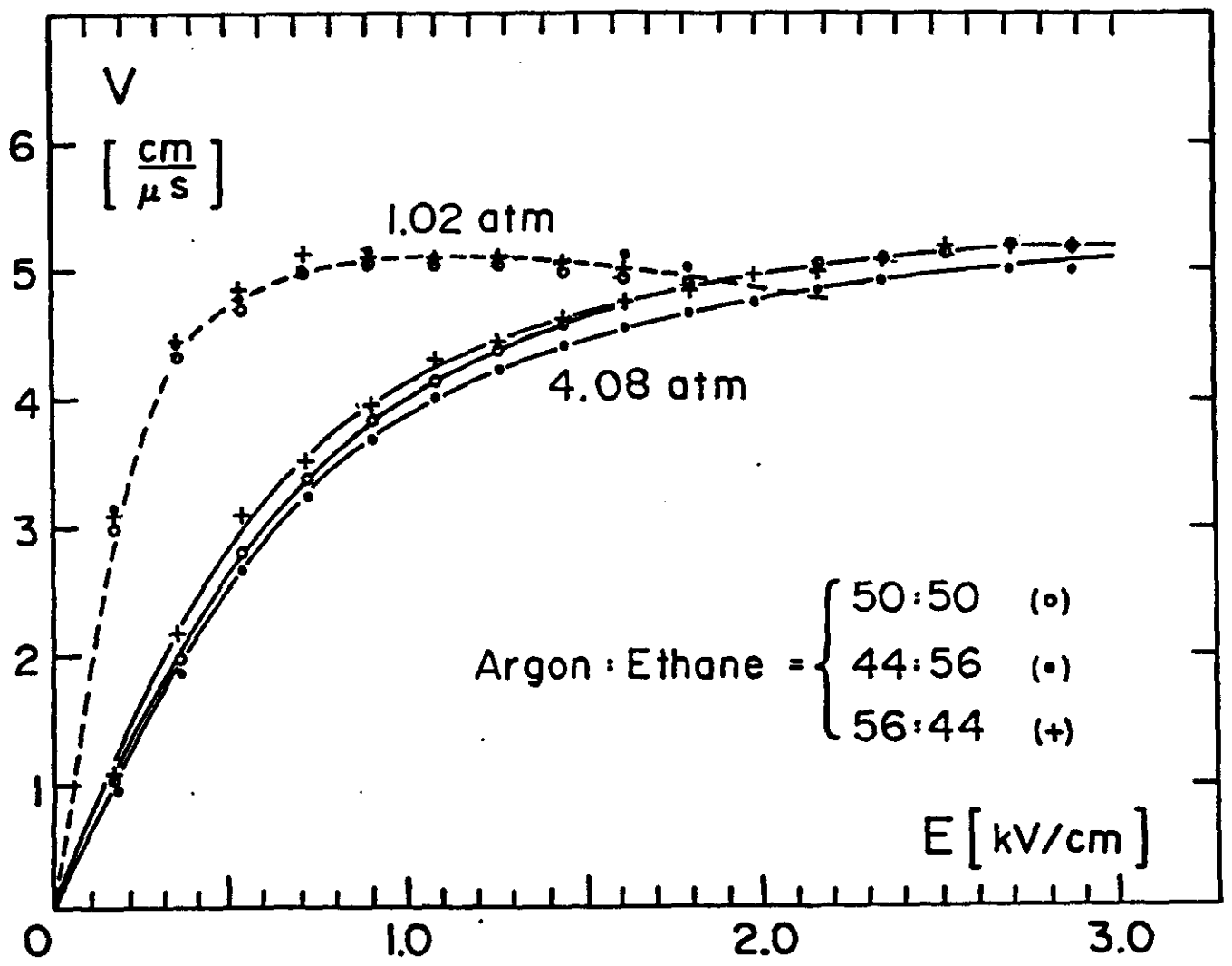

Figure 7 DRIFT VELOCITY vs ELECTRIC FIELD

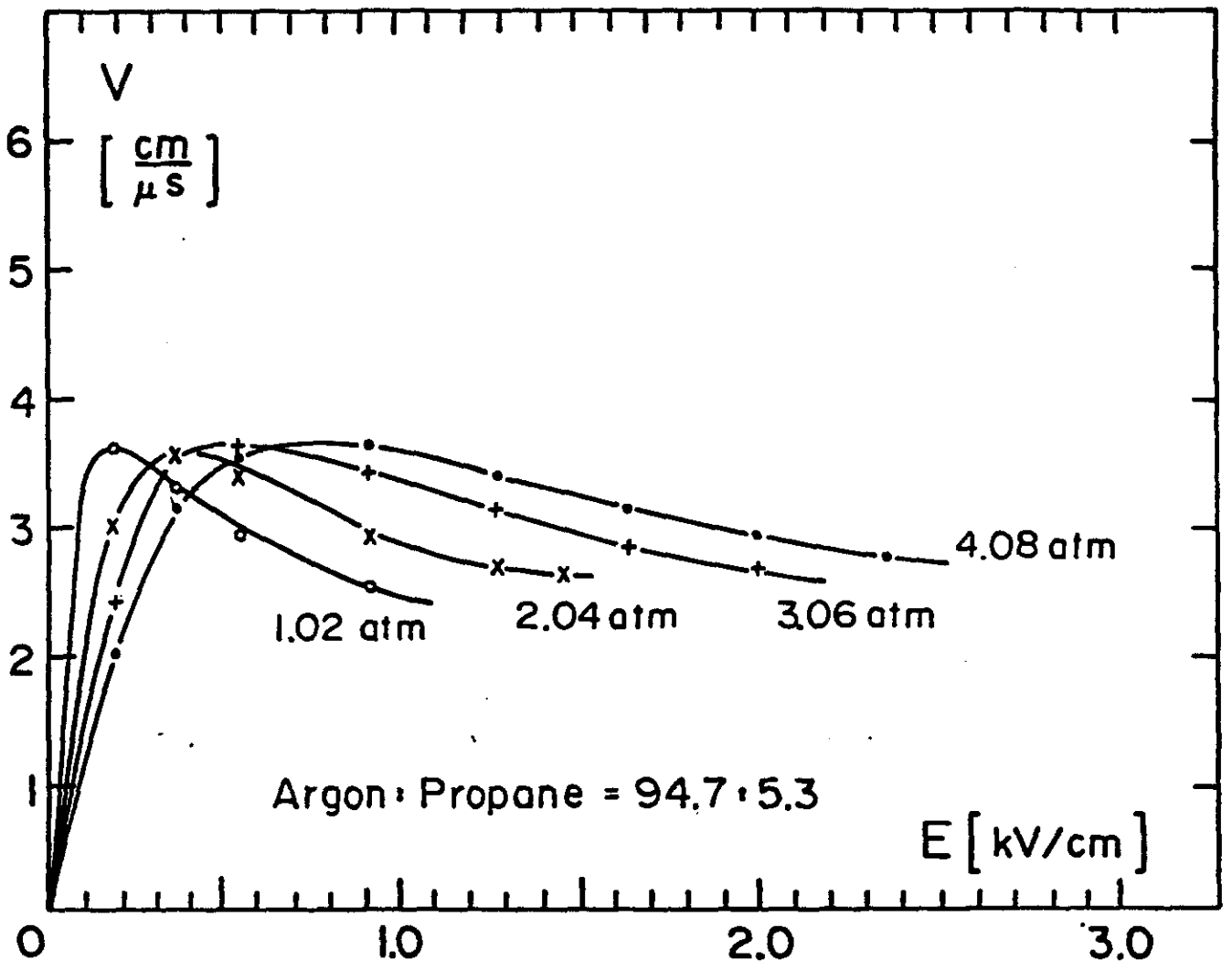

Figure 8 DRIFT VELOCITY vs ELECTRIC FIELD

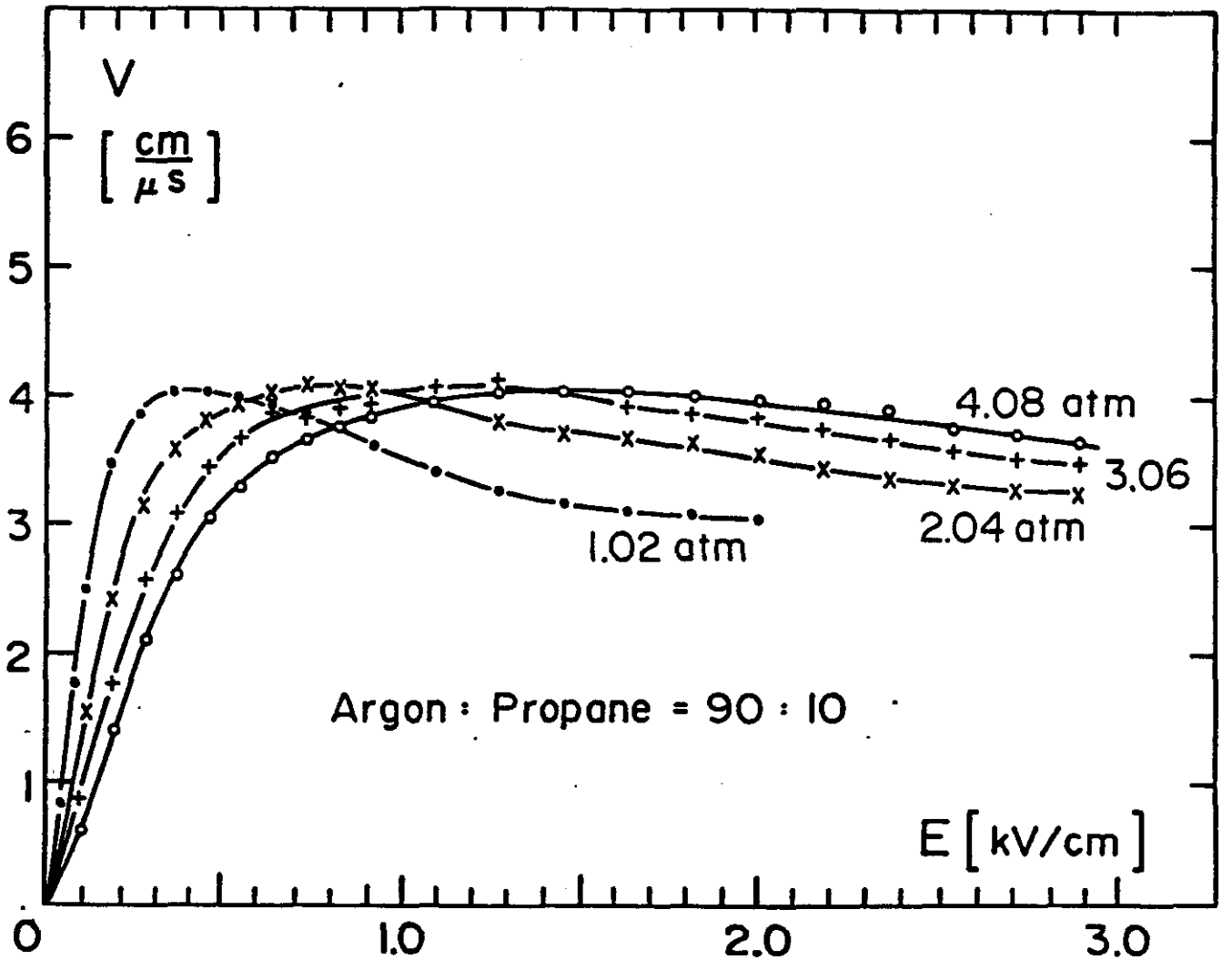

Figure 9 DRIFT VELOCITY vs ELECTRIC FIELD

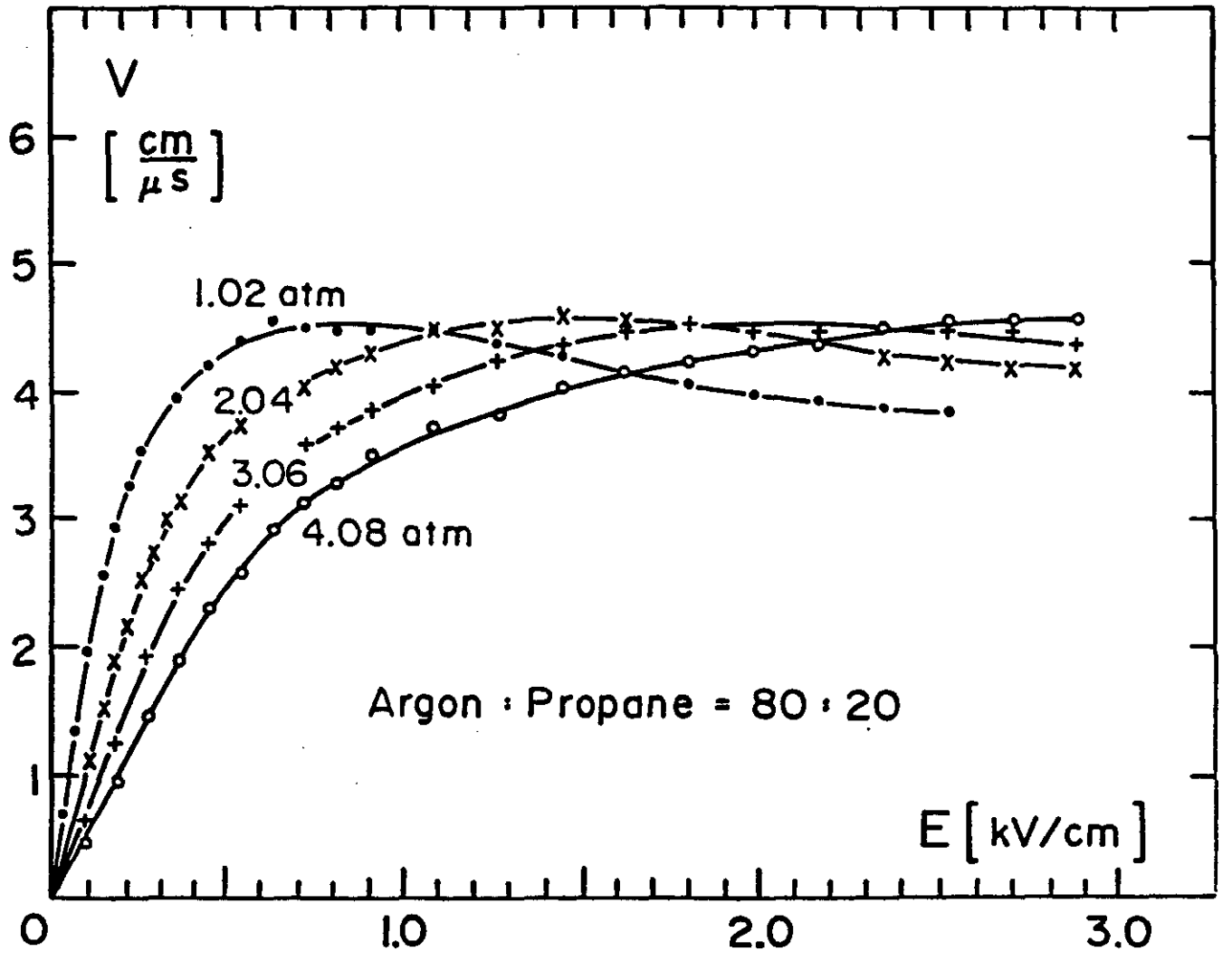

Figure 10 DRIFT VELOCITY vs ELECTRIC FIELD

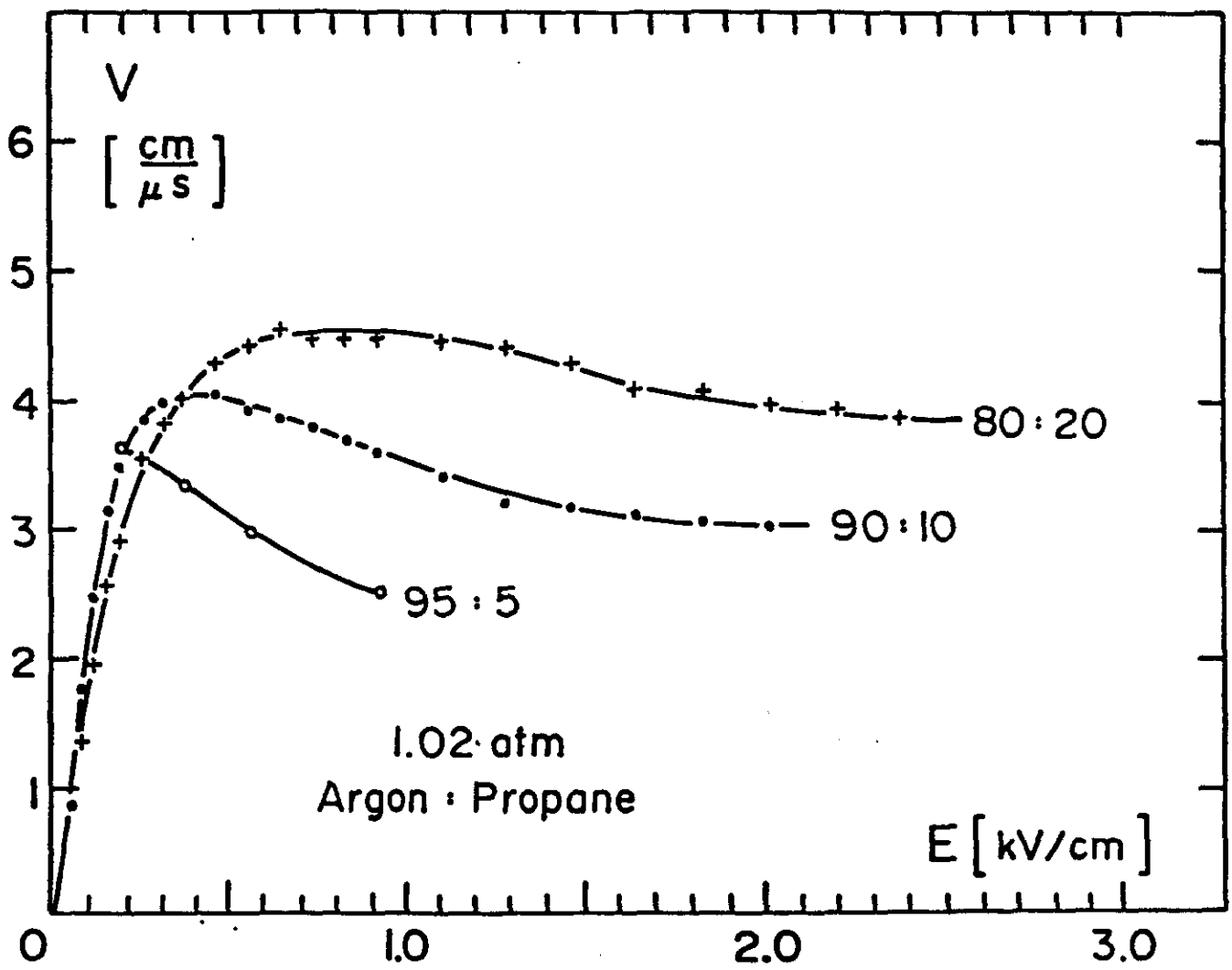

Figure 11 DRIFT VELOCITY vs ELECTRIC FIELD

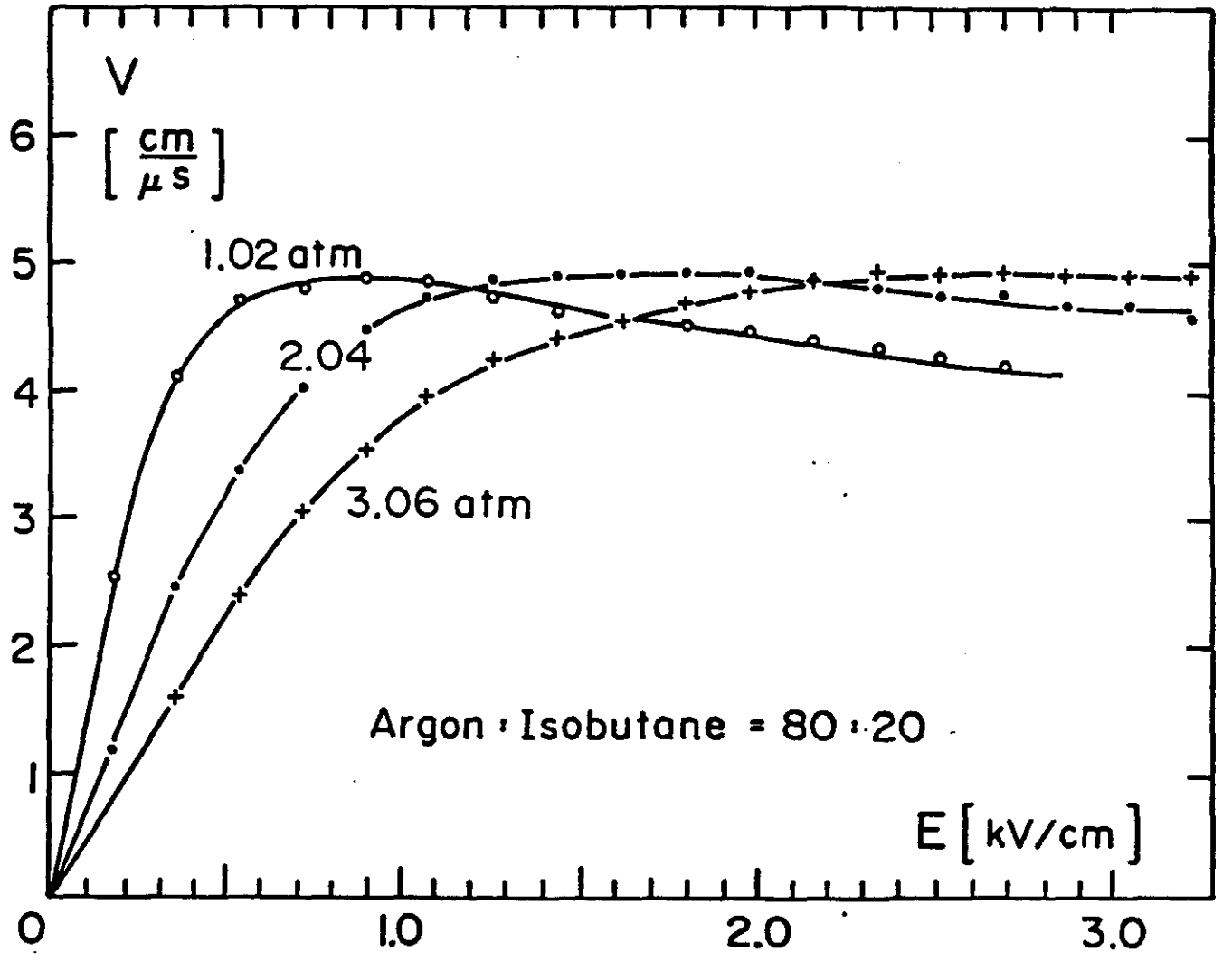

Figure 12 DRIFT VELOCITY vs ELECTRIC FIELD

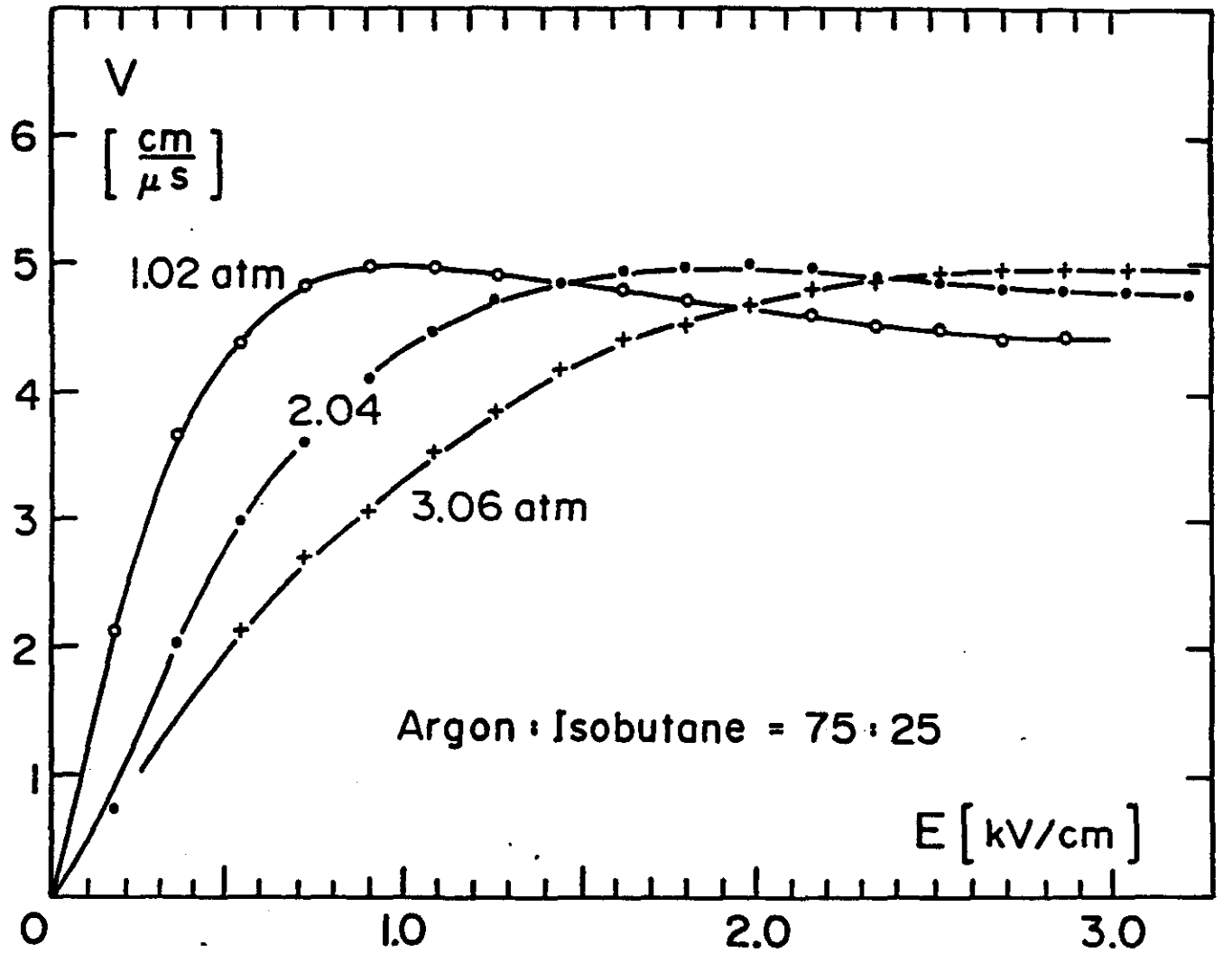

Figure 13 DRIFT VELOCITY vs ELECTRIC FIELD

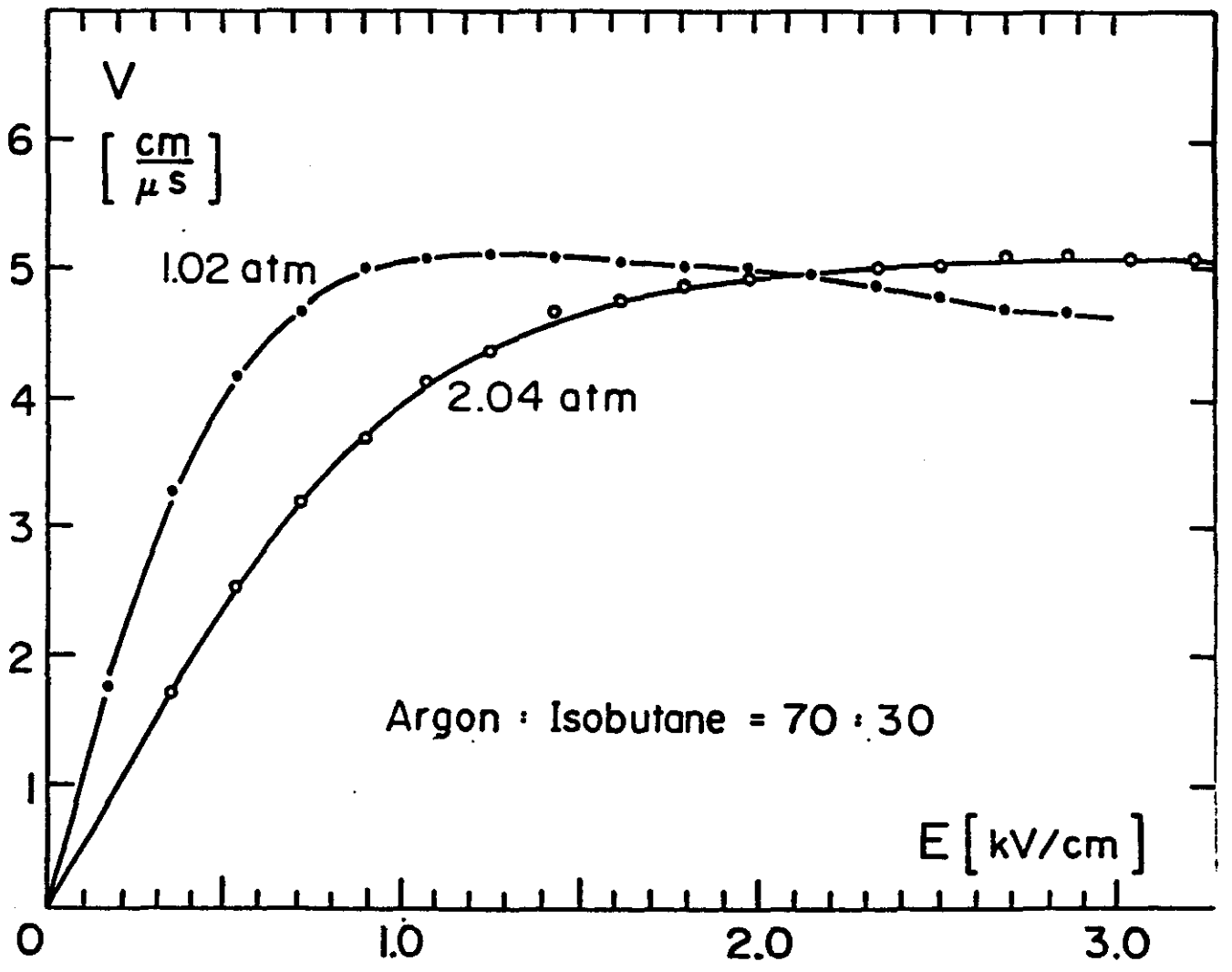

Figure 14 DRIFT VELOCITY vs ELECTRIC FIELD

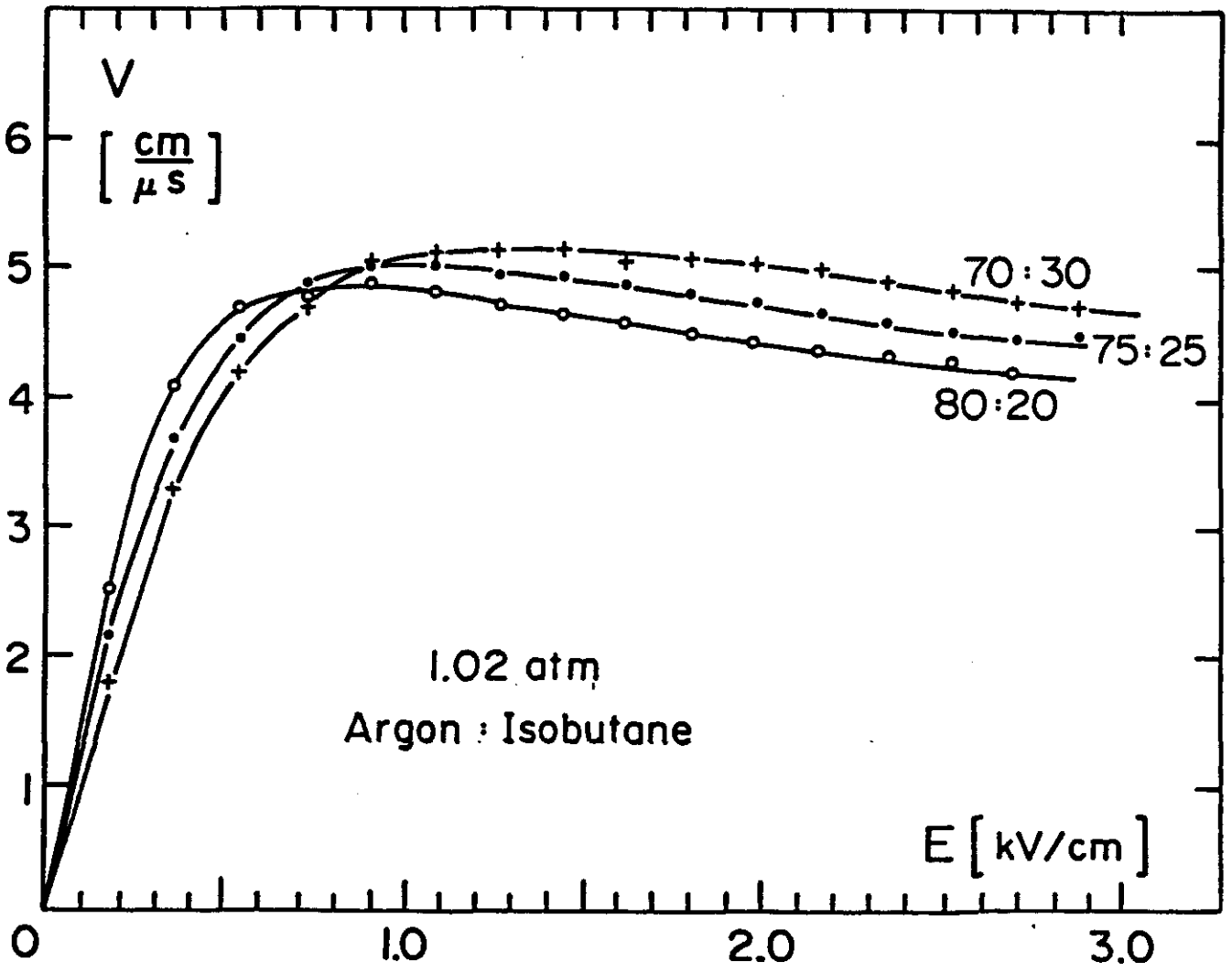

Figure 15 DRIFT VELOCITY vs ELECTRIC FIELD

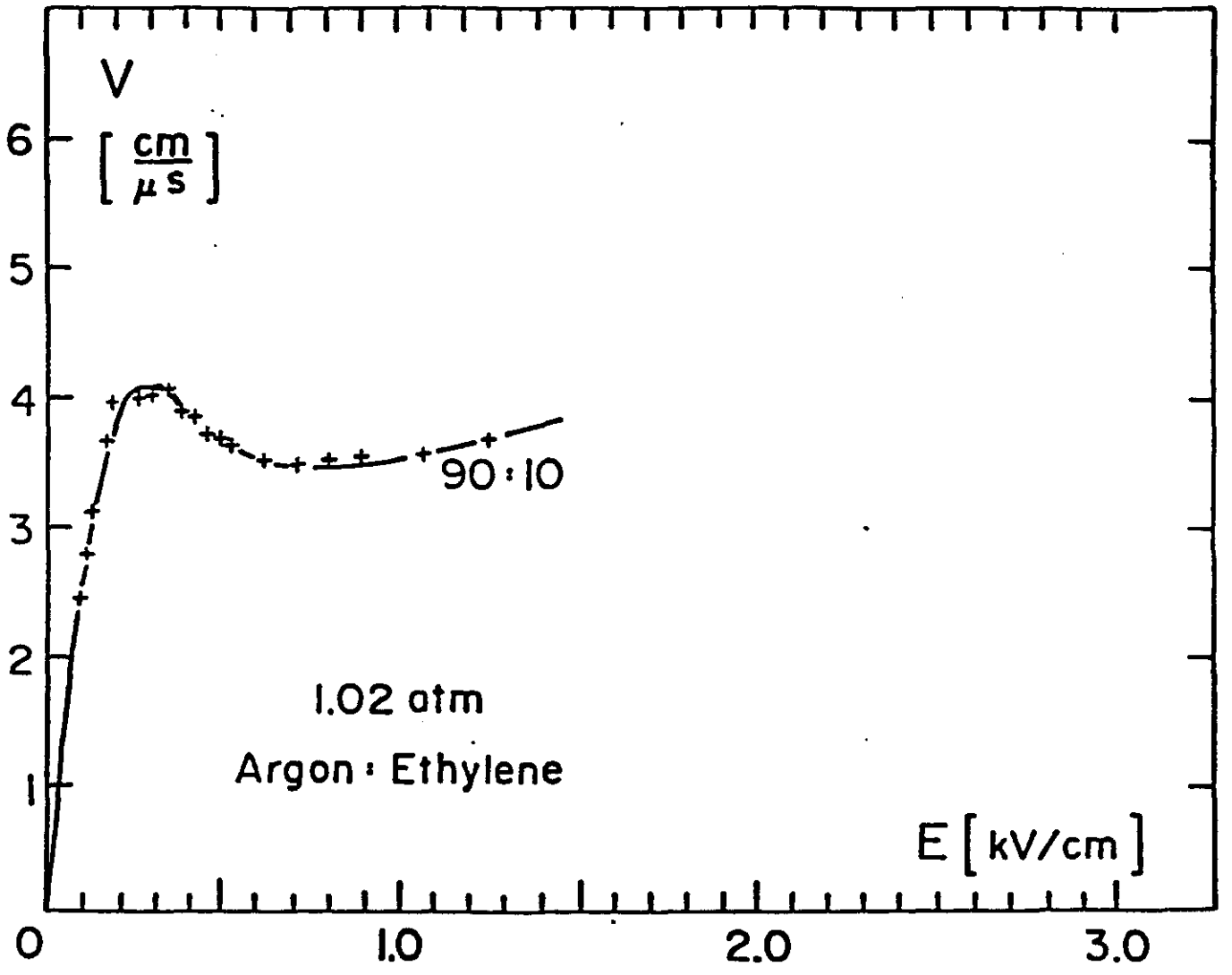

Figure 16 DRIFT VELOCITY vs ELECTRIC FIELD

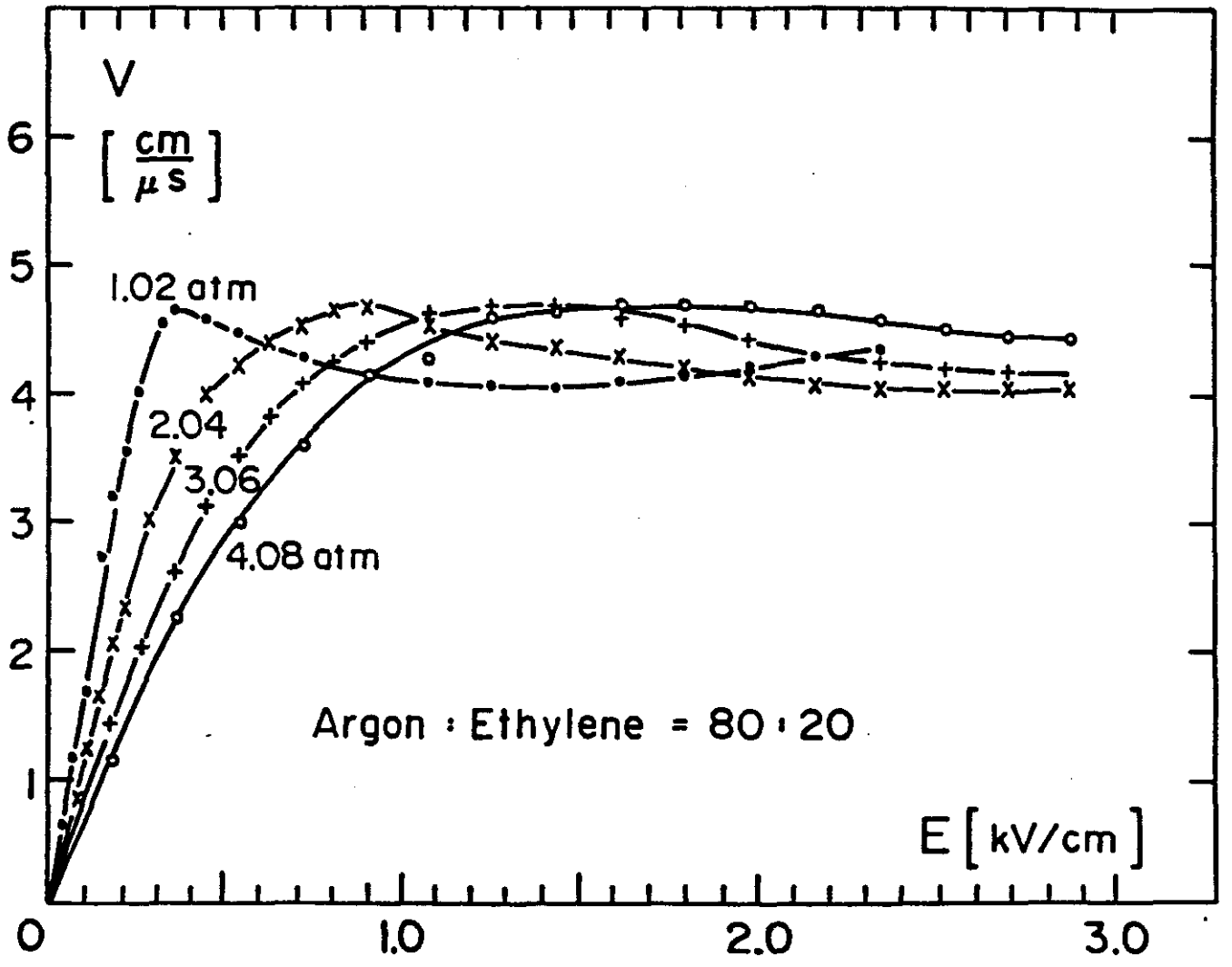

Figure 17 DRIFT VELOCITY vs ELECTRIC FIELD

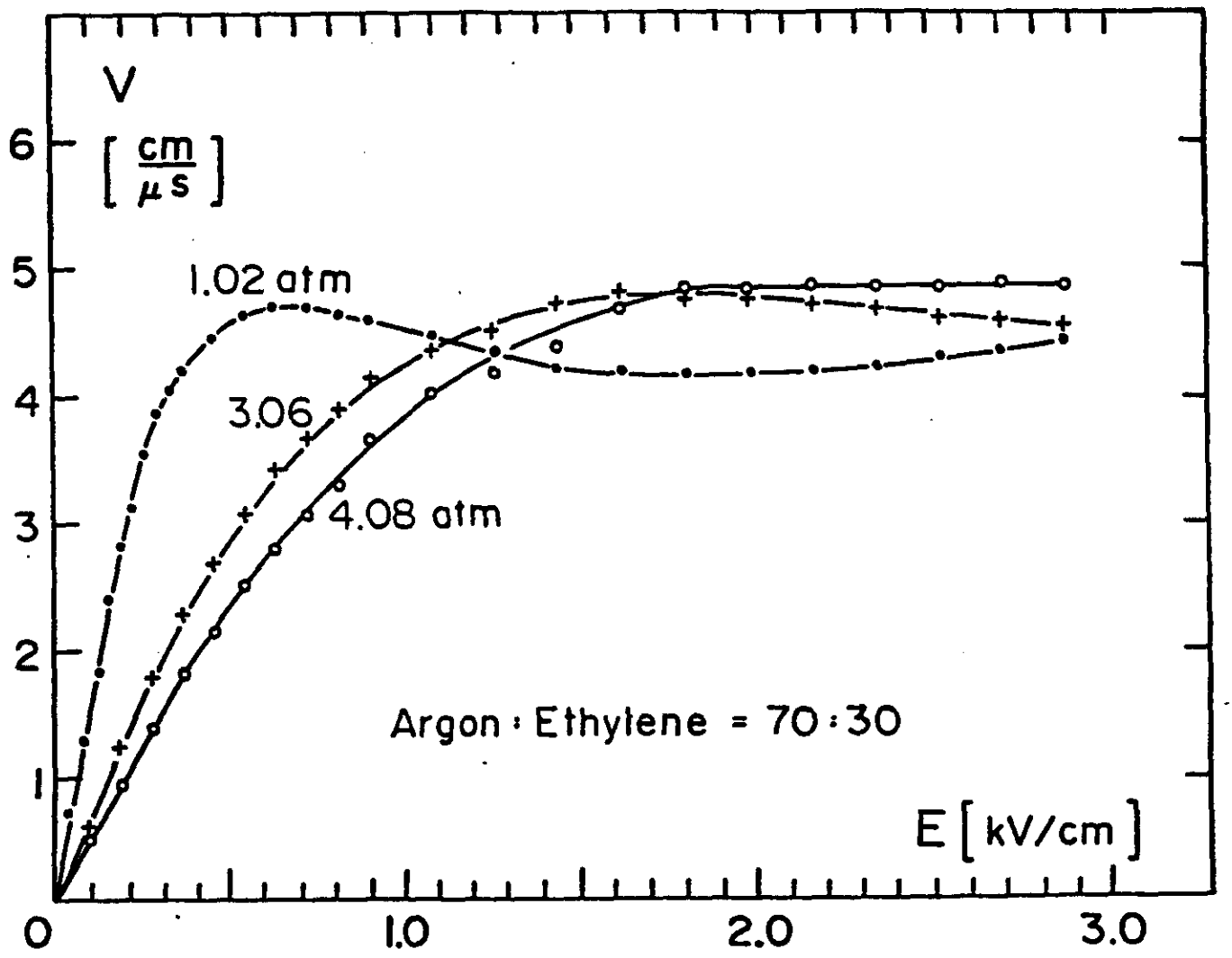

Figure 18 DRIFT VELOCITY vs ELECTRIC FIELD

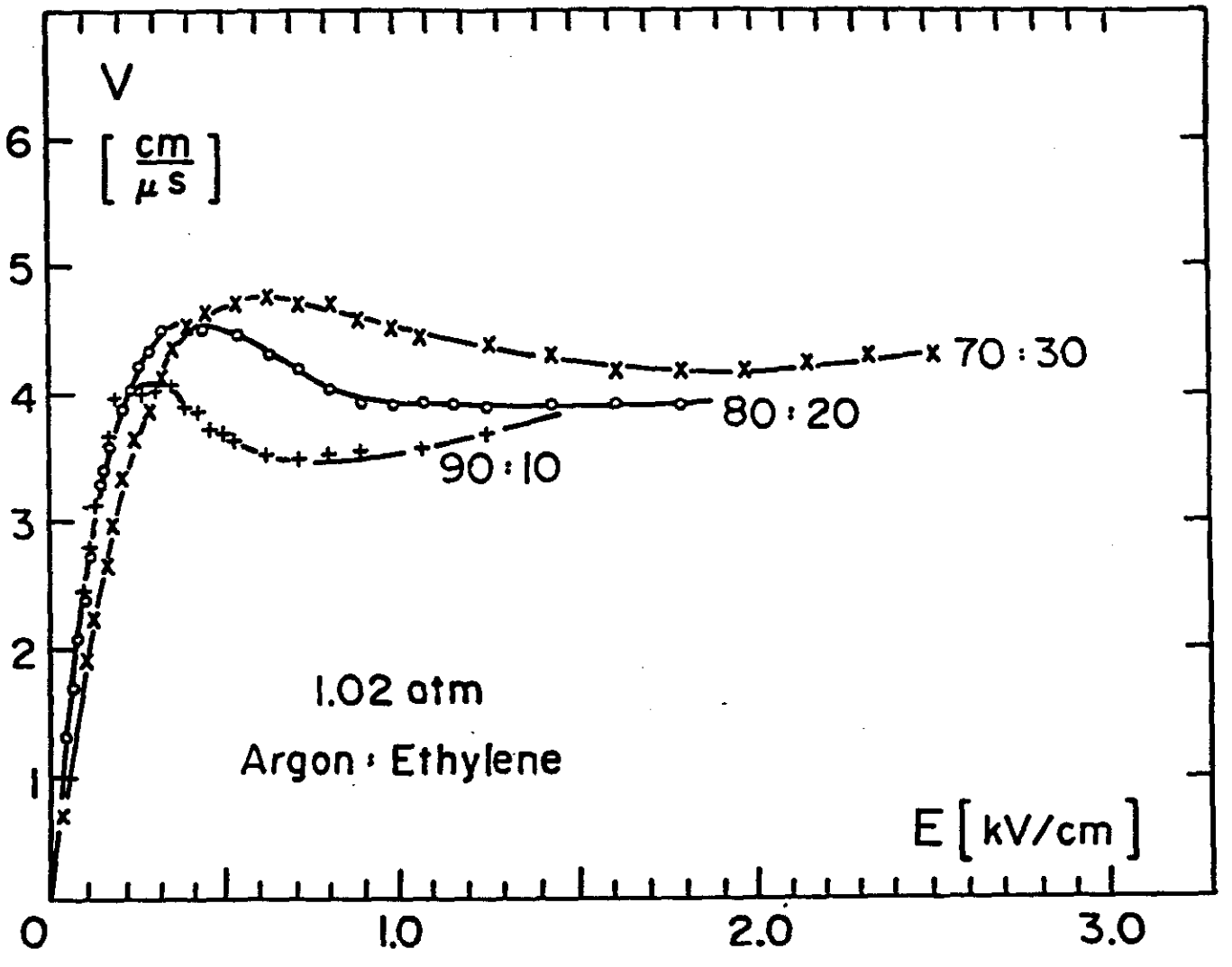

Figure 19 DRIFT VELOCITY vs ELECTRIC FIELD

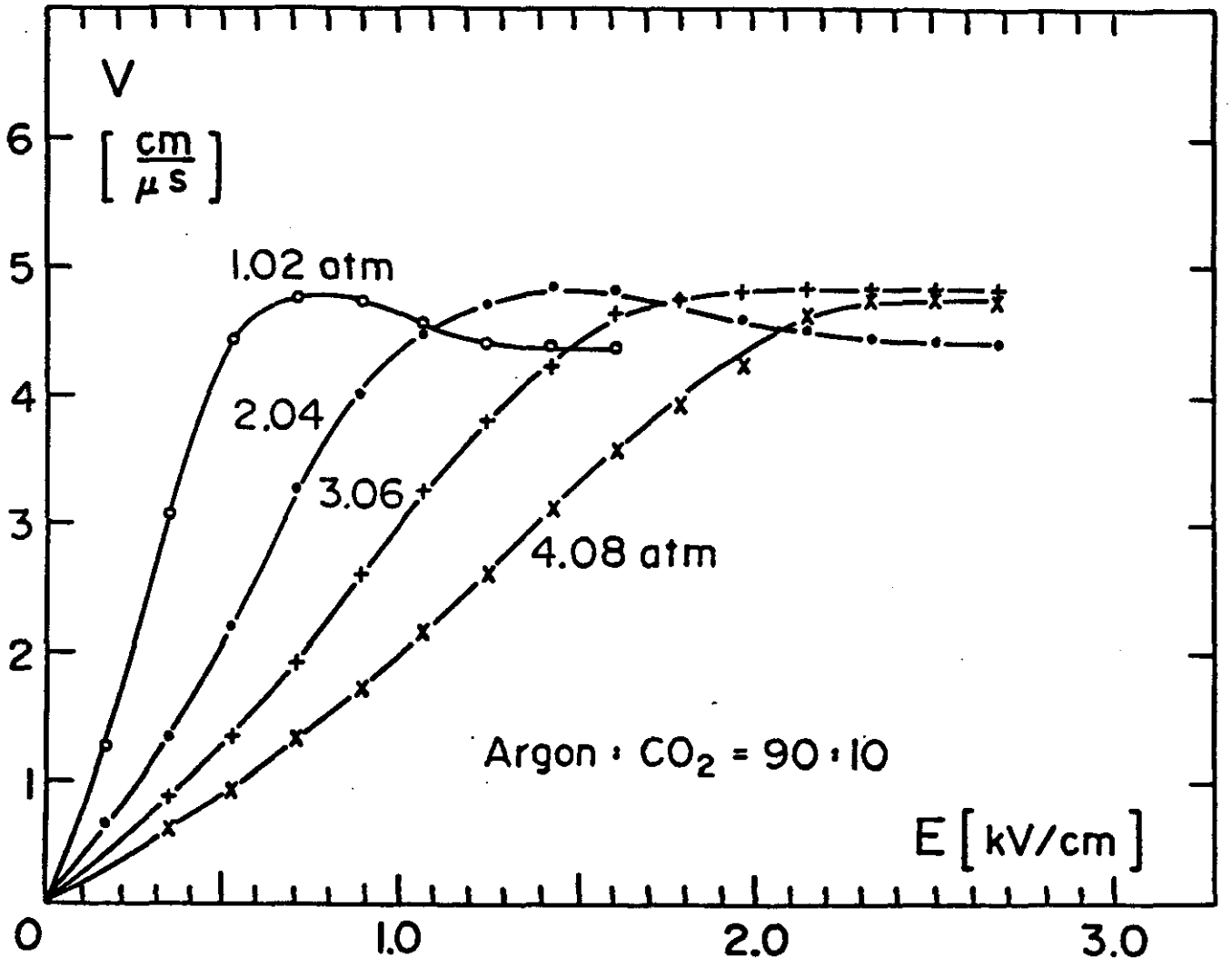

Figure 20 DRIFT VELOCITY vs ELECTRIC FIELD

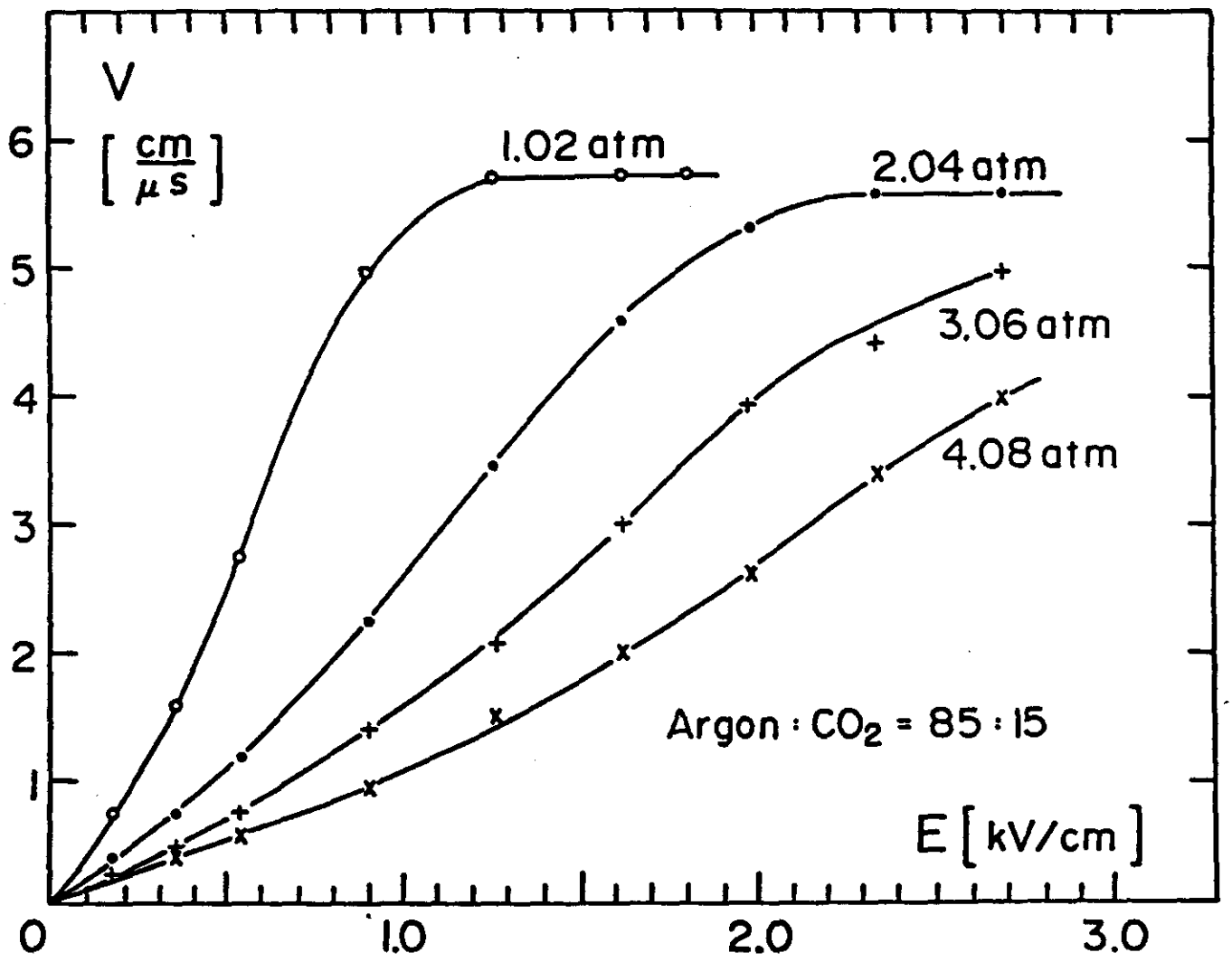

Figure 21 DRIFT VELOCITY vs ELECTRIC FIELD

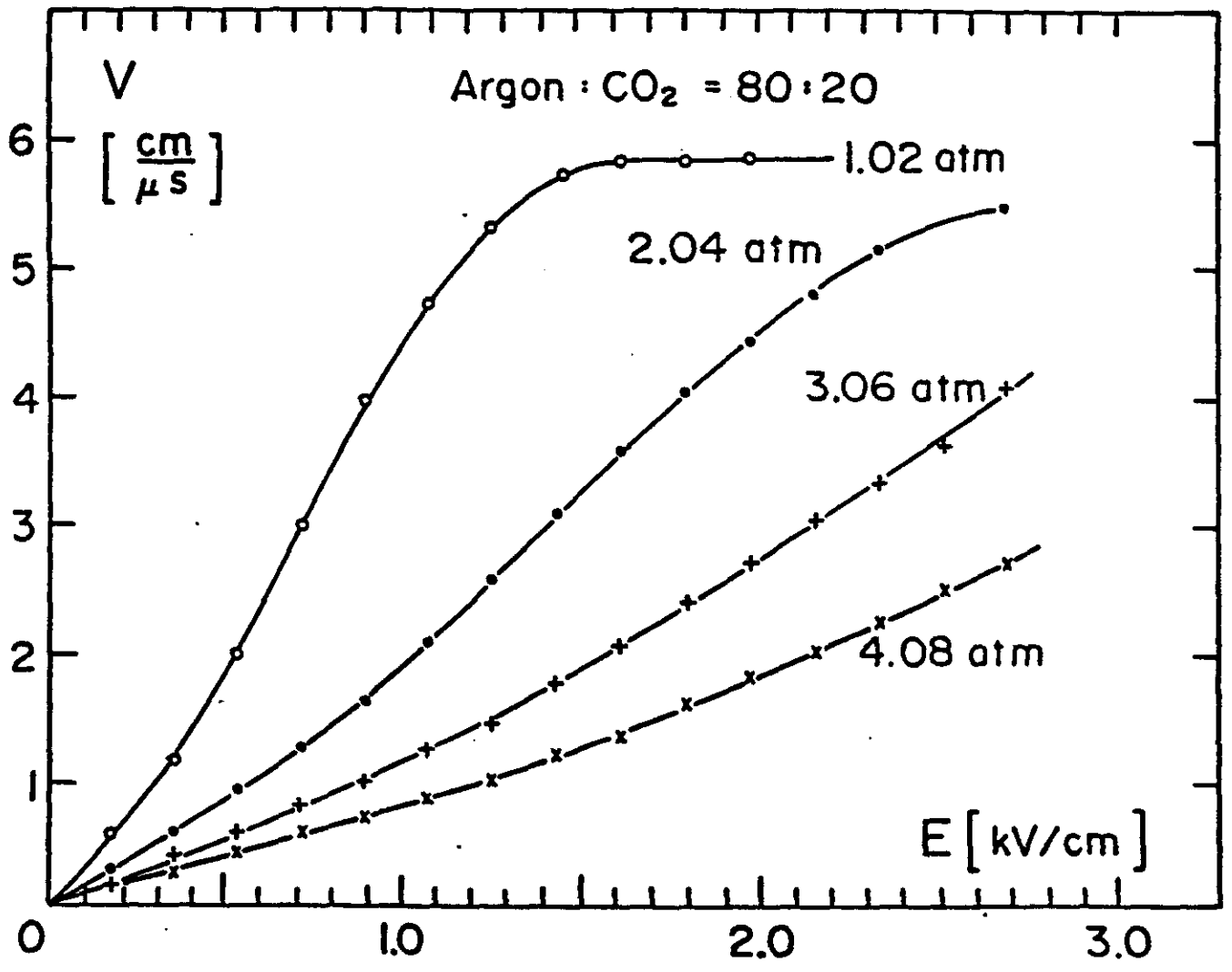

Figure 22 DRIFT VELOCITY vs ELECTRIC FIELD

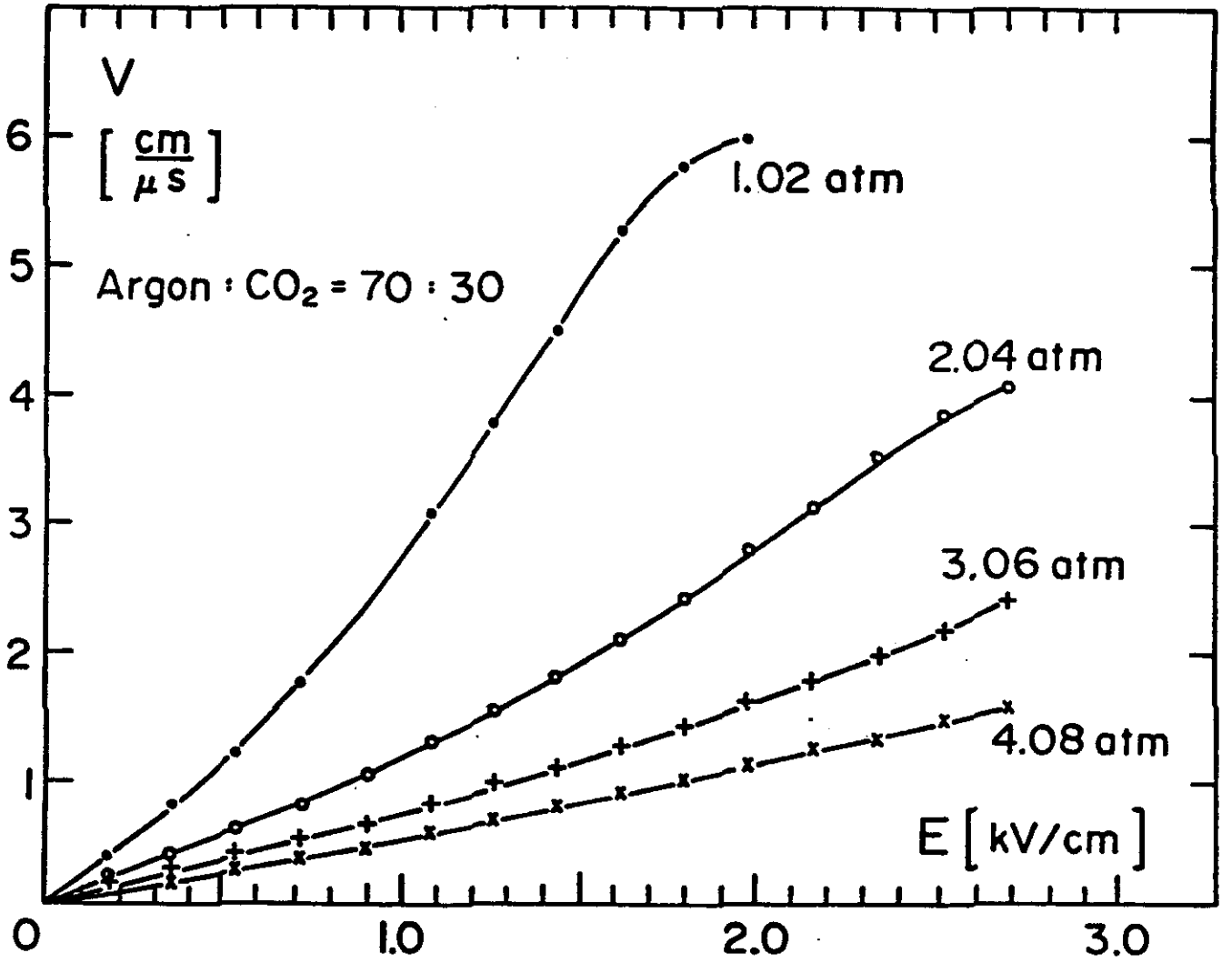

Figure 23 DRIFT VELOCITY vs ELECTRIC FIELD

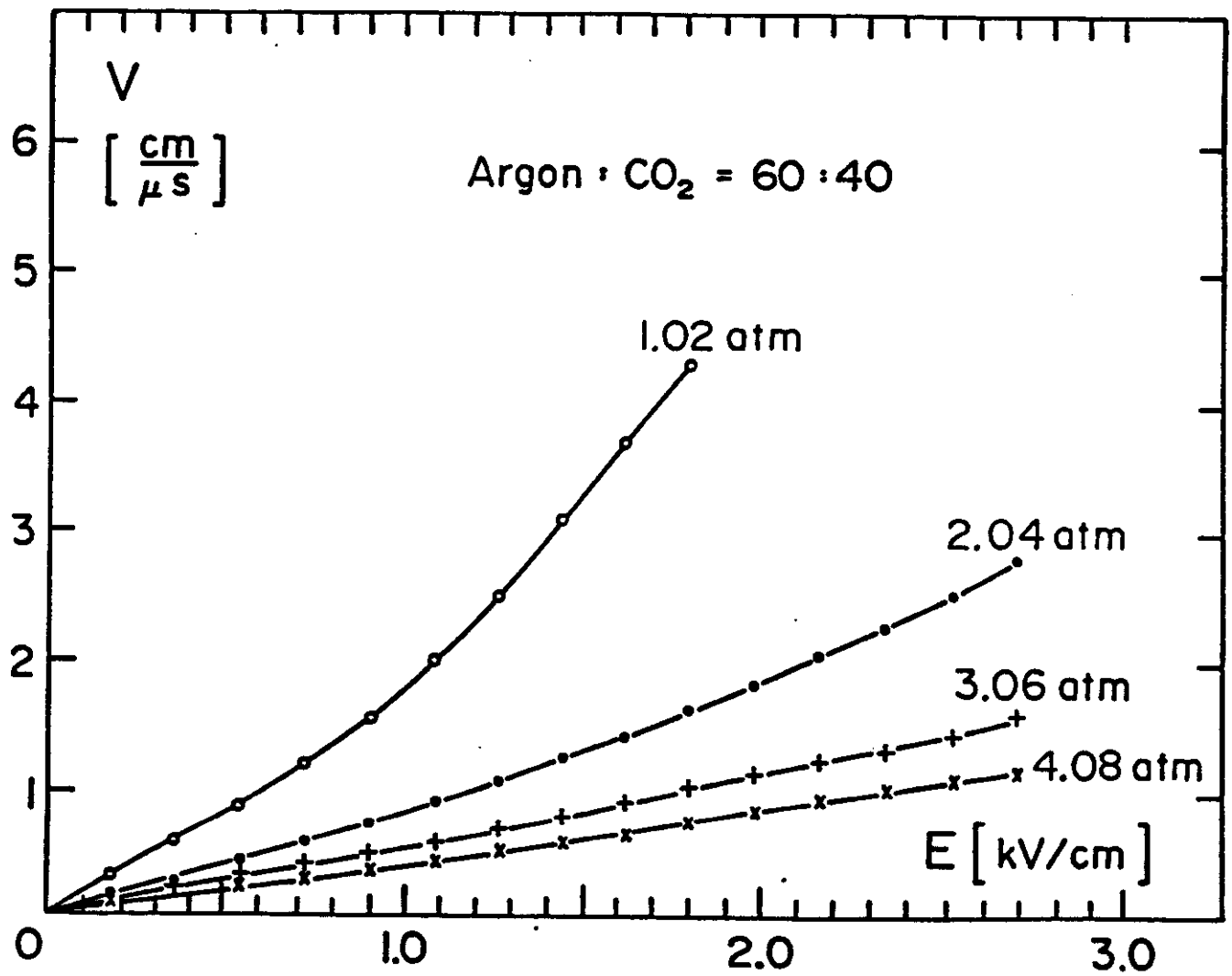

Figure 24 DRIFT VELOCITY vs ELECTRIC FIELD

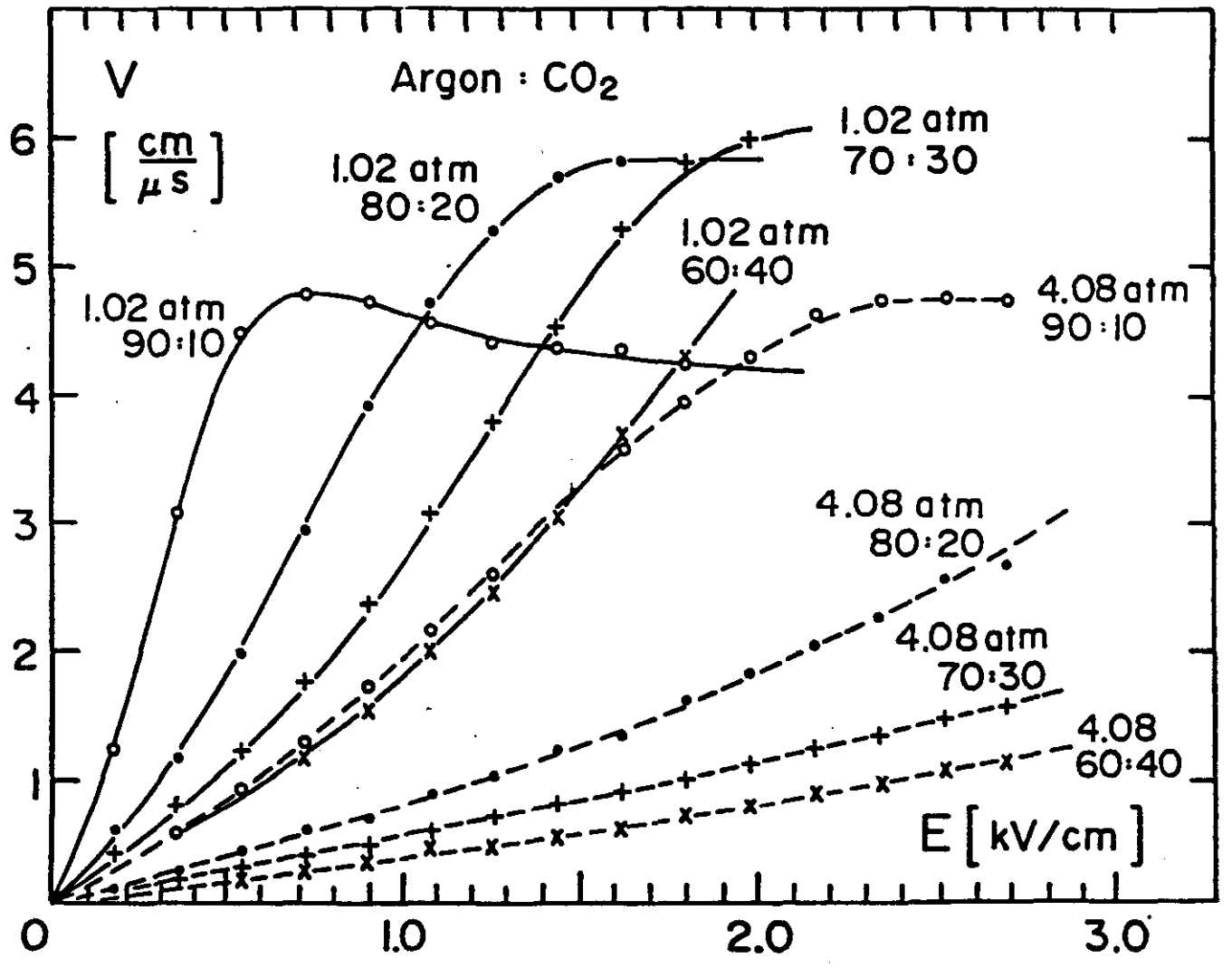

Figure 25 DRIFT VELOCITY vs ELECTRIC FIELD

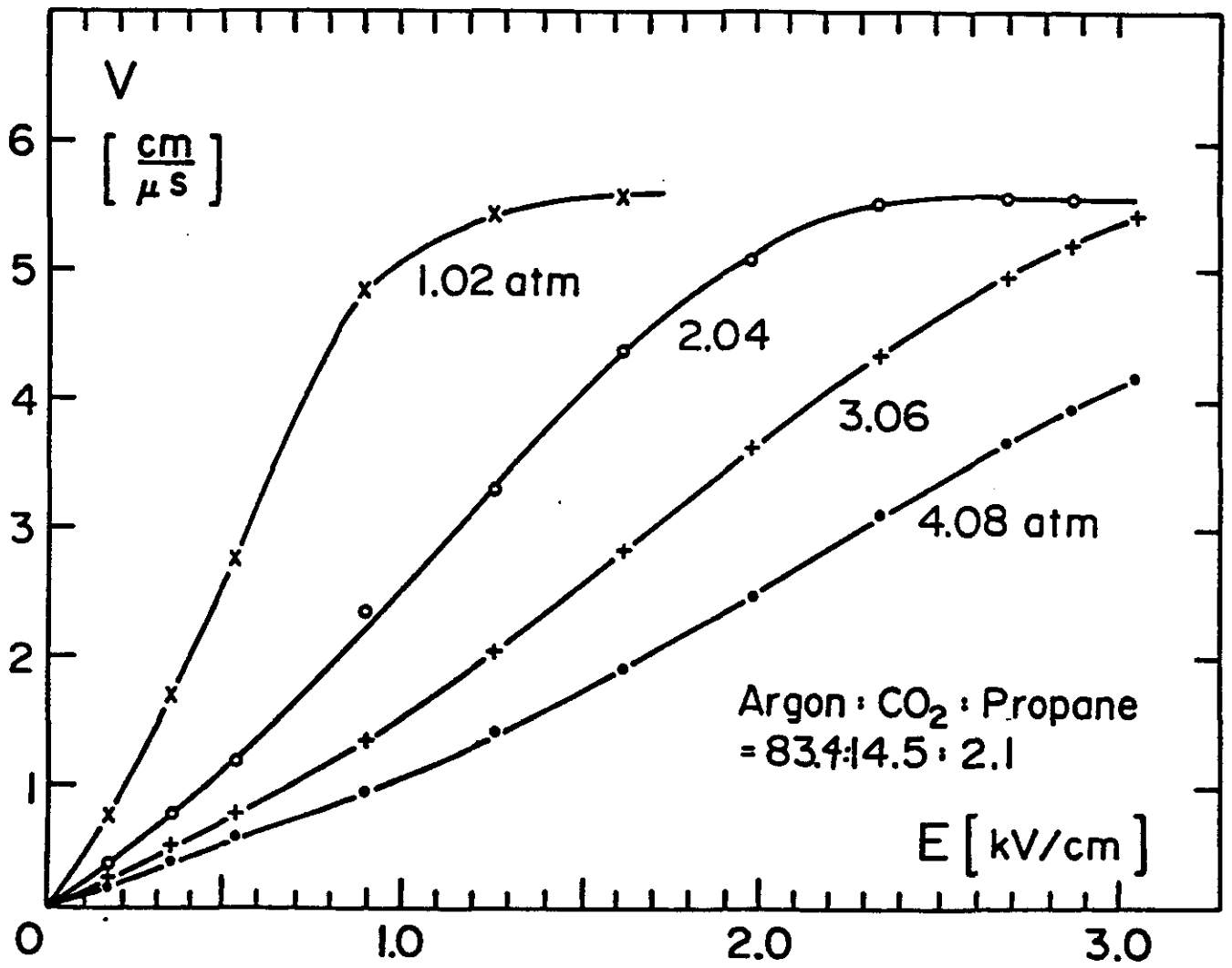

Figure 26 DRIFT VELOCITY vs ELECTRIC FIELD

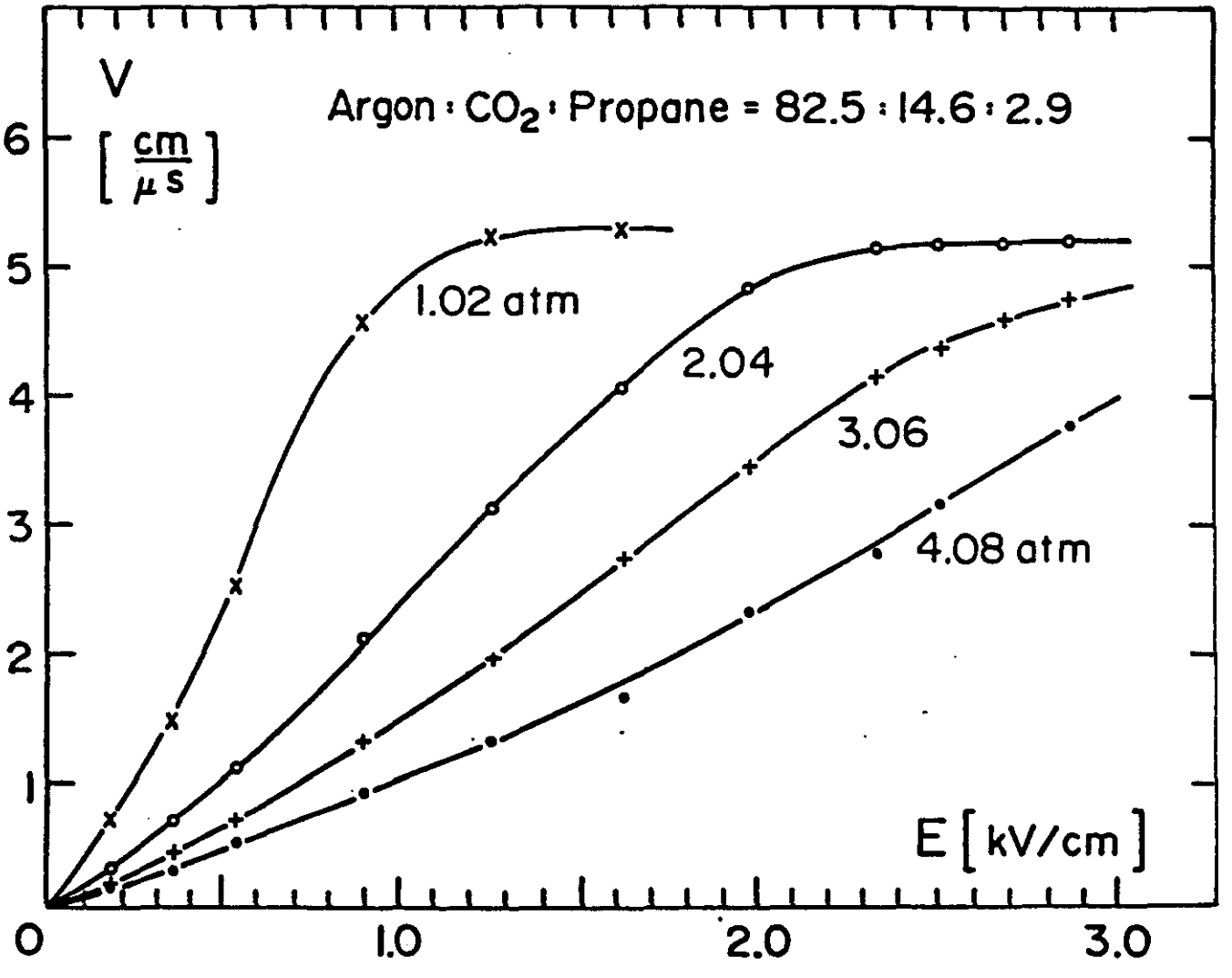

Figure 27 DRIFT VELOCITY vs ELECTRIC FIELD

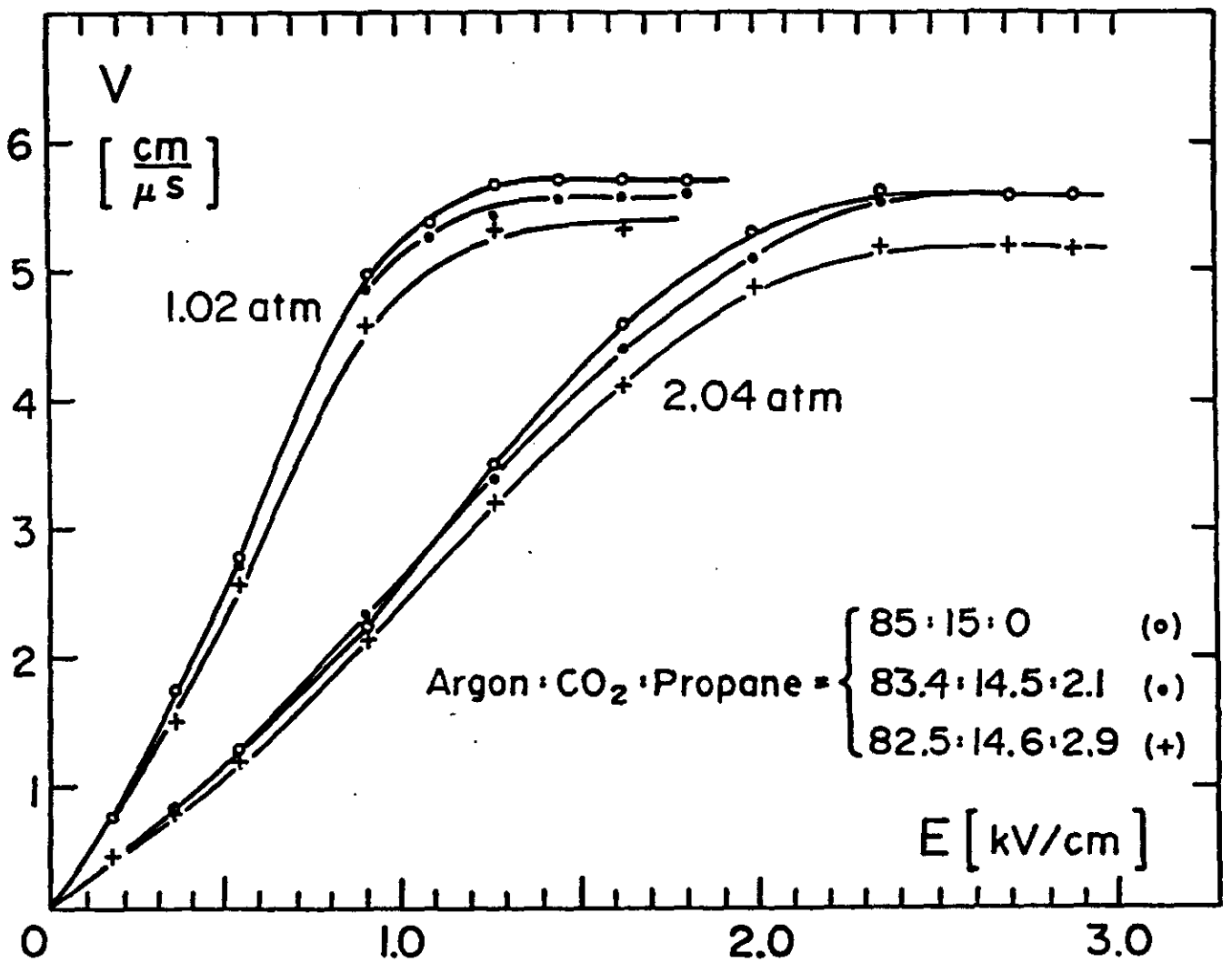

Figure 28 DRIFT VELOCITY vs ELECTRIC FIELD

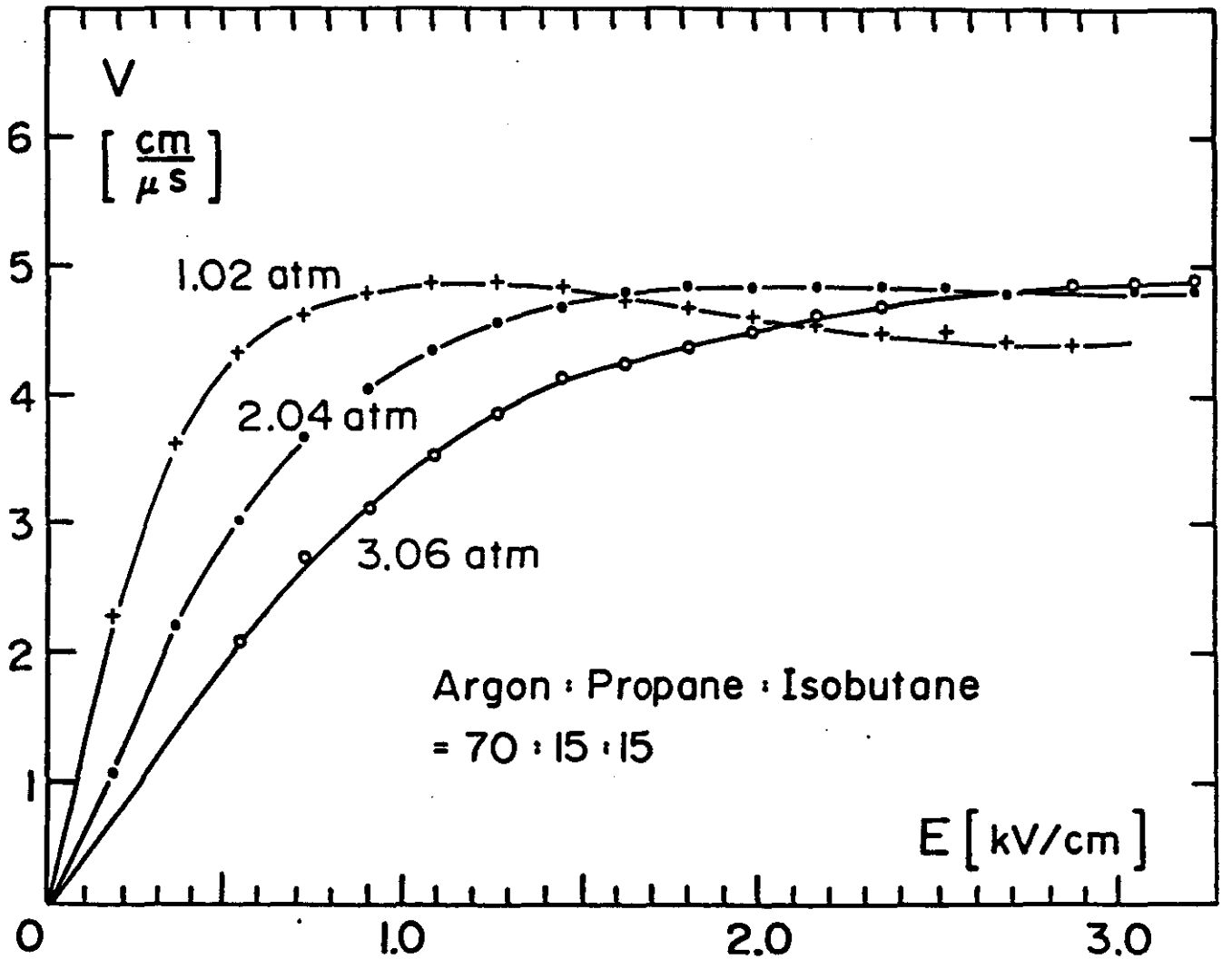

Figure 29 DRIFT VELOCITY vs ELECTRIC FIELD

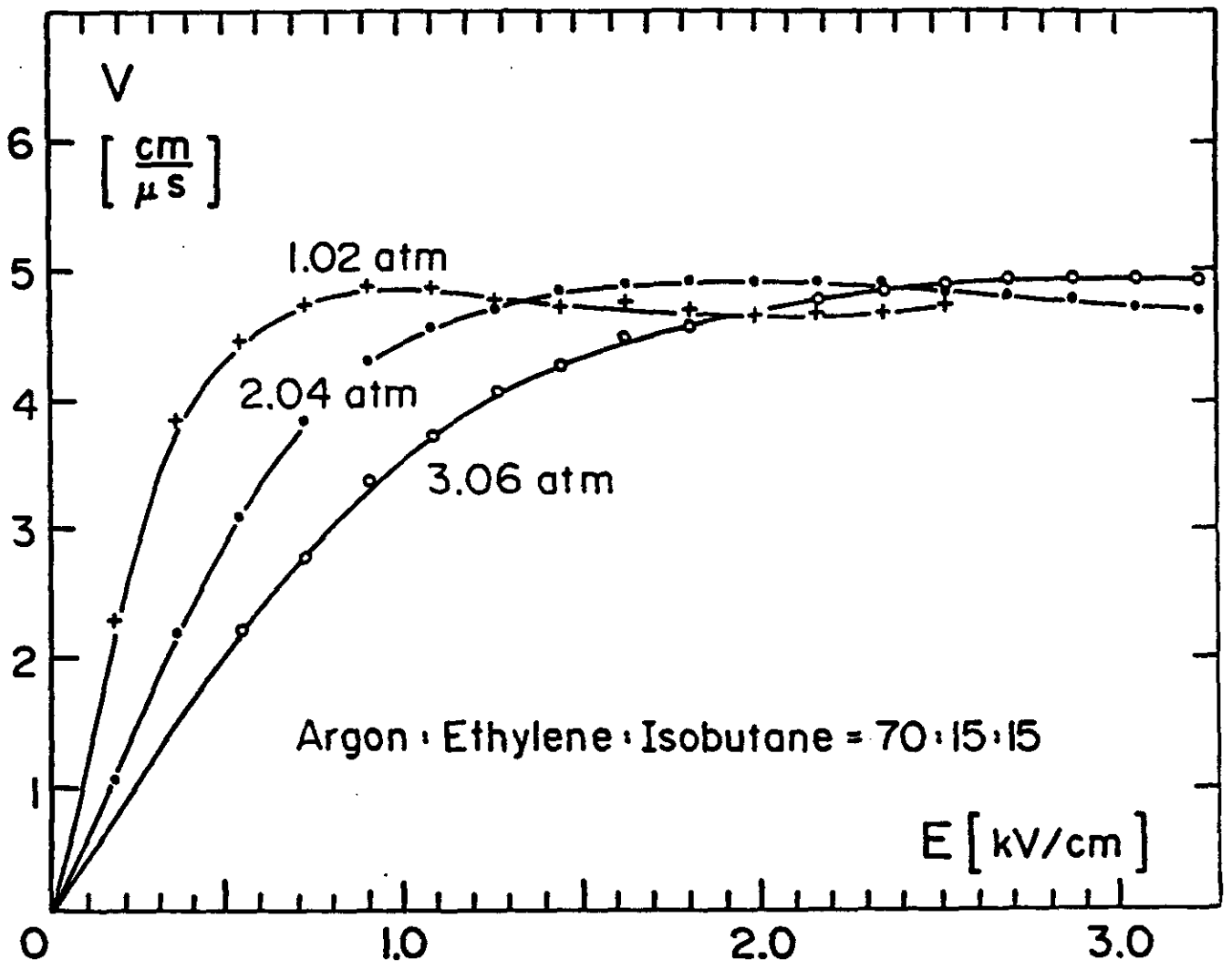

Figure 30 DRIFT VELOCITY vs ELECTRIC FIELD

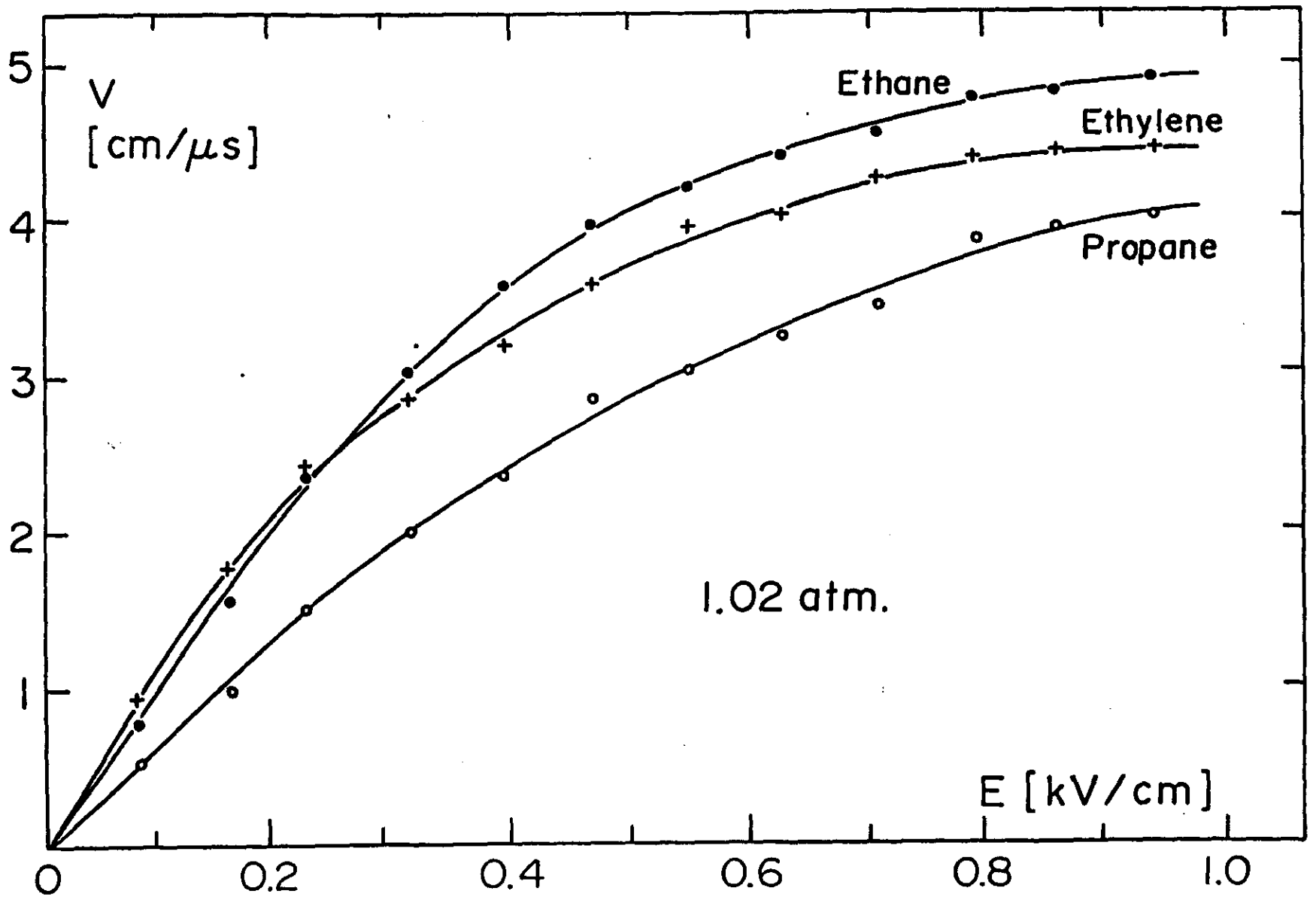

Figure 31 DRIFT VELOCITY vs ELECTRIC FIELD

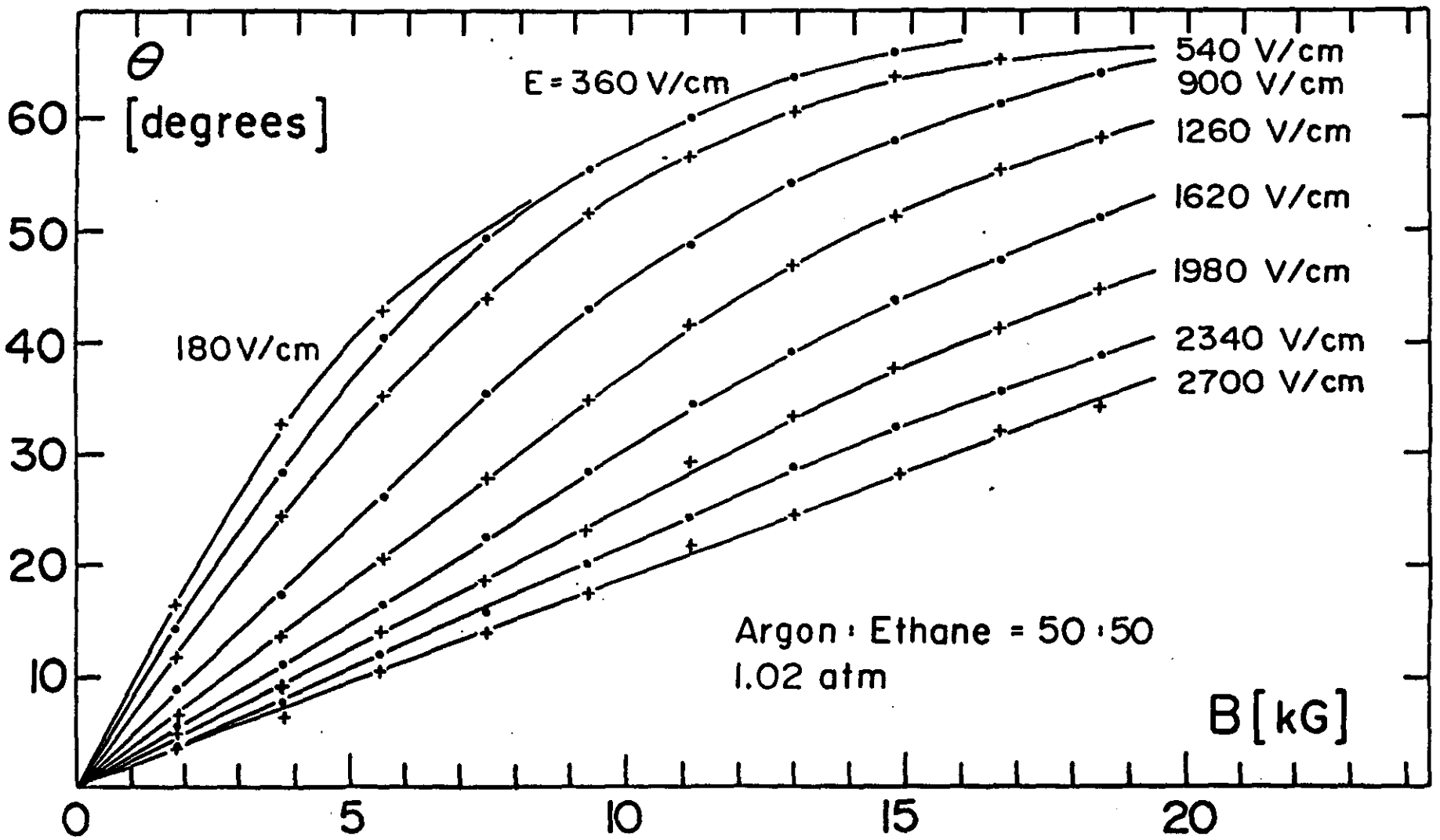

Figure 32 DRIFT ANGLE vs MAGNETIC FIELD

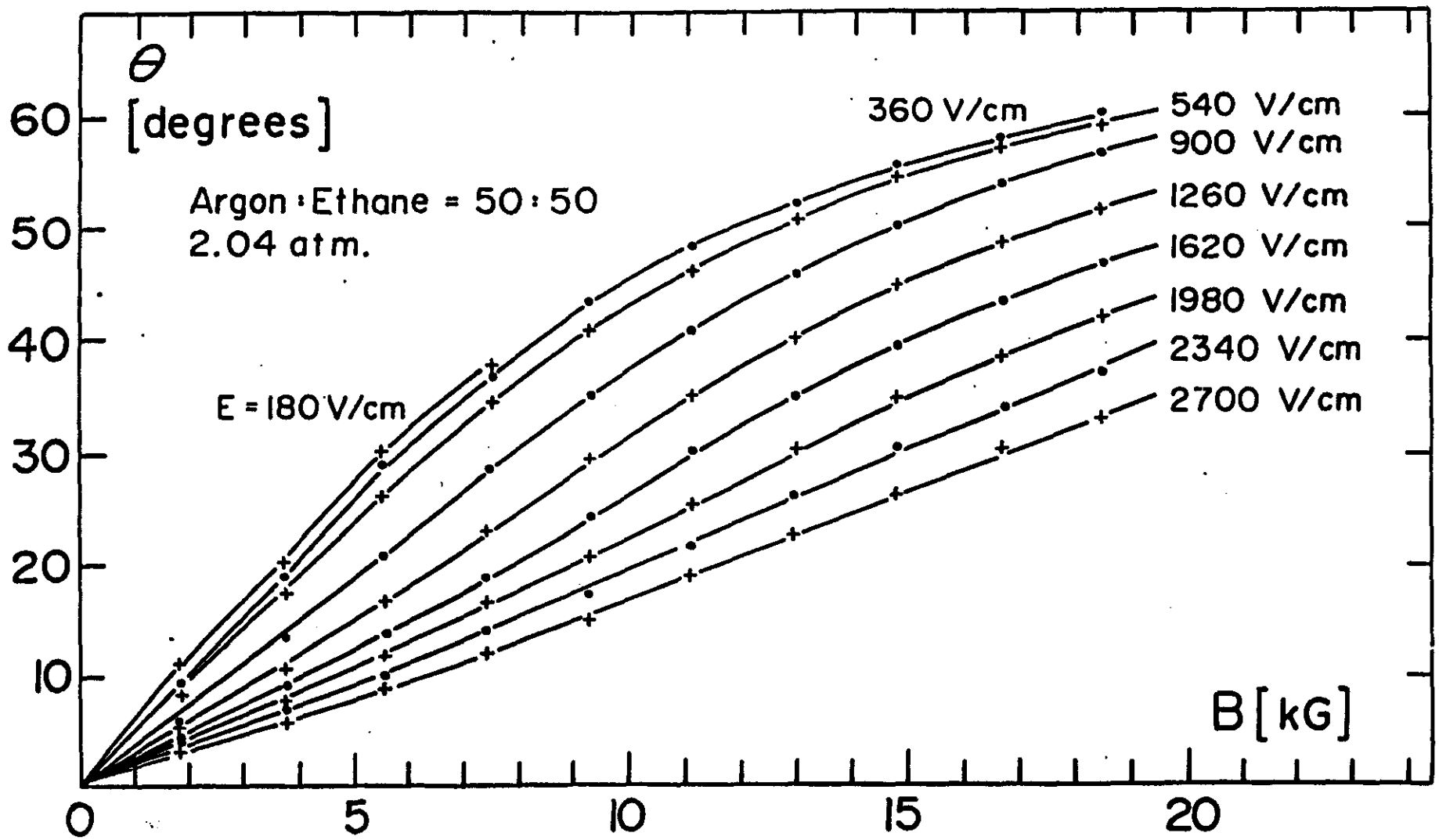

Figure 33 DRIFT ANGLE vs MAGNETIC FIELD

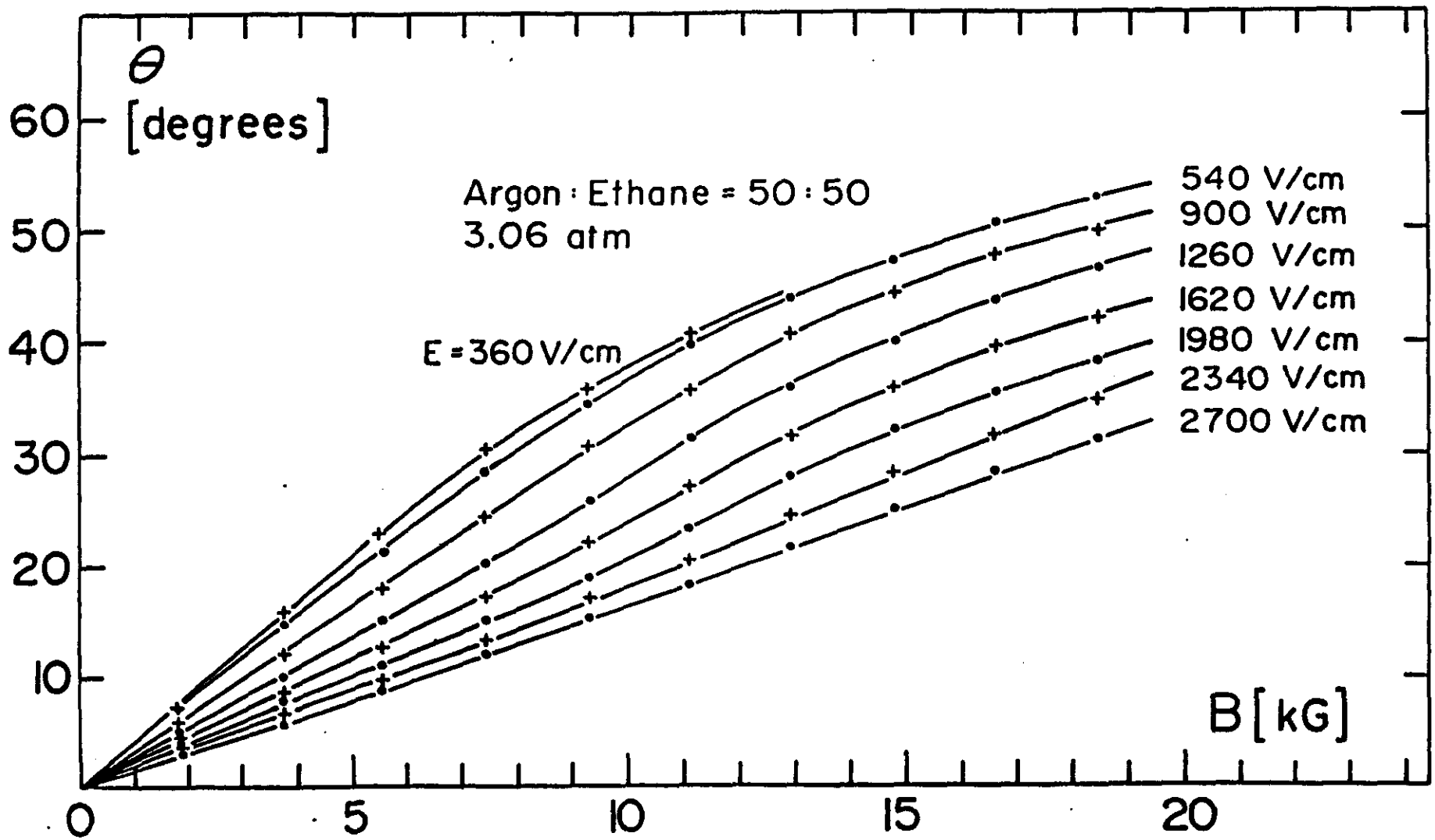

Figure 34 DRIFT ANGLE vs MAGNETIC FIELD

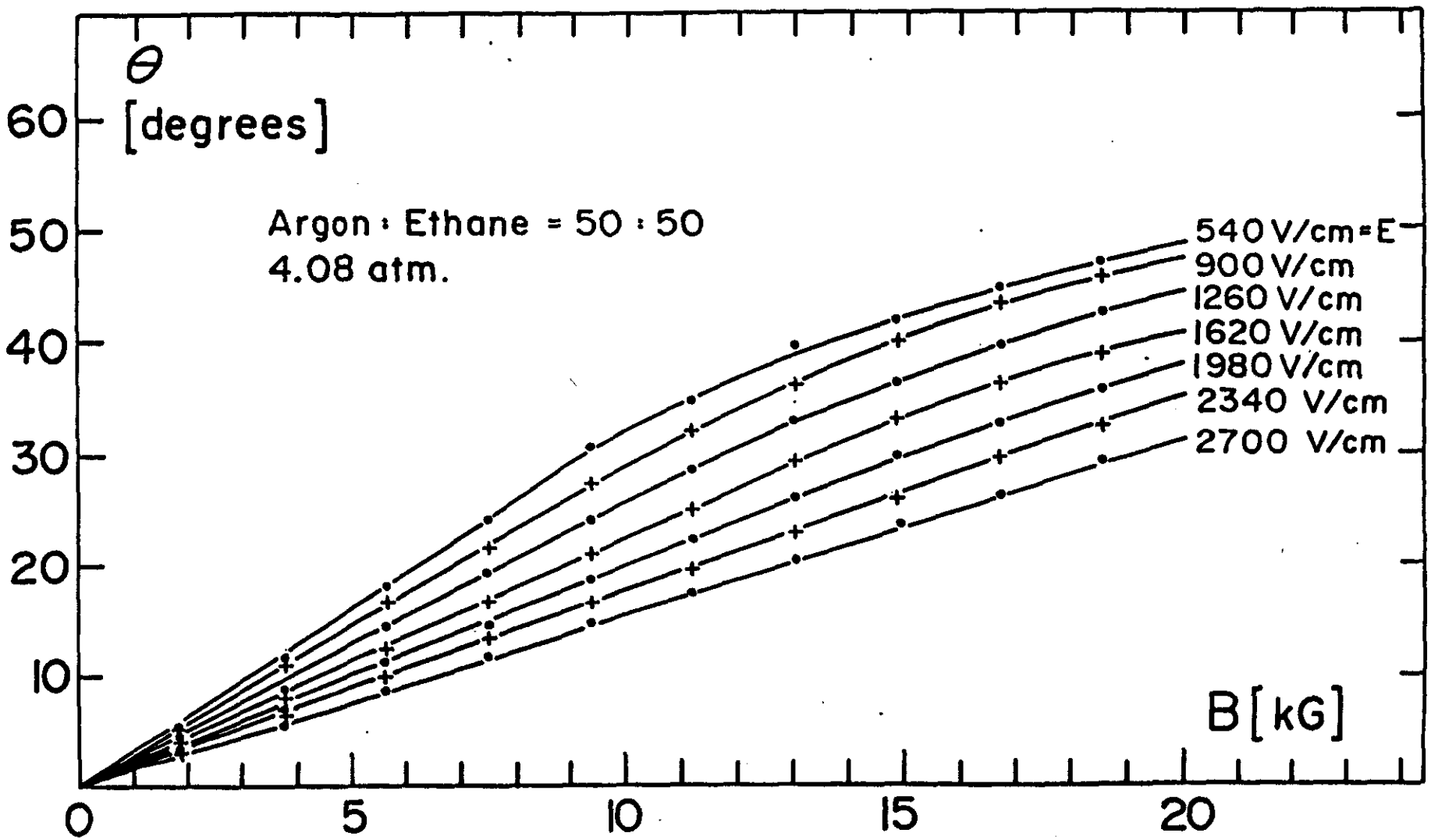

Figure 35 DRIFT ANGLE vs MAGNETIC FIELD

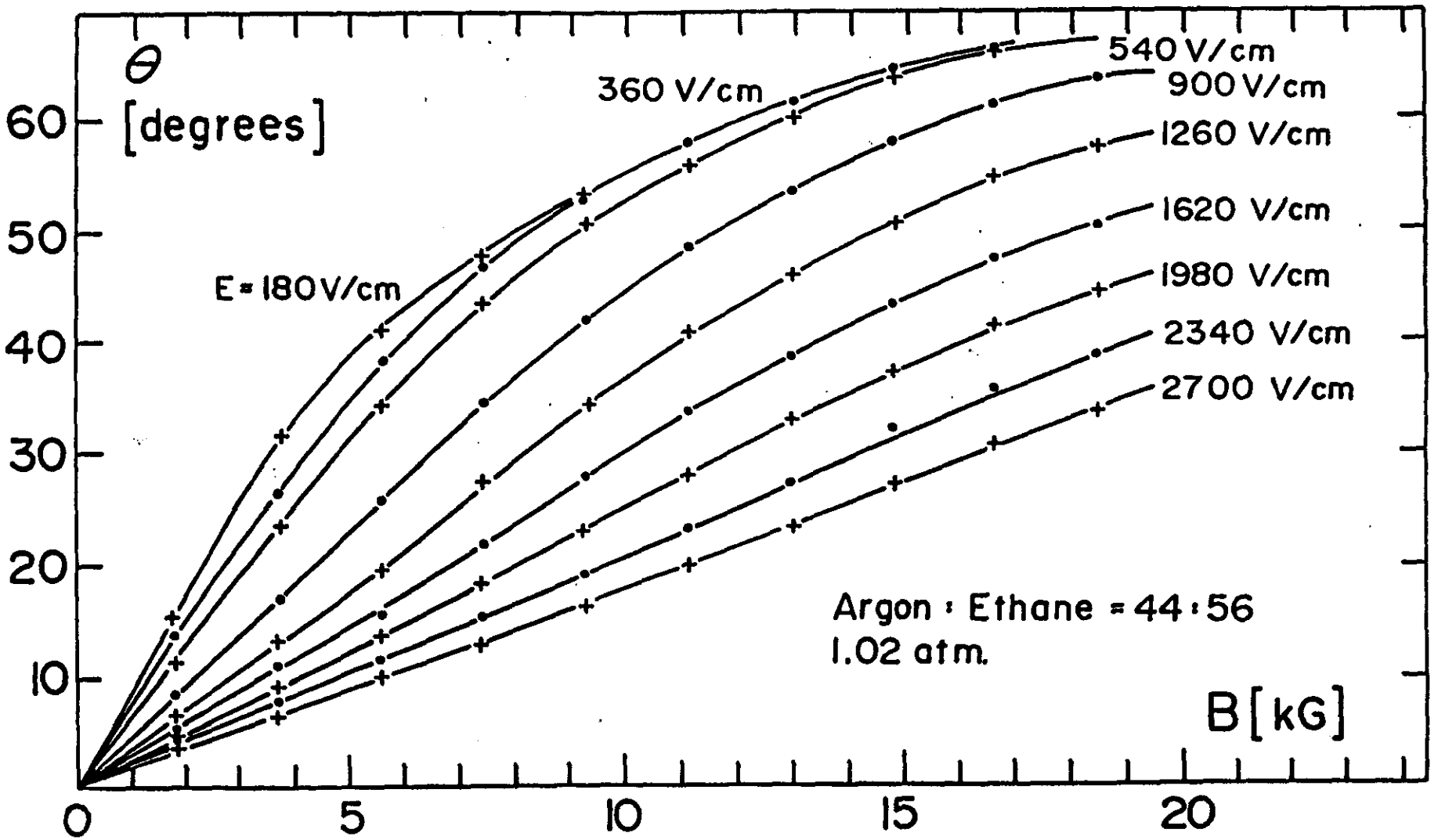

Figure 36 DRIFT ANGLE vs MAGNETIC FIELD

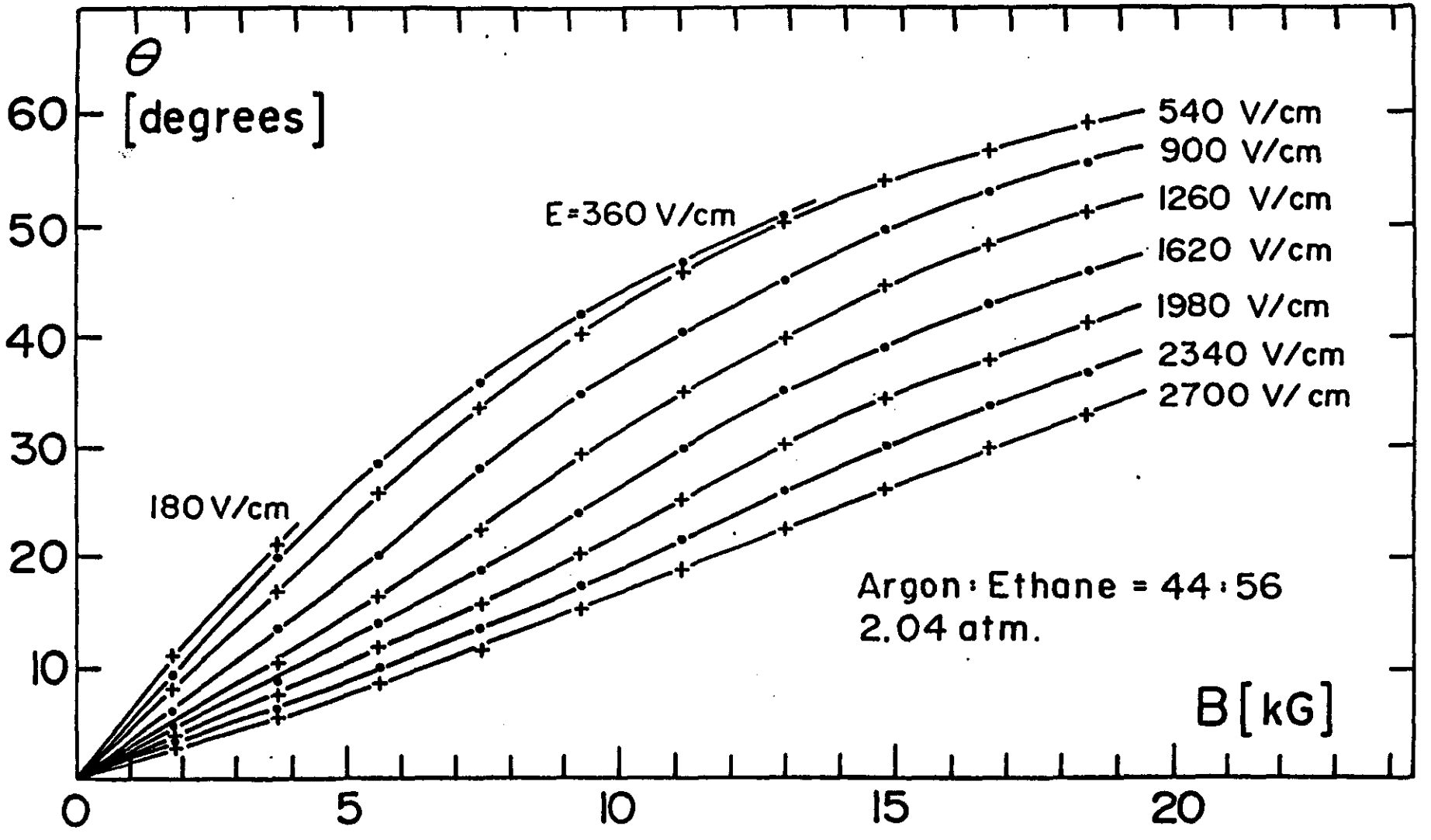

Figure 37 DRIFT ANGLE vs MAGNETIC FIELD

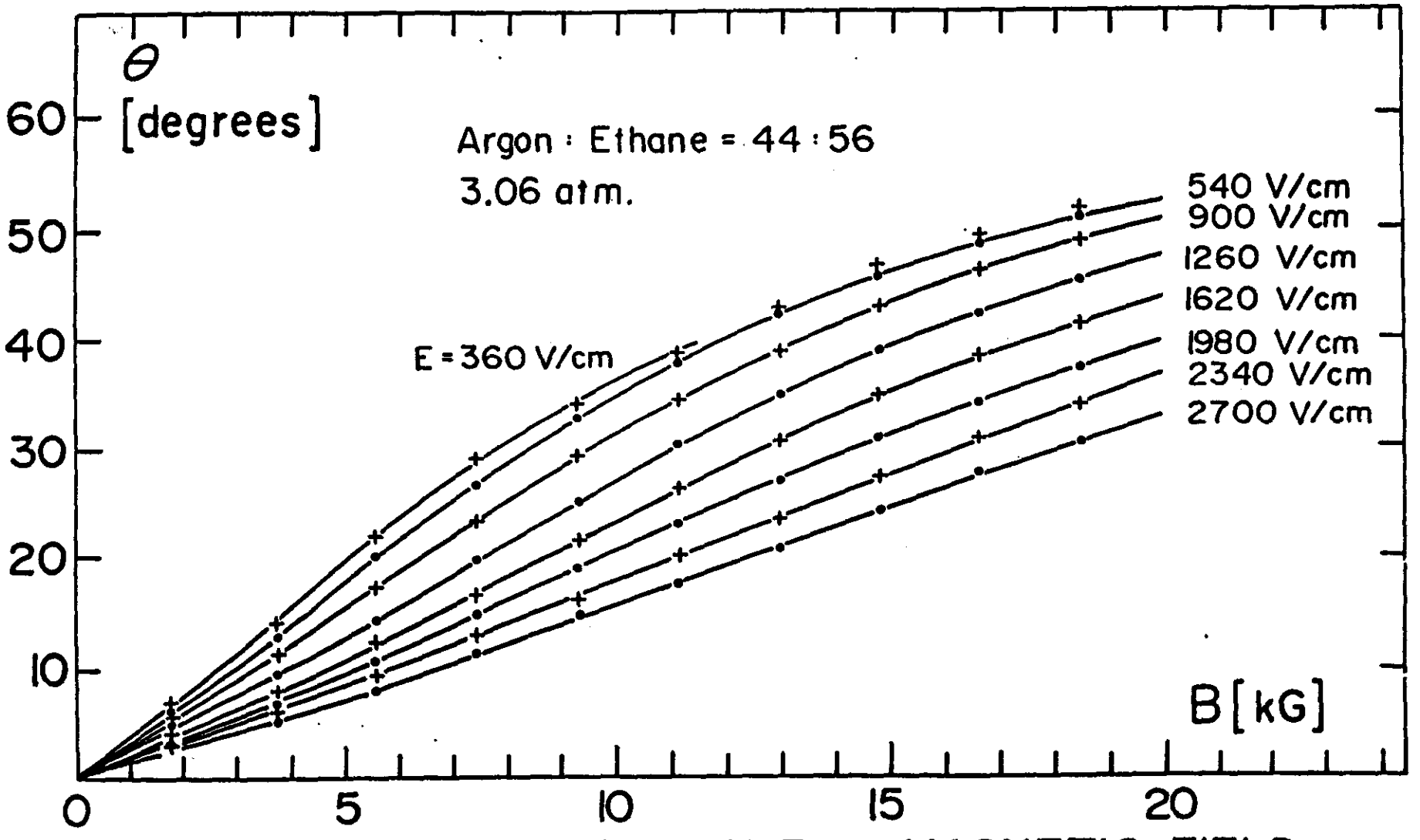

Figure 38 DRIFT ANGLE vs MAGNETIC FIELD

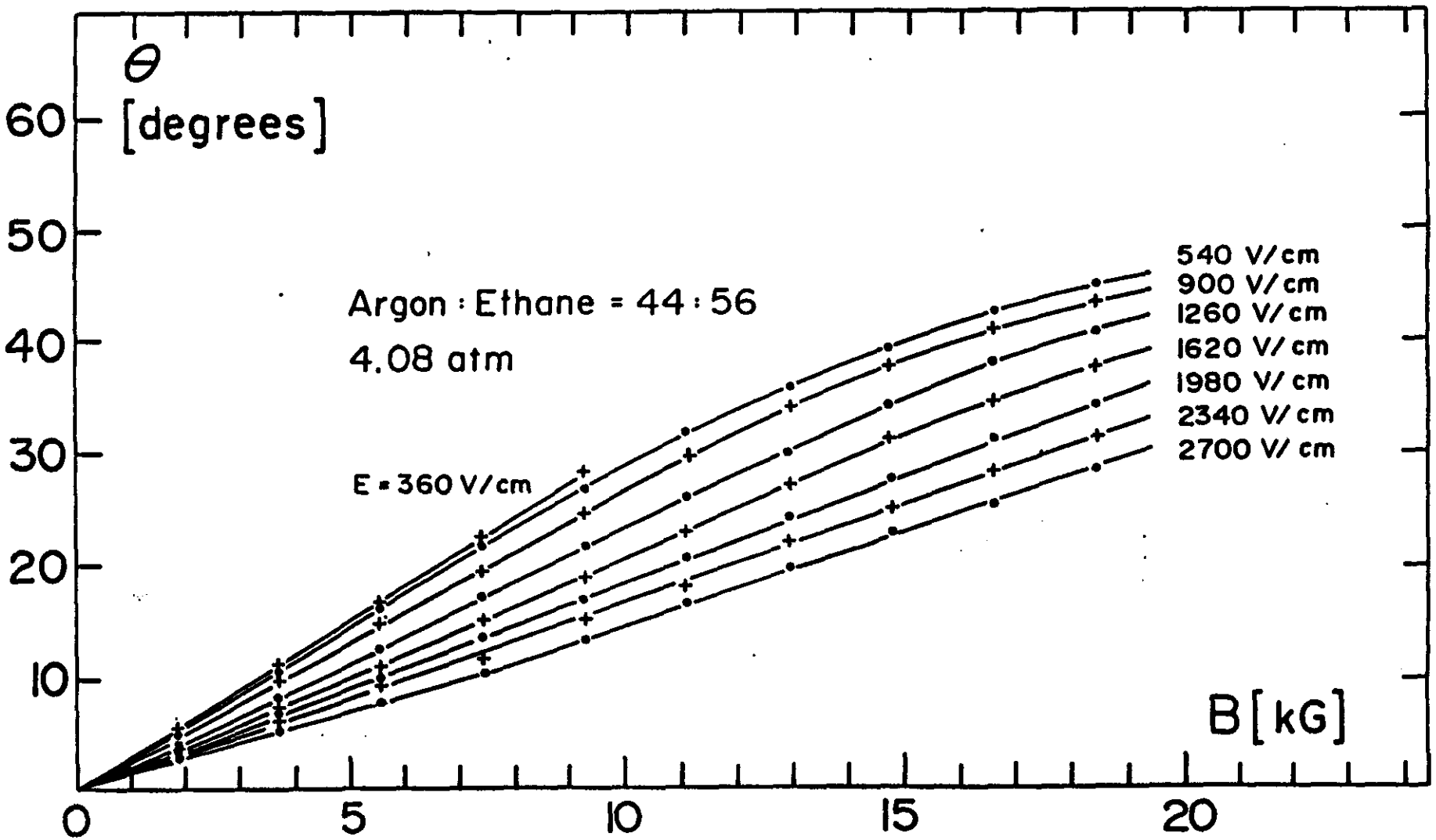

Figure 39 DRIFT ANGLE vs MAGNETIC FIELD

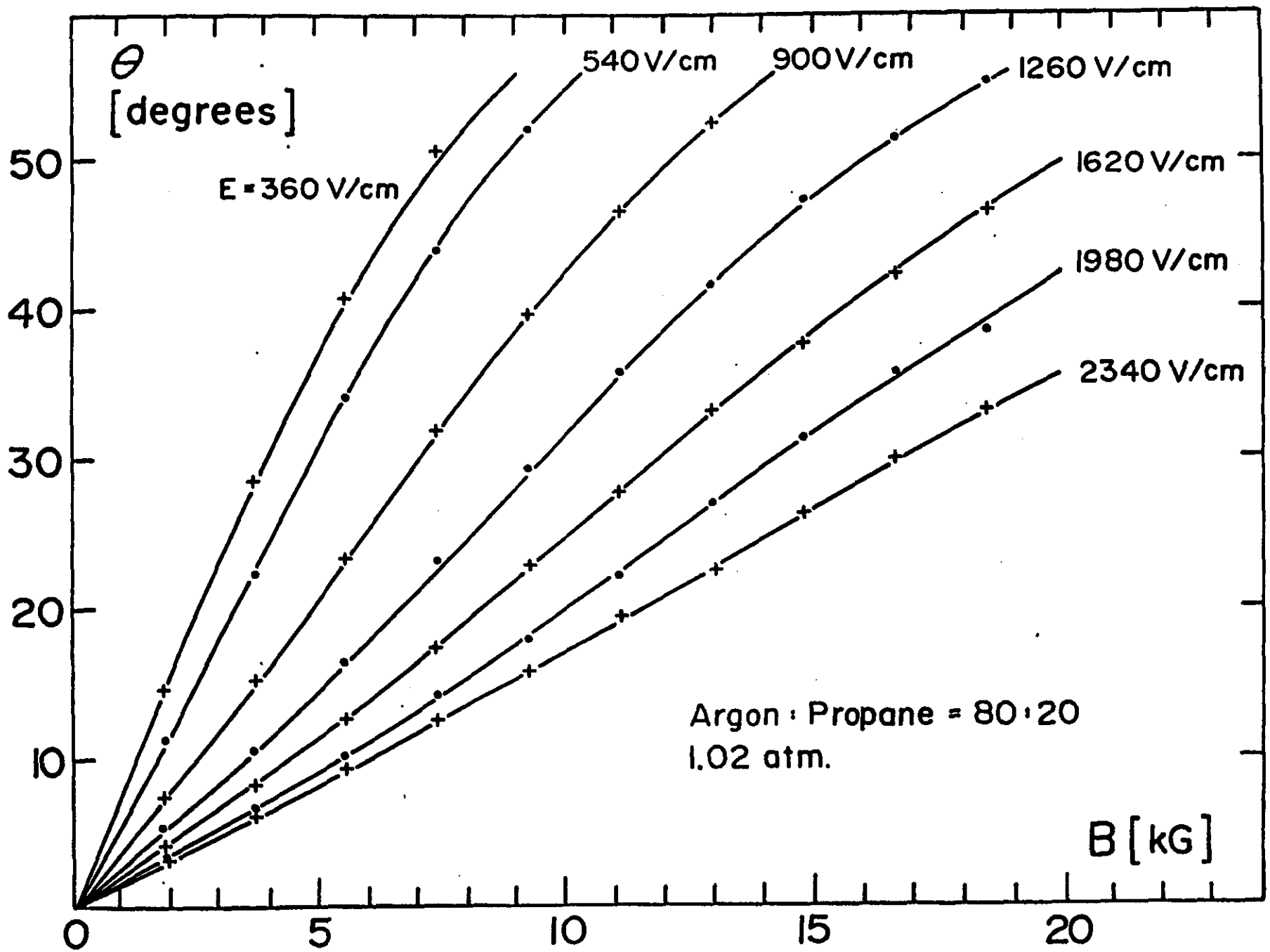

Figure 40 DRIFT ANGLE vs MAGNETIC FIELD

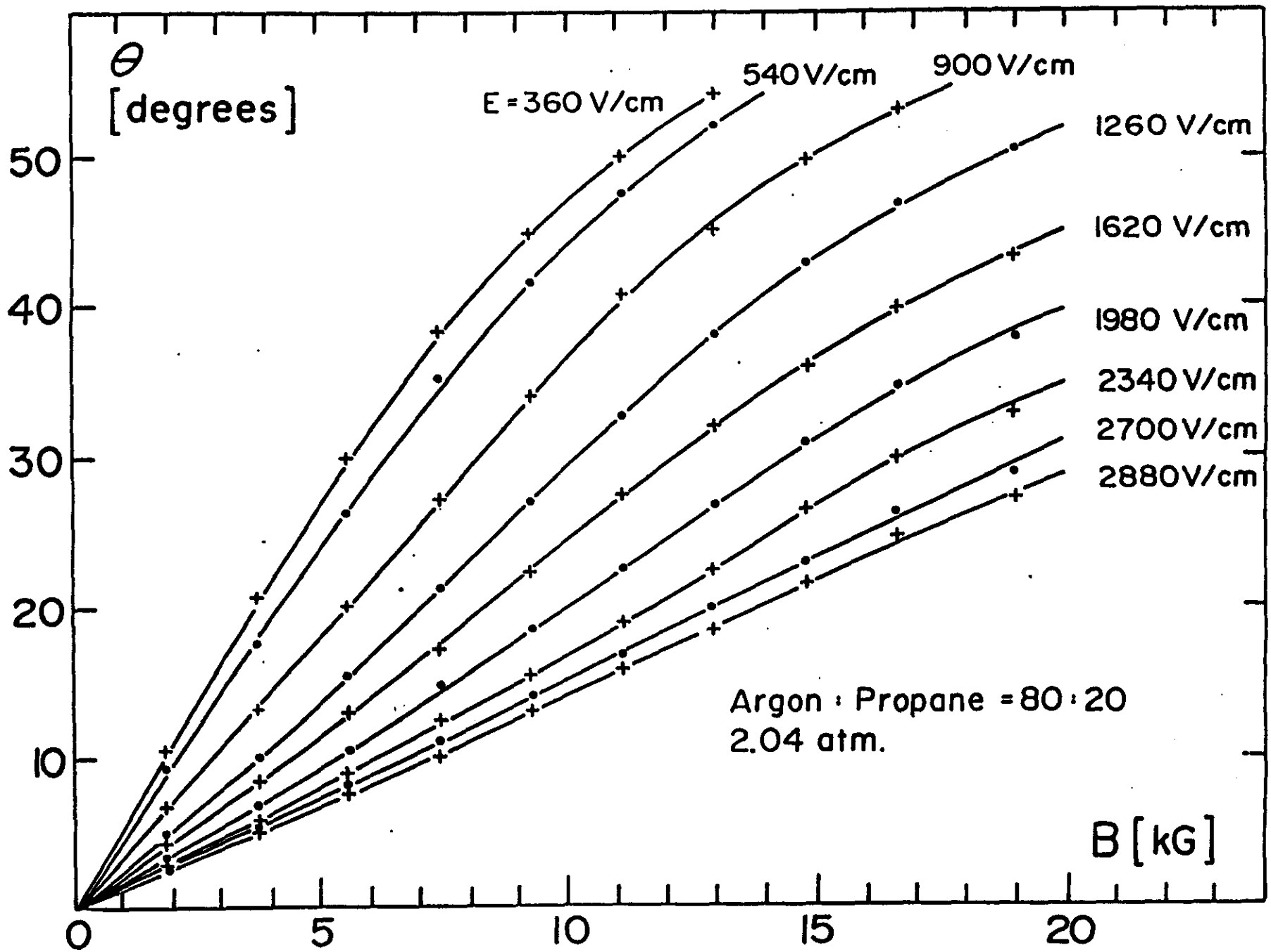

Figure 41 DRIFT ANGLE vs MAGNETIC FIELD

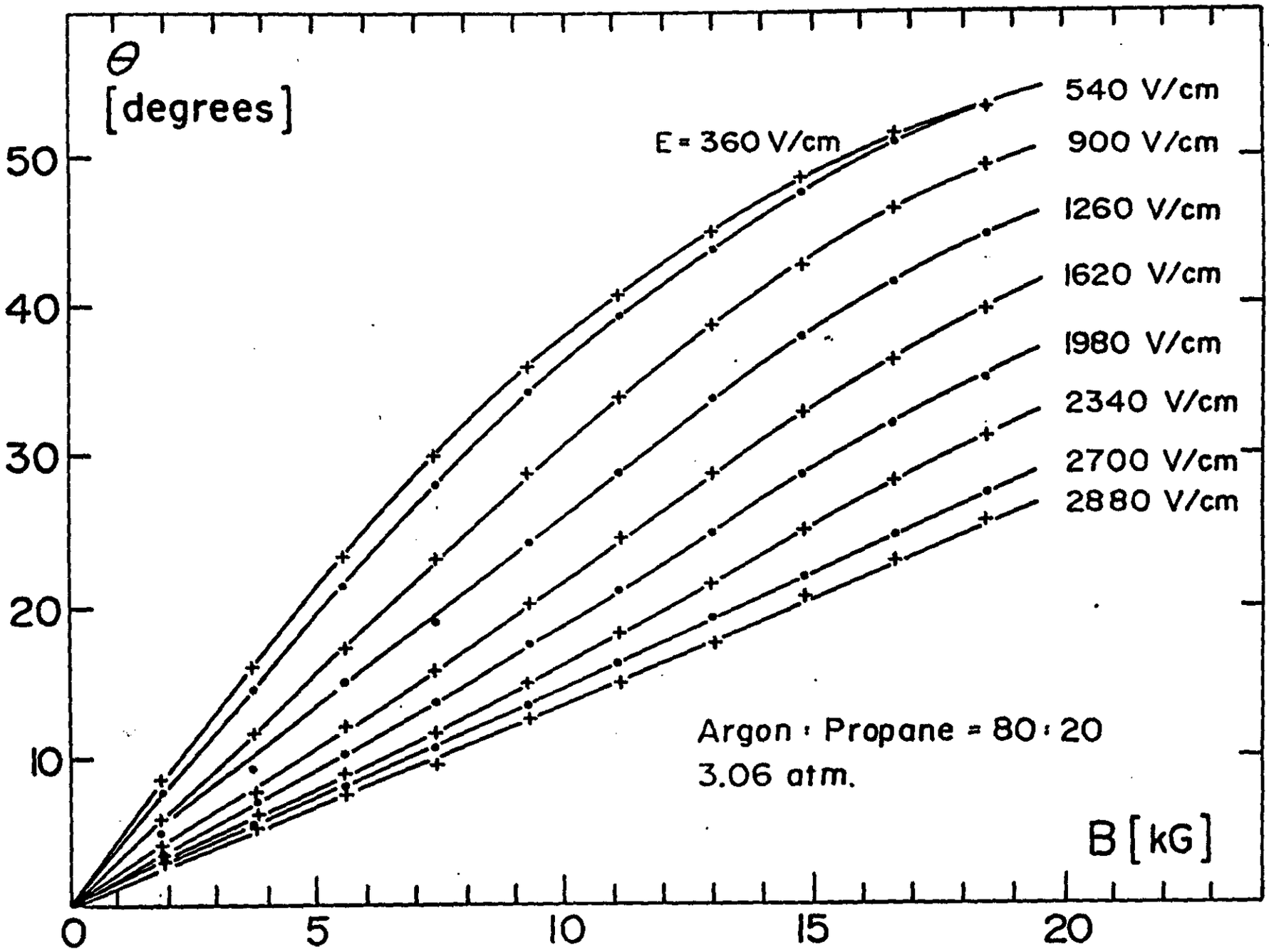

Figure 42 DRIFT ANGLE vs MAGNETIC FIELD

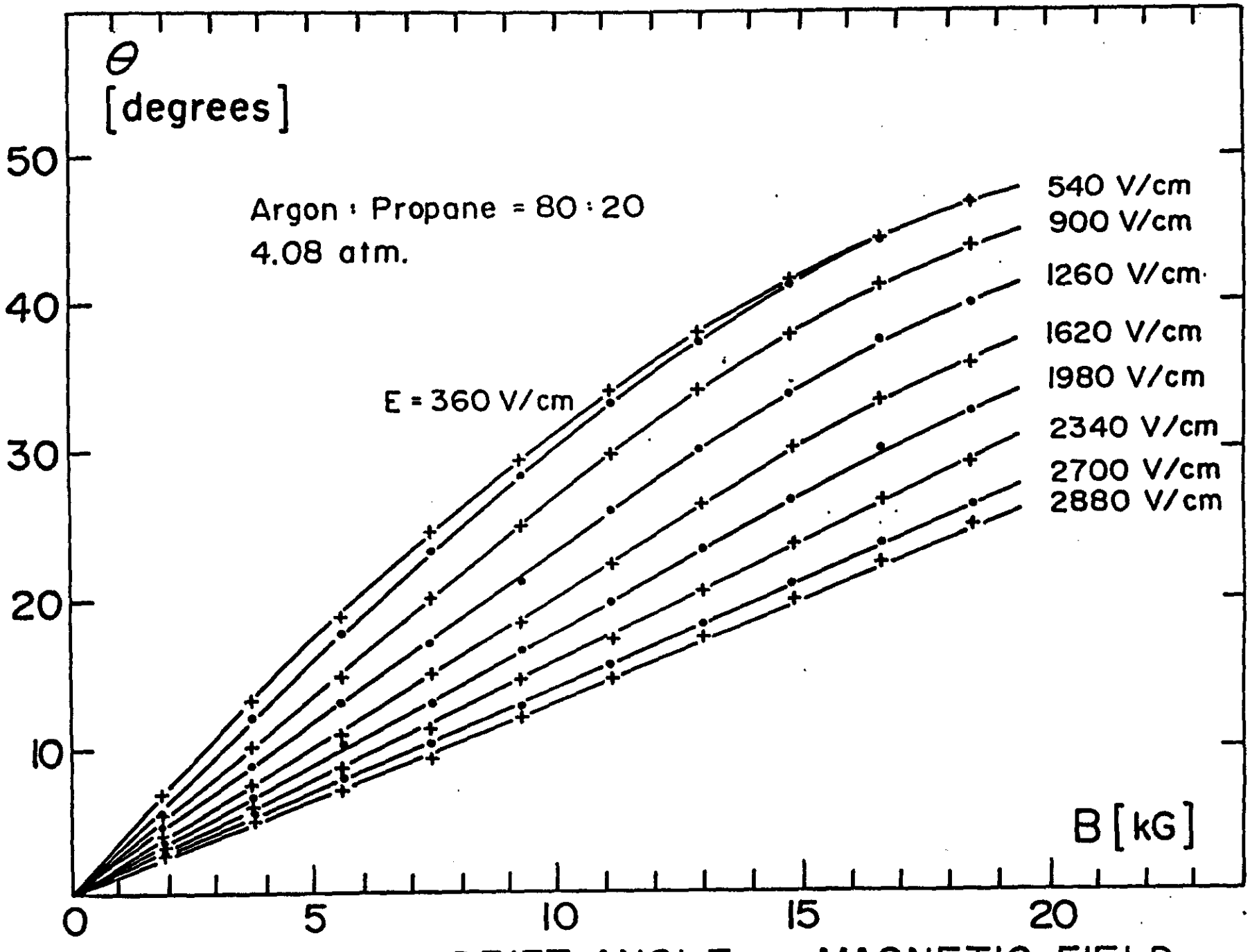

Figure 43 DRIFT ANGLE vs MAGNETIC FIELD

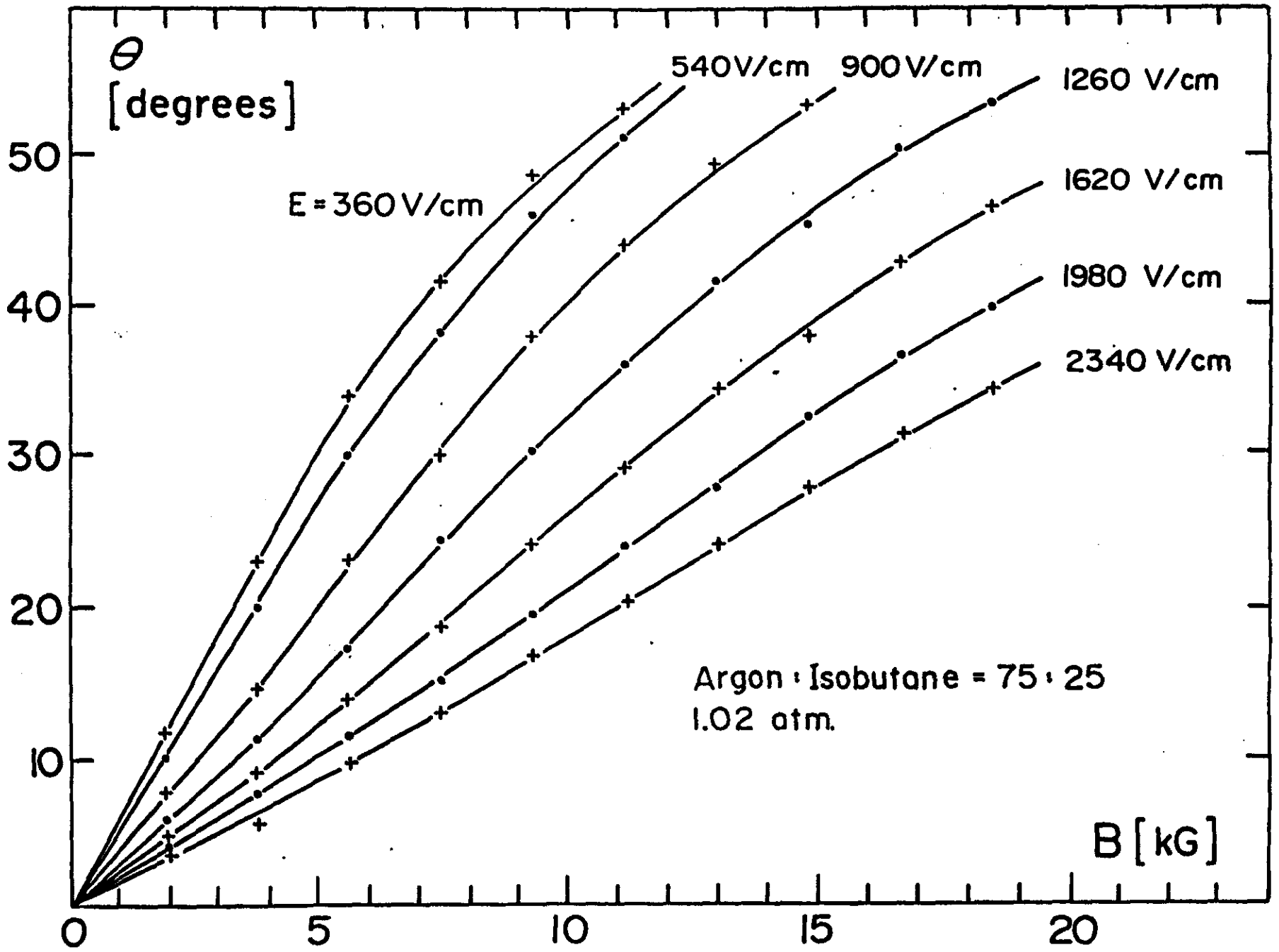

Figure 44 DRIFT ANGLE vs MAGNETIC FIELD

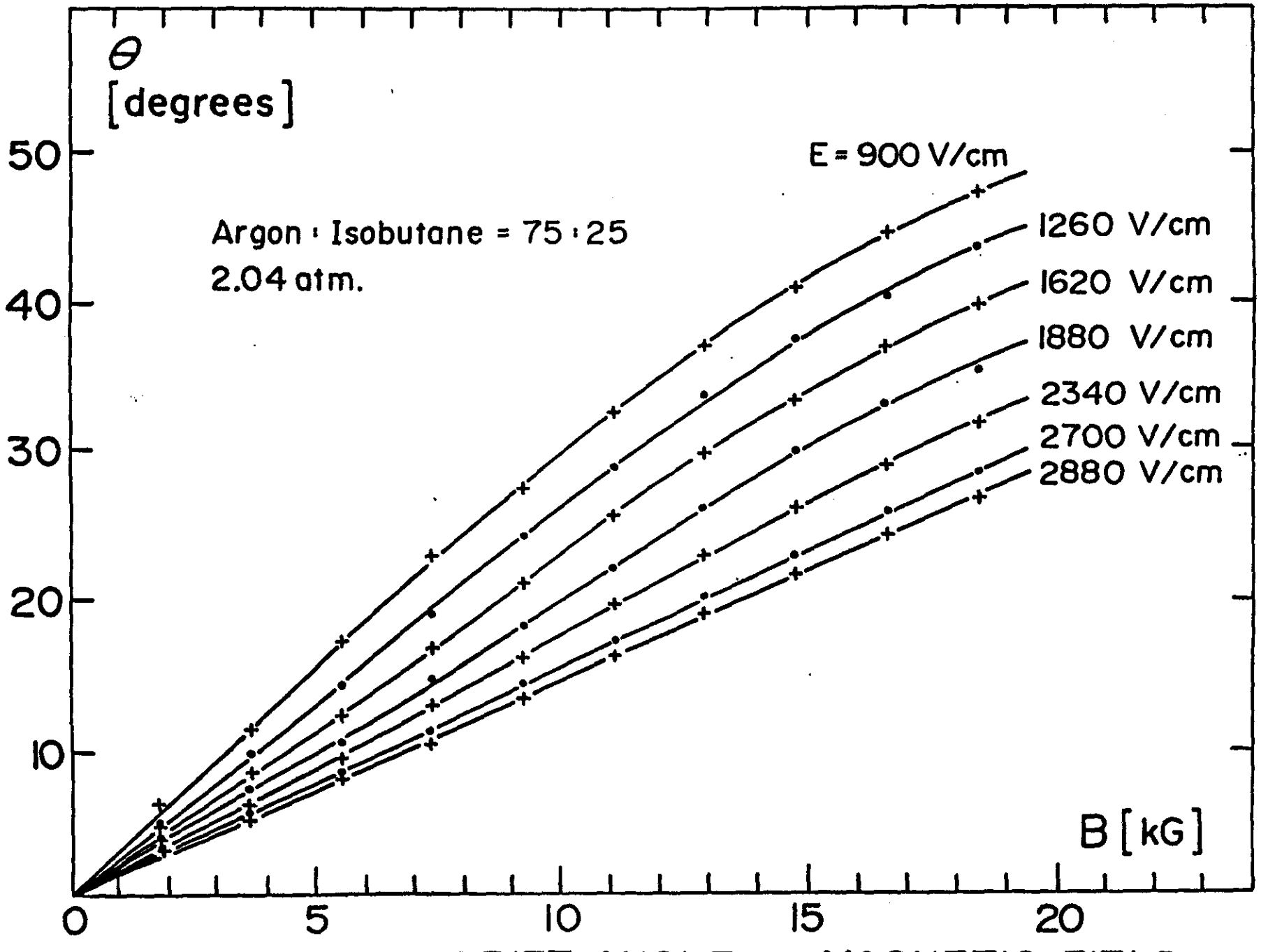

Figure 45 DRIFT ANGLE vs MAGNETIC FIELD

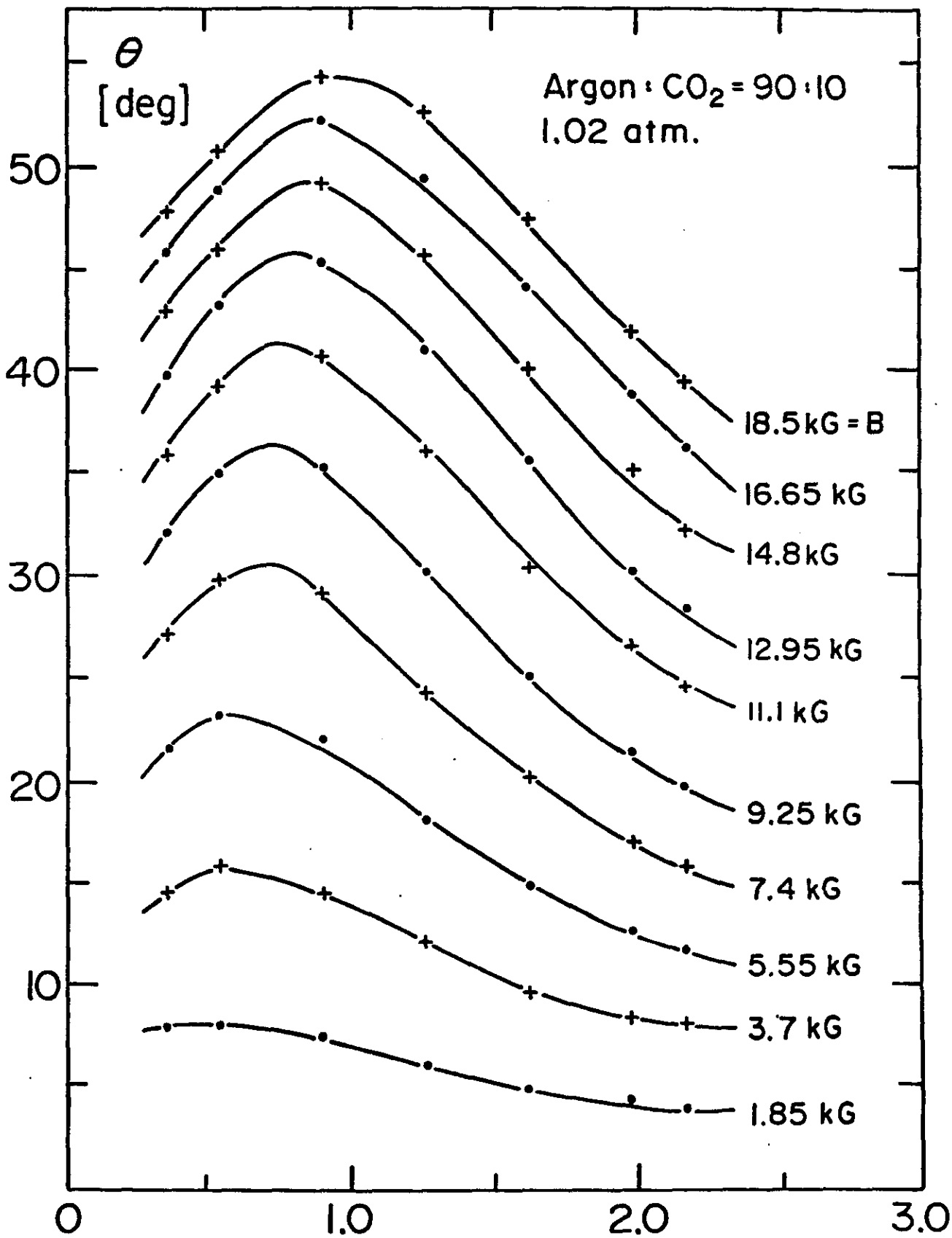
θ
[deg]
Argon : CO_2 = 90 : 10
1.02 atm.
50
40
30
20
10
18.5 kG = B
16.65 kG
14.8 kG
12.95 kG
11.1 kG
9.25 kG
7.4 kG
5.55 kG
3.7 kG
1.85 kG
0
1.0
2.0
3.0
E [kV/cm]

Figure 46

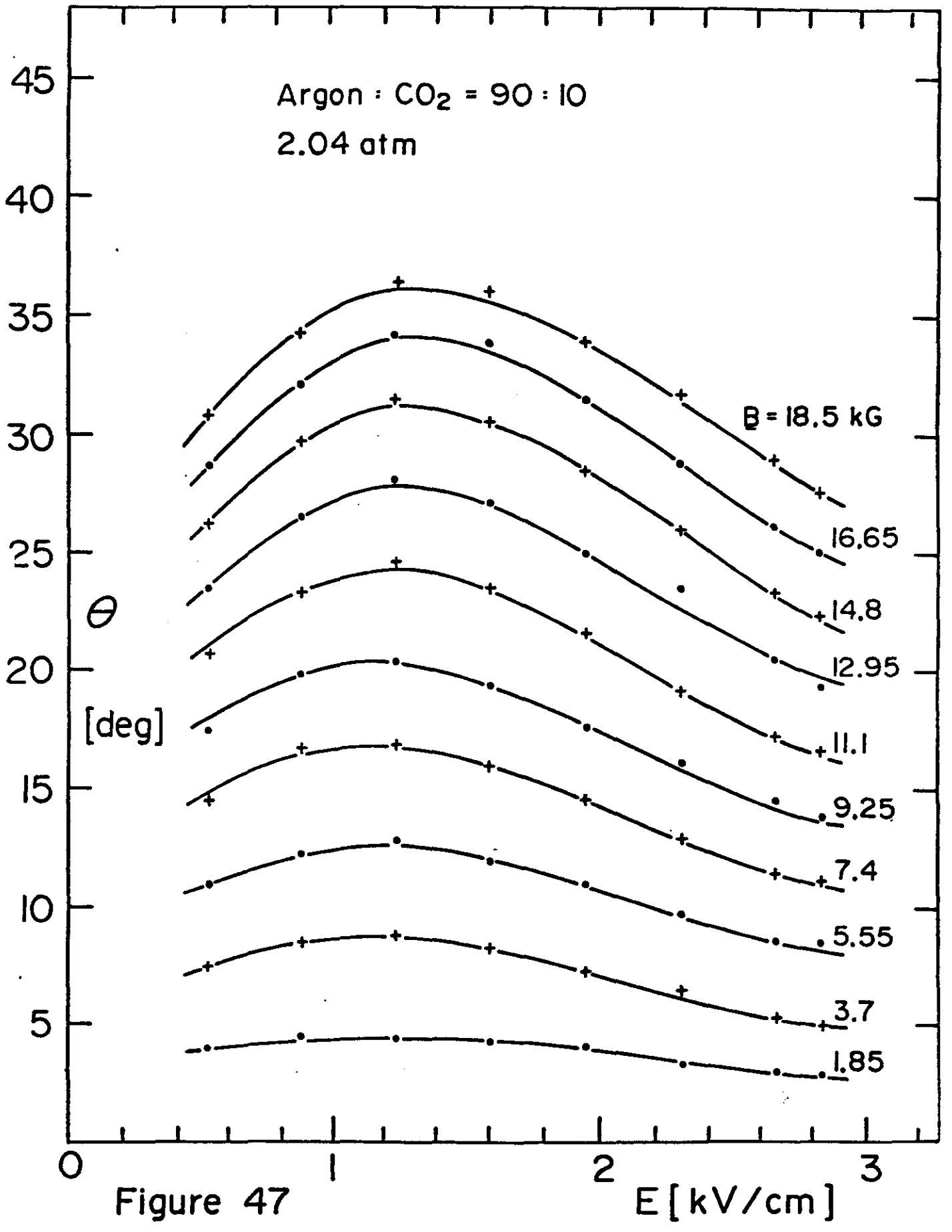
Argon : CO_2 = 90 : 10
2.04 atm
B = 18.5 kG
16.65
14.8
12.95
11.1
9.25
7.4
5.55
3.7
1.85
θ
[deg]
E [kV/cm]
0
1
2
3
5
10
15
20
25
30
35
40
45

Figure 47

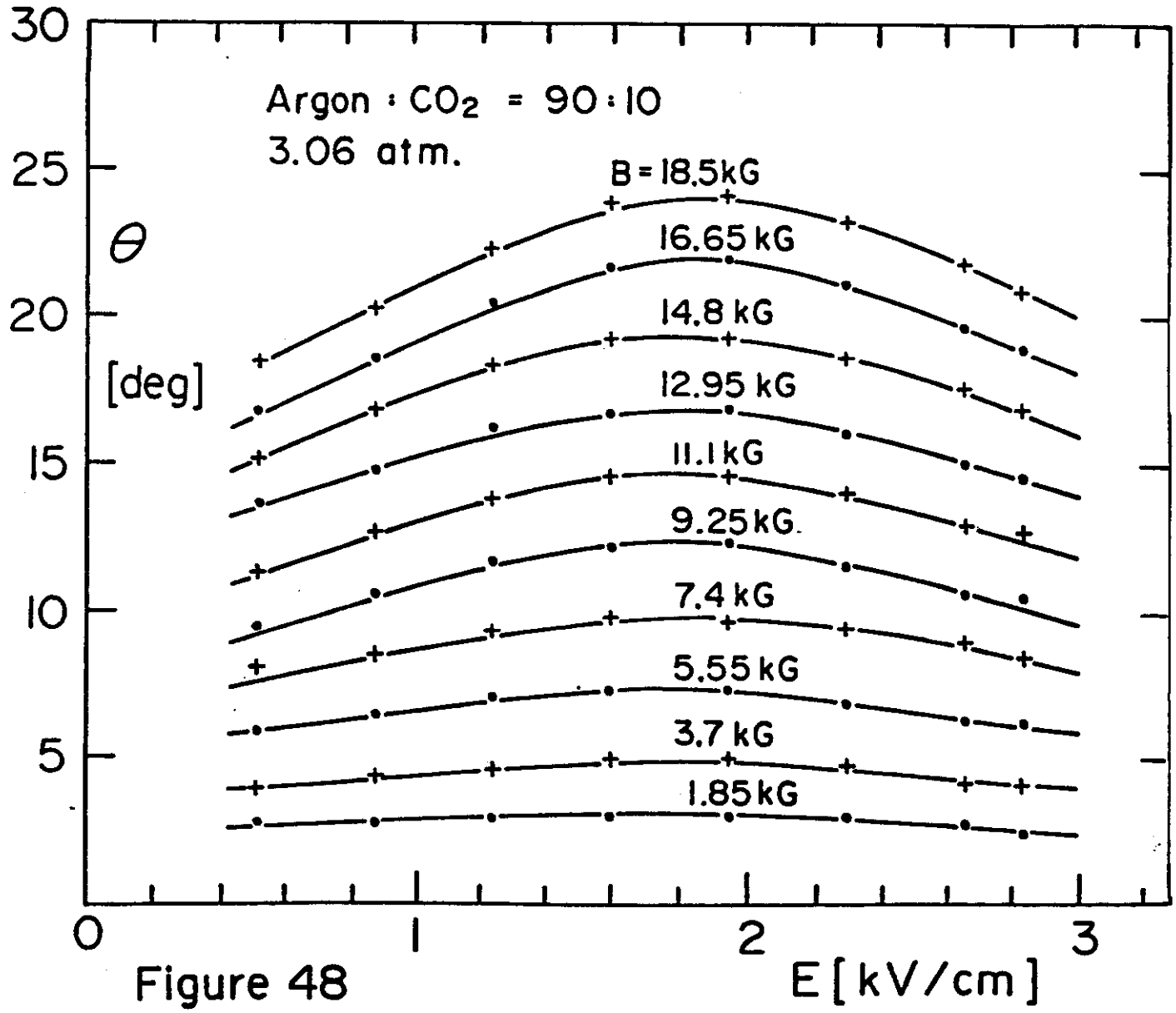
Argon : CO_2 = 90 : 10
3.06 atm.
B = 18.5kG
16.65 kG
14.8 kG
12.95 kG
11.1 kG
9.25 kG
7.4 kG
5.55 kG
3.7 kG
1.85 kG
θ
[deg]
30
25
20
15
10
5
0
1
2
3
E [kV/cm]

Figure 48

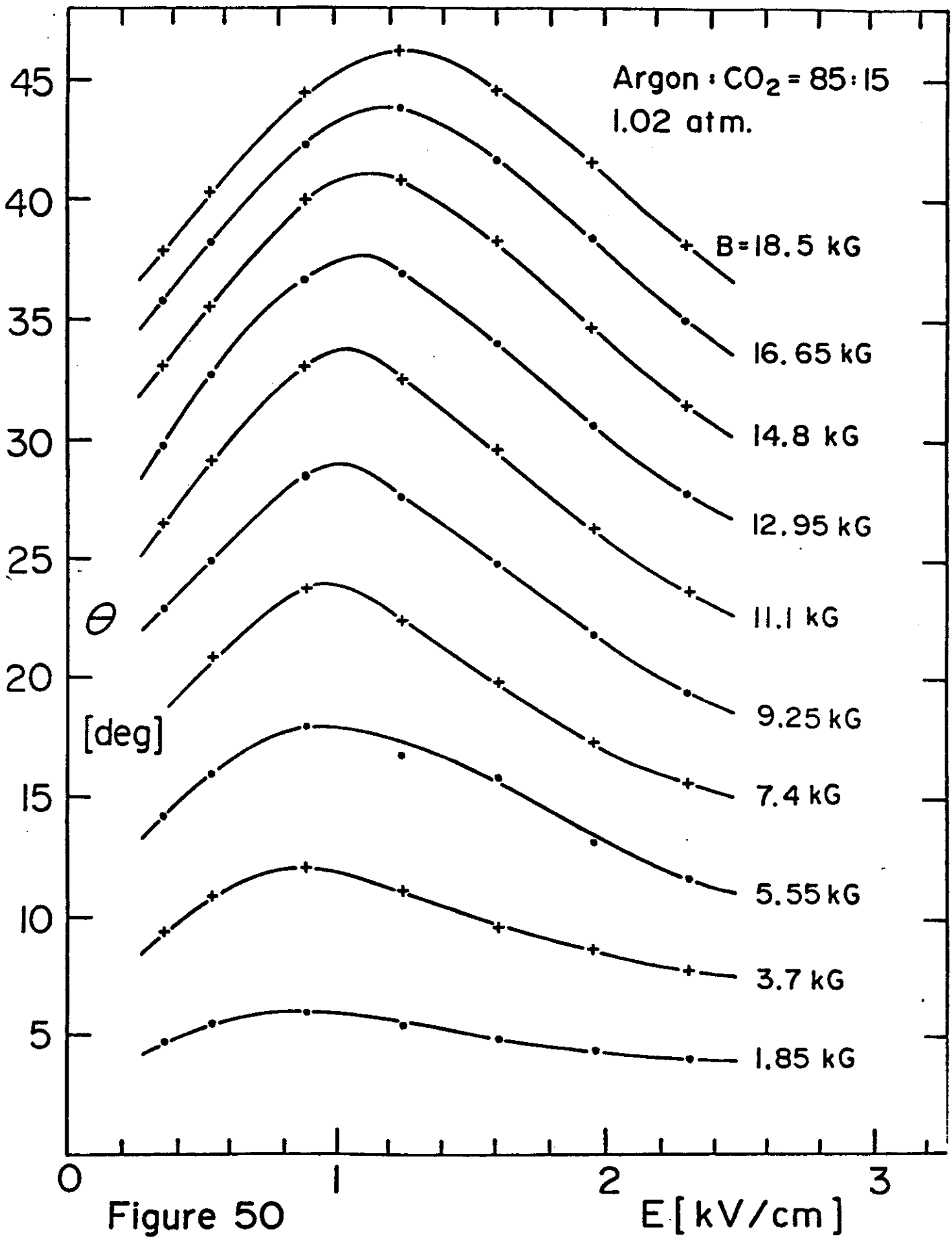
Argon : CO_2 = 85 : 15
1.02 atm.
B = 18.5 kG
16.65 kG
14.8 kG
12.95 kG
11.1 kG
9.25 kG
7.4 kG
5.55 kG
3.7 kG
1.85 kG
θ
[deg]
45
40
35
30
25
20
15
10
5
0
1
2
3
E [kV/cm]

Figure 50

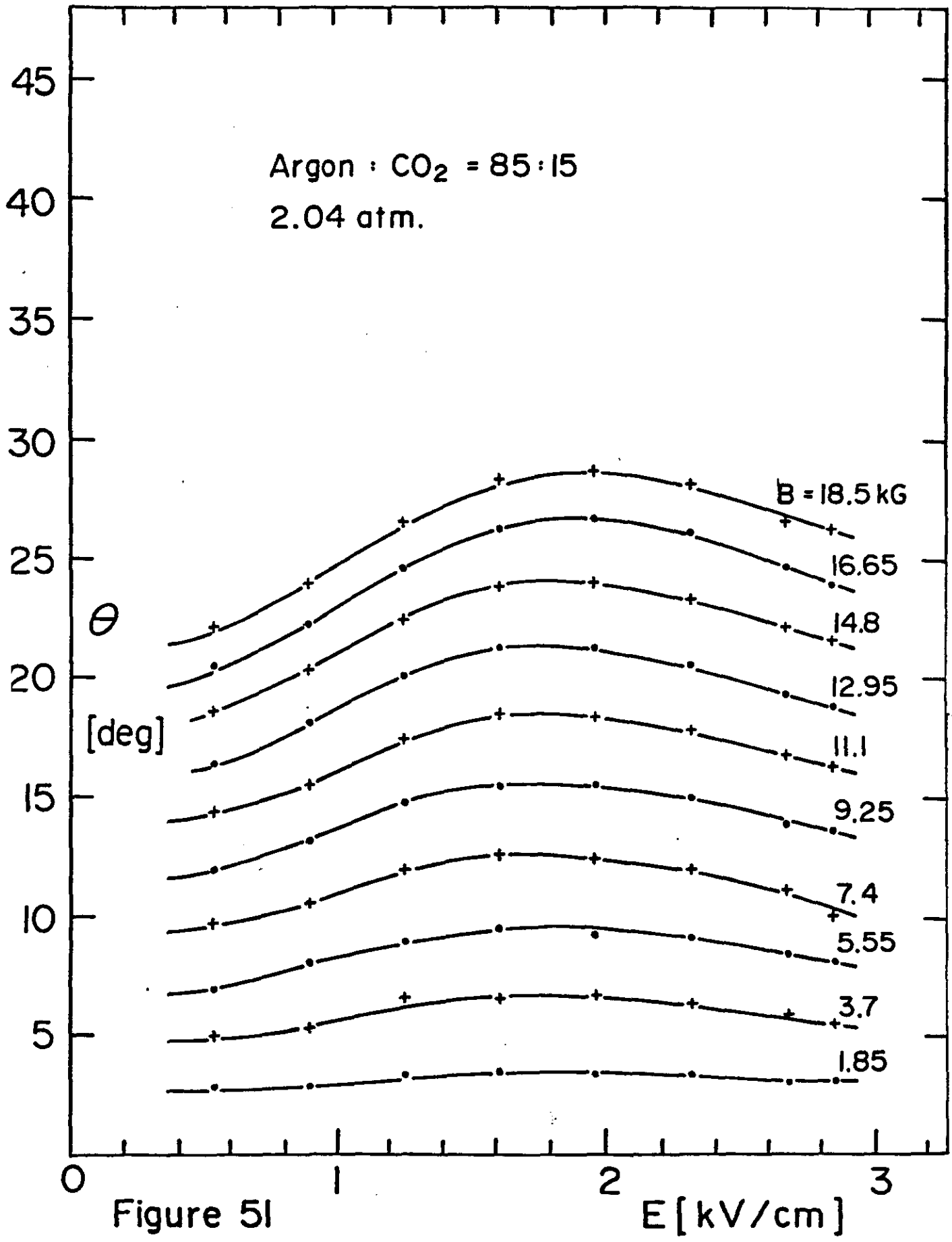
Argon : CO_2 = 85 : 15
2.04 atm.
B = 18.5 kG
16.65
14.8
12.95
11.1
9.25
7.4
5.55
3.7
1.85
θ
[deg]
45
40
35
30
25
20
15
10
5
0
1
2
3
E [kV/cm]

Figure 51

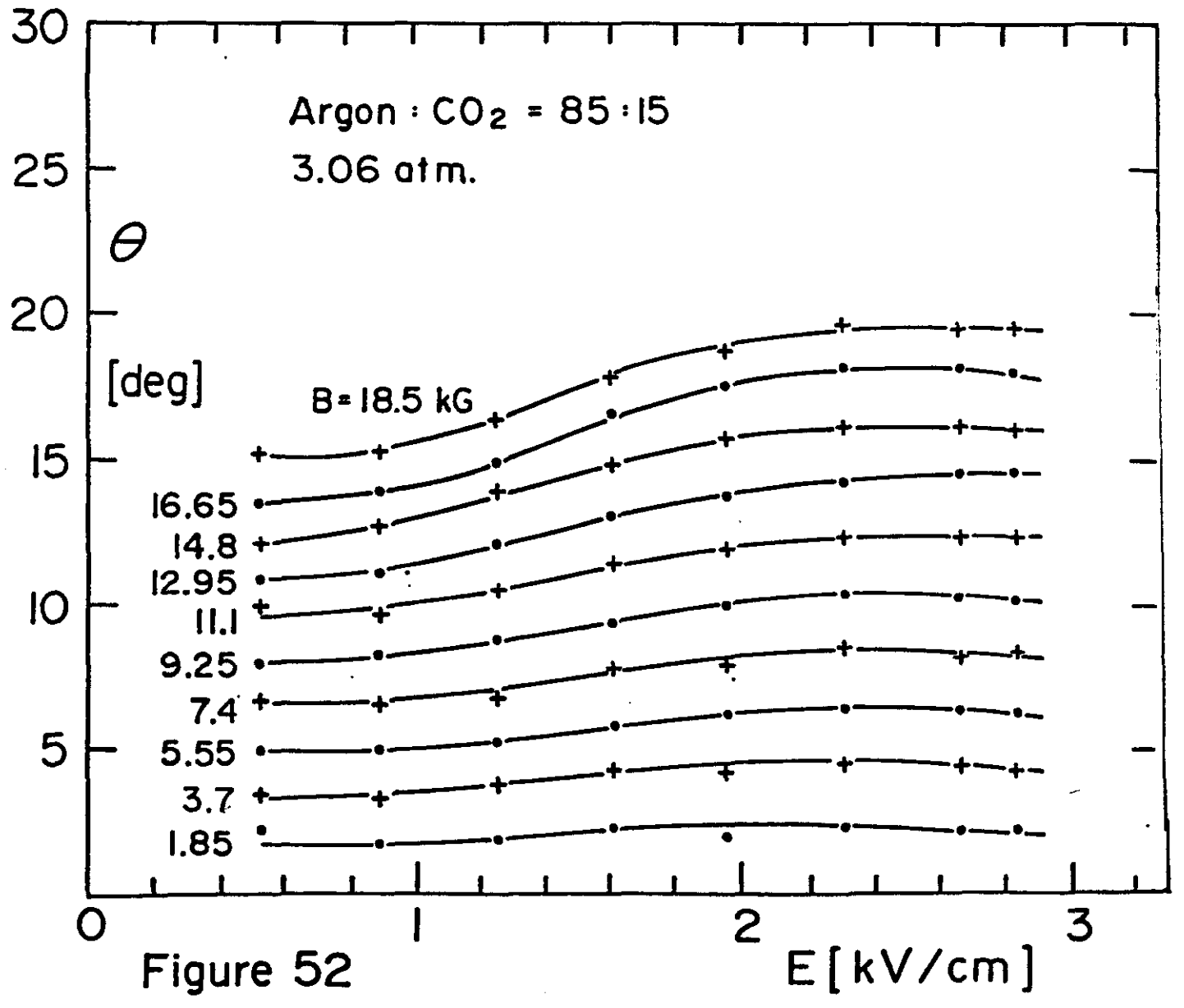
Argon : CO_2 = 85 : 15
3.06 atm.
θ
[deg]
B = 18.5 kG
16.65
14.8
12.95
11.1
9.25
7.4
5.55
3.7
1.85
30
25
20
15
10
5
0
1
2
3
E [kV/cm]

Figure 52

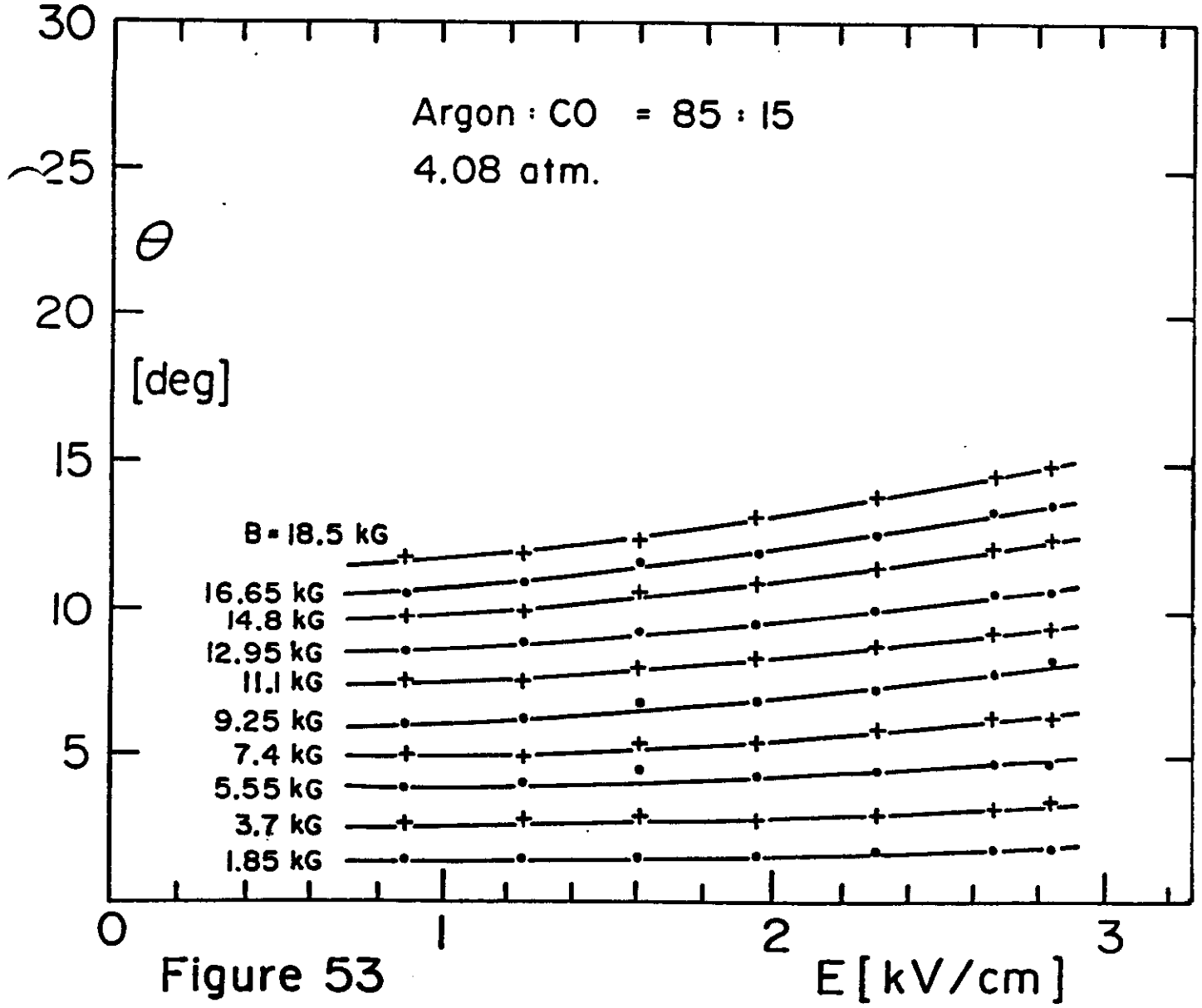
Argon : CO = 85 : 15
4.08 atm.
θ
[deg]
B = 18.5 kG
16.65 kG
14.8 kG
12.95 kG
11.1 kG
9.25 kG
7.4 kG
5.55 kG
3.7 kG
1.85 kG
30
25
20
15
10
5
0
1
2
3
E [kV/cm]

Figure 53

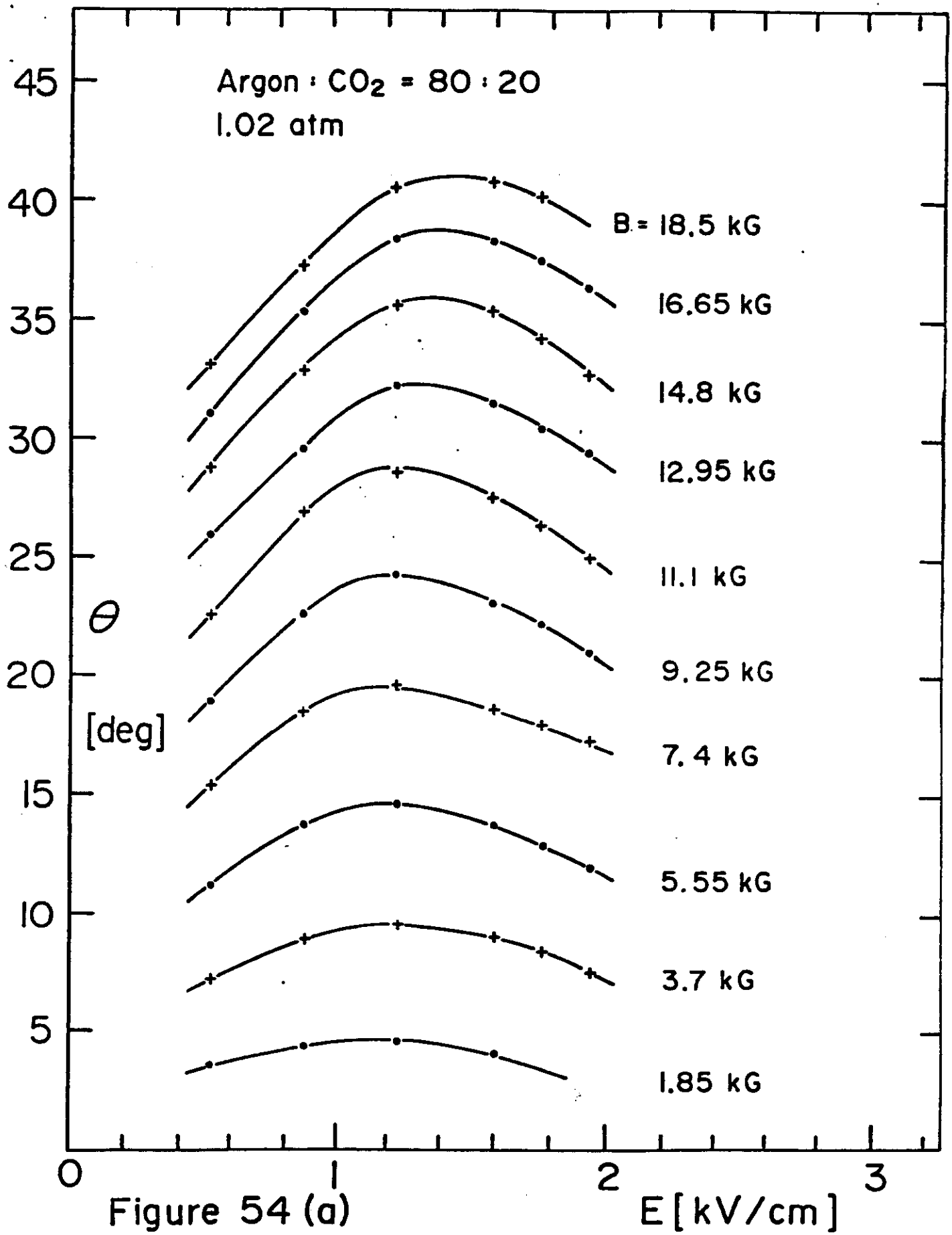
Argon : CO_2 = 80 : 20
1.02 atm
B = 18.5 kG
16.65 kG
14.8 kG
12.95 kG
11.1 kG
9.25 kG
7.4 kG
5.55 kG
3.7 kG
1.85 kG
θ
[deg]
45
40
35
30
25
20
15
10
5
0
1
2
3
E [kV/cm]

Figure 54 (a)

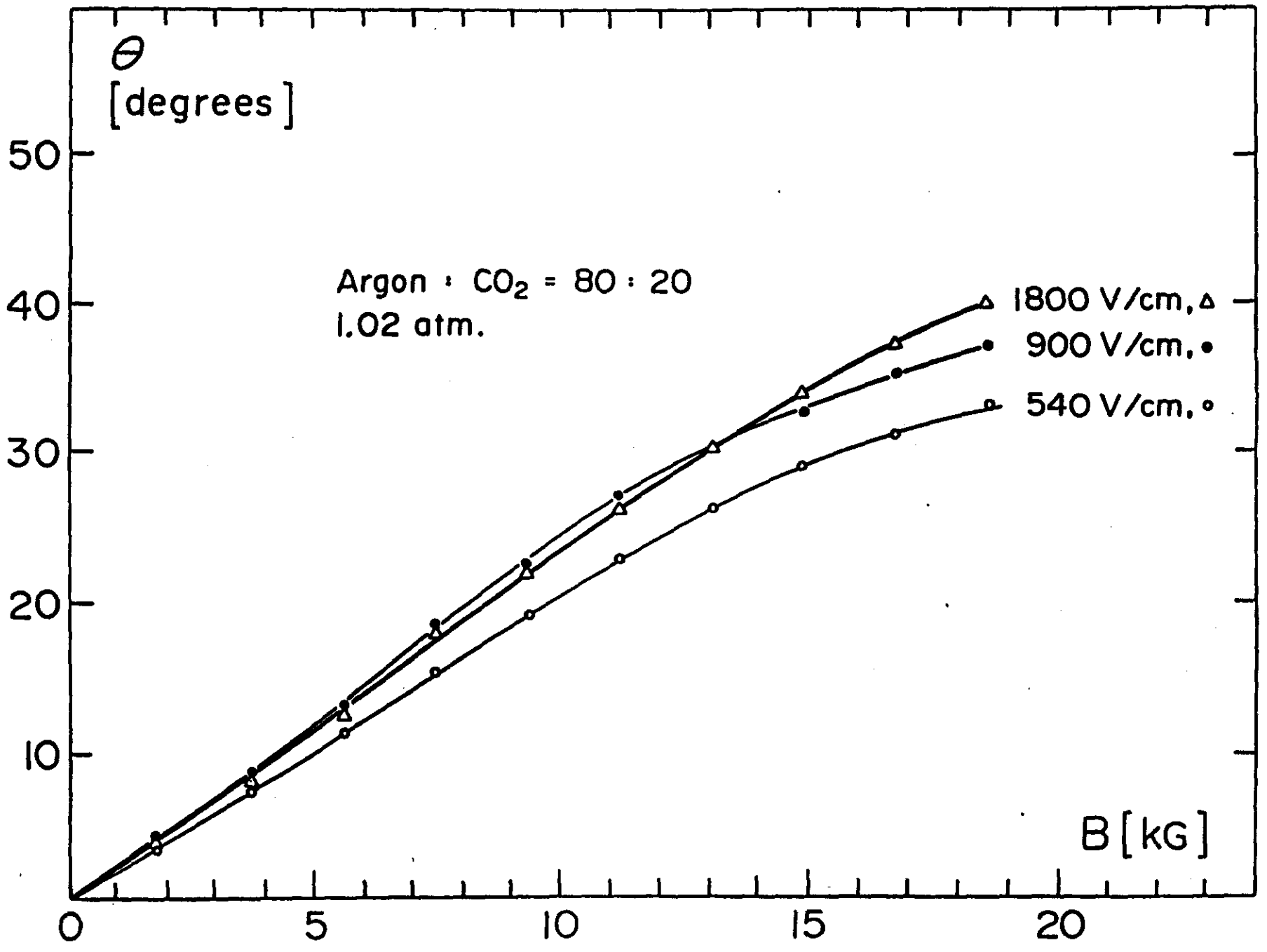

Figure 54(b) DRIFT ANGLE vs MAGNETIC FIELD

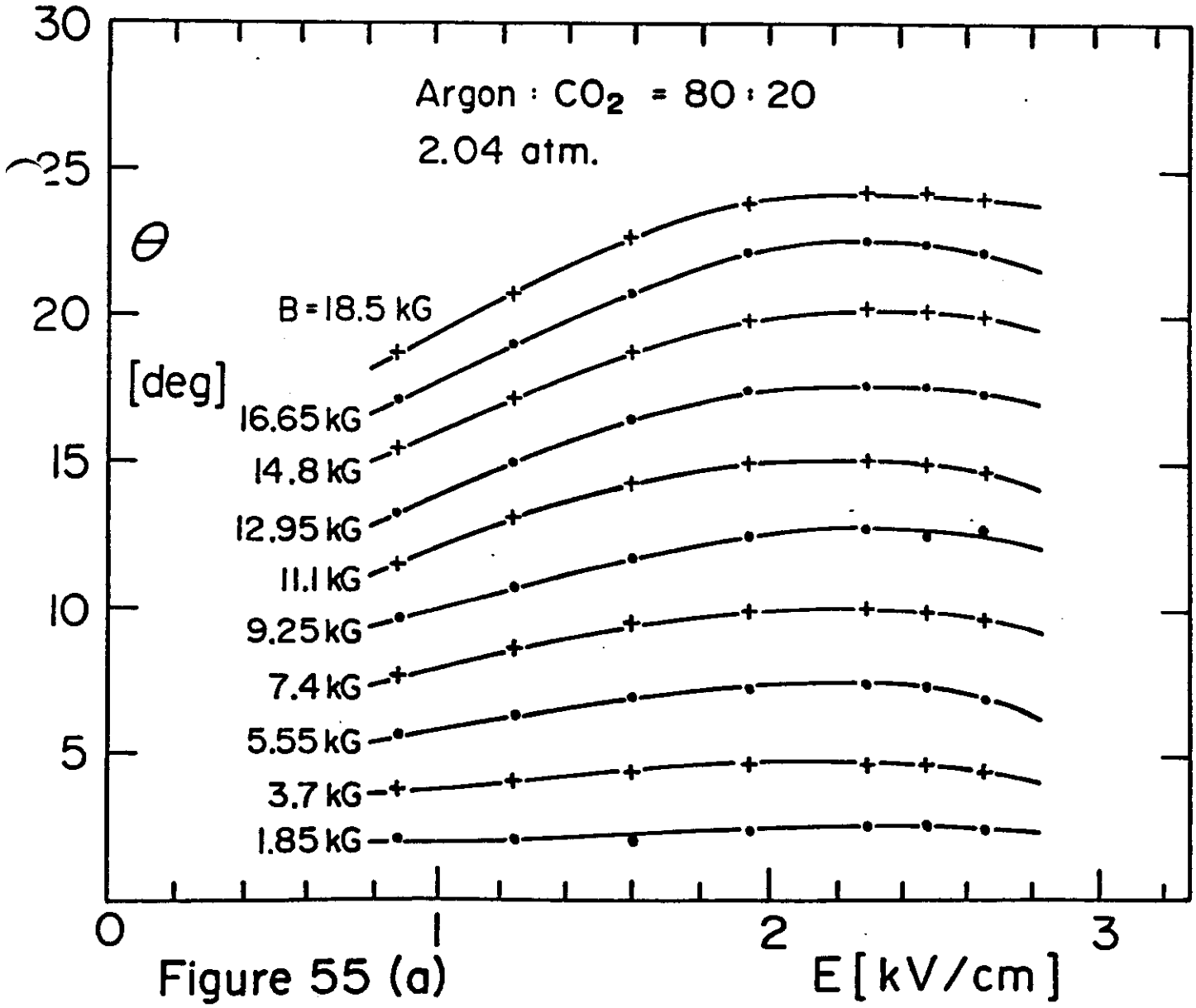
Argon : CO_2 = 80 : 20
2.04 atm.
θ
[deg]
B = 18.5 kG
16.65 kG
14.8 kG
12.95 kG
11.1 kG
9.25 kG
7.4 kG
5.55 kG
3.7 kG
1.85 kG
30
25
20
15
10
5
0
1
2
3
E [kV/cm]

Figure 55 (a)

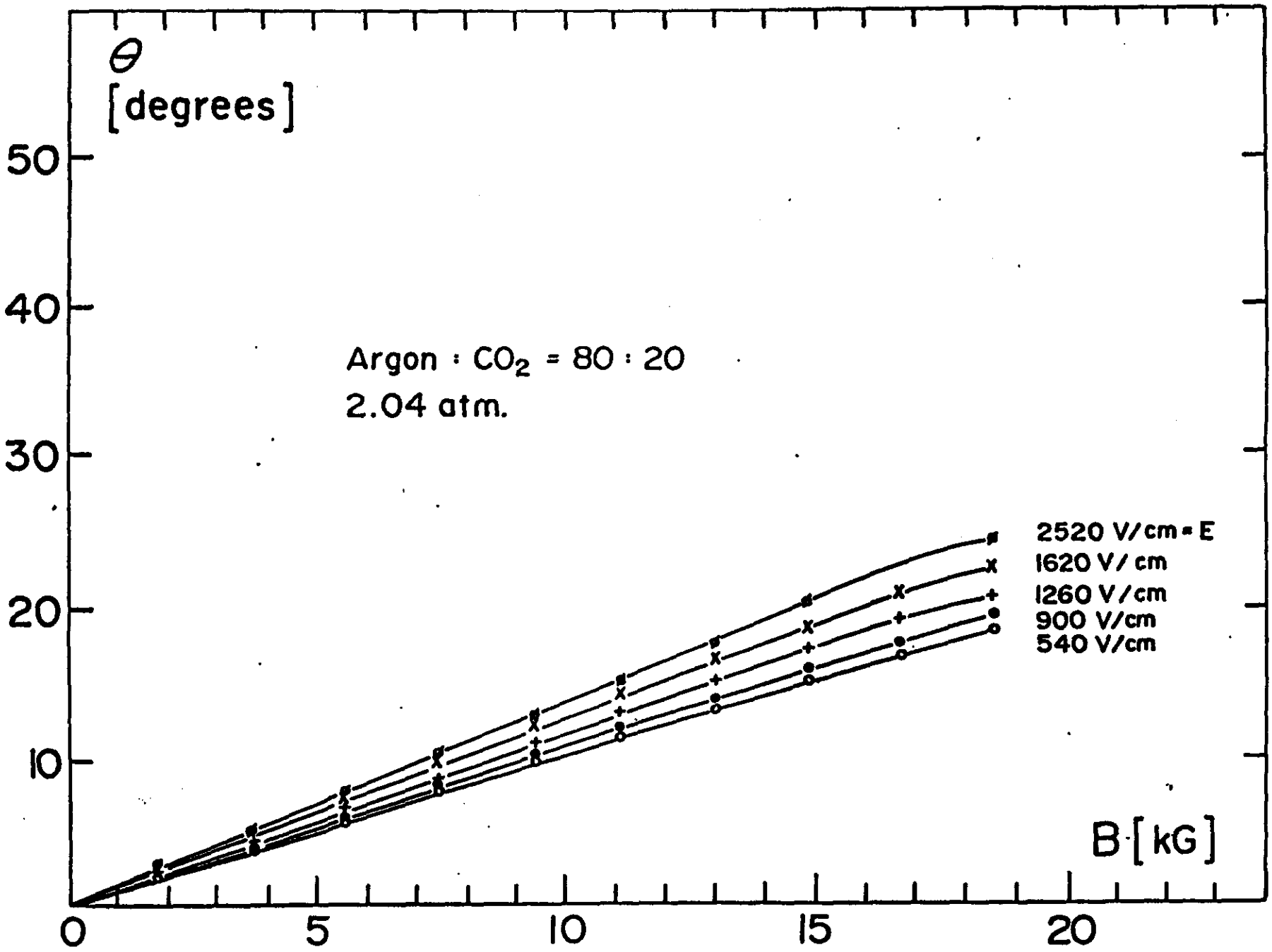

Figure 55 (b) DRIFT ANGLE vs MAGNETIC FIELD

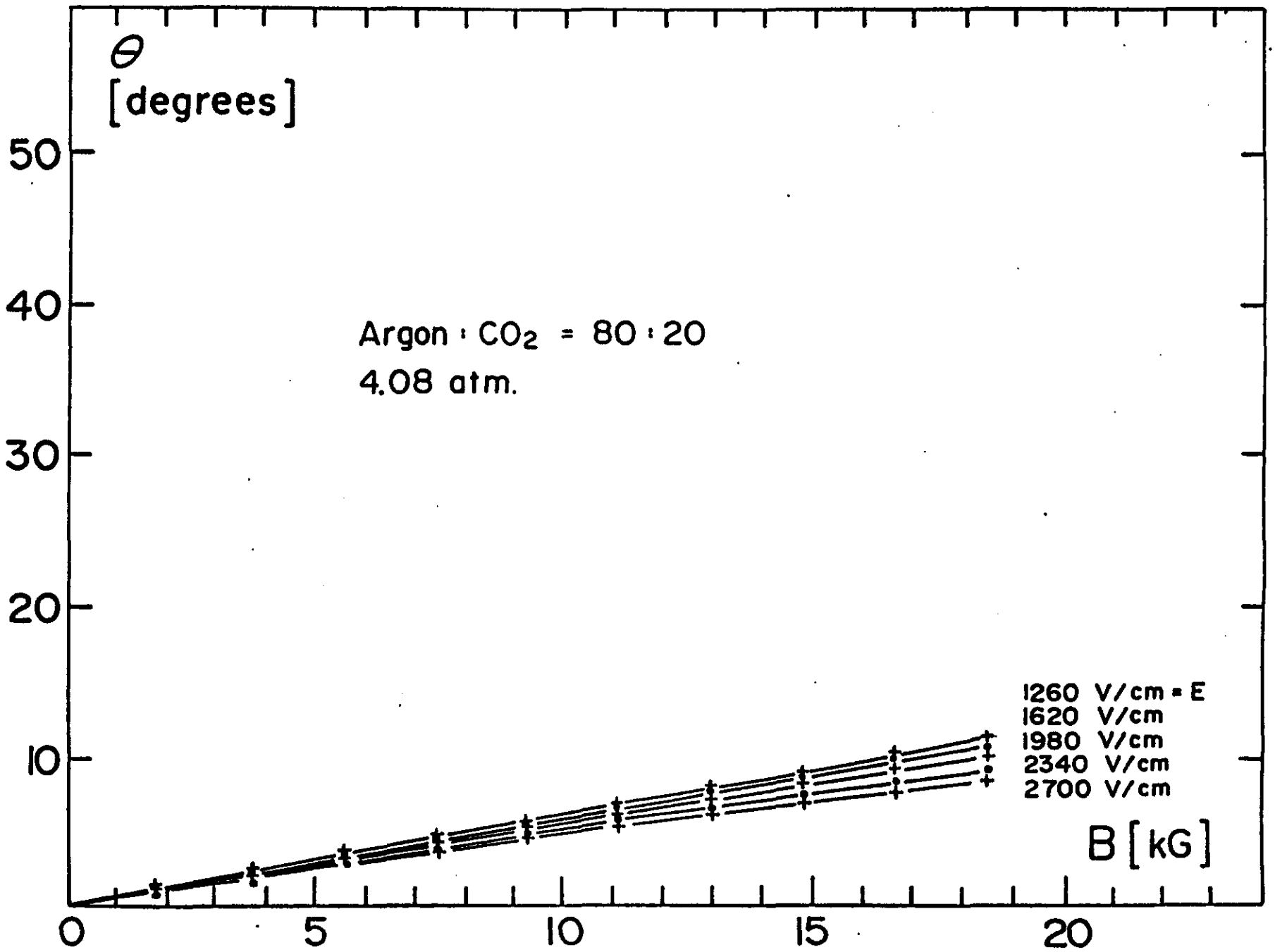

Figure 56 DRIFT ANGLE vs MAGNETIC FIELD

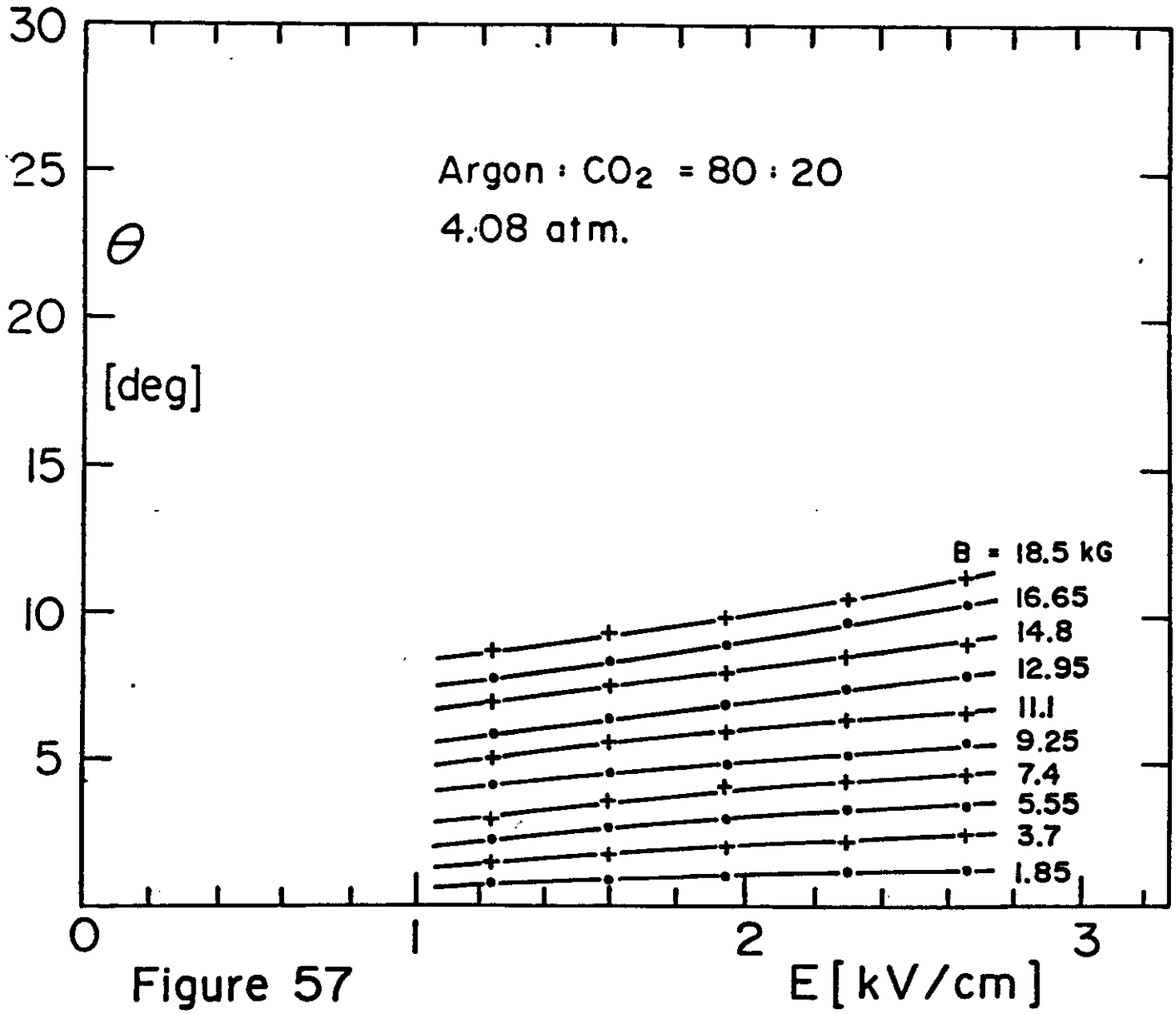
Argon : CO_2 = 80 : 20
4.08 atm.
θ
[deg]
B = 18.5 kG
16.65
14.8
12.95
11.1
9.25
7.4
5.55
3.7
1.85
30
25
20
15
10
5
0
1
2
3
E [kV/cm]

Figure 57

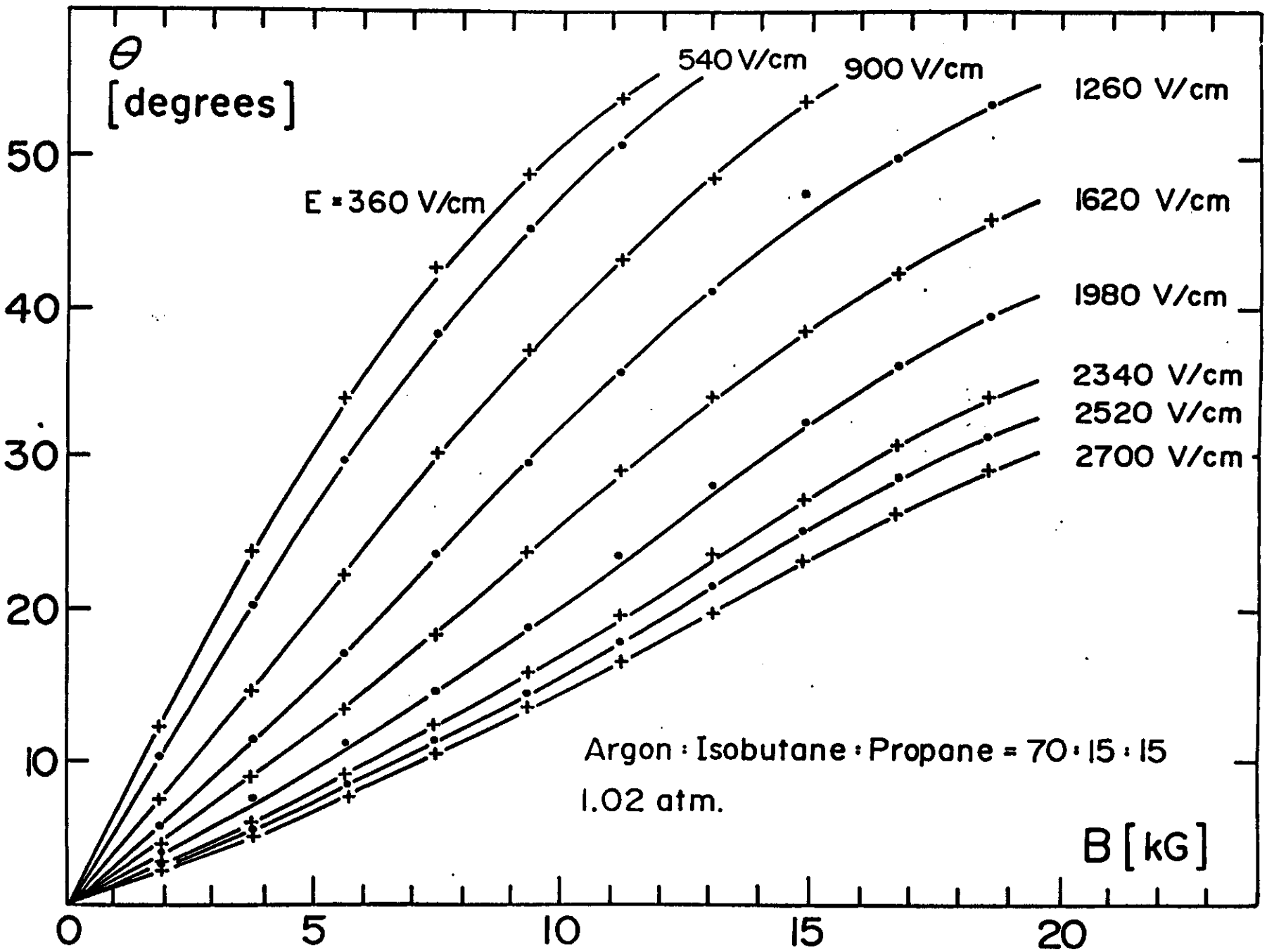

Figure 58 DRIFT ANGLE vs MAGNETIC FIELD

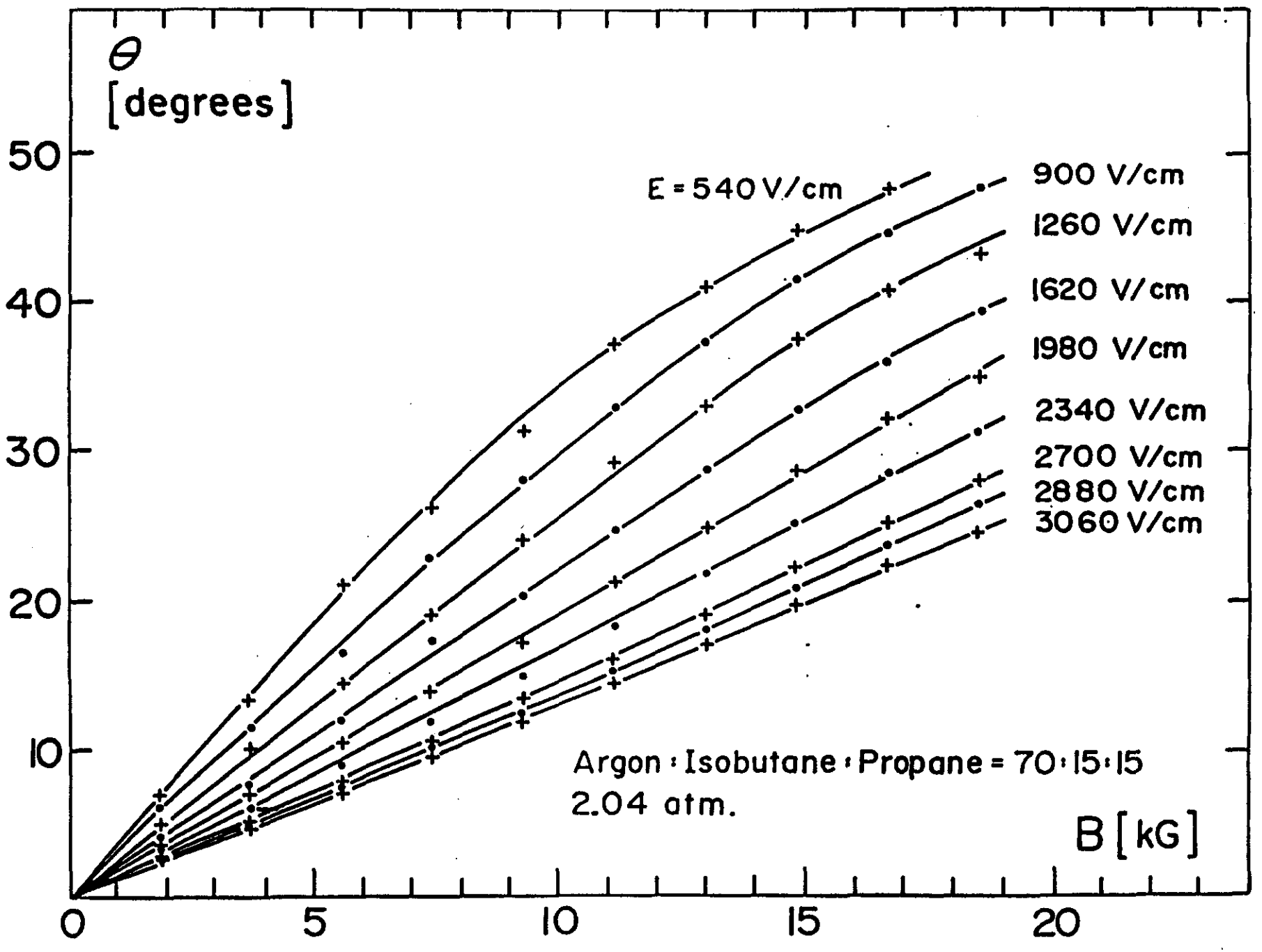

Figure 59 DRIFT ANGLE vs MAGNETIC FIELD

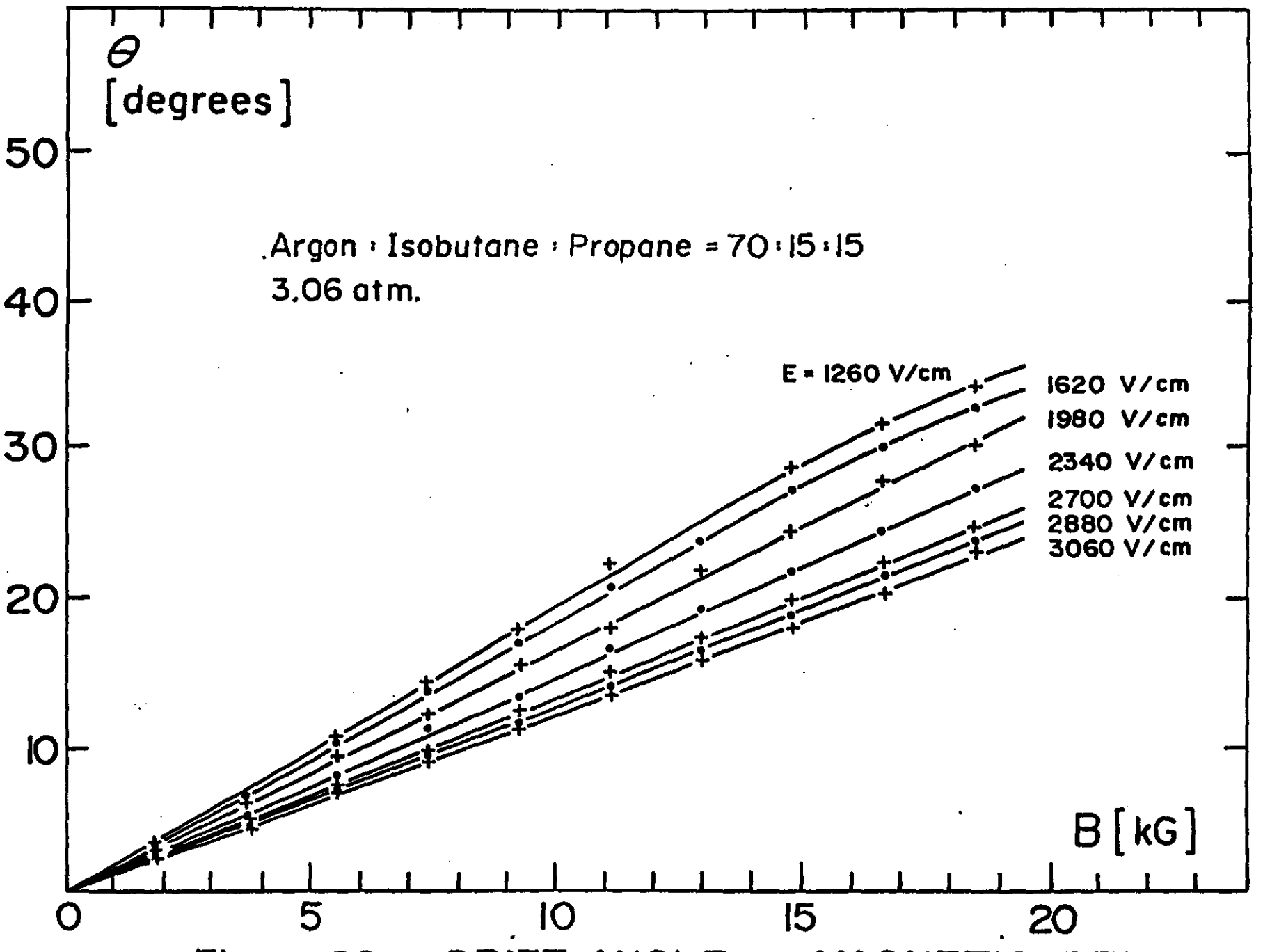

Figure 60 DRIFT ANGLE vs MAGNETIC FIELD

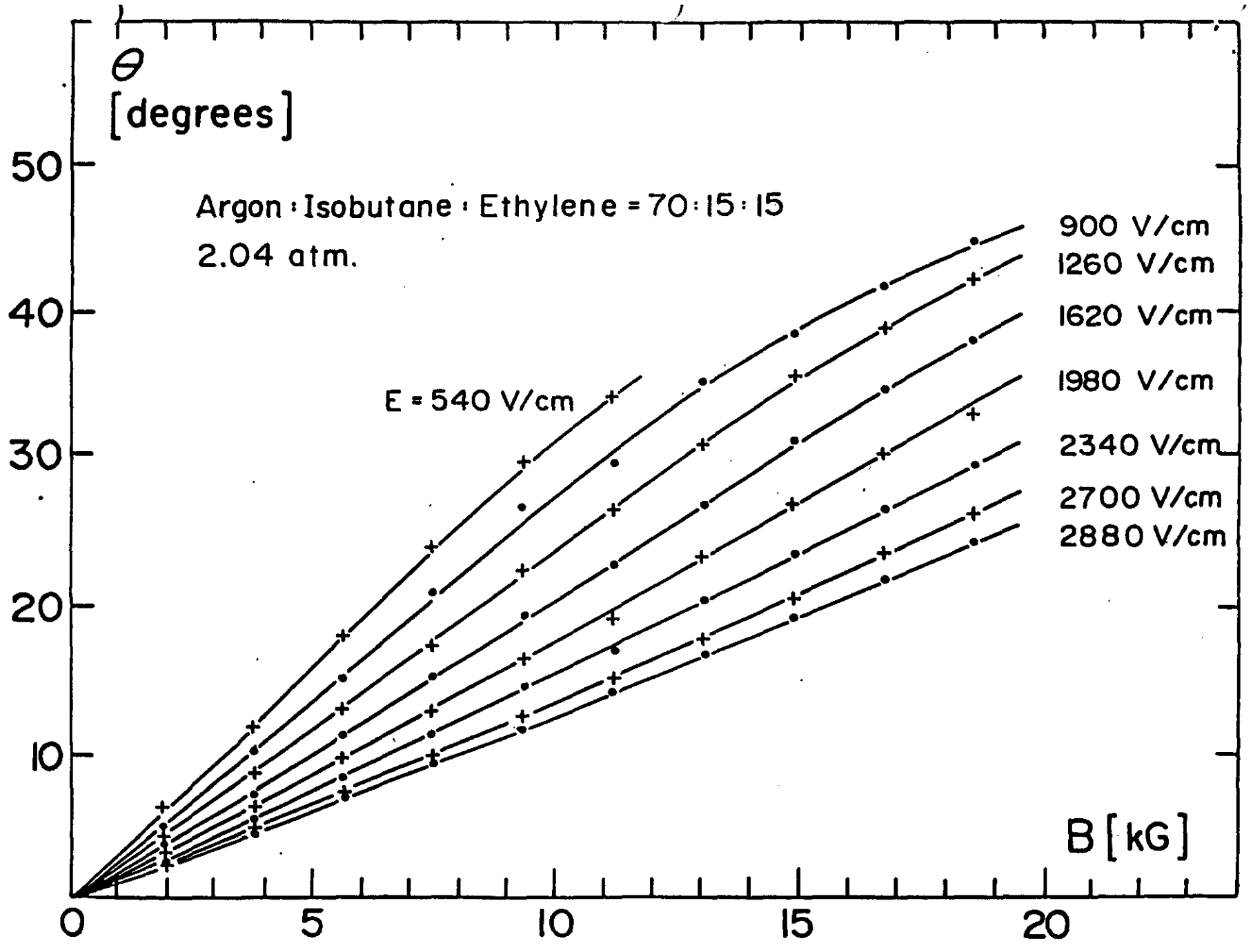

Figure 61 DRIFT ANGLE vs MAGNETIC FIELD

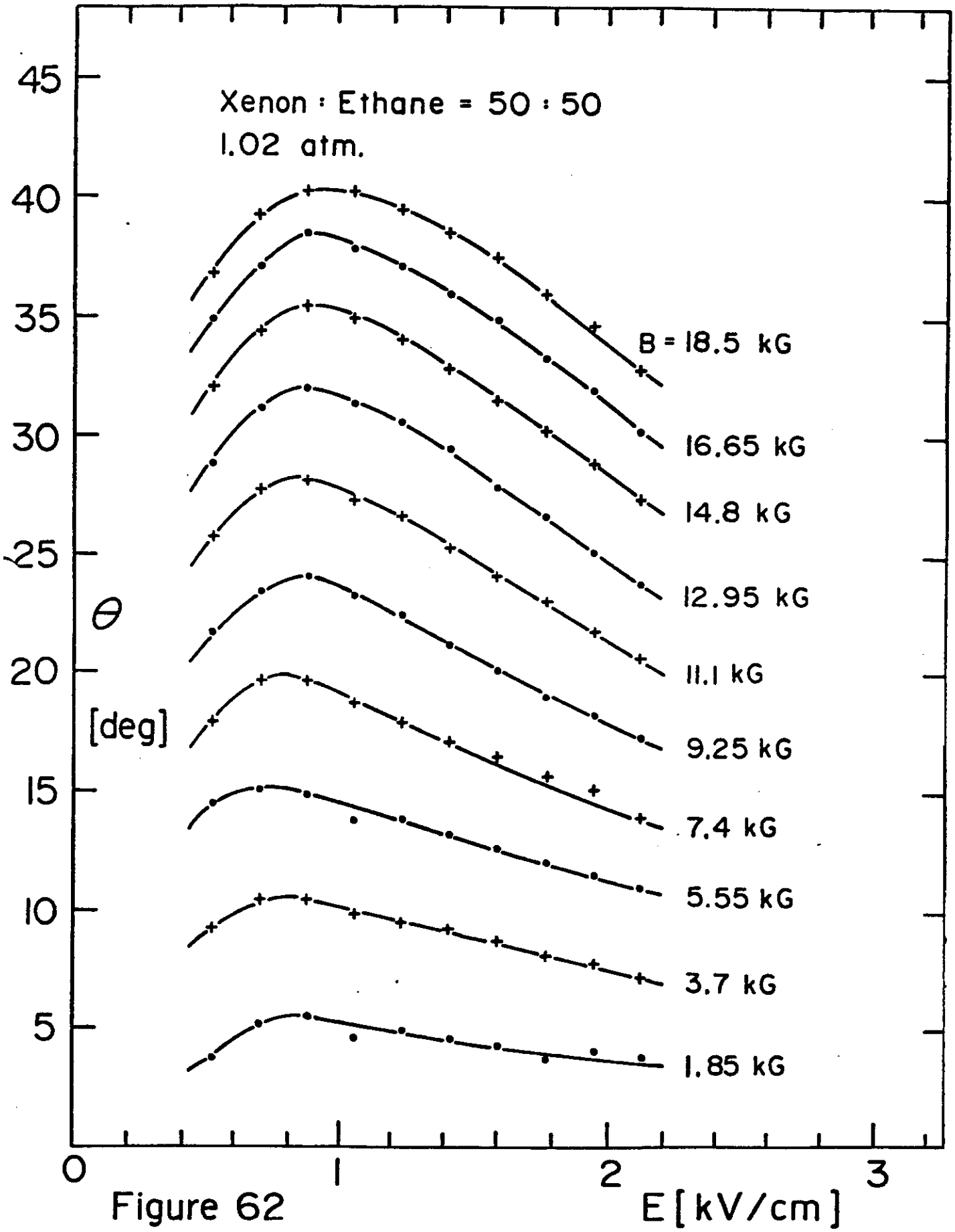
Xenon : Ethane = 50 : 50
1.02 atm.
B = 18.5 kG
16.65 kG
14.8 kG
12.95 kG
11.1 kG
9.25 kG
7.4 kG
5.55 kG
3.7 kG
1.85 kG
θ
[deg]
45
40
35
30
25
20
15
10
5
0
1
2
3
E [kV/cm]

Figure 62

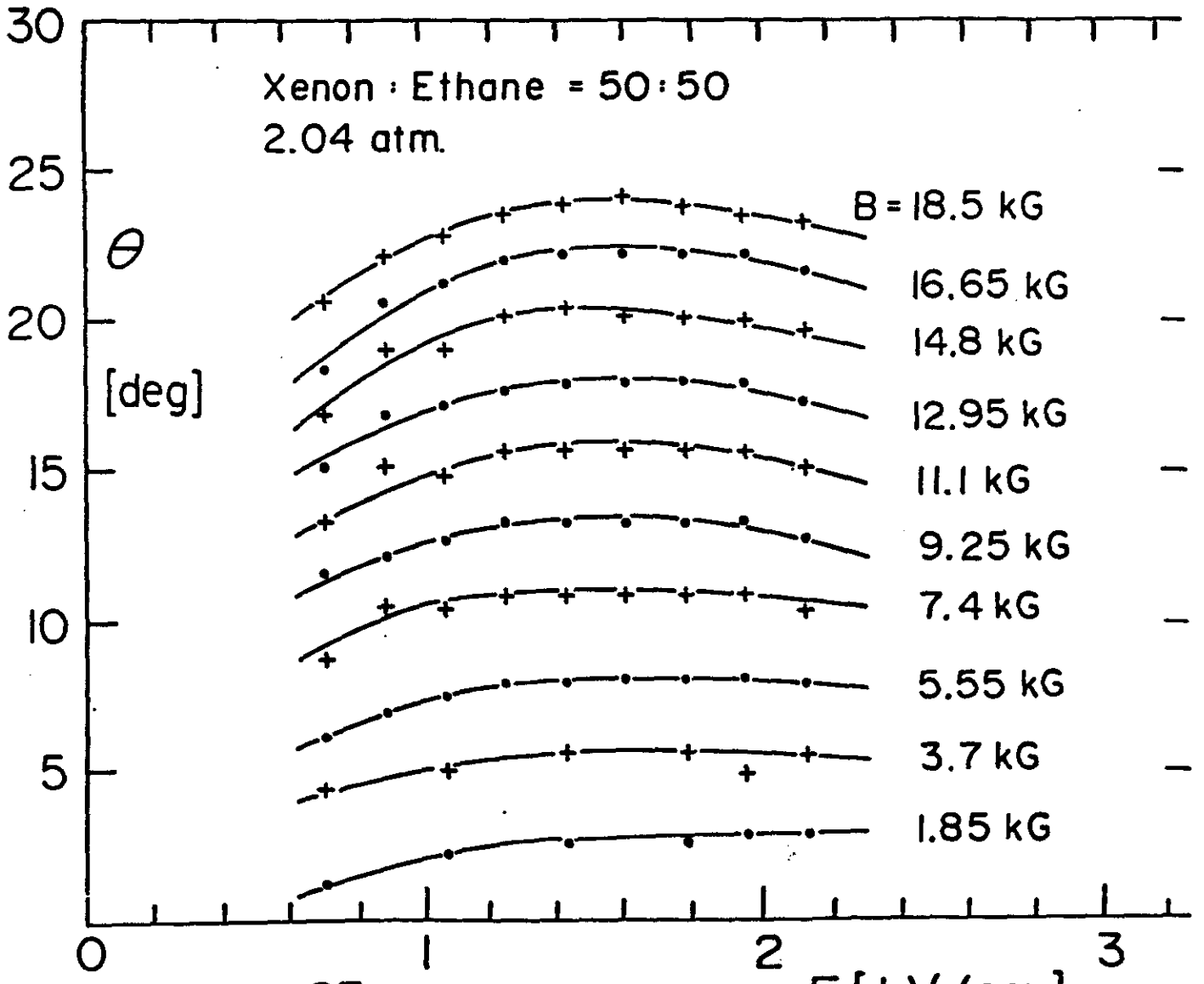
Xenon : Ethane = 50 : 50
2.04 atm.
θ
[deg]
B = 18.5 kG
16.65 kG
14.8 kG
12.95 kG
11.1 kG
9.25 kG
7.4 kG
5.55 kG
3.7 kG
1.85 kG
30
25
20
15
10
5
0
1
2
3
E [kV/cm]

Figure 63

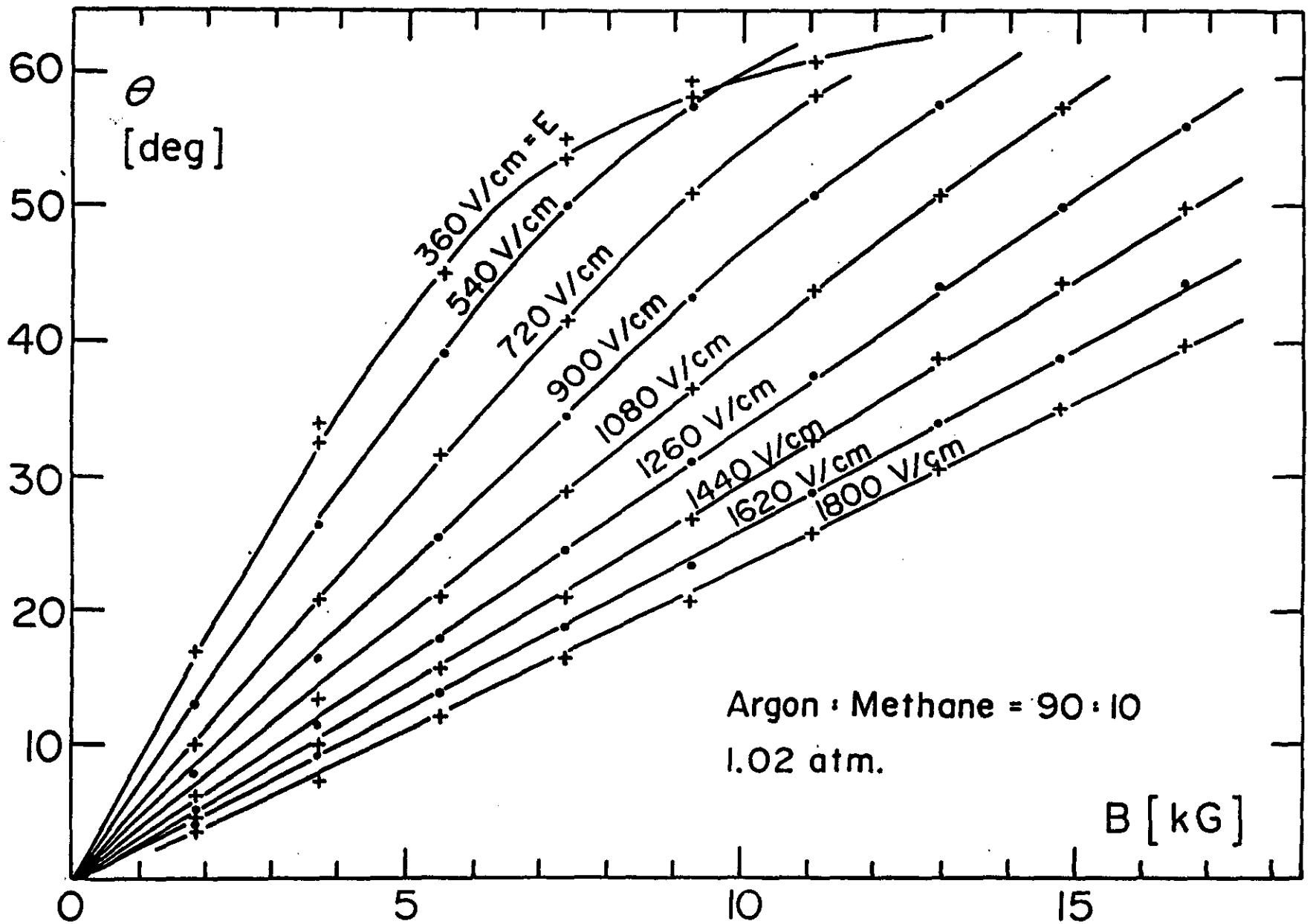

Figure 64 DRIFT ANGLE vs MAGNETIC FIELD